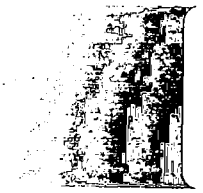

NASA Contractor Report 3726

Helicopter Rotor Wake Geometry and Its Influence in Forward Flight

Volume I - Generalized Wake Geometry and Wake Effect on Rotor Airloads and Performance

T. Alan Egolf and Anton J. Landgrebe

CONTRACT NAS1-14568
OCTOBER 1983

25th Anniversary
1958-1983

NASA

NASA Contractor Report 3726

Helicopter Rotor Wake Geometry and Its Influence in Forward Flight

Volume I - Generalized Wake Geometry and Wake Effect on Rotor Airloads and Performance

T. Alan Egolf and Anton J. Landgrebe
United Technologies Research Center
East Hartford, Connecticut

Prepared for
Langley Research Center
under Contract NAS1-14568

NASA
National Aeronautics
and Space Administration

Scientific and Technical
Information Branch

1983

PREFACE

This investigation was sponsored by the Structures Directorate, U. S. Army Research and Technology Laboratories, Langley Research Center, Virginia, and administered by the National Aeronautics and Space Administration at Langley Research Center under Contract NAS1-14568. The Army technical representative for this contract was Wayne R. Mantay. Henry E. Jones was the technical representative during the initial period of the contract. The Principal Investigator was T. Alan Egolf, Research Engineer, United Technologies Research Center (UTRC). The Program Manager and Co-investigator was Anton J. Landgrebe, Manager, Aeromechanics Research, UTRC. Donna Edwards, Engineering Assistant, UTRC, contributed significantly to the development of the computer graphics used to provide the wake charts presented herein.

This report consists of two volumes:

Volume I - Generalized Wake Geometry and Wake Effect on Rotor Airloads and Performance

Volume II - Wake Geometry Charts

SUMMARY

An analytical investigation is described which was conducted to generalize the wake geometry of a helicopter rotor in forward flight and to demonstrate the influence of including wake deformation in the prediction of rotor airloads and performance.

A first level generalized wake model was developed for a helicopter rotor operating in steady level forward flight based on theoretically predicted wake geometries. The generalized wake model consists of wake geometry equations in which tip vortex distortions are generalized as displacements from the classical undistorted tip vortex geometry. Tip vortex coordinates are generalized in terms of tip vortex age, blade azimuth, rotor advance ratio, thrust coefficient, number of blades, and rotor disk attitude for a selected representative blade design. Emphasis was placed on the region of the wake near the rotor and the predominant axial tip vortex distortions normal to the rotor disk. An exploratory study of the sensitivity of tip vortex geometry to rotor operating condition and design parameters was conducted to guide the generalized wake formulation. The generalized wake equations were programmed in a computer module which can be used to expeditiously generate wake coordinates for use with computer programs for rotor airflow and airloads prediction. A set of wake geometry charts are presented in Volume II to provide a convenient, readily accessible source for approximating rotor forward flight wake geometry and identifying wake boundaries and locations of blade-vortex passage.

Tip vortex geometry and the sensitivity of predicted rotor airloads and related rotor performance, and blade bending moments to various rotor inflow and wake geometry models are demonstrated herein for selected low to moderate high speed flight conditions of a representative rotor and the H-34 rotor. The inflow/wake models consist of uniform rotor inflow and variable inflow based on classical undistorted wake geometry, predicted distorted wake geometry, and the newly developed generalized wake geometry. Relative to the undistorted wake model, the forward and lateral sides of the wake are distorted toward the rotor in forward flight. This results in the prediction of a greater number of close blade-vortex passages and larger local gradients in blade airloads with the distorted wake models. The influence of the wake on blade airloads is related to the degree of proximity of the tip vortices to the rotor and the number of close blade-vortex passages. For steady level flight, this influence is predicted to generally increase with decreasing advance ratio, decreasing rotor disk nose down tilt, and increasing number of blades. Increasing thrust coefficient increases the undistorted wake deflection angle away from the rotor but simultaneously increases the amplitude of

the distortions of the tip vortices toward the rotor. Tip vortex distortions relative to the undistorted tip vortex geometry are predicted to be insensitive to rotor disk attitude.

Although additional experimental data are required, limited data from previous investigations tend to support these theoretical observations. The occurrence of close blade-vortex passages and the high sensitivity of predicted blade airloads to small deviations of blade to tip vortex distance demonstrate the requirement for an improved blade-vortex interaction model. Although the need for further analytical refinement is evident, the degree to which distorted wake models (generalized or predicted) improved the correlation of the measured H-34 airload and bending moment distributions is encouraging and indicates that, with future emphasis on blade-vortex interaction modeling, distorted wake methodology has the potential to provide a more accurate tool for blade airload prediction.

TABLE OF CONTENTS

TABLE OF CONTENTS (Cont'd)

LIST OF SYMBOLS

a_o	blade coning or precone angle, deg
a_{1_s}	longitudinal flapping angle for the first harmonic; i.e., coefficient of $-\cos\psi$ term in Fourier series expansion of blade flap angle with respect to plane normal to the rotor shaft axis, deg
A_y	lateral distortion amplitude parameter
A_o	generalized axial wake distortion envelope function coefficient for the first two revolutions of wake age, represents the slope of the function at zero wake age
A_1	generalized axial wake distortion envelope function coefficient for the first two revolutions of wake age, determines the decay of the function from the linear growth rate with wake age
A_{1_s}	cosine component of first harmonic cyclic pitch; i.e., coefficient of $-\cos\psi$ term in Fourier series expansion of the blade pitch angle with respect to the plane normal to the rotor shaft, deg
AR	blade aspect ratio, AR = $R/\bar{c}$
b	number of blades
B	generalized axial wake distortion envelope function coefficient for all revolutions of wake age greater than two, represents the intercept value at zero wake age of this linear envelope function, or number of blades
b_{1s}	lateral flapping angle for the first harmonic; i.e., coefficient of $-\sin\psi$ term in the Fourier series of blade flap angle with respect to plane normal to the rotor shaft axis, deg
B_{1_s}	sine component of first harmonic cyclic pitch; i.e., coefficient of $-\sin\psi$ term in Fourier series expansion of blade pitch angle with respect to the plane normal to the rotor shaft, deg
c	blade chord, ft.

LIST OF SYMBOLS (Cont'd)

$\bar{c}$	mean blade chord, ft.
C_T	rotor thrust coefficient, directed along shaft, thrust/$\rho\pi R^2(\Omega R)^2$
C_Q	rotor torque coefficient, torque/$\rho\pi R^2(\Omega R)^2 R$
C_W	rotor weight coefficient, $GW/\rho\pi R^2(\Omega R)^2$
D	drag force acting on helicopter
e	exponential function or blade flapping hinge offset
E	generalized wake distortion envelope function
g'_{nc}, g'_{ns}	harmonic coefficients for the generalized axial wake distortion shape function, Fourier cosine and sine terms respectively, for the first revolution of wake geometry
g''_{nc}, g''_{ns}	harmonic coefficients for the generalized axial wake distortion shape function, Fourier cosine and sine terms respectively, for the second and all subsequent revolutions of wake geometry
G	generalized axial wake distortion shape function
GW	gross weight of the helicopter, lb.
L	rotor lift, lb.
M	generalized axial wake distortion envelope function coefficient for all revolutions of wake geometry greater than two, represents the slope of the linear envelope function
N	number of harmonics for the shape function
r	radial coordinate from rotor axis of rotation to blade section or point on tip vortex, may be nondimensionalized by R
R	rotor radius, ft.
S	generalized lateral wake distortion function

TR	blade taper ratio
V	forward velocity or wind tunnel flow velocity, kt
$V_{i_x}, V_{i_y}, V_{i_z}$	induced velocity in the x, y or z direction respectively, fps
$V_{i_{MOM}}$	momentum value of axial induced velocity, see equation in Table VI, fps
x,X	longitudinal coordinate measured from center of rotor disk in tip-path plane, nondimensionalized by R, positive as shown in Fig. 10
y_L	lateral distortion limit parameter
y_u	undistorted lateral coordinate, nondimensionalized by R
y,Y	lateral coordinate measured from center of rotor disk in tip-path plane, nondimensionalized by R, positive as shown in Fig. 10
z,Z	axial coordinate measured from center of rotor disk and normal to tip-path plane, nondimensionalized by R, positive up as shown in Fig. 10
α_s	rotor shaft angle of attack (mast angle). Angle between forward velocity and plane normal to shaft axis, positive nose up, deg
α_{TPP}	rotor tip-path plane angle of attack. Angle between forward velocity and tip-path plane, positive nose up, deg
γ	Lock number, ratio of aerodynamic to inertial loads
δ_y	generalized lateral distortion growth function
ΔC_ℓ	limiting value of change in induced lift coefficient per azimuthal interval as used in the analysis
Δt	numerical time step increment, see $\Delta\psi$, deg

$\Delta x, \Delta X$	longitudinal vortex element coordinate distortions from the undistorted longitudinal coordinate, nondimensionalized by R
$\Delta y, \Delta Y$	lateral vortex element coordinate distortions from the undistorted lateral coordinate, nondimensionalized by R
$\Delta z, \Delta Z$	axial vortex element coordinate distortion from the undistorted axial coordinate, nondimensionalized by R
$\Delta\psi$	numerical azimuth increment used in the analyses corresponding to the time step increment, Δt (deg or rad)
θ_1	rate of change of local blade pitch angle due to built-in linear twist with respect to blade spanwise direction, positive when tip section is twisted leading-edge up relative to root section, deg
θ_{75}	blade collective pitch angle as measured at r = 0.75, deg
λ	rotor inflow ratio; see equation in Table VI
λy	lateral coordinate distortion rate parameter
μ	rotor advance ratio (with respect to tip-path plane), $\mu = V_{cos}\alpha_{TPP}/\Omega R$ ($\alpha_{TPP} \leq 6°$ for this study)
μ'	rotor advance ratio (with respect to free stream velocity), $\mu' = V/\Omega R$
ρ	air density, lb-sec^2/ft^4
σ	rotor solidity ratio, $\sigma = b\bar{c}/\pi R$
χ_{TPP}	undistorted wake deflection angle based on momentum induced velocity, angle between undistorted momentum wake boundary and tip-path plane, positive when wake is below tip-path plane, deg; see equation in Table VI
ψ_{age}	wake age, see ψ_w, deg or rad

ψ_b	blade azimuth angle measured from positive x-axis (downstream direction) to blade in direction of blade rotation, deg or rad; see Fig. 10
ψ_{b_0}	blade azimuth angle of blade that originated (shed) vortex element -- at the time of origination, deg or rad
ψ_w	wake azimuth position or wake age, azimuth angle of vortex element (point on tip vortex) relative to the blade from which it originated; represents the blade azimuth travel between the time the vortex element was shed by the blade and the current blade azimuth, deg or rad; see Fig. 10. Used interchangeably with ψ_{age}
$\bar{\psi}_w$	phased wake azimuth position, represents the wake age with respect to the positive x-axis, deg or rad, $\bar{\psi}_w = \psi_w - \psi_b$, see Fig. 10
ΩR	rotor tip speed, fps

INTRODUCTION

One of the most fundamental factors affecting the performance of rotorcraft systems is the induced influence of the main rotor wake on rotor airloads and related performance. The task of predicting the flow field induced by a helicopter rotor continues to be of primary importance for providing and evaluating improved rotor designs. The continuing development of more accurate aerodynamic methods for predicting the temporal and spatial variation of the induced flow velocities at the rotor blades and in the rotor flow field will result in significant advances in rotor aerodynamic methodology important to nearly every area of rotary wing design. These areas include performance, vibrations, stability, structural reliability, and acoustics. Improved capability to predict the detailed rotor flow characteristics will facilitate the prediction of more accurate blade airloads and a more rational design of the blade structure. This, in turn, can lead to reduced aircraft development and maintenance costs along with improved performance because of the more optimum design. Also, the capability to predict rotor-induced flow velocities away from the rotor is important for the calculation of aerodynamic interference effects at aircraft components such as the fuselage, wing, tail rotor, and empennage surfaces.

The accurate prediction of helicopter rotor blade airloading has been a continuing goal in the helicopter industry. Significant progress has been made as advanced computational methods accounting for wake, aeroelastic, and fuselage interference effects have been developed. However, the helicopter designer cannot yet rely on airloads methods to provide him with sufficient accuracy to determine performance, loads, vibrations, stability, noise, and interference effects over the range of flight conditions. Of the numerous phenomena influencing rotor airloads that require further research, a primary one is wake interaction. For many flight regimes the tip vortices from the main rotor blades pass sufficiently close to, or even impact, following blades such as to produce a complex flow environment which influences both the local blade loading and the vortex characteristics.

Classically, the wake shed from a rotor blade in forward flight has been modeled as a rigid, undeformed helical sheet of vorticity of varying strength, with a trajectory defined by rotor attitude and flight condition. Generally, these vortex sheets are then modeled by assuming that their influence can be approximated by using discrete vortex filaments of appropriate strength positioned within the plane of the vortex sheet (Fig. 1). These wake models are then used to calculate the induced inflow at the rotor blade by applying the Biot-Savart law to the particular rotor-wake geometry.

In recent years, the demand for improved rotorcraft performance and airload prediction has led to the development of more detailed wake models. A major characteristic of the wake geometry, currently ignored in most forward flight analyses in general use in industry, is the deformation of the wake from the rigid helical shape. In particular, the rollup of the sheet into a deformed tip vortex whose position in space is not consistent with the classical geometry is shown in Figs. 2 and 3. Any methodology which does not consider this deformation phenomena may be in question for certain applications.

The major technological advance in recent years to rotor induced velocity methodology has been the improvement in the mathematical modeling of the rotor wake. This has become possible with the advent of high-speed digital computers. Many efforts have been directed toward providing this methodology as shown in the survey presented in Ref. 1 and other examples listed in the References. As a major part of a long-term effort to advance the technology associated with the aerodynamic and aeroelastic behavior of helicopter rotor blades, the United Technologies Research Center, UTRC, has been conducting studies on the influence of the rotor wake on rotor airflow, airloads, and dependent rotorcraft characteristics. Some of the UTRC research programs conducted in this area are discussed in Refs. 1 through 10. The scope of this effort has included both analytical and experimental investigation programs, and the development of distorted and undistorted wake prediction analyses as applied to single- and multi-rotor configurations and compound helicopters operating under hovering and forward flight conditions. Methods developed have been provided to several organizations within the Government and industry. The UTRC Prescribed Wake Rotor Inflow Analysis, the Rotorcraft Wake Analysis, and the Rotor Wake Geometry Analysis are described in Refs. 1 to 10 and brief descriptions will be presented in a later section of this report. The functions and features of the Rotorcraft Wake Analysis are shown in Fig. 4. A major feature of these analyses is the provision for various wake modeling options.

In hovering flight, the need to accurately predict the position of the rotor wake is well documented (Refs. 1 to 13). The use of lifting line or surface models with discrete trailing vortex systems modeling the wake of each blade is state-of-the-art in the industry for general hover performance predictions. Accurate hover performance analyses use prescribed wake models, whose tip vortex and inboard sheet geometry have been determined from empirical studies. Originally the wake geometry in hover was predicted numerically, but this was found to be of insufficient accuracy and computationally costly, and had to be calculated for each flight condition. This method was replaced by empirical methods describing the wake geometry from flow visualization data which was generalized at UTRC for a wide range of parameters (Refs. 9 and 10). This generalization was performed for a range

of hovering rotor geometries and flight conditions to obtain analytical expressions defining the hovering wake geometry in a compact form. Further expansion of the empirical wake geometry generalization for hover was reported in Ref. 11. A validated lifting line hover performance analysis is the Circulation Coupled Hover Analysis Program (CCHAP) developed at Sikorsky Aircraft (Ref. 8). This analysis is an extension of the Ref. 9 prescribed wake hover analysis. CCHAP adjusts the generalized hover wake geometry by coupling the wake geometry and blade airloading in a consistent manner. Other hover method developments have included a lifting surface representation of the blade (e.g., Refs. 11 to 13). The importance of accurately modeling the tip vortex geometry in forward flight is not as extensively documented as for hover, but the need has been recognized by several investigators (e.g., Refs. 4, 14 to 17).

A sample computer plot of the deformed tip vortices for a two-bladed rotor at a 30 kt flight condition, as calculated by the UTRC Wake Geometry Analysis, is presented in Fig. 3. The predicted wake geometry for this condition is compared with that of a hover condition and the predicted distorted and undistorted tip vortex patterns of a 15 kt condition in Fig. 5, which is reproduced from Ref. 6. The tip vortex geometry predicted by the same analysis for one blade of a two-bladed rotor at 89 kt is shown in Fig. 6, which is reproduced from Ref. 5. In several UTRC studies summarized in Ref. 6, experimental and theoretical techniques were applied to investigate rotor wake and airflow characteristics for low speed flight. Flow velocities were measured with a laser velocimeter and wake features were determined from flow visualization techniques. For example, measured wake boundaries and tip vortex locations from Ref. 6 are presented in Figs. 7 and 8 which show that the path of the tip vortices goes above and then down through the rotor at low speed, and blade-vortex impact occurs. The application of laser velocimetry to locate the tip vortex passages under the advancing blade is discussed in Ref. 18. A comparison of calculated and measured airloading for that test program is presented in Ref. 19. Photographs of a model rotor wake in a water tunnel are presented in Ref. 20. In the Ref. 5 study, the water tunnel data of Ref. 20 and the UTRC Wake Geometry Analysis were utilized to explore the forward flight wake problem and the potential of forward flight wake generalization was identified. For forward flight, experimental wake data is extremely limited, and theoretical wake predictions have been limited to isolated cases. A systematic determination of wake geometry and airload sensitivity to wake deformations over a range of operating conditions was required. The theoretical study, reported herein, systematically explored the characteristics and influence of the forward flight wake.

A primary reason for the limited use of distorted wake geometries in rotor analyses is the computer cost and complexity involved in wake geometry computations. Wake coordinates are calculated by large computer programs,

such as the UTRC Rotor Wake Geometry Analysis described in Ref. 4, in which the computer time required is typically many times the combined requirement for the calculation of all of the other rotor aerodynamic and performance characteristics.

Applications of the Rotor Wake Geometry Analysis at UTRC indicated that the potential existed for generalizing rotor tip vortex geometry for forward flight conditions. From information generated during the Ref. 5 study, the development of techniques for generalizing forward flight tip vortex geometry as functions of primary parameters appeared feasible. It was recognized that wake generalization would facilitate the development of a set of generalized equations, charts and/or tables which would define rotor wake geometry in a form suitable for use in computer analyses for predicting rotor airloads and related performance, structural, and dynamic response characteristics. Such generalizations could be programmed in modular form to make wake geometries immediately available in such rotor analyses.

Considering the above, this investigation was conducted with the following objectives:

1. To analytically demonstrate the significance of rotor tip vortex distortions on the aerodynamic environment of a helicopter rotor in forward flight with particular emphasis on rotor airload distribution and associated rotor performance.

2. To generalize rotor tip vortex coordinates in terms of primary variables in equation form for incorporation in a computer subroutine to provide a first level wake geometry generalization for the calculation of rotor inflow and airload distributions required for helicopter rotor performance and blade aeroelastic response programs.

3. To perform an initial assessment of the developed generalized wake representation and its application for analytical rotor flight simulation.

4. To provide a set of graphical wake geometry charts for undistorted and distorted tip vortex coordinates, blade-vortex passages, and wake boundaries for a comprehensive range of primary rotor wake parameters: number of blades (2 and 4), advance ratio, thrust coefficient, rotor attitude, blade azimuth and vortex age.

The investigation is described in the following sections of this report which are entitled (1) Technical Approach, (2) Description of Analyses, (3) Selection of Analytical Parameters and Procedures, (4) Generalized Wake Geometry, and (5) Influence of Wake Geometry on Rotor Airloads and Performance. A set of wake geometry charts is provided in Volume II of this report.

TECHNICAL APPROACH

In accordance with the objectives stated in the Introduction, a technical program was performed which was comprised of the following tasks:

1. Determination of the significance of wake distortions on rotor airloads and related rotor performance and blade bending moments.

2. Wake generalization.

3. Development of a generalized wake computer module.

4. Assessment of the wake generalization.

5. Provision of a set of rotor wake geometry charts.

The technical approach used in the performance of each of these tasks is summarized below.

Significance of Wake Distortions

The computer program for the UTRC Rotor Wake Geometry Analysis was used in conjunction with the UTRC Prescribed Wake Rotor Inflow Analysis (Single Rotor Version of the UTRC Rotorcraft Wake Analysis), and the Sikorsky Generalized Rotor Performance Analysis, as shown in Fig. 9, to determine the significance of main rotor tip vortex distortions on the aerodynamic environment and performance of a helicopter rotor in steady forward flight. The wake geometry, blade loading distribution, and rotor performance characteristics were calculated for varying combinations of rotor design and flight condition, and the results based on a distorted wake geometry were compared with the results based on both an undistorted wake geometry and uniform inflow. The calculated wake distortions consisted of self-induced distortions of the tip vortices of an isolated rotor, and the distorted wake geometry used in the inflow and performance calculations included these tip distortions along with an undistorted inboard wake representation. The time-varying circulation strength of the rolled-up tip vortices of the distorted wake was based on the time-varying peak of the blade radial loading distribution as calculated in the Prescribed Wake Rotor Inflow Analysis. Flight speeds of approximately 20-130 knots (0.05-0.3 advance ratio) were investigated to emphasize the low to moderate speed range where wake effects are most influential. The effects of tip vortex distortions on airloads and overall performance were determined as a function of rotor radius, azimuth, and flight condition for several flight conditions and design variations for a representative rotor. In addition,

three H-34 rotor operating condition combinations were selected on the basis of available test data, and for the above combinations calculated airloads, controls, and bending moments were compared with the test data. An available Sikorsky normal modes aeroelastic rotor analysis was used to predict bending moments.

Wake Generalization

Using results from the UTRC Rotor Wake Geometry Analysis as used in conjunction with the UTRC Prescribed Wake Rotor Inflow Analysis and the Sikorsky Generalized Rotor Performance Analysis, techniques were developed for generalizing rotor tip vortex coordinates in terms of primary parameters. The wake generalization findings reported in Ref. 5 were expanded and investigated analytically for additional rotor designs and flight conditions to establish a data base from which to generalize the tip vortex distortions, develop generalization techniques, and determine the range of values of the variables over which the generalization techniques apply. The computer programs were used to compute distorted and undistorted wake geometries for several combinations of significant parameters such as advance ratio, number of blades, thrust coefficient, rotor disk attitude, blade twist, and blade aspect ratio. A first level wake generalization was successfully developed. Emphasis in the generalization was placed on rotor advance ratio (0.05 to 0.3), number of blades (2 and 4), thrust level and rotor disk attitude.

It is noted that it was not the intent of this investigation to necessarily develop a wake generalization which is all inclusive for every parameter and the complete range of each parameter. Recognizing that this was the first systematic attempt to generalize forward flight wake geometry and the prohibitive costly computer requirements to establish an all inclusive data base in this initial effort, the intent was to develop a first level generalization. The scope of this generalization was determined by the complexity and range of applicability of the generalized techniques that were developed, and the predefined computer utilization limits of the project.

In order to reduce the large number of values required to document the coordinates of the time-varying tip vortex geometries for a specific flight condition, application of several generalization techniques were explored. These included the development and investigation of the adequacy of numerical curve fit equation techniques and the generalization of coordinates for varying rotor positions and wake revolutions. Also, the adequacy of undistorted wake coordinates for certain wake regions was investigated. The wake geometries were generalized in equation form with tabulated coefficients for a representative blade design, which is dependent on the number of blades, advance ratio, thrust coefficient, and disk attitude.

Development of a Generalized Wake Computer Module

The results of the wake generalization were programmed in a computer subroutine and incorporated in the UTRC Prescribed Wake Rotor Inflow Program. The computer subroutine was also provided as a module to the computer program for the Rotorcraft Wake Analysis (Ref. 2). Wake coordinate equations and tabulations with interpolation procedures were coded in the subroutine to generate the wake distortions corresponding to a desired rotor design and operating condition. The resulting generalized wake module coupled with the Prescribed Wake Rotor Inflow Program or the Rotorcraft Wake Analysis provides the capability for calculating distorted wake induced velocities in a computationally efficient manner.

Assessment of the Wake Generalization

The generalized wake module was used in conjunction with the UTRC Prescribed Wake Rotor Inflow Program and the Sikorsky Generalized Rotor Performance Program to perform an initial assessment of the generalized wake. Comparisons of wake coordinates, airloads, and associated performance results based on use of the generalized wake module were compared with the following: (1) corresponding coordinates, airloads and performance based on distorted wake geometries obtained directly from the Rotor Wake Geometry Analysis, (2) corresponding coordinates, airloads, and performance based on undistorted wake geometries, and (3) airloads and performance based on constant rotor inflow. Comparisons were made for a representative rotor and for three flight conditions of an H-34 full-scale rotor for which test data were available.

Rotor Wake Geometry Charts

Wake geometry charts were developed using computer graphics techniques. These charts provide the necessary information to determine the relative position of the tip vortices trailed from helicopter rotor blades for a range of parameters sufficient for most conventional steady forward flight operating conditions. Both the classical undistorted and generalized distorted wake models are included. The charts can be used for a variety of applications which require the geometric relationship between the tip vortices and spatial locations relative to the helicopter. In particular, locations of blade-vortex interactions and wake boundaries beneath the rotor can be rapidly estimated using these charts. A series of tip vortex patterns showing top, side, rear, and isometric views are also included. The wake geometry charts were prepared as Volume II of this report.

The above technical activities and the results therefrom are described in detail in the following sections of this report. Brief descriptions of the computer analyses used in this investigation are presented in the next section.

DESCRIPTION OF ANALYSES

Several computer analyses were used during this investigation to predict rotor wake geometry, inflow, airloads, performance, and bending moments. Included in this section of the report are brief descriptions of these analyses along with a description of the solution procedures required for their use.

The Prescribed Wake Rotor Inflow Program

The UTRC Prescribed Wake Rotor Inflow Program (F389SR) is a single rotor version of the Rotorcraft Wake Analysis (RWA) described in Ref. 2. A chart of the operational status and capabilities of RWA is shown in Fig. 4. These analyses are used in conjunction with other analyses to provide either inflow velocities at the rotor disk for rotor performance and blade response predictions or blade circulation distributions for use in the Rotor Wake Geometry Analysis (Ref. 4). A flow chart of this type of coupling to form a complete "rotor analysis" is presented in Fig. 9. The details of the single rotor version of the inflow program used in this investigation are presented in Ref. 21. A brief technical description for this single rotor version follows.

Technical Description

The UTRC Prescribed Wake Rotor Inflow Program (hereafter referred to as the rotor inflow program or inflow analysis) computes the bound circulation and induced inflow distributions along the rotor blades based on a prescribed wake model and modeling of the aerodynamics at each blade section. As shown in Fig. 9, the section operating conditions are generally prescribed from blade motion and control information obtained from a separate blade airload and response program. The wake model is either generated internally in the computer program (undistorted wake) or prescribed from a separate program.

Briefly, the mathematical model in the rotor inflow program consists of the representation of each blade by a segmented lifting line, and the helical wake of the rotor by discrete segmented vortex filaments consisting of trailing vorticity which result from the spanwise variation of bound circulation. Figure 10 illustrates the coordinate system used in this analysis for the rotor and wake geometry. The circulation of the wake for each blade changes with azimuth position and is periodic for each rotor revolution. The blades are divided into a finite number of radial segments, and the induced velocity at the center of each selected blade segment is computed by summing the contributions of each bound and trailing wake segment (Fig. 11). The contribution of each vortex segment is obtained through use of the Biot-Savart

equation which expresses the induced velocity in terms of the circulation strength of the vortex segment and its geometric position relative to the blade segment at which the induced velocity is desired. The bound circulation distribution is determined by relating the wake circulations to the bound circulations, expressing the wake induced velocities in terms of the unknown bound vortex strengths by means of the Biot-Savart equation, and developing a set of simultaneous equations in which each term relates the bound circulation and local blade angle of attack at each blade segment and azimuth position. These equations thus involve the known flight condition, wake geometry, and blade motion and control parameters and the unknown bound circulation values. Solution of these equations, to include measured airfoil section characteristics, yields the desired bound circulation values, which, when combined with the appropriate geometric relations in the Biot-Savart law, produce the required rotor induced velocity distribution. Many of the fundamental assumptions are based on those of Ref. 22.

The rotor inflow program is based on the following formulation and assumptions:

1. Each blade is represented by a lifting line located at the blade quarter chord line (bound vortex) and divided into a finite number of segments (blade segments) each having a different circulation strength (Fig. 11). The aerodynamic characteristics at the centers of each segment are assumed to be representative of the entire segment over a finite azimuth interval. The use of lifting line rather than lifting surface theory permits the use of empirical airfoil data for nonlinear aerodynamics such as stall.

2. The wake is represented by a finite number of vortex filaments trailing from the blade segment boundaries. Each filament is divided into straight segments, the lengths of which are determined by a specified wake azimuth interval which is equivalent to a specified blade azimuth interval (see Fig. 11). The circulation strength of each trailing vortex segment is constant along its length, and is equivalent to the difference between the circulation values of its adjacent bound vortex segments in accordance with the Helmholtz laws of conservation of vorticity. The circulation strengths of different vortex segments along a vortex filament vary in accordance with the variation of the bound circulations with azimuth position.

3. Viscous dissipation effects on the wake circulation strengths are neglected in that the circulation of a given wake segment is constant with time. However, the number of wake revolutions retained in the analysis can be limited to evaluate an abrupt dissipation of the wake. Also, the viscous rollup of the tip vortex can be approximated by combining tip filaments beyond

a prescribed rollup azimuth interval. In addition, a vortex core size is assigned to each vortex filament. Potential theory is assumed to apply outside the vortex core. Inside the vortex core zero flow or rigid body rotation is assumed. Other vortex core models can be readily incorporated.

4. It is assumed that the rotor is operating in steady-state flight. The inflow and wake from each blade is assumed to be periodic with blade spacing. That is, the inflow and wake geometry are the same for each blade when at a specific azimuth position.

5. Shed wake segments (segments normal to the trailing wake segments mentioned above) arising from the time rather than radial variations of bound vorticity, are not included in the wake model. Although this omission technically violates the Helmholtz law, it is believed that a more accurate representation of the shed wake effects is obtained through the use of experimental unsteady airfoil characteristics in the analysis. This implies that the primary effects of the shed vorticity are those associated with the shed wake immediately behind the blade, and thus can be approximated by those of a fixed-wing type of wake. Miller (Ref. 23) shows that this is generally reasonable. This approach not only permits a factor of two reduction in computer time and prevents unrealistic results associated with a discrete filament wake model, but more importantly, permits nonlinear unsteady stall effects to be included in an empirical manner in the airloads prediction program.

6. The wake geometry is prescribed from analytical or experimental results. Various options are available for selecting the representation of the wake model.

7. The airfoil at the blade is assumed two-dimensional (radial velocity components are neglected). For the linearized circulation solutions and associated calculations, a set of lift curve slopes, stall angles of attack, and angles of zero lift are provided which vary with Mach number and blade thickness. These may be based on unsteady aerodynamic data, if available. Below stall the lift curve slope is assumed constant. The blade section circulation is limited to a constant value for angles of attack above stall. An optional nonlinear solution procedure can be used which employs measured tabulated airfoil data to account for nonlinear aerodynamics including stall.

8. In the blade-wake geometrty calculations the blades are assumed rigid. However, flexibility effects may be included in the circulation solution by providing the necessary noninduced velocity at each segment associated with flexible blade motions and controls from a blade response program. Also, an anhedral or swept tip may be prescribed.

9. Tangential and radial induced velocity components are neglected and small angle assumptions are included in the linear circulation solution. These assumptions are eliminated in the optional non-linear solution.

10. The aerodynamic interference effects of the rotor hub, fuselage, etc. are normally neglected. However, these can be accommodated in the solution, if desired, as superimposed flow velocity increments. The rotor is assumed to be operating out-of-ground effect.

Wake Geometry

The rotor inflow program requires that the rotor wake geometry be specified in order for circulations and induced velocities to be determined. Generality regarding the specification of the wake geometry is provided in the computer program. This is accomplished by allowing the wake coordinates for the wake segment end points to be input from an external source (tape, cards, etc.) for computational purposes, if desired. At the onset of this investigation there were two program options available for wake geometry: (1) a classical undistorted wake model (Fig. 1), available internally, and (2) an analytical wake model (distorted wake, Fig. 3), obtained from a separate wake geometry program. In addition, a generalized wake module developed during the course of this investigation has since been included.

Generally the classical undistorted wake model has been used for performance prediction. It has the least complex wake geometry that is simply a function of the flight condition and momentum inflow velocity. The coordinates of this helical wake, which is skewed in forward flight, are generated internally in the program. A brief description of the classical and distorted wake geometries is provided below.

Undistorted Wake Model

In its simplest form, the wake can be assumed to be a classical undistorted skewed helical sheet of vorticity defined from momentum considerations (hereafter referred to as the classical wake or undistorted wake). A sample undistorted wake representation is shown in Fig. 1. The coordinates of the undistorted wake representation are obtained from the rotor advance ratio, μ, thrust coefficient, C_T, and angle of attack relative to the tip path plane, α_{TPP}. For example, the top view of the tip vortex filaments is obtained directly from the helicoidal path of the blade tip as it translates at the velocity $V\cos\alpha_{TPP}$ and rotates at the velocity ΩR. The side view is dependent on the wake skew angle (angle between normal to the rotor disk and wake boundary), which is normally defined from momentum considerations. Equations for the undistorted wake coordinates will be presented in a later section of the report.

Distorted Wake Model

A distorted wake model may be incorporated in the analysis via tape input. A rotor wake geometry analysis, such as that developed at UTRC and described in the following section, can be used to generate wake coordinates on tape for use in the rotor inflow analysis. Figure 3 is an example of such a distorted wake model.

The Rotor Wake Geometry Analysis

The UTRC Rotor Wake Geometry Analysis predicts the distorted tip vortex geometry of a rotor in steady forward flight. A detailed description of the development and fundamental concepts used in this analysis along with sample applications are presented in Ref. 4. Because this analysis is used to predict the distorted tip vortex geometry, and it is these predicted geometries which determine the influence of wake distortions on the predicted rotor performance for this investigation, a description of the technical approach is presented which provides more detail than the descriptions of the other analyses used in the investigation. The basic technical approach and numerical procedure used in this analysis follow, and the major assumptions and approximations used in the analysis are noted.

Technical Description

The wake model used in the calculation of the wake distortions is composed of trailing and bound vortex filaments. The trailing vortex filaments are divided into finite length straight vortex elements whose end points are free to convect at velocities equal to the vector sum of the free stream velocity and the velocities induced by the trailing and bound vorticity. The lengths of the wake elements are related to the azimuth increment chosen. The wake is truncated at a specified number of revolutions downstream of the blade. Generally, the numerical accuracy of the analysis is increased by decreasing the azimuth increment and increasing the number of wake revolutions. The exact choice of these parameters is dependent upon the flight condition under study and the trade-off between required accuracy and acceptable computing cost. Details of this selection of parameters is noted in another section of this report. The accuracy/computing cost trade-off also influenced the wake interaction model and the selection of interacting elements as described below.

The tip vortex elements distort over successive time increments from an initially prescribed geometry (generally the classical undistorted wake geometry) under the influence of the induced flow distribution velocities contributed by each of the vortex elements of the blade bound vortex, the

inboard trailing wake filaments, and the tip vortex filaments. A regionalization procedure, which distinguishes between "near" and "far" elements to reduce computer cost, described in detail in Ref. 4, will be described briefly at the end of this report section.

The bound vorticity of each blade is represented by a single segmented vortex filament located at the quarter chord (lifting line). In the general case, the strength of this vorticity varies with both radial position and azimuth angle. Up to ten radial values of bound vorticity can be accounted for in the program at each azimuth angle.

The inboard wake elements, representing the inboard vortex sheet of each blade, are generally prescribed as undistorted and their influence at the tip vortices is generally based on the undistorted wake geometry.

The wake elements generated by azimuthal variations in blade bound circulation have not been included in the wake model. This shed wake represents one of the unsteady effects arising from the azimuthal variation of blade bound circulation. It was reasoned during earlier evaluation studies of undistorted wake variable inflow methods that the number of discrete shed wake filaments that could be accommodated in any practical analysis was so limited that the use of discrete filament shed wake model was of questionable accuracy, particularly in the important region near the blade. Although it is recognized, from a rigorous theoretical viewpoint, that the Helmholtz laws of vortex continuity have been violated as far as the wake geometry problem is concerned, the omission of the shed wake effects on the distortions of the trailing vortex filaments is assumed to have only a secondary effect. This assumption is partially based on the fact that the circulation strength of the shed wake is significantly less than that of the trailing filaments, particularly that of the tip vortices.

The input circulation strengths assigned to the wake elements are generally transferred from the Prescribed Wake Rotor Inflow Program (Fig. 9). In such a calculation, a steady flight condition is assumed and the circulation of a given wake element is related to the bound circulation of the blade section at the time the wake element was created. Viscous dissipation effects on wake circulation are currently neglected.

A provision is included in the analysis for eliminating the irrotationality assumption (i.e., applicability of the Biot-Savart law) in computing induced velocities at points located within an arbitrary distance from any vortex element. This distance is considered to be the vortex core radius. Irrotational potential flow induced velocities are calculated at points outside the vortex core with a limiting value at the vortex core boundary. The results presented herein were obtained assuming a vortex core diameter of 1 percent of the rotor radius (approximately 0.1 to 0.15 chord length). Due to

the current limitations of the state-of-the-art concerning rotor vortex core structure, the detailed rotational induced effect for points within the core and changes in core radius consistent with distortions of the lengths of the elements were neglected. Removal of these assumptions can be easily accommodated when more data on the structure and induced influence of the vortex core for helicopter rotor applications become available. Finally, interference effects from sources external to the rotor blades such as the fuselage, hub, and wings were not included in the analysis for this isolated rotor study.

Numerical Procedure

The procedures followed in the numerical computations of the distorted tip vortex geometry are described below. The procedure involves two basic steps -- the use of the Biot-Savart law to compute the wake distortion velocities produced by a given wake geometry and the integration of these velocities over a small time increment (azimuth increment) to establish a new tip vortex geometry. These steps are successively repeated until a converged periodic wake geometry results.

The computation is initiated by specifying the wake geometry and circulation to be those corresponding to the classical undistorted wake solution. The three components of distorting velocities induced by each wake element at the end points of the trailing wake elements are then computed using Biot-Savart relationships (Ref. 4). The resulting changes in the coordinates of a given element are given by the following relations, which also include the effect of the flight velocity, V, the rotor disk attitude, α_{TPP}, and the blade tip speed, ΩR.

$$\Delta x = (V_{i_x} + V\cos\alpha_{TPP})\ \Delta t/R$$

$$\Delta y = V_{i_y}\ \Delta t/R$$

$$\Delta z = (V_{i_z} + V\sin\alpha_{TPP})\ \Delta t/R$$

$$\Delta t = R\Delta\psi/\Omega R$$

where all distances are nondimensionalized by the rotor radius, R.

The equations are based on the assumption that the tip vortex distortion velocities remain constant during the time step, Δt. Also, the length of any vortex element is allowed to vary as the wake distorts and the blades are

allowed to rotate to new positions. The rotation of the blades leads to the generation of new wake elements; however, for convenience and computer cost efficiency, the total number of wake elements retained in the computation is held fixed by discarding elements from the ends of the trailing filaments farthest from the blades. Once the new wake position has been established, the procedure is repeated and the process continues for a sufficient number of time steps to achieve convergence of the periodic distorted tip vortex geometry.

The development of efficient computation techniques and simplifying approximations to the basic technical approach has been emphasized at UTRC to provide a practical computer program for engineering applications. Without these simplifications, the cost of computing the distorted geometry of a typical rotor wake becomes prohibitive for routine applications -- even with the speed of current computers. This is especially true for computations involving inboard vortex filaments, large numbers of blades, large numbers of wake revolutions, and small azimuth increments.

The number of wake elements involved in the basic technical approach outlined above is essentially equal to the product of the number of blades, number of vortex filaments per blade, number of wake revolutions, and number of wake elements per revolution (which is fixed by the azimuth increment). It is therefore essential that simplifying assumptions and efficient computing techniques be used.

To reduce the computational complexity of the basic technical approach described above, an approximate method, described in Ref. 4, was developed based on the rapid reduction of the velocity induced by a wake element with increasing distance from the element. During the development of this analysis, it was initially considered that elimination of interactions between wake elements spaced greater than a specified distance apart might be a reasonable simplification to the analysis. However, it was reasoned that although the individual contribution of any one wake element to the induced velocity at a point in the wake might be insignificant, the elements of a rotor wake system could be oriented in such a way that the integrated effect of a group of such elements could be significant. As a result, the following approximate approach was developed. The wake surrounding each tip vortex element end point was divided into a near and far wake region. The grouping of elements into near and far wake regions is determined by specifying a limiting value on the distortion velocity induced by a single wake element. If the element's induced velocity is greater than the limit value, it is classified as a near wake element. Thus, the near wake region contains the elements which individually contribute significantly to the distortion velocity at a wake point under consideration. The induced effect of each of these near wake elements is therefore recalculated for each time step in the

distortion iteration. In contrast, the distortion velocities at the wake point induced by the far wake elements are only computed once -- for the initial time step. The summation of these individual distortion velocities represents the integrated induced effect of the far wake region on the element end point under consideration and is maintained constant for succeeding time steps. In effect, this assumes that the distortion velocities induced by the elements in the far wake region can be based on the initial undistorted wake model. The neglect of the distortions of the far wake elements when computing their induced effects at a given wake point is reasonable because the induced velocity is insensitive to small changes in the position of a point relative to the vortex when the point and the vortex are widely separated. The retention of the far wake effect by the approximate method described above results in a satisfactory compromise between accuracy and computer cost requirements.

The Generalized Rotor Performance Analysis

The Sikorsky Generalized Rotor Performance (GRP) Analysis, a method for predicting rotor performance, is described in Ref. 24, and has been refined and improved since its inception. The analysis is a rigid, articulated blade response analysis that is a significant refinement of the classical Wheatley-Bailey blade element method (Ref. 25) for rotor performance predictions. The method used in the analysis represents a numerical stepwise (in the direction of rotation) solution in the equations of motion of rigid blades. Tabulated airfoil data are used. Details of the numerical procedure are available in the above references. The latest version of this analysis can be coupled with the UTRC Prescribed Wake Inflow Analysis to obtain compatible inflow and rotor performance predictions.

The Normal Modes Rotor Aeroelastic Analysis

To calculate the flexible blade response and bending moments for this investigation, a version of the Sikorsky Normal Modes Rotor Aeroelastic Analysis (Y200) was used (Refs. 26 to 29). The version chosen for this investigation was the Y200 program version which had been transmitted to the government by Sikorsky Aircraft for use in the Aerodynamically Comformable Rotor Research Program, Refs. 28 and 29. A brief discussion of the analysis is presented below. A detailed description of the equations of motion used is given in Ref. 26.

The computer analysis constitutes a numerical method for solving the differential equations governing the fully coupled flapwise, edgewise, and torsional response of flexible rotor blades. A normal mode approach combined

with a finite difference, step-by-step integration of the equations is employed. The former is widely used throughout the aircraft industry and assumes that the deflections of the rotor blade can be represented by summations of the blade's natural vibratory modes. Although an elastic body has an infinite number of such modes, the normal mode approach owes its success to the fact that only a relatively small number of modes is generally required to adequately approximate the elastic deformations of interest. The use of normal modes also results in certain simplifications of the equations of motion (such as elimination of certain dynamic coupling terms) thereby facilitating the solution of the equations through numerical integration techniques on a digital computer.

The version of the analysis selected for this investigation has the following capabilities (recent versions have increased capabilities):

1. The program includes the effects of up to 4 flapwise, 3 chordwise, and 2 torsional elastic modes as well as the flapping and lagging rigid body modes for an articulated rotor.

2. The chordwise and torsion modes can be suppressed to permit applications for which only the influence of the uncoupled flapwise modes are of interest.

3. The computer program can be applied equally well to blades having many types of root-end boundary conditions by simply providing as input the appropriate mode shapes and natural frequencies. Any degree of hinge restraint from fully articulated (with flapping hinge offset) to rigid in either the flapwise or chordwise direction can be studied and both lag hinge damping and control system flexibility can be included.

4. The elastic deflections of the rotor blade and the aerodynamic forces generated by it are fully coupled. Aerodynamic forces in the blade equations can be considered to be composed of (1) components independent of blade motion (forcing functions), (2) components dependent on blade deflections (spring forces), and (3) components dependent on the rate of change of blade deflections (damping forces). Analyses which do not couple blade deflections and blade loads, therefore, consider only the first of these three components. At high forward speeds the contributions of the coupled aerodynamic loads become increasingly important.

5. The computer program can be used to compute time histories of blade motion even when such motion is unstable. Such conditions of instability or near-instability can exist at high advance ratio flight conditions where either retreating blade torsional divergence or blade flapping instability imposes a limit on maximum speed.

6. Dynamic coupling between the flapwise, chordwise, and torsional degrees of freedom have been included.

7. Airfoil lift, drag, and pitching moment data at angles of attack from 0 to 360 deg and at Mach numbers from 0 to 0.9 are employed.

8. High frequency blade response in the primary modes can be predicted. This can be particularly important at high forward speeds and low rotor speeds when the entire blade enters the reversed flow regime.

SELECTION OF ANALYTICAL PARAMETERS AND PROCEDURES

Numerical Prediction Procedures

In this investigation the analyses were used to predict rotor wake geometry, inflow, airloads, performance, blade response, and bending moments. It is therefore necessary to explain the calculation procedure that was used to predict this information. Details of the individual analyses used in the procedure have been outlined in the preceding section. The procedure used to calculate this information using combinations of these analyses is explained below.

The procedure consisted of running the separate analyses in a sequential and iterative manner to provide compatible solutions. A flow chart of this procedure is shown in Fig. 9. In this chart, either the Generalized Rotor Performance Analysis (GRP) or the aeroelastic analysis (Y200) is indicated as the blade airloads and response program to provide rotor controls and blade motion information for the variable inflow analysis. The airloads program was first run with a uniform inflow model using a parabolic tip loss factor to provide initial input as noted above for the inflow analysis. The inflow analysis was then run with the desired wake model (classical or distorted) to calculate the induced inflow and blade circulation distribution. The airloads program was then rerun using the variable induced inflow as input to calculate new rotor controls and blade response. This procedure was repeated until the resulting inflow solution and rotor controls and blade response were compatible. To obtain the distorted wake geometry, the circulation distributions were first used from the classical wake solution as input to the wake analysis and the resulting wake geometry was calculated. This wake geometry was used as input to the inflow analysis to obtain the distorted wake circulations and induced inflow, and the iterative procedure noted above was used to obtain the resulting rotor performance and blade response solution compatible with the distorted wake inflow. This procedure could have been repeated by using the distorted wake circulation distributions as input to the wake analysis to recompute a new wake geometry and the complete cycle repeated, however past experience has shown that it is generally not required for high flight speed conditions and can result in numerical convergence problems for flight conditions with close blade-vortex encounters using existing blade-vortex interaction models.

Input Parameter Selection for the Wake Geometry Analysis

The UTRC Wake Geometry Analysis can be run with several input options which can affect the speed of computation and numerical accuracy of the results for a given condition. These are: (1) the number of wake revolutions, (2) the blade azimuth increment, (3) the number of blade stations, (4) the number of time step intervals, and (5) the tolerance for selecting near and far wake regions for the computations of the self-induced velocity field (wake distortion velocities).

Because of the significant cost of running the Wake Geometry Analysis and the large number of computer cases required for this study, the need was recognized for determination of the appropriate combination of these parameters considering cost effectiveness, numerical convergence, and accuracy. The number of blade stations is basically determined by the solution resolution required in the rotor inflow calculation program, so this input was kept consistent with the requirements of that program. Nine (9) stations were used for this investigation. Knowledge of the number of wake revolutions required for a given flight condition had been gained from previous experience with the analysis. The number of wake revolutions used in this investigation varied from 5.5 to 7. Initial runs were made with the distorted wake analysis for different blade azimuth increments, number of time steps, and far field tolerance criteria. From these runs it was determined that a blade azimuth increment of 15 degrees would be used for both two- and four-bladed rotors. Thus, throughout these investigations, 15 degrees was used as the blade azimuth increment for computing the tip vortex distortions. The use of one value (15 deg) for all cases also allowed for the generation of a consistent number of wake geometry data points for each condition for the wake generalization portion of the investigation. The number of time steps (incremented blade azimuth positions) required for distorted tip vortex geometry convergence is dependent on the number of blades used, with the four-bladed cases requiring more. The values used, which were determined to give reasonable convergence, were 48 and 72 time steps for the two- and four-bladed configurations respectively. The study of the induced velocity tolerance to determine near and far wake regions for each wake point led to the final value of 0.5 feet per second as a reasonable value for this rotor. Smaller values made the computation time per time step too large without gaining significant increases in numerical convergence and speed of convergence, and larger values did not give reasonable convergence or convergence rates although the computation time per time step is reduced. It should be noted here that the question of convergence is an engineering judgment question, since the solution obtained with an analysis using a finite length wake may never completely converge. Also, it may be cost prohibitive to run the analysis until far wake convergence is obtained. Emphasis was placed on convergence of the wake geometry near the rotor.

Selection of a Representative Rotor

To provide a baseline rotor design to investigate rotor wake effects on the airloads and performance of helicopter rotors in forward flight, and to develop a large data base of distorted wake geometries for the first level forward flight wake generalization, a physical description of a representative rotor system was required. In order to select a rotor blade design which is representative of existing rotor systems, the physical characteristics of nine helicopter rotors were obtained and tabulated in Table I. Four two-bladed rotors and five four-bladed rotors were selected to establish a representative rotor. This information was primarily provided from data furnished by the government for this contract activity. The selection of these nine rotors was based on the desire to include existing military aircraft and newer generation aircraft currently entering the market place. Only two- and four-bladed systems were considered for the definition of a representative rotor because the wake generalization process was planned as a limited first level effort which could be expanded at a future date. Included in the table are the rotor tip speed and aircraft gross weight used to establish representative values of thrust coefficient. With this information, the characteristic parameters of a representative rotor were selected, and are included in Table I. The representative rotor is a two- and four-bladed rotor with rotor radius and constant chord chosen to provide rotor solidity and aspect ratio values which are inclusive of both the two- and four-bladed rotor configurations presented in Table I.

The values presented in Table I are the baseline values for the representative rotor. Variations of these parameters in the course of the study were made about these basline values. In particular, thrust level variations of about 15 to 20 percent were made, resulting in thrust coefficient ranges of 0.0026 to 0.0039 for the two-bladed configuration and 0.0052 to 0.0077 for the four-bladed configuration. For the solidities chosen, the upper thrust coefficient bounds are close but below stall for the NACA 0012 airfoil. The selection of flight speed conditions are not shown in Table I; however, the selection of speeds was made to define a reasonable operating range for the rotorcraft. The low to moderate flight speed range was selected to investigate conditions where wake effects are most significant under normal study flight conditions. The advance ratio range selected was 0.05 to 0.3, and the range of rotor tip path plane angles was 0.0 to -6.0 degrees consistent with typical flight attitudes. Limited variations in blade linear twist and aspect ratio were also made over a range of -6 to -14 degrees and 11 to 16, respectively.

TABLE I. CHARACTERISTIC PARAMETERS OF SEVERAL ROTORS AND THE REPRESENTATIVE ROTOR

AIRCRAFT	AH-1G	UH-1D	HU-1A	OH-58A	OH-6A	BO-105	H-34	S-76	UH-60 BLACK HAWK	REPRESENTATIVE ROTOR
BLADE NO	2	2	2	2	4	4	4	4	4	2 OR 4
RADIUS (FT)	22	24	21.875	17.67	13.17	16.11	28	22	26.83	22.0
CHORD (FT)	2.25	1.75	1.267	1.0833	.5625	.8867	1.366	1.304	1.73	1.3823
TWIST (DEG)	-10	-10.89	-12.0	-10.0	-7.97	-8.0	-8.0	-10.0	-16.0	-10.0
LIFT OR GROSS WEIGHT	9500			3250	2700	5953	10500	9700	16000	5700 11400
BLADE THICKNESS (% CHORD)	9.37	12	9	11.3	15	12	12	9.5	9.5	12.0
ASPECT RATIO	9.8	13.7	17.27	16.31	23.41	18.2	20.5	16.9	15.5	15.9
SOLIDITY, σ	.0646	.0464	.0369	.0390	.0544	.0701	.0621	.0751	.0888	.04 .08
LOCK NUMBER	5.33	2.97	4.76			5.26	10.49	12.04	10.66	10
PRECONE (DEG)	2.75	4.00	3.00	2.25	0.0	2.5	0.0	0.0	0.0	0.0
CW* (X10-3)	4.72			3.25	4.70	5.97	4.28	5.89	5.67	3.22 6.44
CW/σ* (X10-2)	7.31			8.33	8.64	8.52	6.90	7.84	6.38	8.05
AIRFOIL TYPE	BELL 540	NACA 0012	NACA 0009	NACA 0012	NACA 0012	23012	NACA 0012	SIKORSKY SC1095	SIKORSKY SC1095	NACA 0012
TIP SPEED (FPS)	746	800	714.7	655	666	717	647	675	724.4	700
ROTOR TYPE	TEETER	TEETER	TEETER	HINGE-LESS	ARTICU-LATED	HINGE-LESS	ARTICU-LATED	ARTICU-LATED	ARTICU-LATED	ARTICULATED ZERO FLAPPING

* CW = GROSS WEIGHT $/\rho\pi R^2(\Omega R)^2$ AT STANDARD DAY, SEA LEVEL

NOTE: THIS SHOULD NOT BE CONSIDERED CURRENT OR OFFICIALLY ACCURATE DATA OF THE MANUFACTURERS. MOST OF THE DATA WAS FURNISHED BY THE GOVERNMENT AT THE INITIATION OF THE CONTRACT. SOME VALUES ARE APPROXIMATIONS AND SOME VALUES HAVE BECOME OBSOLETE. THE PURPOSE OF THE DATA COMPILATION WAS SPECIFICALLY FOR SELECTION OF THE REPRESENTATIVE ROTOR.

The rotors presented in Table I are representative of the current configurations in the rotorcraft industry. One of the basic differences between several of the rotors presented in Table I is the Lock number, the ratio of air forces to mass forces. Since the intent of this investigation was to study the wake deformations and their effect on airloads and performance, the selection of a representative rotor for the study required a Lock number which was representative of the rotors in use today. Due to the large differences between the Lock numbers of the rotors in Table I, a small sensitivity study was performed to establish the effects of varying the Lock number on performance for the representative rotor. The representative rotor presented in Table I was run for two different Lock numbers (4 and 10) at an advance ratio of 0.2 for a two-bladed configuration with a uniform inflow model, classical wake inflow model and a distorted wake inflow model. Since the analysis used for the performance predictions was run trimmed for zero flapping, the effect of Lock number on performance should be small. This was found to be the case and the results are presented in Table II. As anticipated, the only significant differences occur in the blade coning angle and blade cyclic controls required for zero flapping trim. From this study and the data of Table I it was determined that a Lock number of 10 would be representative and not significantly influence the performance results.

Selection of Trim Procedure

A preliminary activity was performed to determine the relationship between the performance predictions for an articulated rotor with various flapping responses at the same tip-path plane trim attitude. This study was necessary because it was anticipated that rotor tip-path plane attitude would be a primary parameter in the wake generalization procedure.

The Sikorsky Generalized Rotor Performance Analysis (GRP) was used for this initial activity using a uniform inflow model. Variations in shaft angle, flapping with respect to the shaft and flapping hinge offset were investigated for one flight condition of a UH-1D rotor. The tip-path plane attitude was maintained constant using different rotor shaft attitudes and flapping response. From this study it was confirmed that the use of (GRP) for an articulated rotor with zero flapping gave performance results similar to an articulated rotor with non-zero flapping where the appropriate adjustments to blade cyclic controls were made to run at the same rotor disk trim attitude. Thus, an articulated rotor trimmed for zero flapping was used for the course of this first level investigation. It is recognized, however, that nonlinear effects occur at low speed (e.g., $\mu = 0.05$) with nonuniform inflow (Ref. 32). Table III is a summary of the results of this brief trim study.

TABLE II. PERFORMANCE RESULTS FOR THE LOCK NUMBER VARIATION OF THE TWO BLADED REPRESENTATIVE ROTOR AT ONE FLIGHT CONDITION (μ = .2, CT = .0032, α_{TPP} = -3°) TRIMMED FOR ZERO FLAPPING WITH RESPECT TO SHAFT

LOCK NUMBER γ	INFLOW MODEL	TOTAL POWER (HP)	PROFILE POWER (HP)	INDUCED POWER (HP)	CONING (DEG)	COLLECTIVE PITCH θ_{75} (DEG)	CYCLIC PITCH	
							LATERAL A_{1S} (DEG)	LONGITUDINAL B_{1S} (DEG)
4	UNIFORM	247.2	121.2	57.6	1.775	6.54	-0.48	3.17
4	CLASSICAL WAKE	267.6	116.6	80.6	1.798	6.51	-1.00	3.19
4	DISTORTED WAKE	264.9	117.5	76.9	1.799	6.48	-1.01	3.17
10	UNIFORM	247.9	121.5	57.9	4.649	6.62	-1.27	3.27
10	CLASSICAL WAKE	265.0	118.1	76.5	4.729	6.57	-1.70	3.30
10	DISTORTED WAKE	259.8	118.3	71.7	4.790	6.51	-1.72	3.24

TABLE III. BLADE FLAPPING SENSITIVITY STUDY RESULTS FOR THE UH-1D ROTOR AT ONE FLIGHT CONDITION (GW = 10,000, μ = .19, α_{TPP} = -8.9°)

CASE NUMBER	SHAFT ANGLE α_S (DEG)	LONGITUDAL FLAPPING a_{1S} (DEG)	LATERAL FLAPPING b_{1S} (DEG)	CONING α_0 (DEG)	COLLECTIVE PITCH θ_{75} (DEG)	LATERAL CYCLIC A_{1S} (DEG)	LONGITUDAL CYCLIC B_{1S} (DEG)	TOTAL POWER (HP)	PROFILE POWER (HP)	INDUCED POWER (HP)
1	-17.9	8.9	0.0	3.1	8.6	-.9	-5.1	928.	352.	549.
2	0.0	-8.9	0.0	3.1	8.6	-.7	12.7	912.	351.	537.
3	-8.9	-.004	0.0	3.1	8.6	-.8	3.8	912.	350.	537.
4	-8.9	.0087	-5.0	3.1	8.6	-5.8	3.8	915.	350.	542.
5	-8.9	-.0035	5.0	3.1	8.6	4.2	3.8	911.	352.	533.

(A) e/R = 0

CASE NUMBER	SHAFT ANGLE α_S (DEG)	LONGITUDAL FLAPPING a_{1S} (DEG)	LATERAL FLAPPING b_{1S} (DEG)	CONING α_0 (DEG)	COLLECTIVE PITCH θ_{75} (DEG)	LATERAL CYCLIC A_{1S} (DEG)	LONGITUDAL CYCLIC B_{1S} (DEG)	TOTAL POWER (HP)	PROFILE POWER (HP)	INDUCED POWER (HP)
6	-17.9	8.9	0.0	2.7	8.7	.2	-4.6	922.	352.	543.
7	0.0	-8.9	0.0	2.7	8.6	-1.6	12.1	922.	365.	532.
8	-8.9	0.0	0.0	2.6	8.6	-.7	3.8	909.	348.	535.
9	-8.9	0.0	-5.0	2.7	8.4	-5.3	3.2	894.	337.	526.
10	-8.9	0.0	5.0	2.7	8.8	3.9	4.4	944.	376.	549.

(B) e/R = .05

Selection of Wake Geometry Parameters

The major parameters to consider for rotor wake geometry are listed in Table IV. The identification of primary parameters which affect the wake distortions was both a preliminary activity and an ongoing one during the course of the investigation. This was because the determination of the parameters which were significant in terms of forward flight wake distortions was an objective of this project. Initial activities consisted of the selection of several parameters to concentrate on in the investigation. The parameters considered were: thrust coefficient (C_T); rotor advance ratio (μ); blade number (b); rotor tip path plane angle (α_{TPP}); blade twist (θ_1); and blade aspect ratio (AR).

It should be noted that for this investigation, rotor disk attitude, α_{TPP}, was considered as an independent parameter. To eliminate the functionality of disk attitude in rotor advance ratio, μ, the advance ratio is defined as:

$$\mu = \frac{V}{\Omega R} \cos\alpha_{TPP} \simeq \frac{V}{\Omega R}$$

This effectively assumes a small angle for disk attitude. Angles less than 10 degrees are typical of level flight for the low to moderate airspeeds, at which wake effects are important.

In the Ref. 5 investigation, a brief study for a single flight condition was conducted to indicate the sensitivity of wake geometry to several of the parameters. Primary wake parameters and potential wake generalization techniques were identified on a preliminary basis. Specifically, wake sensitivity in terms of thrust level, blade flexibility, rotor disk attitude, blade cyclic pitch, and viscous and compressibility effects on the airfoil characteristics were investigated. From this study and other results reported in Ref. 5, the following primary wake parameters were identified: rotor advance ratio, thrust level, tip-path plane angle and blade number.

To provide a first level wake generalization, the parameters selected for emphasis in this investigation were C_T, μ, α_{TPP}, and the number of blades. By selecting a representative rotor for the wake generalization, typical values of blade design parameters were used. The sensitivity of tip distortions to two of the blade design parameters, blade linear twist and aspect ratio, was investigated, but these parameters were not included independently as generalized wake parameters. It was decided to limit the investigation to two- and four-bladed rotors since these are the more common current configurations.

TABLE IV. WAKE GEOMETRY PARAMETERS

FUNDAMENTAL PARAMETERS (UNDISTORTED WAKE PARAMETERS)

NUMBER OF BLADES, b
ADVANCE RATIO, μ
THRUST COEFFICIENT, C_T
ROTOR DISK ATTITUDE, α_{TPP}

AZIMUTH PARAMETERS

BLADE AZIMUTH, ψ_b
WAKE AGE, ψ_w

TRIM PARAMETERS

CYCLIC PITCH, A_{1S}, B_{1S}
FLAPPING, a_{1S}, b_{1S}
→ ROTOR TRIM FORCES AND MOMENTS

BLADE DESIGN PARAMETERS

BLADE LINEAR TWIST, θ_1
BLADE TAPER RATIO, TR^1
BLADE ASPECT RATIO, AR
AIRFOIL SECTION
TIP DESIGN (SWEEP, ANHEDRAL, NON-LINEAR TWIST, ETC.)

The first computational efforts were directed mainly at the two-bladed configuration to keep computational costs down until a preliminary understanding of the relationships between the parameters under study and the wake distortions were obtained. The range of thrust coefficient (C_T) to be considered was determined by choosing blade loading conditions (C_T/σ) which would not involve stalled operation of the rotor blades and would represent realistic variations in this parameter. Nominal values of blade loading chosen were .06, .08 and .1, with .08 chosen as a baseline condition. The range in advance ratio chosen for this investigation was between .05 and .3. This was due in part to the confirmation during the course of the investigation that the distortions of the tip vortices become smaller and the number of close blade-vortex interactions decrease with increasing advance ratio. However, it is recognized that the effects of the wake distortions at high advance ratio may be important for some conditions even though the wake distortions are small. Limiting the advance ratio range also avoided retreating blade stall conditions which were considered beyond the scope of this initial investigation. Selecting conditions at an advance ratio as low as .05 allowed trending of the wake geometry distortions with advance ratio by comparison with known tip vortex distortions in hover.

The selection of rotor attitudes was based on test data available for two- and four-bladed geometries. The rotor attitude for a given aircraft with a specific center of gravity changes with rotor advance ratio and thrust level. To determine representative tip path plane attitudes associated with current helicopters, the following study was conducted.

From simple balance of force relationships for a single rotor helicopter in forward flight, with no hinge offset, no trimming horizontal stabilizer, and assuming small angles, it can be shown that the rotor tip path angle is

$$\alpha_{TPP} = -\frac{D}{GW}$$

where D is the drag on the fuselage, assumed to act through the center of gravity and GW is the gross weight of the helicopter. For any particular aircraft operating at a fixed flight speed with a fixed center of gravity, this relationship implies that,

$$\alpha_{TPP} C_T = \text{constant} \propto \mu^2$$

for small angles; and thus, for a given gross weight the aircraft must operate at a fixed rotor tip-path plane attitude. To check the validity of this relationship, data were gathered from several sources for various aircraft. Some of the data came from flight test data and some from analytical predictions. Figure 12 presents the data of this study in the form of a plot of $C_T\alpha_{TPP}$ versus flight speed. From this figure it can be seen that for each selected aircraft, the data could be represented by a smooth single valued curve which is a function of flight speed. For similar aircraft (similar gross weight) the curves are similar. Also the effect of center of gravity on the data presented in this manner appears to be small. Normal operating ranges of the rotor tip-path plane attitude with advance ratio were determined for the representative thrust levels from the test data available. From this information, values for the rotor tip-path plane were chosen which were compatible with the rotor configuration (two or four bladed) and the operating conditions.

Selection of Representative Rotor Conditions

The approach taken in this investigation to acquire theoretical information for wake generalization was to build a data base of performance predictions and distorted wake geometries for representative rotor flight conditions in a sequential manner, whereby each case was run and the results analyzed before the next case was run. This technique allowed the generation of a data base of information which was constructed in a logical and consistent manner, where the selection of the following case could be influenced by the most current results of the previous cases as they became available. Table V is a listing of the representative rotor cases studied under the current investigation.

TABLE V. REPRESENTATIVE ROTOR CONDITIONS

CASE NUMBER	b	μ	α_{TPP}	CT	σ	CT/σ	θ_1	
1	2	.05	0	.0032	.04	.08	-10.0	*
2	2	.05	-3	.0032	.04	.08	-10.0	
3	2	.1	0	.0032	.04	.08	-10.0	
4	2	.1	-3	.0026	.04	.064	-10.0	*
5	2	.1	-3	.0032	.04	.08	-6.0	
6	2	.1	-3	.0032	.04	.08	-10.0	*
7	2	.1	-3	.0032	.04	.08	-14.0	
8	2	.1	-3	.0039	.04	.096	-10.0	*
9	2	.1	-3	.0039	.04	.096	-14.0	
10	2	.1	-3	.0039	.06	.065	-10.0	
11	2	.1	-6	.0032	.04	.08	-10.0	
12	2	.1	-6	.0039	.04	.096	-10.0	
13	2	.2	-3	.0032	.04	.08	-10.0	
14	2	.2	-6	.0032	.04	.08	-10.0	*
15	2	.2	-6	.0032	.04	.08	-14.0	
16	2	.3	-6	.0032	.04	.08	-10.0	*
17	4	.05	-0.5	.0064	.08	.08	-10.0	*
18	4	.05	-3	.0032	.08	.04	-10.0	
19	4	.1	-1	.0052	.08	.065	-10.0	*
20	4	.1	-1	.0064	.08	.08	-10.0	*
21	4	.1	-1	.0077	.08	.096	-10.0	*
22	4	.1	-3	.0032	.08	.04	-10.0	
23	4	.2	-2.25	.0064	.08	.08	-10.0	*
24	4	.3	-4	.0064	.08	.08	-10.0	*

* USED FOR TIP VORTEX GENERALIZATION MODULE COEFFICIENTS

GENERALIZED WAKE GEOMETRY

The simplest generalization of forward flight wake geometry is the classical undistorted wake model. This is described first, for it forms the base for the newly developed generalized wake geometry model in which the tip vortex distortions relative to the undistorted tip vortex coordinates have been generalized.

Classical Undistorted Wake Model

Most forward flight variable inflow methods that are currently used in the helicopter industry assume that the rotor wake geometry is undistorted and defined from momentum considerations. The forward flight wake is modeled by undistorted skewed helical vortex filaments. An example of what will hereafter be referred to as the classical undistorted wake model was presented in Fig. 1. The equations for the undistorted wake coordinates of a point on a tip vortex filament are presented in Table VI.

A diagram of the rotor-wake coordinate system is presented in Fig. 10. The origin of the coordinate system is defined as the center of the rotor disk in the tip-path plane. The coordinate axes are oriented with respect to the tip-path plane. The azimuthal wake coordinate, ψ_w (or ψ_{age}), hereafter referred to as "wage age" or "vortex age", is the age of a point on a vortex filament measured in terms of the blade rotation angle. That is, it is equivalent to the blade azimuth travel relative to the blade azimuth at which the wake point was shed by the blade. ψ_w can exceed 360 degrees (2π). For example, ψ_w is 720 degrees for a wake point that is two wake revolutions from the blade that generated it. It is noted that a wake age parameter, ψ_w, was used for the hovering rotor wake generalization in Refs. 9 and 10. Considering a vortex filament model of the wake, such as that shown in Fig. 10, the wake point is a point on a specified vortex filament. For this study, in which the focus is on tip vortex geometry, the wake points will refer to a point on the tip vortex filament. For the distorted wake model, the tip vortex filament represents a rolled up tip vortex in which the vorticity, shed from the outer portion of the blade, is concentrated in the core of a single vortex filament.

The coordinates of the undistorted wake representation are obtained from the rotor advance ratio, μ, thrust coefficient, C_T, and angle of the tip-path plane, α_{TPP}. For example, the top view of the tip vortex filaments is obtained directly from the helicoidal path of the blade tip as it translates at the velocity $V\cos\alpha_{TPP}$ and rotates at the velocity ΩR. These two velocity

TABLE VI. CLASSICAL UNDISTORTED WAKE GEOMETRY EQUATIONS

UNDISTORTED LONGITUDINAL COORDINATE

$$x/R = \cos(\psi_w - \psi_b) + \mu\,\psi_w$$

UNDISTORTED LATERAL COORDINATE

$$y/R = -\sin(\psi_w - \psi_b)$$

UNDISTORTED AXIAL COORDINATE

$$z/R = -\mu\psi_w \tan\chi_{TPP}$$
$$= \lambda\psi_w$$

WAKE DEFLECTION ANGLE

$$\chi_{TPP} = \tan^{-1}\left(-\frac{\lambda}{\mu}\right)$$

MOMENTUM INFLOW ANGLE

$$\lambda = (V\sin\alpha_{TPP} - v_{i_{MOM}})/\Omega R$$
$$= \mu'\sin\alpha_{TPP} - v_{i_{MOM}}/\Omega R$$

MOMENTUM INDUCED VELOCITY

$$v_{i_{MOM}} = \frac{\Omega R\, C_T}{2\sqrt{\mu^2+\lambda^2}}$$
$$\simeq \Omega R\, C_T/2\mu \quad \text{for} \quad \mu > 0.15$$

components are contained in the advance ratio, μ. The side view of the classical undistorted wake is defined by the wake deflection angle, χ_{TPP}, which determines the skewed linear path of each wake point, and thus also the wake boundaries. The wake deflection angle, χ_{TPP}, is a function of advance ratio and inflow ratio. Inflow ratio is dependent on the momentum value of induced velocity normal to the rotor disk.

Formulation of the Generalized Wake Model

A primary task of this study was to investigate forward flight wake geometry to gain insight into the behavior of wake distortions with variations in selected parameters. The objective was to develop a first level generalized wake model which could form the basis for future refinement, expansion, and validation. In this report section, the wake distortion characteristics are demonstrated along with the relationship of the distortions to rotor design and flight parameters. Tip vortex distortions are modeled mathematically and the distorted wake coefficients of the wake model are generalized as a function of the identified wake definition parameters. This results in the development of a first level generalized wake model which is coded to provide a computer module for use in conjunction with other computer codes requiring rotor wake coordinates. An important feature of the generalized wake module is that its use requires insignificant computer time.

Initial activity toward formulating the mathematical relationship required to model the distorted wake geometry consisted of studying available wake geometry predictions and experimental data. Predicted wake geometries and flow visualization techniques applied in model rotor tests conducted in a water tunnel (Ref. 20) and a wind tunnel (Ref. 6) have shown that forward flight wake geometry is significantly distorted from the classical (undistorted) geometry. In Fig. 5, reproduced from Ref. 6, 15 kt and 30 kt distorted tip vortex geometries, predicted at UTRC for a rocket interference investigation, are compared with the hovering and undistorted 15 kt tip vortex geometries. Key features of the predicted tip vortex distortions were confirmed by smoke visualization and laser velocimeter measurements. The predicted tip vortex geometry from Ref. 5 for a UH-1D rotor at 89 kt is compared with the undistorted geometry in Fig. 6 further illustrating the features of the wake distortions. Photographs from Ref. 20 of the tip vortices from a two-bladed model rotor at two simulated flight speeds, 35 and 90 kts, were reduced to coordinate form and compared to coordinates obtained by applying the UTRC Wake Geometry Analysis to predict the distorted wake geometry. These comparisons are reported in Ref. 5, and although the test data is limited, the key features of the wake geometry appear to be well predicted.

Figures 13 and 14 illustrate the comparisons of the experimental axial tip vortex coordinates with the distorted wake predictions for the two advance ratios, 0.074 and 0.19, corresponding to 35 and 90 kts, respectively. These comparisons show that the analysis predicted the tip vortex distortion amplitudes and distribution with wake age, ψ_w, reasonably well. However, it will be shown later in this report that the remaining differences can be significant for rotor airload applications.

At this point, it is necessary to define the coordinates for wake distortions as used in this report. The axial wake coordinate, z, is the coordinate of a point on a vortex filament representing the distance from the rotor tip-path plane. The lateral and longitudinal wake coordinate axes, x and y, are in the tip-path plane (Fig. 10). Distortion is defined as the change in a wake coordinate from the classical undistorted wake definition of that coordinate. In particular, the axial distortion (Δz) of a point on the tip vortex is

$$\Delta z = z - \lambda\psi_w$$

where λ and ψ_w are the inflow ratio and wake age as defined earlier.

A graph of the axial coordinates of the tip vortex for varying wake azimuth position (wage age), such as presented in Figs. 13 and 14, displays the distance to the rotor disk of all the points on the distorted, skewed, helical tip vortex for several helical revolutions from its origin at the blade. The tip vortex coordinates are dependent on the particular blade azimuth selected, such as shown in Figs. 13 and 14 for the 0, 90, 180 and 270 degree blade azimuths. The axial coordinates of the undistorted tip vortex lie along a straight line in these figures with slope equivalent to the momentum inflow ratio, λ, as shown in Table VI. The axial distortion of a point on a tip vortex filament in these figures is simply the Δz displacement from the undistorted tip vortex line.

In the predicted and experimental wakes, exemplified in the figures presented, some common features of tip vortex geometry are consistently evident. Several of these characteristic distortion features are listed below:

1. Relative to the undistorted geometry, large tip vortex distortions occur in the axial direction. The distortions near the rotor are significantly smaller in the in-plane (longitudinal and lateral) directions.

2. The magnitude of the distortions generally decrease with increasing flight speed.

3. The forward portion of the rotor wake tends to be displaced toward the rotor, the aft portion is displaced downward, and the sides are displaced upward.

4. Portions of tip vortex filaments can be at or above the plane of the rotor. Upward tip vortex distortion increases with decreasing advance ratio, decreasing thrust coefficient, and decreasing rotor disk attitude (nose down tilt).

The first task in generalizing the tip vortex coordinates x, y, and z was to develop analytical expressions for each of these coordinates in terms of the blade azimuth position, ψ_b, and wake age, ψ_w. This was essentially the task of developing curve fit equations for these coordinates as functions of ψ_b and ψ_w. From these equations, the coordinates of any point on a tip vortex filament could be calculated from its wake age, ψ_w, and the azimuth position of the blade from which the tip vortex originated, ψ_b. In the equations, coefficients of terms containing these parameters would be dependent on the rotor design and flight condition parameters.

From the limited flow visualization data from the water tunnel, it was observed that the tip vortex distortions in the longitudinal and lateral directions, x and y, are generally small near the rotor compared to the axial distortions. This is shown in Fig. 15. Predicted wake geometries have shown agreement with this observation at advance ratios above approximately 0.1. It was thus decided to concentrate the activity for the first level wake generalization on the axial tip vortex distortions, and initially generalize the top view of the wake (longitudinal and lateral coordinates) by the undistorted wake coordinates as defined in Table VI. This generalizes the x and y coordinates in simple equations in terms of advance ratio and number of blades. An alternative generalization which considers the distortions of the lateral coordinate will be described later.

As can be seen in Figs. 13 and 14, the variation of the distorted axial tip vortex coordinate with wake age is blade azimuth dependent. Tracking each axial coordinate peak with blade azimuth, through one blade revolution, it can be seen that the peak follows a consistent pattern. The peak grows in amplitude at approximately a constant rate away from the blade that generated it. This behavior is better illustrated if the axial coordinate distributions for the various blade azimuth positions are superimposed on one another and phase adjustments are made for blade azimuth position. Figure 16 is a plot of such a superposition for the predicted wake geometries of Fig. 13. From this figure the behavior of the tip vortex geometry with rotor position is more clearly evident. Phasing the wake age by the azimuth angle of the blade that

generated the tip vortex, as in Fig. 16, aligns tip vortex points shed from the same blade azimuth. For example, the first set of vertically aligned negative peaks in Fig. 16, points A, were all shed from a blade when it was near the downstream position (ψ_{b_o} = 330°). In fact, the aligned positive peaks in Fig. 16, spaced nearly one-half revolution apart, generally represent those portions of the tip vortex that were shed when the blade was near the lateral azimuth locations (ψ_{b_o} = 90° and 270°), points B and C in Fig. 16. The aligned negatively directed peaks, also spaced by nearly one-half revolution, represent portions of the tip vortex that were shed when the blade was near the downstream and upstream locations (ψ_{b_o} = 0° and 180° respectively). However, the much lower peaks from the downstream location, point D, are distinguished from the upstream locations (E) which, although negatively directed, remain near the rotor disk. The above is consistent with the wake distortion observations noted earlier (up on sides, down in rear, near rotor disk in front). The phasing of the wake coordinates as in Fig. 16 effectively results in plotting them versus a phased wake age, $\psi_w - \psi_b$ which is designated, $\bar{\psi}_w$. This was found to be a useful parameter to generalize the shape of the plotted axial coordinate curve. It is noted that $\psi_w - \psi_b$ also appears in the undistorted wake equations in Table VI. $\bar{\psi}_w$ is shown in Fig. 10 to be the wake azimuth relative to the downstream directed x axis.

Recognition of these consistent wake features was an important step leading to a mathematical formulation for the tip vortex distortions. It was noted that the peaks in the distortions (relative to the undistorted wake line) in Fig. 16, and in similar plots for other conditions, grow smoothly in amplitude with wake age. Graphical analysis showed that the growth in amplitude resembled an exponential function.

Observation of the above mentioned wake features was instrumental in the selection of the fundamental mathematical relationships for the representation of the axial distortion coordinate. It was decided to introduce two functions, an amplitude scaling function, E, and a geometric shape function, G, which when multiplied together equal the tip vortex axial distortion, Δz. As will be discussed, E is acquired from an exponential curve fit of the variations of the distortion peaks with wake age, and thus represents an "envelope function". The fundamental mathematical relation for the nondimensional axial distortion is simply,

$$\Delta z/R = E \cdot G$$

where E = envelope function
G = shape function

and the axial coordinate relation is retained as,

$$z/R = \lambda \psi_w + \Delta z/R$$

The intent of the envelope function is to generalize the amplitude of the distortions with wake age, and the intent of the shape function is to generalize the characteristic azimuthal distribution of the distortions with wake age.

An analytical study was performed in which several mathematical expressions for the envelope function and the shape function were postulated and evaluated to develop accurate curve fit relations for the tip vortex axial distortion. The study was based on distorted wake predictions for several actual and representative rotors and operating conditions. The study resulted in the generalized wake equations listed on the following page in Table VII. These equations with defined coefficients make available a procedure for mathematically describing and calculating the tip vortex axial distortions at all combinations of blade azimuth and wake age for selected rotor designs and operating conditions. Sample plots of the axial tip vortex coordinate variation with wake age and the corresponding envelope function and shape function are presented in Fig. 17 for a sample rotor and operating condition.

The independent variable in the equation for the envelope function is the previously defined wake age, ψ_w. The independent variable in the equation for the shape function is $\bar{\psi}_w$ which is defined as the difference between the wake age, ψ_w, of a point on the tip vortex and the azimuth position of the blade from which it was shed, ψ_b.

As indicated in Table VII, the envelope function is an exponential function of the wake age, ψ_w, for the first two tip vortex filament revolutions and a linear function of ψ_w thereafter. The shape function is in the form of a Fourier series with one set of harmonic coefficients for the first tip vortex revolution and a second set for the following revolutions. As indicated, the envelope and shape function coefficients are dependent on rotor design and operating condition parameters.

Generalization for the Blade Azimuth and Wake Age Parameters

Tip vortex geometry is both blade azimuth, ψ_b, and wake age, ψ_w, dependent. Primary objectives in the selection of the envelope and shape functions were to make the function coefficients independent of blade azimuth and wake age, and generalize the functions over multiple wake revolutions. Accuracy near the rotor was emphasized. It was recognized that the achievement of these objectives, while retaining acceptable accuracy, would greatly

VII. GENERALIZED TIP VORTEX AXIAL COORDINATE EQUATIONS

DISTORTED TIP VORTEX AXIAL COORDINATE

$$\underbrace{z/R}_{\substack{\text{Tip vortex axial coordinate /R} \\ \text{(Normal to tip path plane)}}} = \underbrace{\lambda\psi_w}_{\substack{\text{Classical undistorted z coordinate/R} \\ \text{(Based on momentum } \lambda\text{)}}} + \underbrace{\Delta z/R}_{\substack{\text{Tip vortex} \\ \text{axial distortion /R}}}$$

TIP VORTEX AXIAL DISTORTION

$$\Delta z/R = \underbrace{E}_{\text{Envelope Function}} \cdot \underbrace{G}_{\text{Shape Function}}$$

ENVELOPE FUNCTION

$$E = A_0\,\psi_w\, e^{A_1\psi_w} \qquad \text{for } \psi_w \le 4\pi$$

$$= M\psi_w + B \qquad \text{for } \psi_w > 4\pi$$

$$A_0, A_1, M, B = f(b, \mu', C_T) \text{ for rep. rotor}$$

SHAPE FUNCTION

$$G = \sum_{n=0}^{N} (g'_{nc} \cos n\,\bar{\psi}_w + g'_{ns} \sin n\,\bar{\psi}_w) \qquad \text{for } 0 \le \psi_w \le 2\pi$$

$$= \sum_{n=0}^{N} (g''_{nc} \cos n\,\bar{\psi}_w + g''_{ns} \sin n\,\bar{\psi}_w) \qquad \text{for } \psi_w > 2\pi$$

$$g'_{nc}, g'_{ns}, g''_{nc}, g''_{ns}, = f(b, \mu') \text{ for rep. rotor}$$

$$\bar{\psi}_w = \psi_w - \psi_b$$

simplify the generalization and result in a large reduction in the number of function coefficients. As evident in the generalized equations, these objectives were accomplished. Background and justification for the generalization of the blade azimuth and wake age parameters in the envelope and shape functions are presented below.

Envelope Function

Following the formulation and evaluation of several mathematical relationships for the envelope function, the equation in Table VII was selected as one that provided an acceptable scaling function for the amplitudes of the tip vortex distortions while satisfying the above objectives for blade azimuth and wake age generalization.

To emphasize accuracy near the rotor, an exponential function was formulated for the first two wake revolutions ($\psi_w \leq 4\pi$), and a separate linear function was formulated for the following wake revolutions ($\psi_w > 4\pi$). The independent variable in both expressions is wake age, and both expressions are blade azimuth independent. The coefficients A_0 and A_1 were obtained by a least squares fit through all of the positive axial distortion peaks in the first three wake revolutions from all blade azimuth positions, ψ_b. The positive peaks (e.g., see Fig. 16) were selected to increase the accuracy of the tip vortex geometry near the rotor. It was found that the negative peaks were still approximated with this formulation. The tip vortex regions at the negative peaks are sufficiently removed from the rotor disk so that the influence of small deviations do not generally have a significant effect on rotor blade inflow calculations. Exclusion of consideration of the negative peaks may somewhat compromise flow field velocity predictions in the immediate vicinity of the negative peak regions. The coefficient M for the second part of the envelope function was obtained by using a least squares fit through all of the positive axial distortion peaks in the second and third wake revolutions from all blade azimuth positions. The coefficient B was obtained by matching the second part of the envelope function, which is linear with slope M, to the first part at two wake revolutions ($\psi_w = 4\pi$). Least squares averaging of the envelope function coefficients over all blade azimuths eliminated blade azimuth as a variable when the envelope function is implemented.

Shape Function

Based upon the consistent character of the axial tip vortex coordinate variation with wake age when phase shifted by blade azimuth (Fig. 16), it was assumed that the envelope function could be blade azimuth independent, and the shape function would fully accommodate the blade azimuth dependence. Preliminary mathematical formulations for the generalization of the tip vortex distortions were explored for the two-bladed UH-1D, 35 and 90 kt conditions

using the predicted distorted tip vortex geometry as the reference. In Fig. 18, the axial tip vortex distortions for the 90 kt condition are plotted versus wake age for a blade azimuth position of 0.0 degrees. Division of the distortions by the envelope function value at each wake age results in the shape distribution shown in Fig. 18. It is noted that the indeterminate shape distribution value at the blade (at $\psi_w = 0°$) was set to the value at one wake revolution ($\psi_w = 360°$) to provide a periodic formulation for the geometric shape function. This is possible because the tip vortex distortion at zero wake age will be forced to a zero value at the blade when the shape distribution is multiplied by the envelope function. From Fig. 18, it is evident that the second revolution of the shape distribution is similar to the first. Figure 19 is a comparison of the shape distributions for various blade azimuth positions. From this figure, the similarities in the character of the curves for different blade azimuths is illustrated. When these curves are phased for blade azimuth position and superimposed, the similarity is more clearly demonstrated, as shown in Fig. 20. This shape distribution phasing, accomplished by shifting the wake age variation by the blade azimuth value, is similar to the phasing of the axial tip vortex coordinates shown in Fig. 16. The insight gained from Fig. 20, along with similar results for other rotors and conditions, led to the inclusion of the phasing of the wake age by the blade azimuth position in the shape function equation in Table VII. This resulted in combining the wake age, ψ_w, and blade azimuth, ψ_b, into a single independent parameter for the shape function, $\bar{\psi}_w = \psi_w - \psi_b$.

In order to emphasize the accuracy of the wake generalization in the vicinity of the rotor, the coefficients, g, of the Fourier series for the shape function in Table VII, are separately acquired for the first and following wake revolutions. For each revolution the harmonic coefficients obtained at each blade azimuth position are averaged. The averaging eliminates the blade azimuth dependency when the coefficients are implemented. Separate sets of shape function coefficients are noted in Table VII where g' indicates those for the first wake revolution and g" indicates those applicable to all revolutions beyond the first. The shape function coefficients acquired from second wake revolution information are assumed to be applicable to the second and all subsequent revolutions. Twelve harmonics, N, were used to determine the shape function coefficients currently stored in the computer module for the generalized wake geometry.

Assessment of Generalization for the Blade Azimuth and Wake Age Parameters

Reconstructions of the axial tip vortex geometry using the generalized wake equations are compared with the original predicted geometry in Figs. 21 to 25 for several combinations of rotor and operating condition parameters. These figures demonstrate the capability of the generalized wake equations to curve fit the wake age variations of the axial coordinate for various blade

azimuths. The range of parameters in these sample comparisons includes two- and four-bladed rotors, advance ratios from 0.05 to 0.3, thrust coefficients from 0.0025 to 0.0064, and rotor disk attitudes, α_{TPP}, from -0.5 to -4 degrees. These sample comparisons are generally representative of the complete range investigated for these variables. The degree of accuracy achieved by the wake generalization for wake age and blade azimuth was sufficiently encouraging to proceed with the detailed study of the generalization for the primary rotor design and operating condition parameters to be discussed in the following section.

Generalization for Rotor Operating Condition Parameters and Number of Blades

Following the establishment of the generalized wake equations, the dependency of the envelope and shape function coefficients on the operating condition paramaters (μ, C_T, α_{TPP}) was investigated, and the generalization for these parameters was performed for two- and four-bladed rotors with the blade design of the "representative rotor":

Blade twist = -10°
Taper Ratio = 1
Aspect Ratio = 16
Airfoil: NACA 0012

As will be shown in following sections, the rotor disk attitude, α_{TPP}, can be eliminated as a distortion parameter. Furthermore, thrust coefficient, C_T, will be shown to be a parameter defining the envelope function and not the shape function. Based on these findings, a computer module was developed which contains the generalized wake equations and their coefficients. The coefficients were stored in tabular form for interpolation over a range of advance ratio, μ, and thrust coefficient, C_T, values. The envelope function coefficients were predicted to increase smoothly with increasing thrust coefficient, to decrease smoothly with increasing advance ratio, and to be insensitive to nominal rotor disk attitude variations in steady forward flight. The shape function coefficients were found to be insensitive to thrust coefficient variations and disk attitude variations. This reduced the interpolation requirement in the computer module to a bivariant parameter generalization for the envelope function (μ, C_T) and a single parameter generalization for the shape function (μ). Separate sets of coefficients were included for two and four blades, and rotors with other numbers of blades were assigned the coefficients of the four-bladed rotor as a first level approximation. The sensitivity of the coefficients of the generalized wake functions to blade twist and aspect ratio was explored, thereafter, using the "representative rotor" as a baseline design. (The effect of taper ratio on wake

geometry is similar to that of blade twist. Airfoil section, if uniform in the spanwise direction, is primarily accounted for by the thrust coefficient generalization.)

These wake generalization activities and results related to the rotor design and operating condition parameters will now be discussed in greater detail.

Rotor Disk Attitude

In the Ref. 5 investigation, the sensitivity of rotor wake geometry to rotor disk attitude (tip-path plane angle), α_{TPP} was explored. The predicted effect of rotor disk attitude on blade loading and the tip vortex axial coordinate variation with wake age is shown in Figs. 26 and 27, which are reproduced directly from Ref. 5. The relatively large tip vortex coordinate differences for the two disk attitudes in Fig. 26 were found to be primarily due to the inflow component of the forward velocity (V sin α_{TPP}) which changes the undistorted wake deflection angle defined in Table VI. The change in wake deflection angle influences the axial positioning of the undistorted wake relative to the rotor disk, as shown in Fig. 26. However, it was found that the tip vortex distortions relative to the undistorted wake location are not significantly influenced by the variation in rotor disk attitude. This is shown in Fig. 27. It was concluded in Ref. 5 that disk attitude is an important parameter for rotor wake geometry. However, its influence is mainly on the fundamental undistorted wake geometry and not the axial distortions of the wake from that geometry.

In order to confirm the conclusion from Ref. 5, the envelope functions and shape functions were computed for a disk attitude variation at several advance ratios. The insensitivity of the shape function to disk attitude was clearly demonstrated at values of 0, -3, and -6 degrees for advance ratios as low as 0.05. Insensitivity of the envelope function was demonstrated within limited extents of disk attitude for fixed thrust level. These limited extents were determined from Fig. 12, discussed earlier, to be within the range of typical values associated with current helicopters. That is, using the range of realistic disk attitudes from Fig. 12 for several advance ratios and thrust coefficients, it was found that the effect of disk attitude variations on the wake distortion is sufficiently limited to justify removing disk attitude as a parameter for defining the envelope function as well as the shape function.

Based on these results, disk attitude was removed as an independent parameter for the axial tip vortex distortion (Δz). Figure 12 was used in the selection of disk attitudes for given thrust levels used in calculating the wake distortion coefficients for the representative rotor stored in the generalized wake computer module. It is noted that, although α_{TPP} is not a parameter for the tip vortex axial distortion, it is a primary parameter for the total axial coordinate in that it appears in the momentum inflow ratio used to define the undistorted portion of the coordinate (see Table VI).

Advance Ratio and Thrust Coefficient

With the removal of the rotor attitude as a parameter for definition of the tip vortex distortions, the task of generalizing the wake equation coefficients for advance ratio and thrust coefficient proceeded next. First, a preliminary computer program was coded to calculate and tabulate the wake coefficients for the predicted distorted tip vortex geometries generated for the representative rotor over the investigated range of wake definition parameters ($0.05 \leq \mu' \leq 0.3$; $0.0026 \leq C_T \leq 0.0039$ for b=2; $0.0052 \leq C_T \leq 0.0077$ for b=4). Envelope function and shape function coefficients were tabulated for bivariant interpolation on thrust coefficient and advance ratio (C_T, μ'). Many coefficients for the computer program were obtained by interpolation or extrapolation of the available coefficient data to regions within the bounds of the matrix of conditions studied for which no data were calculated. Judgment for the interpolation and extrapolation task was based on trend observations from the available coefficient data and the expected behavior of the coefficients from past experience and other data sources. For example, the behavior of the coefficients at low advance ratio was influenced by information available from hover distorted wake data. Figure 29 presents the advance ratio variation of the envelope functions for the two- and four-bladed configurations.

The above analytical study resulted in a generalized wake computer module which linearly interpolates between thrust coefficient levels and advance ratio to obtain required envelope coefficients. The geometric shape function coefficients for the first and second wake revolutions are also bivariantly interpolated for advance ratio (μ) and thrust level (C_T). If the required C_T goes beyond the range for this parameter in the computer module, the boundary values are currently used to define the envelope function coefficients. For advance ratios beyond 0.4, the module extrapolates to zero distortion at an advance ratio of 1.0. The computer module generates separate sets of coefficients for two- and four-bladed configurations. It will be shown that the coefficients are less sensitive to blade number variations, and thus, for three or more blades this first generation computer module currently uses the coefficients for four blades.

Figures 30 through 35 contain plots of the envelope and shape functions which show the behavior of these functions with advance ratio and thrust level for two- and four-bladed rotors. It can be seen that the behavior of the functions follow consistent and definable patterns with the μ and C_T variations. It is observed that the functions are most sensitive to advance ratio variations. In fact, the shape function is shown in Figs. 34 and 35 to be insensitive to thrust coefficient variations. This is consistent with the observation from Fig. 28, reproduced from Ref. 5, from which it is shown that the amplitude and not the shape of the wake age distribution of the distortions is influenced by C_T. It was hypothesized in Ref. 5 that the tip vortex axial distortions are approximately proportional to thrust coefficient. Considering the observed insensitivity, thrust coefficient was eliminated as a dependent variable for the shape function, and the generalized wake computer module was modified to reflect this.

Number of Blades

Two advance ratio conditions were investigated for two and four blades at the same thrust level to explore the sensitivity of tip vortex geometry to blade number. Figures 36 and 37 are comparisons of the generalized wake formulations (envelope and shape functions) for the two advance ratios, 0.05 and 0.1, for two- and four-bladed rotors. These figures indicate a small but significant difference in envelope function between two and four blades. The shape functions are generally similar at values above 0.5, but notable differences are evident for the lower peaks which apply to points away from the rotor. In Fig. 38, variations of the envelope function coefficients with thrust coefficient are presented for two and four blades. Although large differences in the coefficients for two and four blades are evident for the hover condition, the differences appear to be significantly decreased in forward flight. In fact, the agreement at the 0.1 advance ratio indicated the possibility of using single curves for A_0 and A_1 by combining the two- and four-bladed coefficients at each forward flight advance ratio for interpolation on thrust coefficient. In the computer module, the two-bladed results are used for lower thrust coefficients typical of two-bladed rotors, and four-bladed results are used for the higher thrust coefficients typical of four-bladed rotors. If the thrust level for a two-bladed condition exceeds the range used for the generalization, the module will use the four-bladed results. Similarly, if the thrust level for a four-bladed condition is too low for the four-bladed generalization, the module will use the two-bladed results. It is also noted from Fig. 38 that the curves are sufficiently smooth for reliable interpolation on thrust coefficient.

Smooth curves for the envelope function coefficients for two and four blades were shown in Fig. 29, and, as previously mentioned, a bivariant interpolation is included in the generalized wake module for thrust coefficient and advance ratio. Separate sets of shape function coefficients were retained in the generalized wake module for two and four blades. The current generalized wake module thus separately accommodates two- and four-bladed rotors. The four-bladed generalization is currently used for other numbers of blades. Future investigations should expand the generalization beyond four blades.

Overall, blade number appears to have a smaller influence on wake geometry in forward flight than in hover, and its influence appears to be less than that of advance ratio and thrust level. For hover, tip vortex geometry was found to be C_T/b dependent. For forward flight the dependence seems to be more on the overall rotor thrust, C_T, than on blade loading, C_T/b. The rapid transition from blade loading to overall thrust dependence is indicated by the A_1 coefficient in Fig. 29 between an advance ratio of 0 and 0.05.

Some differences due to blade number are expected considering that as blade number is increased there are more tip vortices within any given wake region, and thus, the tip vortices move under a different self inducing flow field. Also, the spanwise distribution of peak blade circulations which define the tip vortex strengths are predicted to be different for two versus four blades for the same integrated thrust level. That is, the peak tip vortex circulation strengths do not directly scale by blade number, but are also dependent on other criteria.

Sensitivity to Blade Design Parameters

Aspect Ratio

The sensitivity of tip vortex geometry to blade aspect ratio was investigated for the two-bladed rotor at one advance ratio, 0.1, and at a constant thrust coefficient, 0.0039. The aspect ratio was varied from 10.5 to 16. The corresponding rotor solidity ($\sigma = b\bar{c}/\pi R = b/\pi\ AR$) variation was 0.06 to 0.04. Figure 39 presents the comparison of the envelope function and shape function for this independent aspect ratio variation. From this figure it is evident that the envelope functions are essentially identical and the shape functions are similar. In Fig. 38, the A_o and A_1 envelope function coefficients for this single condition are also shown to be similar for this aspect ratio

variation. Although limited in scope, these results indicate that aspect ratio is at most a secondary wake geometry parameter in forward flight. It is noted that aspect ratio is not a parameter in current hovering rotor wake generalizations. For hover, solidity changes through number of blades, not aspect ratio, were found to be significant, resulting in C_T/b as the important parameter (Ref. 11).

Blade Twist

Parameters which affect the spanwise distribution of blade loading for a given thrust level after the blade bound circulation distribution. This in turn changes the self induced flow field produced by the trailing wake system. Thus, it would be expected that changes in such parameters would alter the wake geometry for the same flight condition. Blade twist and taper are two design parameters representing spanwise variations in blade pitch and chord. Since the net effect of changing these parameters is similar, this initial investigation was limited to exploring the influence of blade twist as a representative parameter which significantly alters the blade spanwise circulation distribution. For hovering flight, twist distribution is known to be a primary wake geometry definition parameter.

The sensitivity of tip vortex geometry to blade twist was investigated for the two-bladed rotor at two forward flight advance ratios of 0.1 and 0.2 and two thrust coefficients, 0.0032 and 0.0039. Blade linear twist, θ_1, values of -6, -10, and -14 degrees were investigated. Wake geometry information available for hover was used for comparison and to assist in the understanding of the behavior of the tip vortex distortions with blade twist variations. The sensitivity of the envelope function to blade twist is shown in Figs. 40a and 40b for the 0.0032 and 0.0039 thrust coefficient, respectively. The conditions which showed the larger envelope function sensitivity (wake distortion amplitude sensitivity) to twist were selected for presentation of the shape function comparisons in Figs. 41 and 42. In Figs. 40 through 42 it is shown that the sensitivity to twist varies depending on the flight condition, but overall it appears that twist should be considered as a primary parameter in future investigations. The current wake generalization module is based on a linear twist of -10 degrees for the representative rotor.

Lateral and Longitudinal Tip Vortex Distortions

The investigation of wake distortions was primarily focused on axial distortions of the tip vortex geometry for reasons noted earlier. This section of the report will describe the results of a preliminary investigation of the lateral and longitudinal distortions and the formulation of an initial model to describe these in-plane ("top view") distortions, Δx and Δy. This model is programmed into the computer module as an option to the user.

As noted in Figs. 5 and 6, the Δx and Δy tip vortex distortions near the rotor are relatively small when compared with the axial distortions, Δz. Figures 43 and 44 present plots of the predicted longitudinal and lateral tip vortex coordinates, respectively, versus wake age at several advance ratios for one thrust level, one blade azimuth position, and the two-bladed representative rotor. The differences noted in these figures for the blade azimuth noted ($\psi_b = 0°$) are similar for other blade azimuth positions. Figures 45 and 46 present the same results for the four-bladed rotor.

The most noticeable differences between the two- and four-bladed distortions are that the four-bladed geometries show larger predicted in-plane distortions; and that at the lowest advance ratio, 0.05, the four-bladed longitudinal distortions are of the same order as the lateral distortions. For both the two- and four-bladed geometries the Δx and Δy distortions become small with increasing advance ratio, and generally the lateral distortions are significantly larger than the longitudinal distortions. Based on this information, it was decided to neglect the longitudinal tip vortex distortions. This assumption, that the longitudinal distortions are insignificant, is justifiable for most rotor airload calculations because the regions where the longitudal distortions differ significantly from the undistorted wake occur beneath the aft longitudinal axis of the rotor disk where the distorted wake geometries are generally displaced downward from the rotor after one wake revolution. Generally, within the first wake revolution, the longitudinal tip vortex distortions are small, and therefore the longitudal distortions can be neglected. Thus, the undistorted longitudinal coordinate equation in Table VI is used to represent the generalized longitudinal coordinates.

The lateral coordinates versus wake age show the most distortions on the advancing and retreating sides of the rotor disk. These are the regions where the tip vortices shed from each blade interact to effectively approximate two trailing vortices similar to the fixed wing trailing vortex system. As a result, the lateral distortions may be important for locally predicting the blade inflow distributions on the advancing and retreating sides of the rotor disk. Therefore, a brief investigation was performed to provide a preliminary lateral distortion model as a correction to the undistorted lateral coordinate relationship defined in Table VI.

A mathematical model which modifies the lateral coordinates of the classical wake was formulated and applied to the existing data base of predicted tip vortex geometries. This model scales the classical relationship used to define the lateral coordinate to obtain a distortion model,

$$y/R = S \cdot y_u/R$$

where y is the distorted lateral tip vortex coordinate,
y_u is the classical undistorted lateral coordinate (see Table VI), and
S is the scaling function;

$$S = 1 - \delta_y \, (|y_u| - y_L)/(1 - y_L) \quad \text{for } |y_u| > y_L$$

$$S = 1.0 \quad \text{for } |y_u| \leq y_L$$

and δ_y is a function of the form:

$$\delta_y = A_y \, (1 - e^{-\lambda_y \, \psi_w})$$

A_y, λ_y and y_L are coefficients which are flight condition dependent. The values for A_y, λ_y and y_L were determined by an iterative least squares curve fit to the predicted data for each flight condition. The value for the coefficient, y_L, was chosen to be constant for both the two- and four-bladed geometries but varies as a function of advance ratio. The other coefficients vary with advance ratio and blade number. It was found that the variations of the coefficients with thrust level gave only slight differences in the resulting curve fitted geometries, and thus thrust dependence was omitted. These lateral distortion coefficients were programmed into the generalized wake coefficient module for use with the axial distortions as an option. Figure 47 is an example of the resulting lateral coordinates compared with the original coordinates at several advance ratios for one blade azimuth position of the four-bladed rotor. Figure 48 presents similar plots for a thrust level variation at four different blade azimuth positions for one advance ratio. Two-bladed rotor results, not shown, demonstrate better agreement than the four-bladed results. This may be due to the fewer number of tip vortex interactions with the two-bladed rotor.

This alternate lateral distortion model is provided as an option to the undistorted tip vortex model. This model should be used with the recognition that it represents a preliminary attempt to model the lateral distortions. For most first level generalized wake applications, it is advised that the undistorted wake generalization be used for the longitudinal and lateral coordinates and that attention be focused on the predominant axial distortions.

Generalized Wake Summary

In summary, a first level generalized wake geometry has been developed. This generalization uses the undistorted wake equations of Table VI as a base and increments the undistorted wake coordinates with the generalized distortions. Emphasis was placed on generalizing the predominant axial tip vortex distortions normal to the rotor disk. However, an optional lateral distortion generalization is also provided. The axial tip vortex distortions are expressed in equation form in Table VII in terms of the product of an envelope function and shape function. The envelope function describes the amplitude variation with wake age and the shape function describes the characteristic distribution of the tip vortex distortion locations with wake age phased by blade azimuth. The tip vortex distortion equations were programmed in a generalized wake computer module for two- and four-bladed rotors. The coefficients for the envelope function are dependent on rotor advance ratio and thrust coefficient. The coefficients for the shape function are dependent on advance ratio. Rotor disk attitude was eliminated as a tip vortex distortion parameter, but is a primary parameter in the basic undistorted portion of the tip vortex coordinates. Although tip vortex coordinates can be generated for any combination of advance ratio, thrust coefficient, disk attitude, and number of blades, emphasis in the generalization was placed on advance ratios between 0.05 and 0.3, and thrust coefficients between 0.0025 and 0.0075 for two- and four-bladed rotors. The four-bladed wake coefficients are currently used as an estimate for other numbers of blades. Complete generalization for the blade design parameters such as aspect ratio, twist, and taper ratio were beyond the scope of this initial study. The generalized wake module was developed for a representative untapered blade design with an aspect ratio of 16 and a linear twist rate of -10 degrees. An exploratory sensitivity study revealed that tip vortex distortions are sensitive to blade twist variations in forward flight, but aspect ratio appears to be a secondary parameter.

The computer time requirement for application of the generalized wake module to generate tip vortex coordinates is insignificant relative to the large time requirement of a freely distorting wake geometry prediction analysis. For a typical case the difference is 1000 to one in computation speed.

Wake Geometry Charts

A set of wake geometry charts were developed which provide a convenient, readily accessible source for approximating rotor forward flight wake geometry and identifying potential locations of close blade-vortex passage. The charts are presented as a self-contained reference in Volume II of this report. Charts for both the classical undistorted wake model and the generalized distorted wake model are included. The charts provide the necessary information to determine tip vortex coordinates for a range of parameters sufficient

for most conventional steady level flight operating conditions. They can be used for a variety of applications which require the geometric relationship between the tip vortices and spatial locations relative to the rotor blades and other helicopter components. In particular, blade/tip vortex interaction locations and rotor wake boundaries can be rapidly defined. A series of sample three-views and isometric views of tip vortex patterns for two- and four-bladed rotors are also included.

Generalized wake envelope function and shape function charts are included from which generalized tip vortex coordinates can be determined for the range of operating condition parameters investigated. Charts are presented in Volume II for advance ratios of 0.05, 0.10, 0.15, 0.20, 0.30, and 0.40 and thrust coefficients between 0.0025 and 0.0075 for both two-and four-bladed rotors. Sample envelope function and shape function charts are presented herein in Figs. 49 and 50. Through interpolation within the charts to a specified operating condition and by multiplying envelope function and shape function values at prescribed wake age values, the user can determine the incremental tip vortex distortions, which when added to the undistorted axial coordinates, $\lambda\psi_w$ (see Table VI), provide the distorted tip vortex axial coordinates. Nomographs for expediently determining rotor inflow ratio, λ, and the undistorted axial coordinates are included in the Volume II charts. Charts are also included for the rapid determination of the undistorted lateral and longitudinal coordinates based on the equations in Table VI.

Samples from Volume II of the three-view and isometric view of the tip vortices based on the generalized wake model and the undistorted wake model are presented in Figs. 51 and 52. A series of these tip vortex patterns are included in Volume II for representative variations of advance ratio, thrust level, disk attitude, and two and four blades. A representative series for varying rotor azimuth position is also included in Volume II. Plots of the loci of blade-vortex passage locations, based on undistorted in-plane wake coordinates, are also contained in Volume II, from which a sample is presented in Fig. 53. By superimposing the rotor blades on the charts at selected azimuth positions, the user can determine from the charts the locations where the projections of the tip vortices into the rotor disk plane intersect the blades. In reality the vortices are displaced axially from the rotor disk, but these plots provide the user with the potential locations for close blade-vortex passages. Actual close passage locations are determined through determination of the tip vortex axial coordinates for these locations. Wake age, ψ_w, values are indicated on the plots which identify the azimuth travel of a blade since it shed the tip vortex at the blade passage point. This information can then be used to determine the axial position of the wake. The series of these plots in Volume II cover two- through six-bladed rotors for advance ratios between 0.05 and 0.4. In addition to this polar format plot, charts

for direct determination of the blade radial locations for blade-vortex intersections and charts for the determination of the blade/tip vortex intersection angles are presented in Volume II in a cartesian format.

Charts for the determination of fore and aft wake boundaries are included in Volume II for both the undistorted and distorted wake geometries. A sample of the generalized distorted wake boundaries is presented in Fig. 54.

The wake charts supplement the wake equations and generalized wake computer module by providing a source for expediently acquiring approximate wake geometry information for a preselected forward flight rotor operating condition.

INFLUENCE OF WAKE GEOMETRY ON ROTOR AIRLOADS AND PERFORMANCE

A primary objective of this study was to apply theoretical wake geometries to investigate the influence of tip vortex distortions on the aerodynamic related characteristics of a rotor in forward flight. The rotor analysis described earlier (Fig. 9), was applied using various combinations of the computer analysis components and wake/inflow models to compute rotor wake geometry, inflow, airloads, performance, and blade bending moments. The Generalized Rotor Performance Analysis (GRP) was used to provide blade airloads and rotor performance predictions. The Normal Modes Aeroelastic Rotor Analysis (Y200) was used to provide blade bending moment predictions. The rotor wake/inflow models used are listed below:

(1) "uniform inflow" based on a constant momentum value of rotor induced velocity (calculated in GRP and Y200).

(2) "variable inflow" based on "classical undistorted wake geometry" (wake and induced velocities calculated in the Prescribed Wake Rotor Inflow Program, F389SR).

(3) variable inflow based on "predicted distorted wake geometry" (wake calculated by the Rotor Wake Geometry Analysis, F506; induced velocities calculated by F389SR).

(4) variable inflow based on a "generalized wake geometry" (wake distortions calculated by the Generalized Wake Module; induced velocities calculated by F389SR).

In wake/inflow models (3) and (4), the wake was represented in the rotor analysis by distorted tip vortex filaments and undistorted inboard wake filaments.

In accordance with the above objective, the intent of this study was to demonstrate the sensitivity of the aforementioned rotor characteristics to the selection of rotor wake/inflow model and to perform an initial assessment of the new first level generalized wake. This was accomplished through application to the "representative rotor" described previously and the H-34 rotor. The H-34 rotor was selected as a rotor for which test data for blade airloads and bending moments were available. In this report section, results for the representative rotor are presented first to demonstrate the sensitivity of predicted performance and airloads to the wake/inflow models. The H-34 results are presented next to demonstrate sensitivity and compare airload and bending moment predictions for the various wake/inflow models with test data. It will be shown that the rotor characteristics are sensitive to wake

distortions for a wide range of flight conditions that position the tip vortices near the rotor, and the degree of this sensitivity and the associated accuracy of the distorted wake models are dependent on the blade-vortex interaction model used to predict local blade airloads for close vortex encounters.

Representative Rotor--Influence on Predicted Rotor Power

The sensitivity of integrated rotor performance to the choice of wake/inflow model is shown in Table VIII and Figs. 55 and 56 for the two-and four-blade representative rotor conditions listed earlier in Table V. Comparisons of predicted rotor torque at advance ratios between 0.05 and 0.3 for constant rotor thrust coefficient are presented in Fig. 55. Comparisons of predicted rotor torque at representative thrust coefficients for 0.1 advance ratio are presented in Fig. 56.

It is shown that rotor power predictions based on the classical undistorted wake model are consistently higher than those based on the uniform inflow model. This is in agreement with the previous findings as stated in Ref. 8. Classical wake variable inflow resulted in a predicted average torque coefficient increase of 5 percent and 3 percent for the two-and four-bladed rotors, respectively. The extent of variation from the average is ± 3 percent for both rotors. It is noted that these differences would have been larger if a tip loss factor had not been used with the uniform inflow model in the Generalized Rotor Performance Analysis (GRP). The tip loss model in GRP is a parabolic tip loss factor for which the lift diminishes parabolically to zero at the tip from 2 chord lengths inboard of the tip (approximately 0.87R for the representative rotor blade).

The use of variable inflow based on the predicted distorted wake model and the generalized wake model generally resulted in power requirements within a few percent of the undistorted wake results. However, distinct exceptions were noted and no consistent trends are apparent as the values are both higher and lower than the classical wake values.

The generalized wake power predictions relative to those based on the predicted distorted wake are similar for some conditions and notably different for others, with no well-defined trends except that the larger differences generally occur for the four-bladed rotor conditions.

It will be shown in the following discussion of the blade airload results that the mixed sensitivity results for the influence of tip vortex distortions on predicted power are related to the predicted severity of local blade-vortex interactions associated with local tip vortex distortions at specific flight conditions.

TABLE VIII. INTEGRATED PERFORMANCE RESULTS FOR THE REPRESENTATIVE ROTOR

CASE NUMBER	b	μ	α_{TPP}	NOMINAL CT*10-3	UNIFORM INFLOW CQ*10-4	VARIABLE INFLOW CLASSICAL CQ*10-4	VARIABLE INFLOW DISTORTED CQ*10-4	VARIABLE INFLOW GEN. WAKE CQ*10-4	
1	2	.05	0	3.20	1.392	1.459	1.524	1.535	*
2	2	.05	-3	3.20	1.462	1.533	1.624	NS	
3	2	.1	0	3.20	.999	1.042	1.021	NS	
4	2	.1	-3	2.60	.907	.938	.943	.942	*
5	2	.1	-3	3.20	1.199	1.283	NS	NS	
6	2	.1	-3	3.20	1.168	1.233	1.216	1.270	*
7	2	.1	-3	3.20	1.164	1.192	NS	NS	
8	2	.1	-3	3.90	1.515	1.588	1.554	1.655	*
9	2	.1	-3	3.90	1.474	1.523	NS	NS	
10	2	.1	-3	3.90	1.600	1.676	NS	NS	
11	2	.1	-6	3.20	1.340	1.410	1.351	NS	
12	2	.1	-6	3.90	1.732	1.814	NS	NS	
13	2	.2	-3	3.20	1.100	1.175	1.075	1.133	
14	2	.2	-6	3.20	1.439	1.543	1.504	1.527	*
15	2	.2	-6	3.20	1.402	1.497	NS	NS	
16	2	.3	-6	3.20	1.798	1.936	1.920	1.936	*
17	4	.05	-0.5	6.40	4.071	4.154	4.085	4.501	*
18	4	.05	-3	3.20	1.799	1.824	1.678	NS	
19	4	.1	-1	5.20	2.258	2.344	2.289	2.373	*
20	4	.1	-1	6.40	3.075	3.248	3.283	3.316	*
21	4	.1	-1	7.70	4.160	4.313	4.652	4.503	*
22	4	.1	-3	3.20	1.489	1.550	1.310	NS	
23	4	.2	-2.25	6.40	2.549	2.601	2.291	2.393	*
24	4	.3	-4	6.40	3.281	3.439	3.106	3.550	*

* USED FOR TIP VORTEX GENERALIZATION MODULE COEFFICIENTS

NS - NOT STUDIED FOR PERFORMANCE

Representative Rotor--Wake Geometry and Influence on Predicted Blade Airloads

To investigate the sensitivity of blade airload prediction to the various wake/inflow models, the predicted wake geometries and airload distributions for the representative rotor conditions were examined. From these, the following three conditions were chosen for presentation herein:

$b = 2$	$\mu = 0.3$	$C_T = 0.0032$	$\alpha_{TPP} = -6^\circ$
$b = 2$	$\mu = 0.1$	$C_T = 0.0032$	$\alpha_{TPP} = -3^\circ$
$b = 4$	$\mu = 0.05$	$C_T = 0.0064$	$\alpha_{TPP} = -0.5^\circ$

For the representative rotor tip speed of 700 fps, the three advance ratios correspond to 124, 41, and 21 kts, respectively. These three conditions were selected to show conditions representative of various levels of wake influence. Results for two- and four-bladed rotors and advance ratio conditions from 0.05 to 0.3 are included. The two low advance ratio conditions were selected as conditions for which the wake is typically closer to the rotor and significant blade-vortex interactions occur. The 0.3 advance ratio condition was selected as a relatively wake insensitive condition. Emphasis in the following discussion will be placed on the 0.1 condition.

Before concentrating on the detailed wake and airload results of each condition, presented in Figs. 57 to 78, a summary of the observations obtained from these results are presented. A significant influence of tip vortex distortions on blade airloads is noted which is related to the local proximity of the tip vortices to the blades. Airloads predicted by the classical wake model exhibit some higher harmonic content in the azimuthal variations relative to the uniform inflow model. Tip vortex distortions increase the harmonic amplitudes relative to those of the classical wake model, and also introduce additional harmonic content. This is directly attributable to the predicted displacement of the tip vortices closer to the rotor disk. Harmonic airloads increase with combinations of operating condition parameters that result in more numerous blade-vortex interactions and/or place the tip vortices closer to the rotor; i.e., in general, decreasing advance ratio, and shallow rotor disk attitude. Regarding thrust coefficient, the tip vortex distortions increase with thrust coefficient; however, the deflection angle of the undistorted wake increases, which tends to compensate the positioning of the tip vortices near the rotor. The use of the generalized wake model results in airload distributions that are characteristically similar to the

predicted distorted wake model airloads, but the local amplitudes are often different. This results from small but significant changes in the relative position of the tip vortices to the blades. The inverse relationship of induced airload to vortex distance, from the Biot-Savart law used in the analysis, can result in high airload sensitivity. This was recognized prior to this investigation and will be discussed in more detail. In the absence of a validated blade-vortex interaction model for close tip vortex passages it was decided to use a simple solid body rotation vortex core model and assume that the potential flow relation (Biot-Savart law) was applicable outside of a vortex core, 0.01R (approximately 0.15 chord) in diameter. This blade-vortex interaction model does not account for the complex interactive aerodynamics associated with a close passage which can include expansion and even bursting of the vortex core and local suction and flow separation of the blade surface (Refs. 6, 39, 40). However, it does demonstrate the airload prediction sensitivity to the interaction model and the requirement for an improved local blade-vortex interaction model.

First Sample Representative Rotor Condition--Advance Ratio = 0.3

A condition for which the airloads were found to be relatively insensitive to tip vortex distortions is the following:

$$b = 2,\ \mu = 0.3,\ C_T = 0.0032,\ \alpha_{TPP} = -6^\circ$$

This condition corresponds to a 124 kt flight speed. The distorted (generalized wake) and undistorted tip vortex geometry patterns for one rotor azimuth position are shown in Figs. 57 and 58, respectively. Comparing the tip vortex patterns in these figures, it is observed that the generalized wake and classical undistorted wake geometries are similar for this flight condition, and the tip vortex distortions in Fig. 57 are shown to be generally small and occur primarily on the lateral sides of the wake. Fig. 59 shows the loci of points where tip vortices pass directly beneath the blades at each blade azimuth position.

The variation of the spanwise integrated blade loading (total blade lift) with blade azimuth is shown in Fig. 60 for this condition. The integrated blade loading for the three wake models are similar, but they are different from the uniform inflow results, particularly on the advancing side of the rotor. Although generally similar, local airload differences for the wake models were noted in the vicinity of the tip vortex passage from the opposite blade (forward locus of vortex passages in Fig. 59).

The results for this flight condition demonstrate the general insensitivity of blade airloads to tip vortex distortions for typical steady flight of a two-bladed rotor at moderately high advance ratios, where the disk is sufficiently inclined to prevent close blade-vortex passages. However, later in this report it will be shown for the four-bladed H-34 rotor that local airload deviations due to blade-vortex interaction occur on the advancing side for a similar advance ratio (0.29) and disk attitude (-6 degrees) condition.

Second Sample Representative Rotor Condition--Advance Ratio = 0.1

Wake geometries and predicted blade airloads are presented in Figs. 61 to 72 for the following 41 kt flight condition of the representative rotor:

$$b = 2,\ \mu = 0.1,\ C_T = 0.0032,\ \alpha_{TPP} = -3^\circ$$

Because of a lower advance ratio than the previous condition, the number of blade-vortex passages is increased as shown in Figs. 61 through 65. Distorted tip vortices (Figs. 61, 63) are much closer to the rotor than the undistorted vortices (Figs. 62, 64).

Two rotor azimuth positions were selected for a detailed presentation of the wake geometry and airload distributions. For the first selected rotor position the blades are at 0 and 180 degrees (Figs. 61, 62), and for the second selected rotor position the blades are at 90 and 270 degrees (Figs. 63, 64). The locations where the tip vortices pass under the blades at these blade azimuth locations, identified from Fig. 65, are marked on Figs. 61, 63, 65, and 66 as (1) through (11). Close blade-vortex passages can be identified from the axial coordinate plots for the tip vortex from each of the four blade azimuths in Figs. 66a to 66d where the eleven blade-vortex passages are labeled (1) through (11) with the azimuth location of the blade that is involved in the blade-vortex passage. It is noted that the blade location points marked in Figs. 66a to 66d are blade tip locations, and thus, considering coning, inboard portions of the blades are closer to the tip vortices than indicated by the marked points. Close blade-vortex interactions, within approximately 0.03R (one-half chord length), can be identified from Figs. 66a to 66d at locations (1), (2), (7), (8), (9), (10), (11).

Regarding the first rotor position (blades at 0°, 180°), two close vortex passages, (1) and (2), are indicated in Figs. 66a and 66c. In Fig. 66a it is shown that the tip vortex from the downstream blade (at 0 degrees) is predicted to pass close to the upstream blade (at 180 degrees). The wake age (ψ_w = 180°) and blade radial location (0.68R) for this blade-vortex passage (1) is acquired from Fig. 65. This tip vortex passage location (1) is shown in the side view of Fig. 61 to be very close to the blade. This is the

portion of the tip vortex that is emitted from the upstream blade tip and is distorted up and close to the rotor disk as it travels back in time. This upward distortion is consistent with the experimental observation of Ref. 6 in which it is shown that a blade-vortex impact typically occurs near 180 degrees at low advance ratios. In Fig. 61, the tip vortex from the upstream blade (at 180 degrees) is also shown to be close to the upstream blade at a radial location of 0.38R (from Fig. 65), and this is indicated as blade-vortex passage (2). Blade-vortex passages (3) through (6) are progressively older in age and further from the rotor which results in an absence of close blade-vortex passages for the downstream blade (0 degrees azimuth).

Regarding the second selected rotor position shown in Fig. 63 (blades at 90°, 270°), five close blade-vortex passages are evident in Figs. 66b and 66d. These are identified in the figures as passages (7) through (11), and are shown in Fig. 65 to occur on the advancing blade (90°) at 0.96, 0.83, and 0.54R and on the retreating blade (270°) at 0.93 and 0.71R. Even considering a blade coning angle of 5 degrees, all seven of the indicated tip vortex passages are within an axial displacement of 0.03R of the blade. The three close blade-vortex passage locations at the 90 degree blade azimuth are shown schematically in Fig. 67 for the three wake models, and the close proximity of the distorted tip vortices to the blade, compared to the undistorted wake, is clearly evident. It will now be shown that, as would be anticipated, most of the close blade-vortex passages cited above are predicted to have a significant influence on blade airloads.

The effects of the four wake/inflow models on blade airloading are shown in Figs. 68a and 68b. These figures show contours of the blade airload (lift) distributions as the blade rotates around the rotor disk for each specified blade segment and azimuth location of the rotor analysis. Although not shown, the loading does diminish to zero at the edge of the rotor disk (blade tip). Each case was trimmed to the same thrust, disk attitude, and zero flapping. It is observed in these figures that the wake distortions make the character of the airload distributions more irregular and increase the peak amplitudes. This is particularly noticeable on the advancing and retreating sides of the disk. The generalized wake model produces the same general characteristic distributions as the predicted distorted wake model.

The azimuth variation of the total blade lift resulting from a spanwise integration of blade loading is presented in Fig. 69. The blade lift variation based on the two distorted tip vortex representations is shown to fluctuate significantly more than the two simpler wake/inflow representations. The harmonic content from the generalized wake model is similar to that from the predicted distorted wake model, but the amplitudes differ, particularly near 90 degrees blade azimuth. These differences are attributable to the slightly different positions of the tip vortices of the distorted and generalized wake models which produce significant changes in local blade loading.

The influence of the different wake/inflow models on the spanwise loading distributions is shown in Figs. 70a to 70d for the 0, 90, 180, and 270 degree blade azimuths. These loading distributions can be related to the wake geometries presented in the earlier figures. In Fig. 70a, the smooth blade loading distribution of the downstream blade (0°) reflects the absence of close blade-vortex interactions for all wake models. In Fig. 70c, the blade loading distribution of the upstream blade (180°) reflects the very close blade-vortex passage (1) at 0.68R and the moderately close passage (2) at 0.38R for the tip vortex distortion models. Nearly equivalent blade-to-vortex distances were predicted by both the distorted wake and generalized wake models (Figs. 66a and 66c), which resulted in similar loading distributions for this blade azimuth.

In Fig. 70b, for the advancing blade (90°), the tip vortex distortion models show a significant change in the loading distribution when compared to the results of the classical wake and uniform inflow models. The predicted airloads of the distorted and generalized wake models reflect the presence of the previously identified close blade-vortex passages (7), (8), and (9) near 0.96, 0.83, and 0.54R. These blade-vortex passages were presented schematically for the 90 degree blade in Fig. 67. The sensitivity of the predicted blade airloads to what might appear to be small differences in these tip vortex locations is shown in Fig. 70b. The predicted blade airloads are very sensitive to relative vortex location in regions of close blade-vortex passage. This sensitivity is also evident in the effective angle of attack and the blade drag distributions presented in Figs. 71 and 72 for this 90 degree azimuth position. This sensitivity is exemplified further in the blade loading distribution at 270 degrees azimuth shown in Fig. 70d where two close blade-vortex passages, (10) and (11), were predicted at 0.71R and 0.93R. As was shown in Fig. 66b, the tip vortex location (11), for both the distorted wake and generalized wake models, is in extreme proximity to the 270° blade near 0.93R. The generalized wake produces large airload gradients in that blade region. The airload distribution of the predicted distorted wake model does not exhibit an extreme variation. This difference is attributable to the finite element blade representation in the rotor analysis in which the induced velocities and related airloading are calculated at the blade element centers. With the distance between blade element centers larger than the vortex core size, a vortex filament with finite core located near the blade element center can produce an unbalanced induced influence, the magnitude of which is extremely dependent on whether or not the nearest blade element center lies within the vortex core. For this condition (Fig. 70d) the distorted wake model has actually positioned the tip vortex within the vortex core (point (11) in Fig. 66b), thus significantly reducing the induced velocity at this location and the influence on the airloads compared with the generalized wake model results. This sensitivity demonstrates the requirement for attention to

the blade and wake segmentation as well as the aerodynamic representation for the vortex and its influence on blade airloads in future blade-vortex interaction models.

Third Sample Representative Rotor Condition--Advance Ratio = 0.05

To demonstrate the application of the wake/inflow models to a low speed condition with numerous blade-vortex passages the following condition was selected:

$$b = 4,\ \mu = 0.05,\ C_T = 0.0064,\ \alpha_{TPP} = -0.5^\circ$$

This condition corresponds to a 21 kt flight speed.

Relative to the previous 41 kt condition, decreasing the advance ratio and increasing the number of blades by a factor of two results in an extensive increase in the number of blade-vortex passages as shown in Figs. 73, 74, and 75. The thrust was increased and disk attitude decreased to provide typical values consistent with a low advance ratio condition of a four-bladed rotor. The generalized wake geometry, presented in Fig. 73, is highly deformed from the classical wake geometry of Fig. 74. The upward deformation of the forward and lateral portions of the wake and downward deformation of the aft wake is typical of low speed wake geometry. These characteristic features and the displacement of the tip vortices to locations near and above the rotor disk have been observed in model rotor tests (Ref. 6).

The azimuth variation of spanwise integrated blade loading (total blade lift) for this condition is presented in Fig. 76. Although some differences will be shown in the local blade loading, the classical wake and uniform inflow results are quite similar on an integrated loading basis. The results for the tip vortex distortion models again exhibit higher harmonics due to blade-vortex passages. A comparison of the generalized wake results with the distorted wake results indicates some changes in both the peak loading locations and the loading amplitudes due to generally small differences in the tip vortex locations. Details of the spanwise lift distribution are presented in Figs. 77 and 78 for two selected azimuth positions, 0 and 210 degrees.

In Fig. 77, it is shown that the airloading of the downstream blade (0 degrees) is again relatively insensitive to the wake/inflow model, even at this low speed. This is associated with the displacement of the tip vortices away from the rotor in the central downstream region. The blade loading for the 210 degree azimuth (Fig. 78), was selected as an example of a blade position where several distorted tip vortices pass above the outboard half of the blade (vortices of wake age 92, 185, 278, 369, and 460 degrees in Fig. 75), impinge on the center of the blade (552 degrees in Fig. 75), and pass beneath the inboard half of the blade (641, 773, 824, 916, and 1012 degrees in Fig. 75). These are the portions of the tip vortices that are shed from the

forward edge of the rotor disk and travel rearward in a parallel pattern as shown in Fig. 73. A complex induced flow distribution is produced at the blade, particularly in the mid-span region where the tip vortex filaments pass down through the rotor for this condition. The blade loading distribution for this azimuth position is presented in Fig. 78. The classical wake and uniform inflow models are shown to completely ignore the influence of the characteristic wake distortion. The influence of the close blade-vortex passages in the central blade region is evident in the tip distortion models. A significant difference in local mid-span loading between the generalized and predicted distorted wake models is evident. This difference is not typical of all azimuth positions, but this 210 degree azimuth position was purposely selected to further exemplify the requirement for an improved blade-vortex interaction model in the airload analysis. Similar to the findings for the 270 degree azimuth for the previous 0.1 advance ratio condition, a vortex filament was predicted to impinge on the blade. The high sensitivity of the airload prediction to small differences in the vortex core location relative to the nearest preselected analytical blade station results in the airload differential for the two wake models. Since close blade-vortex passages and blade-vortex encounters are prevalent at low advance ratios, awareness of the limitation of the current airload prediction model for quantitative loading accuracy is important, and improved blade-vortex interaction modeling should be stressed.

Prior to proceeding to the results of the H-34 rotor investigation, for which test data was available, the primary observations from this initial representative rotor study can be summarized.

1. Regarding rotor performance prediction, the classical wake calculation of rotor power for constant thrust was consistently higher than the uniform inflow calculation. The calculated power values from the predicted distorted and generalized wake models were scattered about the classical wake values with no well-defined trend.

2. As previously recognized, the influence of wake distortion on blade airloads is directly related to the close proximity of the tip vortices to the rotor and the number of close blade-vortex interactions. The wake influence generally increases with decreasing advance ratio, decreasing nose down tilt of the rotor disk, and increasing number of blades. Increasing thrust coefficient increases the wake deflection angle but also increases the wake distortion toward the rotor, and thus its influence on blade airloads is more difficult to generalize.

3. Relative to the classical undistorted wake model, the forward and lateral sides of the wake are distorted toward the rotor in forward

flight. This results in the prediction of close blade-vortex passages which introduce higher harmonic content and local spanwise gradients in blade airloads.

4. The prediction of tip vortex distortions which are in close proximity to the blades at localized regions of the rotor results in a high sensitivity of predicted airloads to small differences in tip vortex geometry. For such conditions, differences were observed in the airload predictions of the generalized and predicted distorted wake models even though the wake geometry appeared to be approximated well by the generalized wake model.

5. The occurrence of close blade-vortex passages and the high sensitivity of blade airloads to small deviations of blade station to tip vortex distance in the airloads analysis, demonstrate the requirement for an improved blade-vortex interaction model and further wake generalization refinement.

H-34 Rotor--Wake Geometry, Performance, Airloads, and Bending Moments

The previous section presented results illustrating the effect of tip vortex distortions on rotor performance for the representative rotor. The rotor selected was representative but fictitious and no test data were available for comparative purposes. This section presents comparisons between measured results and the predictions using the uniform inflow, classical, distorted, and generalized wake inflow models. Three conditions were investigated over an advance ratio range from 0.064 to 0.29 to provide comparative results to investigate the applicability of distorted wake methodology for rotor performance and airload predictions. The four-bladed H-34 rotor was selected for the comparison because it had, at the time of the study, a large base of test data readily available in the open literature (Refs. 30 and 31).

Three flight conditions were selected from available flight test and wind tunnel data for the H-34 rotor.

Airspeed	Advance Ratio	Thrust Coefficient	Disk Attitude
23 kt	0.064	0.005	-0.61°
48 kt	0.129	0.005	-1.13°
110 kt	0.29	0.0036	-5.7°

Flight test data were available in Ref. 30 for the 23 and 48 kt conditions. Wind tunnel test data of a full-scale rotor were available in Ref. 31 for the 110 kt condition. Emphasis in the selection of these test conditions was

placed on including combinations of airspeed, disk attitude and thrust coefficient that would result in significant wake interaction effects. Selection of the 0.064 and 0.129 advance ratios provides a severe test of distorted wake methodology because of the predicted occurrence of a large number of blade/vortex interactions. These 23 and 48 kt conditions are commonly referred to as transition conditions where helicopters are known to experience irregular control characteristics (Ref. 32) and high vibratory excitations due to rotor/wake interaction. The 0.29 advance ratio condition is a moderately high speed condition (110 kt) for which some blade-vortex interaction was evident in the available blade airloads test data for the disk attitude and lower thrust coefficient of the selected condition.

The H-34 rotor design characteristics and a listing of the test parameters for each of the three operating conditions are presented in Table IX.

The rotor analysis was run using the uniform inflow, classical undistorted wake, predicted distorted wake, and generalized wake models for all three conditions. The Generalized Rotor Performance Analysis was used to predict rotor performance and blade airloads based on the four wake/inflow models. The Normal Modes Aeroelastic Rotor Analysis was used to predict blade bending moments based on flexible blade airloads and the four wake/inflow models. For each case in the prediction procedure the rotor was trimmed to the test thrust coefficient and tip-path plane attitude based on test values of shaft and flapping angles.

H-34 Rotor Wake Geometry

Tip vortex geometry patterns at one rotor azimuth position for the undistorted and generalized wake models are presented for the three H-34 operating conditions in Figs. 79 to 84. The general wake distortion features are consistent with those shown earlier for the representative rotor and those demonstrated in test (e.g., Refs. 5, 6, 20). That is, the distortions increase with decreasing advance ratio and result in displacing the forward and lateral sides of the wake upward and the rear of the wake downward. The upward distortions move the vortices near and even above the rotor, particularly at the lower advance ratios. The number of blade-vortex passages also increase with decreasing advance ratio as shown in Figs. 85 to 87. The combination of four-blades and low advance ratio results in a particularly large concentration of vortex passages near the rotor for the 0.064 advance ratio condition.

Figure 88 shows an example of the capability of the generalized wake model to represent the H-34 axial tip vortex distortions predicted with the Rotor Wake Geometry Analysis. The general agreement is good between the coordinates of the two wake models. This is encouraging, considering that the representative rotor parameters were used to develop the generalized wake.

TABLE IX. H-34 ROTOR CHARACTERISTICS

PHYSICAL CHARACTERISTICS OF THE H-34 ROTOR

RADIUS	28 FT
NUMBER OF BLADES	4
CHORD	1.366 FT
HINGE OFFSET	.0357R
TWIST	-8 DEGREES
AIRFOIL TYPE	MODIFIED NACA 0012

TEST OPERATING CONDITIONS FOR THIS INVESTIGATION

	CASE 1	CASE 2	CASE 3
REFERENCE			
V (KNOTS)	23.0	48.0	110.0
ΩR (FPS)	607.0	628.0	650.0
μ	.064	.129	.29
C_T	.0050	.0050	.0036
α_{TPP} (DEG)	-0.61	-1.13	-5.70
α_S (DEG)	-.6	-.7	-5.0
a_{1S} (DEG)	-.012	-.43	-.7
L (LBF)	11600	11600	8252
ρ (SLUG/FT**3)	.00254	.00212	.002221
a_0 (FPS)	1116	1116	1116
θ_{75}	6.326	5.259	6.6
A_{1S}	-2.216	-1.966	2.4
B_{1S}	.345	2.579	6.0

However, as indicated previously, even small differences near the rotor can have a significant effect on airload prediction. The degree of correlation of the two wake models shown in Fig. 88 is generally typical for advance ratios above 0.1. At low advance ratios, such as the 0.064 condition, greater differences can occur which are partially attributable to a more irregular distorted wake geometry predicted by the Rotor Wake Geometry Analysis.

H-34 Rotor Performance

Rotor power was predicted for the three H-34 conditions using the four wake/inflow models and the Generalized Rotor Performance Analysis (GRP). The horsepower values are presented in Table X. Due to the complications of separating out the main rotor power from other power requirements (tail rotor, gear box, etc.) in flight test, rotor power data were not available from Ref. 30 for the two lower speed conditions. These two conditions were selected for the airloads data comparison to be presented in the next report section.

The uniform inflow model consistently resulted in the lowest power prediction. The classical undistorted wake power values are approximately 6 percent higher than those for the uniform inflow model. An increase of 3 to 5 percent was predicted in the preceding representative rotor study. The power predictions of the two tip distortion models are again scattered about the classical wake results at the two lower speeds due to the occurrence of close blade-vortex passages and the sensitivity to the blade-vortex interaction model. The fact that the variations between the power predictions of the three wake models (classical, distorted, and generalized) are essentially equivalent at the 0.29 advance ratio indicates that wake distortions are generally not significant for power prediction at high advance ratio conditions with typical high nose-down disk attitudes associated with steady level flight. At this condition the power predictions using any of the wake models are closer to the test value, but generally a 6 percent differential remains between test and theory. Based on past experience, this differential is not typical, and may be primarily attributable to difficulty in measuring flapping values to the required degree of accuracy. The Generalized Rotor Performance Analysis, as routinely used with the classical wake model to predict power, consistently agrees with test data within approximately three percent. Thus, the degree of correlation for this one test point should not be considered typical. Emphasis for comparison with test data will be placed on forthcoming airloads predictions.

The collective and cyclic pitch control parameters required in the analysis to trim each condition are presented in Table XI and Fig. 89 for the three operating conditions. Control values for the four wake/inflow models are presented along with the test values. In addition to rigid blade results from the GRP analysis, flexible blade results from the Y200 Aeroelastic Rotor Analysis are included for the distorted wake model. It is noted that test

TABLE X. H-34 ROTOR HORSEPOWER

INFLOW MODEL	μ = .064	.129	.29
UNIFORM INFLOW WITH PARABOLIC TIP LOSS	635.2	468.4	511.4
CLASSICAL WAKE	681.1	499.1	543.8
DISTORTED WAKE	645.8	447.5	538.0
GENERALIZED WAKE	690.6	468.1	542.8
TEST RESULTS	NA	NA	579.0

TABLE XI. TABLE OF PREDICTED AND MEASURED CONTROL PARAMETERS USING RIGID AND FLEXIBLE BLADE RESPONSE ANALYSES FOR VARIOUS WAKE/INFLOW MODELS

CASE I $\mu = .064$

INFLOW MODEL	θ_{75}	A_{1S}	B_{1S}
TEST RESULTS	6.3	-2.2	0.3
UNIFORM	8.0	-0.1	1.3
CLASSICAL WAKE	7.9	-1.5	1.1
DISTORTED WAKE	8.0	-2.1	1.3
GENERALIZED WAKE	8.2	-2.5	0.9
DISTORTED WAKE FLEXIBLE BLADE	7.4	-2.1	1.2

CASE II $\mu = .129$

INFLOW MODEL	θ_{75}	A_{1S}	B_{1S}
TEST RESULTS	5.3	-2.0	2.6
UNIFORM	6.5	-0.4	2.4
CLASSICAL WAKE	6.4	-1.7	2.3
DISTORTED WAKE	6.3	-2.0	2.6
GENERALIZED WAKE	6.3	-1.7	2.2
DISTORTED WAKE FLEXIBLE BLADE	5.8	-1.8	2.7

CASE III $\mu = .29$

INFLOW MODEL	θ_{75}	A_{1S}	B_{1S}
TEST RESULTS	6.6	2.4	6.0
UNIFORM	7.2	2.1	5.0
CLASSICAL WAKE	7.2	1.5	5.0
DISTORTED WAKE	7.1	1.4	5.0
GENERALIZED WAKE	7.2	1.5	5.0
DISTORTED WAKE FLEXIBLE BLADE	6.9	-1.8	5.0

pitch control angle and flapping angle measurements are difficult to acquire accurately on a full-scale rotor, and accuracy limits around 1 degree are not unusual, particularly for flight test.

The theoretical control values presented in Table XI and Fig. 89 are associated with the analytical trim procedure used. Because the geometric relationship between the wake and rotor disk is of fundamental importance for this type of study, the analysis was run in such a manner as to trim to the measured rotor disk attitude. To do this, the shaft angle and first harmonic of blade flapping angle are prescribed in the analysis. The response analysis then alters the blade cyclic controls to obtain equilibrium of forces on the blades for the prescribed condition. That is, the rotor control values were varied in the computer analysis until the test thrust coefficient and longitudinal tip path plane attitude ($\alpha_{TPP} = \alpha_s + {}^{a}1_s$) were achieved. Lateral flapping trim, b_{1_s}, was achieved based on test values. An alternate trim procedure would have been to trim to thrust, propulsive force, and hub moments. This was not selected for this study because of the primary importance of matching disk attitude for wake geometry simulation and the objective to study the influence of wake distortions in a controlled manner.

Considering the expected degree of accuracy of test control angles, Fig. 89 is presented to demonstrate the outstanding trends rather than the absolute values. The theoretical collective pitch values, θ_{75}, are similar for all wake/inflow models, but are consistently higher than the test values. All predicted control values for the three wake models are in agreement at the 110 kt condition ($\mu = 0.29$) and within 1/2 degree at the 23 and 48 kt conditions ($\mu = 0.064$ and 0.129), with the exception of the lateral cyclic, A_{1_s}, at 23 kt. The primary observation in Fig. 89 is the inability of the uniform inflow model to predict the lateral cyclic pitch requirement for trim at the lower speeds and the significant improvement in lateral cyclic prediction that results from the wake models, particularly the two tip distortion models. Lateral cyclic control, A_{1_s}, principally affects the lateral flapping, b_{1_s}, which determines sideward tilt of the rotor disk. Due to the 90 degree phase lag of the response of an articulated blade, sideward tilt is very sensitive to inflow variations from front to rear of the disk. At low forward speed, the fore-aft wake distortion produces a large fore-aft inflow variation which must be represented in any analysis to predict lateral flapping and related cyclic pitch. This phenomenon was previously demonstrated experimentally by Harris (Ref. 32) and theoretically by Johnson (Ref. 33). The model test of Ref. 32 indicated a peak response at an advance ratio of 0.08 where the wake distortions and influence on airloads are severe. At high speeds the predominant inflow is due to the flight velocity acting through the tilted disk, and the effect of wake distortion on airloads and flapping is reduced. The wake influence on blade airloads is the subject of the following discussion.

H-34 Blade Airloading

Azimuth variations of blade airloads for the three selected H-34 conditions at 23, 48 and 110 kt are presented in Figs. 90 through 95. These figures consist of time history plots of local blade lift force at specified blade radial stations (Figs. 90a,b; 92a,b; and 94a,b) and spanwise integrated lift (total blade lift; Figs. 91, 93, and 95). The airload predictions for the four wake/inflow models are compared with test data. It is noted that the test airloads were reconstructed from harmonic data at specific blade radial stations from Refs. 30 and 31, and the predicted airloads were interpolated to these blade radial stations. The flight test data from Ref. 30 for the 23 and 48 kt conditions extended to the 0.95R blade station. The wind tunnel test data from Ref. 31 for the 110 kt condition extended to the 0.99R blade station. The available test data had a limited number of radial stations (7 to 9) and harmonics (10), combined with a limited number of chordwise pressure transducers (3 to 11; 5 to 7 typical) to integrate to blade section lift. This could result in the elimination and/or reduction of local loading peaks that occur within the discrete data points. It is, of course, recognized that a discrete representation of the blade and wake was also used for the predicted airloads.

To qualitatively separate out the more direct wake influences from the time histories of blade airloads, it is necessary to use the uniform inflow results as a basis for comparison. The uniform inflow model does not include a discrete wake representation, and thus provides airload variations which are related to variations of the local non-induced flow velocities, such as the one-per-rev variation in the relative combination of forward and rotational speeds and the associated blade motions. The figures show the well-known character of the uniform airload variations. That is, the low amplitude first harmonic content at low flight speed and the higher amplitude, predominantly first and second harmonic content at higher speed are evident. A local peak due to reversed flow is observed at the inboard station in Fig. 94a. When compared to the test data, it is clearly evident that the airloads predicted by the uniform inflow model are completely devoid of the airload fluctuations attributable to the wake.

The test airloads have peaks in local azimuth regions that are indicative of blade/wake interaction. These are observed for each condition in Figs. 90, 92, and 94 where they are shown to be primarily located on the lateral sides of the rotor. The severity of the local peaks are greatest for the two lower flight speed conditions (23 and 48 kt). However, local peaks, in addition to those related to the non-induced flow, are evident at the 110 kt condition where they are mainly concentrated on the advancing side of the rotor. The most obvious difference between the test airloads for 23 and 48 kts is the difference in the azimuth locations of the high loading gradients and

associated peaks. This is believed to be directly related to the azimuthal difference in blade-vortex intersection locations between the two speeds. It is shown in Figs. 80 and 82 that, at low speeds, the tip vorticies shed from the upstream edge of the rotor move above the disk and then down through it. The tip vortices thus impact the blades where they cross the disk. As mentioned earlier, this behavior has been verified experimentally. For example, for the two-bladed rotor of Ref. 6, the tip vortex from the opposite blade impacted each blade near the upstream azimuth (180 degrees) as shown in Figs. 7 and 8. For the 23 kt condition, the test airloads data appear to show that points of extreme blade-vortex interaction progressively move inward on the blade from the blade tip near 60 degrees to approximately 0.75R near 180 degrees (Fig. 90a). A similar progression takes place on the retreating side of the rotor. Similar behavior is evident at the 48 kt condition (Fig. 92a) except that it is concentrated more toward the blade tip over a smaller azimuth range on the lateral sides of the rotor. This implies that the regions of close blade-vortex interaction change accordingly. Also, near 60 and 300 degrees the tip vortices are in a more parallel alignment with the blade. For close passage regions near the tip this may lead to large airload gradients caused by the abrupt change in induced flow direction as the blade passes the vortex. The central aft region of the rotor, where the wake is displaced down from the disk, is the least affected by local wake effects. However, the integrated wake influence increases the total blade lift in this aft region.

Regarding the wake models, the figures reveal that the time histories of blade airloads progress from a smooth low amplitude harmonic variation for the classical undistorted wake to a high amplitude variation with additional harmonic content for the deformed wake models. This behavior is consistent with the increased amount of blade/vortex interaction associated with the more complex wake models.

Relative to uniform inflow results, the classical wake model improves the harmonic airload content correlation with test data. Compared to the test data, the classical wake model considerably underpredicts the amplitudes of the local airload fluctuations attributable to the wake. This is primarily due to the more distant axial coordinate positioning of the tip vortices from the rotor in regions where the distorted wake theory and limited available experimental wake geometry data from model tests indicate tip vortex distortions near the blades.

For the conditions investigated, the local measured airload fluctuations tend to average out such that, when integrated spanwise at each blade azimuth, the correlation of classical wake total blade lift with test data is much improved over the correlation of local airloads. Although improved, notable discrepancies still exist such as the 40 degree phase shift in the negative peak airloading on the advancing side.

The deformed wake models result in the best prediction of the high harmonic behavior of the airloads and the related locations of the local airload peaks and gradients with respect to the test data. This supports the contention that the local airload fluctuations are due to blade-vortex interaction. However, the amplitudes of the local airload peaks in regions of close blade-vortex passage are frequently not predicted accurately with the deformed wake models.

The harmonic content of the airloads from the generalized wake is similar to that from the predicted distorted wake, and thus the local airload fluctuations generally occur at similar azimuth locations. In some regions, notably the advancing side for the 48 kt condition, the generalized wake tends to damp out some of the excessive amplitudes of the total blade lift for the predicted distorted wake model. This may well be a fortuitous feature of the generalized wake model associated with the fact that it is a curve fit of the outstanding features of the deformed wake. However, as was noted for the representative rotor application, it is also possible for the generalized wake model to over-accentuate the local airloads for any tip vortex distortion perturbation which places the vortex closer to but beyond a vortex core distance from a blade segment center. Of course this is also possible for any distorted wake model.

The over-prediction or under-prediction of the amplitudes of the local airload peaks in regions of close blade-vortex passages are due to limitations of the close blade-vortex interaction theory, coarse discrete element blade/wake modeling, and the high sensitivity of the airloads to small blade-vortex displacements for close passages. This is exemplified by examining in greater detail the most obvious airload over-prediction at 90 degrees azimuth for the 48 kt condition (Fig. 92b). The geometric locations of the tip vortices relative to the 90 degree blade are shown in Fig. 96 for each wake model and the corresponding spanwise airload distributions are presented in Fig. 97. A rear view is presented showing axial and lateral positions of the local tip vortex filament segments that pass directly under (or over) the blade. The specific blade-vortex passage points, as observed in the top view (Fig. 82), are indicated on each segment.

From the geometry presented for the classical undistorted wake at the 48 kt condition, it is apparent that the predicted tip vortex segments are removed from the blade, and thus the related loading distribution in Fig. 97 is much smoother than those of the two deformed wake models.

For this condition, the predicted distorted wake places the tip vortex segments very close to the blade with one impacted by the blade. This is a severe situation for which no reliable blade-vortex interaction model is known to exist that adequately represents the physics of the interaction. The over-predicted amplitude of the airload peak in Fig. 92b corresponds to the peak in

Fig. 97 near 0.85R produced by the close vortex passage. In fact, a very slight displacement could reduce the peak to the test level. A local airload peak is evident in the test data nearer to the blade tip which indicates that the strong blade-vortex interaction does occur in the vicinity of the tip.

The generalized wake model for this condition under-predicts the peak tip loading. This was found to be due to the extreme proximity of the vortex segment and the preselected 0.85R blade station in the computer analysis which results in the interaction being modeled as a blade-vortex core impact with an associated severe reduction in induced velocity. In addition to limitations of the blade-vortex interaction model, the discrete blade station selection, which is somewhat arbitrary, becomes involved in the problem. For example, the aerodynamics at the 0.85R station are modeled to be representative of a finite blade segment. If the radial station had been selected to be at 0.86R, for example, the blade station would have been outside the prescribed vortex core diameter of 0.01R and a high loading peak would have been predicted. This identifies a needed refinement for such close blade-vortex encounters. Similar problems can result from coarse discrete azimuth increments.

The differences in mid-span loading between the wake models and test data at 90 degrees are also due to the close blade-vortex interaction modeling and blade-vortex displacement. A rapid change in the axial position of a vortex segment near mid-span is shown to occur in Fig. 96 for the predicted distorted wake between azimuths of 90 and 105 degrees. This rapid position change occurs slightly sooner for the generalized wake model (between 75 and 90 degrees). This, coupled with the slight but significant blade-vortex displacement differences of the adjacent inboard vortex segment, results in the mid-span loading differences in Fig. 97. It is noted that the impact of the inner vortex segment on the blade loading was much weaker than the impact of the segments at the blade tip for both distorted wake models because an analytical blade station was not as near the impact point. This further exemplifies the problem with discrete point modeling. If the inflow points on the lifting line were repositioned, the loading response could be altered. The response could be improved or degraded depending on the selection of the inflow points.

The above examples have served to demonstrate that close blade-vortex interactions do occur in forward flight and that there is a high degree of sensitivity of predicted blade airloads to wake geometry and blade-vortex interaction modeling in regions of close proximity of rotor and wake.

The observed trend with advance ratio is that differences between the airloads of the three wake models decrease with increasing advance ratio. This characteristic is consistent with the increased influence of the non-induced airflow, the decreased number of blade-vortex passages, the decreased amplitude of tip vortex distortions, and the increased rotor-wake displacement

due to increased rotor tilt and high forward speed. However, at the highest selected advance ratio condition (0.29), the peak-to-peak amplitudes of the local airloads predicted with the three wake models are shown in Fig. 94 to be subdued on the advancing side of the rotor relative to the test amplitudes. This implies that for this 110 kt condition, wake distortions are still significant and the predicted wake may not be sufficiently close to the advancing side of the rotor.

In summary, the test airloads of the three selected conditions generally lie between the airloads predicted by the classical undistorted wake model and the deformed wake models. All of the local airloading results clearly show that the use of a distorted wake inflow model is needed for improved correlation over the uniform inflow results. However, the results also indicate that the current aerodynamic interaction models still need to be refined to some degree. The use of a uniform inflow model will not yield the correct local blade airloading or integrated spanwise airloadings. This lack of correlation is the least at the highest advance ratio, but the correlation is still lacking in the details of the problem. The classical wake results are clearly an improvement over the uniform inflow results, especially on an integrated spanwise load basis. However, this just demonstrates the fact that the integrated results can mask pertinent local features of any prediction analysis. The local airloading results clearly illustrate deficiencies in the classical wake results as compared with the test measurements. The distorted wake model offers an improvement in the local airload prediction capabilities, particularly in locating the airload fluctuations. However, the amplitudes are often overpredicted. The generalized wake results tend to mimic the distorted wake results as they should, but the slight variations in the tip vortex locations between the two models sometimes result in significant local loading amplitude differences. These local loading differences can translate into noticeable variations between the models for the integrated spanwise loading results. Also, the differences are amplified by the current close blade-vortex interaction modeling, and the discrete modeling of the blades and wake.

H-34 Blade Bending Moments

Another measure of the predictive accuracy of the wake/inflow models is the comparison of measured and predicted bending moments. Bending moment time histories are directly dependent on the harmonic variation of the spanwise distribution of the airloads along the blade induced by the flow field. Figures 98 through 100 present the flatwise bending moments at several spanwise locations on the blades, as predicted for the different wake/inflow models, compared with test data for the various advance ratio conditions studied, low to high advance ratio respectively. The Y200 Aeroelastic Rotor Analysis was used for the bending moment prediction. Overall, for all three conditions, the results indicate that the general character of the flatwise

bending moments is significantly better predicted using the predicted distorted wake inflow model as opposed to the classical wake results. However, local peaks tend to be out of phase and/or exaggerated at some locations when using the distorted wake model. The peak-to-peak bending moments are generally underpredicted using the classical wake inflow model at the lower speeds as compared with the test measurements. This is an important limitation for stress analysis. The best correlation in peak-to-peak bending moments is obtained at the lowest advance ratio (0.064) using the distorted wake model. The correlation in terms of peak-to-peak variation at this advance ratio is quite good as can be seen in Fig. 98. At the 0.129 advance ratio the distorted wake model predictions still provide the best correlation with test results in peak-to-peak amplitude, but the predicted results are now lower than the test results as shown in Fig. 99. At the highest advance ratio, 0.29, the character of the azimuth variation of bending moment is predicted with the distorted wake model, but the peak-to-peak moment is overpredicted, as shown in Fig. 100.

Although the need for further analytical refinement is evident, the degree to which the distorted wake model was able to reproduce the measured bending moment distributions is encouraging and indicative that, with future emphasis on blade-vortex interaction modeling, distorted wake methodology will provide an improved predictive tool for blade stress analysis.

Exploratory Blade-Vortex Interaction Study

The accurate prediction of helicopter rotor blade airloading has been a continuing but elusive goal in the helicopter industry. Of the numerous phenomena influencing rotor airloads that require further research, a primary one is blade-vortex interaction. For many flight regimes the tip vortices from the main rotor blades can pass sufficiently close to, or even impact, following blades such as to produce a complex flow environment which influences both the local blade airloading and the vortex characteristics in a currently unpredictable manner. Several investigators have addressed this problem, but much still remains to be learned of the fundamentals of this phenomenon before it can be accurately modeled in airload methods.

The occurrence and importance of blade-vortex interaction and the requirement for improved modeling in rotor analyses are documented in numerous references. For example, survey papers on rotor aerodynamics, such as Refs. 1 and 34 through 36, all point this out. Johnson in Ref. 37 showed that a lifting surface representation for the blade succeeded in reducing the overpredicted loading peaks. However, he also concluded that a very accurate vortex model and wake geometry is required when the vortex is close to a

blade. That is, the vortex structural characteristics should be accurately represented. Such features as vortex core size, vortex bursting propagation, and local blade wake-tip vortex interaction (effects of the interaction on vortex geometry and blade aerodynamics) should be considered. The requirement for such considerations are consistent with the findings from UTRC wake studies listed in the References.

The requirement for improved vortex core modeling in wake/airloads methods was addressed by Scully in Ref. 15 with his distorted wake analysis. He found that the use of a sufficiently large tip vortex core radius reduced the distorted wake induced airloads. However, the vortex core radius required to achieve this result was much larger than that observed experimentally. This led to the concept of including tip vortex-core bursting due to a close blade-vortex interaction in the analytical vortex model. A hypothetical model of vortex bursting was generally successful in reducing the distorted wake airloads to levels approximating those of measured airloads.

Considering that the model based on the propagation of vortex-core bursting was speculative, as recognized by Scully, Ham in Ref. 38 hypothesized that local blade separation induced by a vortex in the vicinity of the blade limits the maximum incremental airload due to close blade-tip vortex interaction. He performed an experiment to study blade-vortex interaction by subjecting the mid-section of a pressure-instrumented airfoil, mounted horizontally and perpendicular to the wind-tunnel airstream, to the impingement of a vortex moving periodically in the vertical plane from a point below the airfoil to a point above the airfoil and back again. This investigation was limited to nearly right angle intersections between the blade and airfoil. The results of this investigation, reported in Ref. 39, indicated that the maximum vortex-induced lift coefficients are of the order of 0.2 to 0.3. The vortex-induced peak loadings were found to be independent of the frequency of vortex impingement (i.e., vortex approach velocity), proportional to vortex strength, and only weakly dependent upon the airfoil angle of attack and angle of yaw. He noted that these results have important implications with respect to predictions of the unsteady loading on helicopter rotor blades due to blade-vortex interaction. They show that the maximum incremental lift coefficients induced on the blade by a returning tip vortex may be limited to values of the order of 0.3 or less, and may be relatively unaffected by vortex approach velocity, blade mean lift coefficient, or blade radial flow. Although Ham's results are significant in identifying local vortex-induced blade separation as a potential mechanism, additional fundamental studies remain to be conducted to demonstrate this for a helicopter rotor.

As has been noted herein in the example conditions investigated, the local blade loading is predicted to be significantly influenced by the induced inflow of a near tip vortex. As indicated by comparison with H-34 rotor test data, this induced influence is over-predicted for many of these encounters. The analytical formulation for this investigation was based on quasi-steady aerodynamics, a lifting line/2D airfoil data representation of the blade, and a simple vortex model. Lifting surface models, when applied to close blade-vortex encounters, will distribute the induced influence over the blade surface rather than concentrate it at coarsely selected collocation points. However, current inviscid lifting surface models are not sufficient for close blade-vortex interaction modeling because nonlinear viscous phenomena, such as local blade stall due to vortex induced separation, are neglected. The simple vortex model used for the airload comparisons presented herein is based on potential flow theory for the induced flow outside a vortex core of prescribed diameter which was selected without regard to the influence of a close blade passage (no vortex core expansion, bursting, etc.). Recognizing that the development of a consistently accurate and physically representative analytical blade-vortex interaction model is the subject of ongoing and future studies, a simple blade-vortex interaction model was used herein to demonstrate the limitations. However, an exploratory study of an empirical blade-vortex interaction model was also performed as described below.

An exploratory blade-vortex interaction model was hypothesized based on the above mentioned empirical results obtained by Ham which indicated a limiting change in the lift coefficient ($\Delta C_{\ell} = 0.2$ to 0.3) due to the presence of an isolated vortex near a fixed wing in a wind tunnel (Ref. 39). The limit in the change in lift coefficient is attributed to the flow separating on the blade in the presence of the vortex. Although the fixed wing/vortex interaction, as tested in Ref. 39, is not completely representative of unsteady vortex encounters which occur for a rotor, it is supportive of the hypothesis of including a limit in the change in local blade section lift coefficient in the rotor analysis. Thus, a blade-vortex interaction model was incorporated in the Prescribed Wake Rotor Inflow Program (F389SR) and the Generalized Rotor Performance Analysis (GRP) which allows the user to prescribe the allowable change in blade section lift coefficient per change in blade azimuth position. The limit on the change in lift coefficient was formulated in the analysis in a manner such that the change is applied only to the portion of the local lift due to the vortex induced flow field as it changes with blade azimuth. The analytical model does not identify individual vortex encounters, but assumes that a rapid change in the local induced inflow which produces the lift coefficient change is primarily attributable to an individual vortex encounter.

In a brief exploratory investigation, the empirical blade-vortex interaction model was applied to the 0.129 advance ratio condition for the H-34 rotor using the predicted distorted wake geometry and several different prescribed limits for the change in lift coefficient per change in azimuth position (0.1 to 0.3 per 15 degree azimuth increment). The resulting air load predictions are compared with test data and the previously presented results with no lift coefficient limit in Figs. 101 and 102. As anticipated, application of the new blade-vortex interaction limit model, hereafter "the BVI limit model", did result in decreasing the local airload peaks on the advancing side of the rotor where close blade-vortex passages were predicted (Fig. 42). The BVI limit of 0.2 generally produced predicted airloads which compared most favorably with the test airloads, particularly the local airloads in Fig. 101. The peak amplitude of the spanwise integrated airloading on the advancing side was improved but still somewhat over-predicted (Fig. 102). A BVI limit of 0.1 reduced the local airloads more severely than required to meet the test levels on the retreating side of the rotor disk. Overall, the BVI limit model succeeded in modifying the amplitudes of the peak airloads on the advancing side, but improvement of the general airload distribution is not evident. In particular, the correlation between test results and the predicted results on the retreating side was degraded. Additional brief investigations, in which the BVI limit model was applied for the generalized wake geometry and a lower advance ratio condition (0.064), produced airload changes which were inconsistent in their degree of correlation with test data.

Because of the degradation of the correlation on the retreating side of the rotor disk with the "BVI limit model", further investigation of the H-34, 0.129 advance ratio condition was performed using other BVI models. First, the interaction model of Johnson (Refs. 17 and 37) was used. This model is based on the ratio of lifting surface to lifting line solutions for an infinite span fixed wing model interacting with an infinite vortex filament at variable planform intersection angles and axial displacements. It is then applied to the lifting line solution for helicopter rotors. The ratio obtained from the fixed wing solution for comparable planform intersection angles and axial displacements in the rotor case is used to scale the local vortex segment induced velocity influence. This model was incorporated into the available inflow analysis and applied to the above condition using the predicted distorted wake geometry. The results of the application of this model to the above case had very little effect on the local airloads. The large airloading spike in Fig. 101a for the distorted wake model was not significantly altered. However, it is recognized that the results from this limited study of one rotor condition are not necessarily conclusive. In order to more accurately account for the blade-vortex interaction in the wake/airflow/airloads analyses a finer numerical grid in the region of the interaction may be necessary.

A final model was used based on introducing a large vortex core radius applied to the individual vortex segments influence, inside which the influence is assumed to be zero. This model could be considered as a hypothetical representation of a burst vortex. For example, vortex bursting was previously simulated in Ref. 38. The vortex core radius was assumed to be .03R (approximately one-half chord) to ensure that the close blade/vortex interaction occuring near the 90 degree azimuth position at approximately .85R on the blade (Fig. 96) would be nullified. It is recognized that the vortex bursting concept as applied to the rotor blade-vortex interaction has not been fully explored experimentally. Also, the choice of vortex core radius in the wake model is clearly arbitrary at this stage. The results of the application of this model are shown in Fig. 103 for the airloading and Fig. 104 for the integrated blade loading which can be compared with the results of Fig. 101 and 102. This model improved the airload correlation by reducing the local airloading on the advancing side of the rotor disk without strongly influencing the solution on the retreating side.

In summary, this brief limited scope study of these BVI interaction models indicates the need for continued activity toward the development and evaluation of a blade-vortex interaction model which can consistently produce accurate blade airload predictions when a blade is subject to close vortex encounters.

CONCLUDING REMARKS

1. Generalized Wake Model - A first level generalized wake model was developed for a helicopter rotor operating in steady level forward flight based on theoretically predicted wake geometries. The generalized wake model consists of equations for wake geometry in which tip vortex distortions are generalized as displacements from the classical undistorted tip vortex geometry. The equations are focused on the predominant distortions normal to the rotor disk. In the generalized tip vortex geometry equations, the locations of points on a tip vortex are defined in terms of tip vortex age and blade azimuth, and the coefficients of the distortion functions in the equations are dependent on rotor advance ratio, thrust coefficient, and number of blades. It was shown that rotor disk attitude, a recognized parameter for the undistorted wake coordinates, is not a significant parameter for the incremental tip vortex distortions. For typical operating conditions, for this initial generalization, the rotor operating condition parameters were emphasized, and a representative untapered blade design with a linear twist of -10 degrees and a blade aspect ratio of 16 was used. A limited study indicated that tip vortex geometry is sensitive to twist variations but insensitive to aspect ratio variations. Rotor wake geometry generalization for forward flight should proceed beyond this initial first level generalization to extend the range of operating and blade design parameters and to refine the generalization as experimental data and improved wake methodology, particularly for blade-vortex interaction, become available.

2. Generalized Wake Program Module - The generalized wake equations for forward flight were programmed in a generalized wake subroutine which can be used to expediently generate wake coordinates for use with airflow and airloads prediction computer programs. Numerical interpolation procedures are provided in this generalized wake module to acquire wake coordinates for user selected combinations of advance ratio, thrust coefficient, disk attitude, and number of blades. Although tip vortex coordinates can be generated for any combination of these parameters, emphasis in the generalization was placed on advance ratios between 0.05 and 0.3 and thrust coefficients between 0.0025 and 0.0075 for two- and four-bladed rotors. The computer time requirement for application of the generalized wake module to generate tip vortex coordinates is insignificant relative to the large requirement of a freely distorting wake geometry prediction analysis.

3. Wake Geometry Charts - A set of wake geometry charts were developed which provide a convenient, readily accessible source for approximating rotor forward flight wake geometry and identifying potential locations of close blade-vortex passage. The charts are presented as a self-contained

reference in Volume II of this report. Charts for both the classical undistorted wake model and the generalized distorted wake model are included. The charts provide the necessary information to determine tip vortex coordinates for a range of parameters sufficient for most conventional steady level flight operating conditions. They can be used for a variety of applications which require the geometric relationship between the tip vortices and spatial locations relative to the rotor blades and other helicopter components. In particular, blade/tip vortex interaction locations and rotor wake boundaries can be rapidly defined. Sample three-views and isometric views of tip vortex patterns for two- and four-bladed rotors are also included.

4. Tip Vortex Geometry and Influence on Airloads, Performance, and Bending Moments - Tip vortex geometry and the sensitivity of predicted rotor airloads and related rotor performance and blade bending moments to various rotor inflow and wake geometry models were demonstrated for forward flight conditions. The inflow/wake models consisted of uniform rotor inflow and variable inflow based on classical undistorted wake geometry, predicted distorted wake geometry, and the newly developed generalized wake geometry. The principal findings of this analytical study are:

   - Although sufficient experimental data is not available for a point-by-point comparison of measured and predicted forward flight wake geometry, the characteristic wake distortion features observed from test results are present in the predicted and generalized tip vortex geometries. Relative to the classical undistorted wake model, the forward and lateral sides of the wake are predicted to be distorted toward the rotor. This results in the prediction of close blade-vortex passages for typical low and moderate flight speed conditions which introduce high harmonic content and severe local spanwise gradients in blade airloads which are not predicted with the uniform inflow model and the undistorted wake model.

   - Advance ratio, thrust coefficient, disk attitude and number of blades determine the classical undistorted wake geometry in forward flight based on momentum considerations. Tip vortex distortions from the undistorted wake geometry were predicted to be most sensitive to advance ratio variations and are insensitive to disk attitude variations. Unlike the hovering condition, for which the tip vortex coordinates are blade loading (C_T/b) dependent, the forward flight wake is predicted to be more disk loading (C_T) dependent. The amplitude of the tip vortex distortions are proportional to thrust coefficient, but the characteristic shape of the principal distortions are insensitive to thrust coefficient.

- The influence of wake distortion on blade airloads is related to the degree of proximity of the tip vortices to the rotor and the number of close blade-vortex passages. For steady level flight, the wake influence on blade airloads generally increases with decreasing advance ratio, decreasing disk attitude and increasing number of blades. Increasing thrust coefficient increases the undistorted wake deflection angle away from the rotor but also increases the distortions of the tip vortices towards the rotor, and thus the influence of thrust coefficient on blade airloads is not necessarily as consistent as the other parameters. The wake distortions and related airload influence are most complex at low advance ratios (e.g., 0.05) where the difficulty of accurate wake geometry and airloads prediction is compounded by the large number of close blade-vortex passages and the movement of the tip vortices above and then down through the rotor disk resulting in blade-vortex impingement.

- The prediction of tip vortex distortions which are in close proximity to the blades at localized regions of the rotor results in a high sensitivity of predicted airloads to small differences in tip vortex geometry. For such conditions, differences were observed between the airload predictions of the generalized and predicted distorted wake models even when the predicted wake geometry was well approximated by the generalized wake model. The occurrence of close blade-vortex passages, and the high sensitivity of blade airloads to small deviations of blade station to tip vortex distance in the airloads analysis, demonstrate the requirement for an improved blade-vortex interaction model and further refinement of wake geometry prediction and generalization techniques. Fundamental experimental and theoretical studies of blade-vortex interaction involving vortex structure and blade surface flow separation influences are required to provide a physically accurate, and dependable blade-vortex interaction model for incorporation in rotor wake and airloads methodology. Attention must also be given to the elimination of analytical modeling inaccuracies due to discrete blade segment modeling and discrete time steps in the vicinity of close blade-vortex passages.

- Regarding rotor performance prediction, the classical undistorted wake calculation of rotor power for constant thrust was consistently higher than the uniform inflow calculation. Previous investigations have indicated that this increase induced power results in improved correlation with test data. The calculated power values from the predicted distorted and generalized wake models were scattered about the classical wake values with no well defined trend. The consideration of

wake distortions is necessary for the prediction of rotor control angles at low speed. Although the need for further analytical refinement is evident, the degree to which the distorted wake model was able to reproduce the measured airload and bending moment distributions is encouraging and indicative that, with future emphasis on blade-vortex interaction modeling, distorted wake methodology has the potential to provide an accurate predictive tool for blade airload and stress analysis.

REFERENCES

1. Landgrebe, A. J., and M. C. Cheney, Jr.: Rotor Wakes - Key to Performance Prediction, Presented at the Symposium on Status of Testing and Modeling Techniques for V/STOL Aircraft, Mideast Region of the American Helicopter Society, October 1972; also, Aerodynamics of Rotary Wings, AGARD CP-111, February 1973, pp. 1-1 - 1-9.

2. Landgrebe, A. J., and T. A. Egolf: Rotorcraft Wake Analysis for the Prediction of Induced Velocities. USAAMRDL TR-75-45, January 1976. (Available from DTIC as AD A021 202.)

3. Landgrebe, A. J., and T. A. Egolf: Prediction of Helicopter Induced Flow Velocities Using the Rotorcraft Wake Analysis. Proceedings of the 32nd Annual National V/STOL Forum, American Helicopter Society, May 1976. Preprint No. 1002.

4. Landgrebe, A. J.: An Analytical Method for Predicting Rotor Wake Geometry, Jl. American Helicopter Society, Vol. 14, No. 4, October 1969.

5. Landgrebe, A. J., and E. D. Bellinger: An Investigation of the Quantitative Applicability of Model Helicopter Rotor Wake Patterns Obtained from a Water Tunnel, USAAMRDL TR-71-69, December 1971. (Available from DTIC as AD 739 946.)

6. Landgrebe, A. J., R. B. Taylor, T. A. Egolf, and J. C. Bennett: Helicopter Airflow and Wake Characteristics for Low Speed and Hovering Flight from Rocket Interference Investigations, Proceedings 37th Annual Forum, American Helicopter Society, May 1981, pp. 51-65; also, Journal of the American Helicopter Society, Vol. 27, No. 4, October 1982.

7. Landgrebe, A. J., and T. A. Egolf: Prediction of Rotor Wake Induced Flow Velocities Along the Rocket Trajectories of an Army AH-1G Helicopter. Picatinny Arsenal Technical Report 4797, U.S. Army Picatinny Arsenal, Dover, N.J., March 1975. (Available from DTIC as AD A007 878.)

8. Landgrebe, A. J., R. C. Moffitt, and D. R. Clark: Aerodynamic Technology for Advanced Rotorcraft. Journal American Helicopter Society, Vol. 22, Nos. 2 and 3, April and July 1977 -- Parts I (pp. 21-27) and II. Also, Proceedings of Symposium on Rotor Technology, American Helicopter Society, August 1976.

9. Landgrebe, A. J.: An Analytical and Experimental Investigation of Helicopter Rotor Hover Performance and Wake Geometry Characteristics. USAAMRDL TR-71-24, U.S. Army, June 1971. (Available from DTIC as AD 728 835.)

10. Landgrebe, A. J.: The Wake Geometry of a Hovering Helicopter Rotor and Its Influence on Rotor Performance, Journal of the American Helicopter Society, Vol. 17, No. 4, October 1972 (Also Preprint No. 620, 28th Annual National Forum of the American Helicopter Society, May 1972.)

11. Kocurek, J. D., and J. L. Tangler: A Prescribed Wake Lifting Surface Hover Performance Analysis, Presented at the 32nd National V/STOL Forum of the American Helicopter Society, Washington, D.C., May 1976, Preprint No. 1001.

12. Johnson, W.: A Lifting-Surface Solution for Vortex-Induced Airloads, AIAA Journal, Vol. 9, No. 4, April 1971, pp. 689-695.

13. Summa, J. M., and D. R. Clark: A Lifting-Surface Method for Hover/Climb Airloads, Preprint No. 79-3, Presented at the 35th Annual National Forum of the American Helicopter Society, Washington, D.C., May 1979.

14. Sadler, G. S.: Development and Application of a Method for Predicting Rotor Free Wake Position and Resulting Rotor Blade Air Loads. Volume I - Model and Results. NASA CR-1911, December 1971.

15. Scully, M. P.: Computation of Helicopter Rotor Wake Geometry and its Influence on Rotor Harmonic Airloads, M.I.T. Aeroelastic and Structures Research Laboratory, ASRL-TR-178-1, March 1975.

16. Crimi, P.: Prediction of Rotor Wake Flows. Aerodynamic Problems Associated with V/STOL Aircraft. CAL/USAAVLABS Symposium Vol. I - Propeller and Rotor Aerodynamics, Cornell Aeronautical Lab., Inc., and U.S. Army Aviat. Mater. Lab., June 1966.

17. Johnson, W.: A Comprehensive Analytical Model of Rotorcraft Aerodynamics and Dynamics. Part 1: Analysis Development. NASA TM-81182, AVRADCOM TR-80-A-5, 1980.

18. Biggers, J. C., A. Lee, K. L. Orloff, and O. J. Lemmer: "Measurements of Helicopter Rotor Tip Vortices," 33rd Annual National Forum of the American Helicopter Society, Washington, D.C., May 1977.

19. Johnson, W.: Comparison of Calculated and Measured Model Rotor Loading and Wake Geometry. NASA TM-81189, AVRADCOM TR-80-A-4, April 1980.

20. Lehman, A. F.: Model Studies of Helicopter Rotor Flow Patterns, 24th Annual Forum of the American Helicopter Society, Paper No. 207, May 1968. Also, Report with same title: USAAVLABS Technical Report 68-17, April 1968.

21. Egolf, T. A., and A. J. Landgrebe: A Prescribed Wake Rotor Inflow and Flow Field Prediction Analysis - User's Manual and Technical Approach. NASA CR-165894, June 1982.

22. Piziali, R. A., and F. A. Duwaldt: A Method for Computing Rotary Wing Airload Distributions in Forward Flight, TREC Tech. Rep. 62-44, U.S. Army, November 1962.

23. Miller, R. H.: On the Computation of Airloads Acting on Rotor Blades in Forward Flight, Journal of the American Helicopter Society, Vol. 7, No. 2, April 1962.

24. Loiselle, James, W.: Generalized Rotor Performance Predictions. NAVAL Post Graduate School, Monterey, CA, September 1977. (Available from DTIC as AD A046 368.)

25. Bailey, F. J.: A Simplified Method of Determining the Characteristics of a Lifting Rotor in Forward Flight. NACA Report 716, 1941.

26. Arcidiacono, P. J.: Prediction of Rotor Instability at High Forward Speeds. Vol. I, Differential Equations of Motion for a Flexible Helicopter Rotor Blade in Steady Flight Including Chordwise Mass Unbalance Effects. USAAVLABS Technical Report 68-18A, U.S. Army, February 1969. (Available from DTIC as AD 685 860.)

27. Bergquist, R. R., et. al.: User's Manual for the Coupled Mode Version of the Normal Modes Rotor Aeroelastic Anaysis Computer Program. NASA CR-137899, 1974.

28. Blackwell, R. H.: Investigation of the Compliant Rotor Concept, Sikorsky Aircraft Division, United Technologies Corporation, USAAMRDL TR 77-7 Eustis Directorate, USAAMRDL, Fort Eustis, VA, June 1977. (Available from DTIC as AD A042 338.)

29. Blackwell, R. H., and D. J. Merkley: The Aeroelastically Conformable Rotor Concept. Preprint No. 78-59, American Helicopter Society, 34th Annual National Forum, May 1978.

30. Harris, F. D.: Articulated Rotor Blade Flapping Motion at Low Advance Ratio. Journal of the American Helicopter Society, Vol. 17, No. 1, January 1972.

31. Scheiman, J.: A Tabulation of Helicopter Rotor-Blade Differential Pressures, Stresses, and Motions as Measured in Flight. NASA TM X-952, March 1964.

32. Rabbott, Jr., J. P., A. A. Lizak, and V. M. Paglino: A Presentation of Measured and Calculated Full Scale Rotor Blade Aerodynamic and Structural Loads, USAAVLABS TR 66-31, July 1966. (Available from DTIC as AD 639 981.)

33. Johnson, W.: Comparison of Calculated and Measured Helicopter Rotor Lateral Flapping Angles. Journal of the American Helicopter Society, Vol. 26, No. 2, April 1981.

34. Ward, J. F., and W. H. Young: A Summary of Current Research in Rotor Unsteady Aerodynamics with Emphasis on Work at Langley Research Center, Proceeding of AGARD, CP-111, 1972.

35. Johnson, W.: Comprehensive Helicopter Analyses: A State-of-the-Art Review. NASA TM-78539, AVRADCOM TR-78-56, November 1978.

36. Johnson, W., and M. P. Scully: Aerodynamic Problems in the Calculation of Helicopter Airloads, Presented at the Symposium on Status of Testing and Model Techniques for V/STOL Aircraft, Mideast Region, American Helicopter Society, Philadelphia, Pennsylvania, October 26-27, 1972.

37. Johnson, W.: Application of a Lifting-Surface Theory to the Calculation of Helicopter Airloads, Preprint No. 510, Presented at the 27th Annual National V/STOL Forum of the American Helicopter Society, Washington, D.C., May 1971.

REFERENCES (Cont'd)

38. Ham, N. D.: Some Preliminary Results from an Investigation of Blade-Vortex Interaction. Journal of the American Helicopter Society, April 1974.

39. Ham, N. D.: Some Conclusions from an Investigation of Blade-Vortex Interaction. Journal of the American Helicopter Society, October 1975.

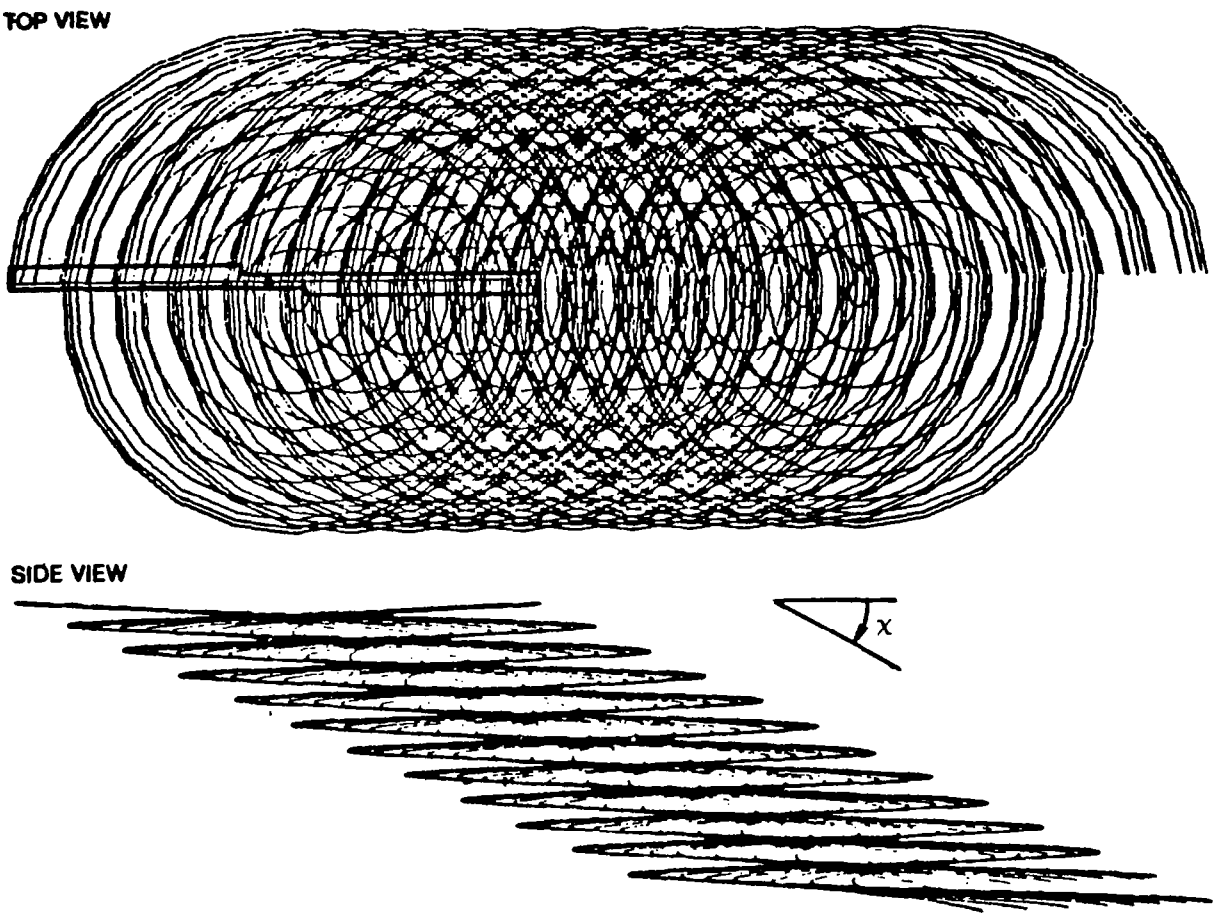

FIGURE 1. COMPUTER WAKE REPRESENTATION-CLASSICAL UNDISTORTED WAKE

4-bladed rotor Advance ratio = 0.1 $C_T = 0.008$ $\alpha_{TPP} = -1°$
Generalized wake from UTRC rotor wake geometry analysis

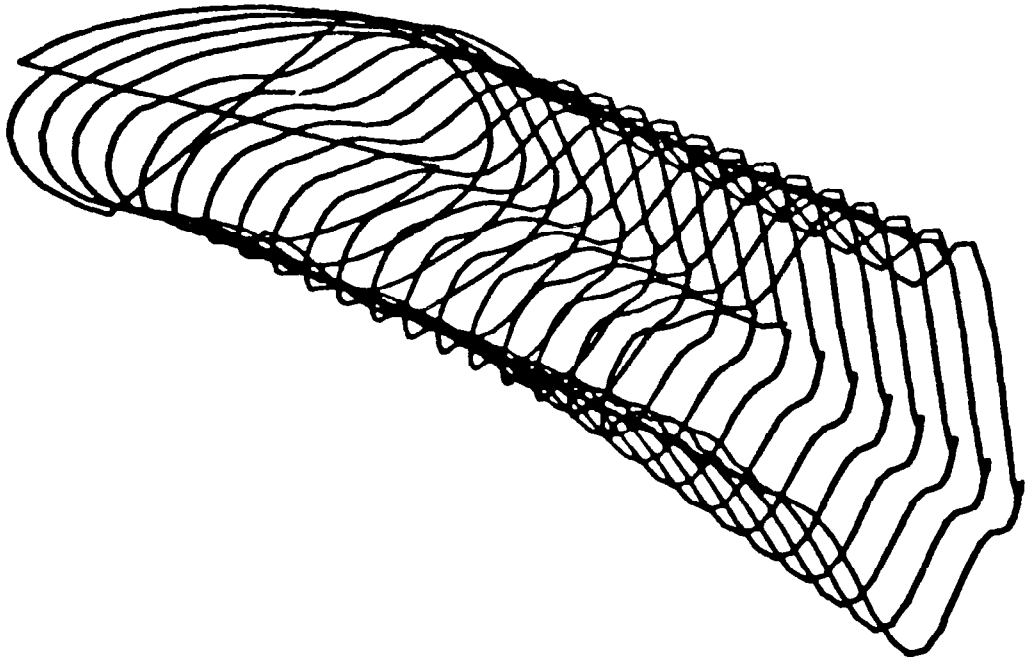

FIGURE 2. ISOMETRIC VIEW OF HELICOPTER TIP VORTICES

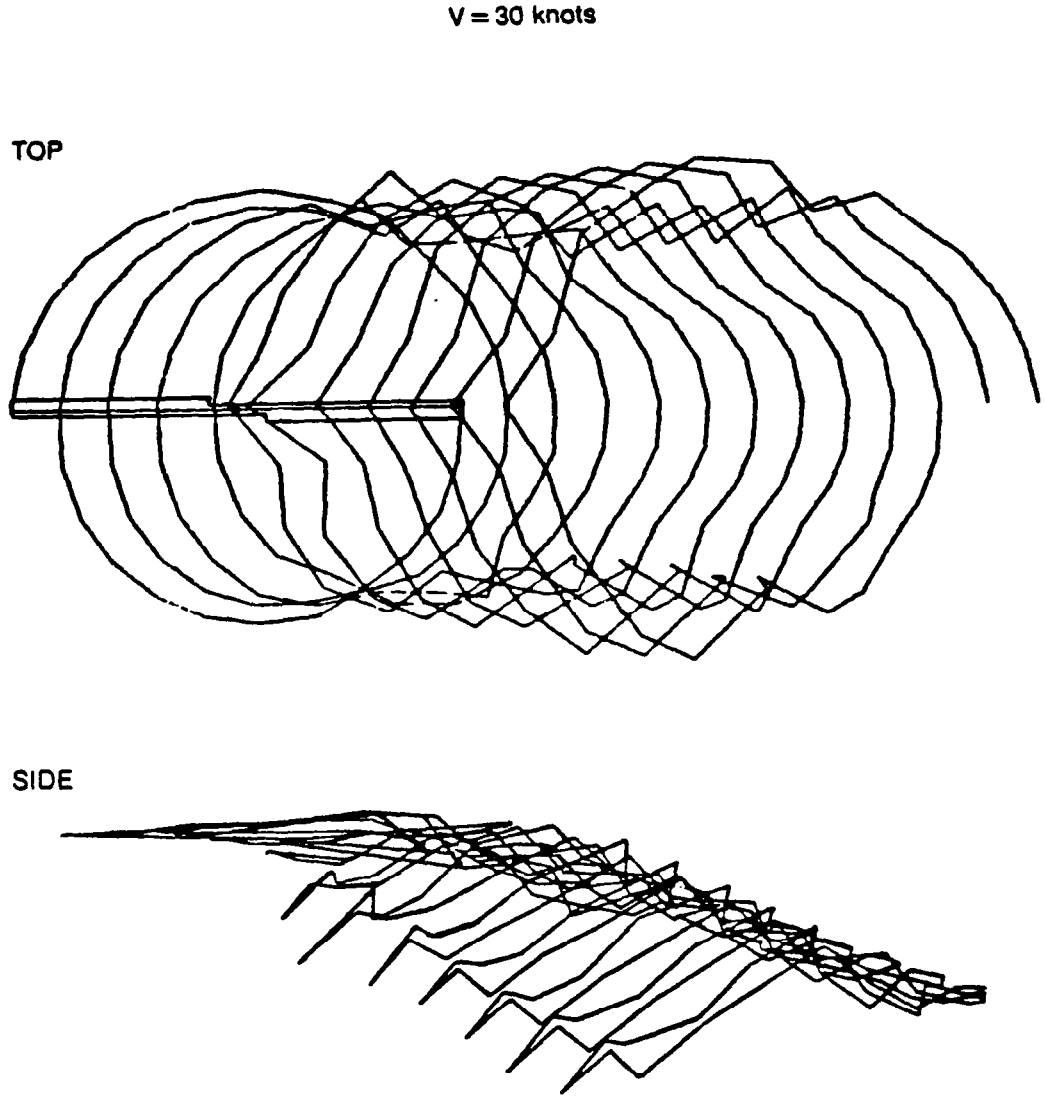

FIGURE 3. PREDICTED TIP VORTEX GEOMETRY FROM UTRC ROTOR WAKE GEOMETRY ANALYSIS

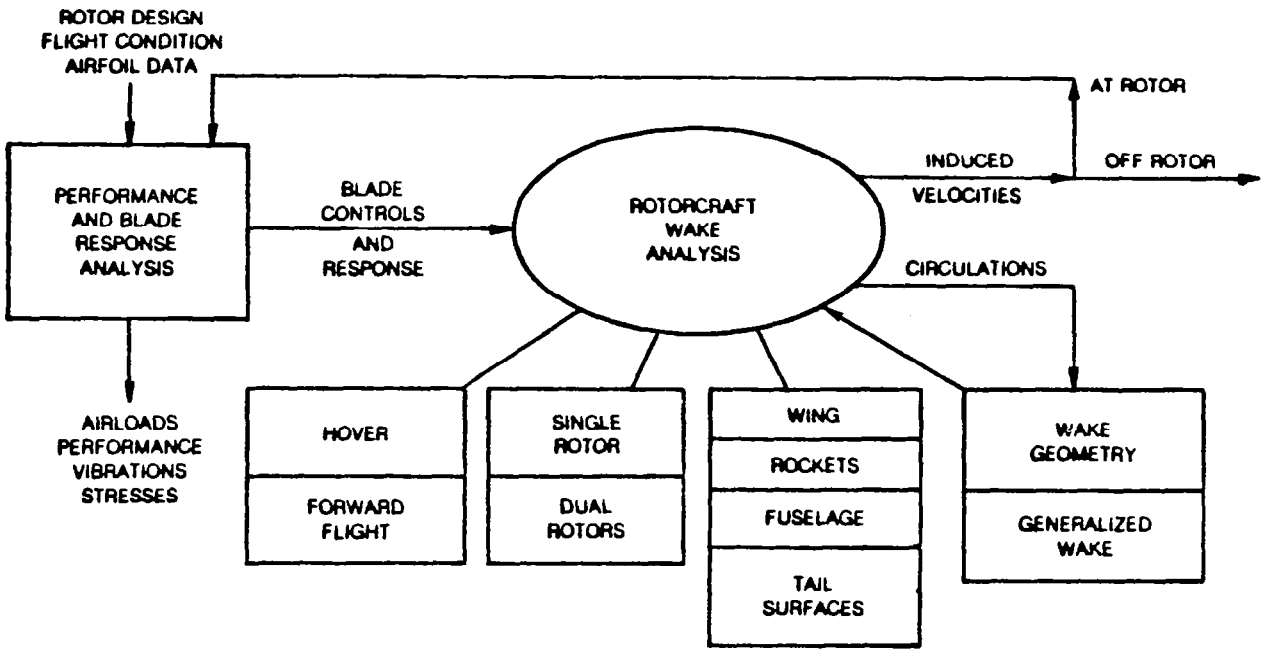

FIGURE 4. UTRC ROTORCRAFT WAKE ANALYSIS

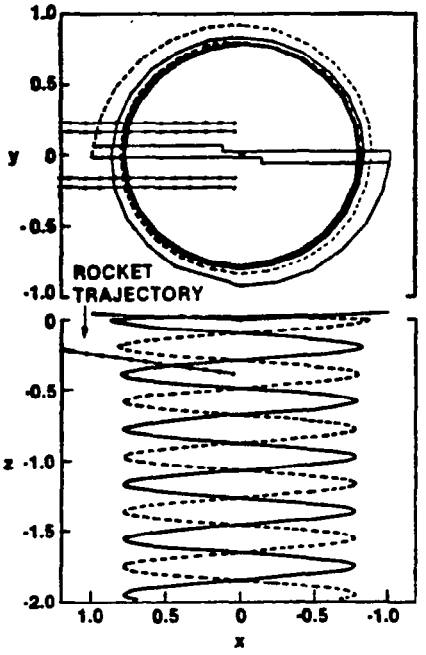

Tip vortex geometry for the hovering condition.

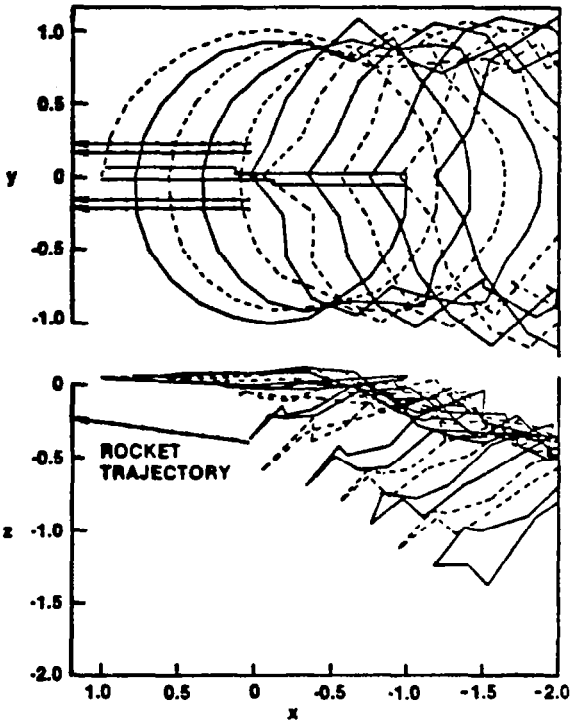

Predicted tip vortex geometry for the 30 kt flight condition.

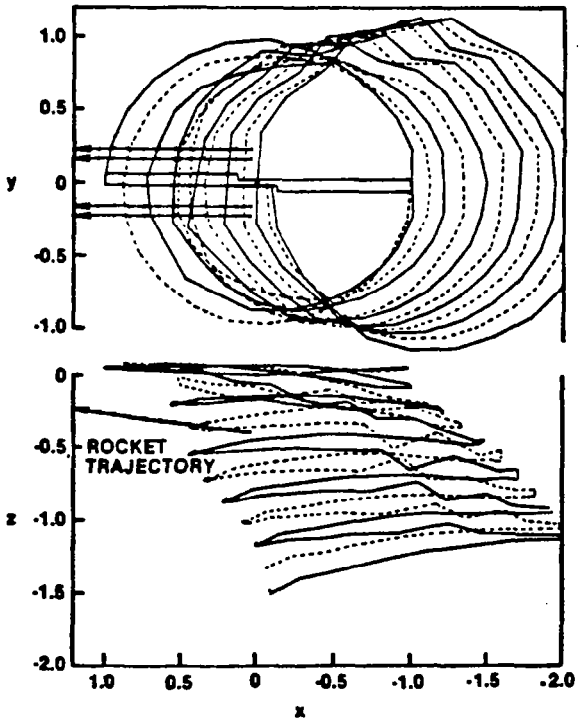

Predicted tip vortex geometry for the 15 kt flight condition.

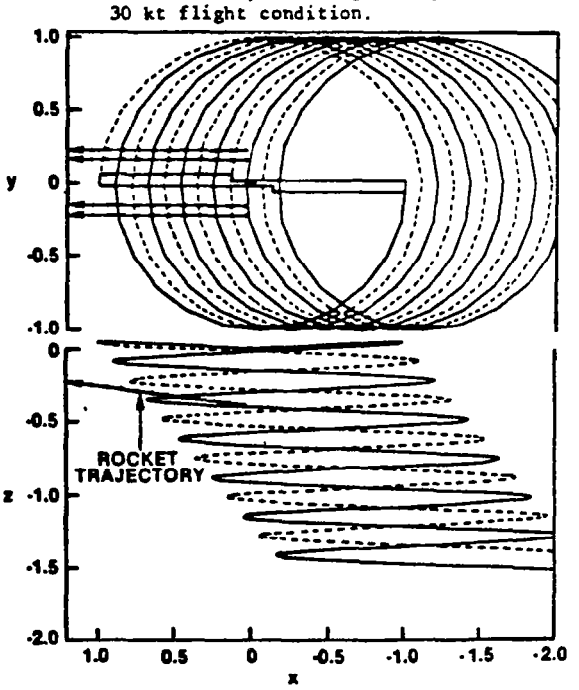

Undistorted tip vortex geometry for the 15 kt flight condition.

FIGURE 5. WAKE GEOMETRY FOR LOW SPEED CONDITIONS
(REPRODUCED FROM REF. 6)

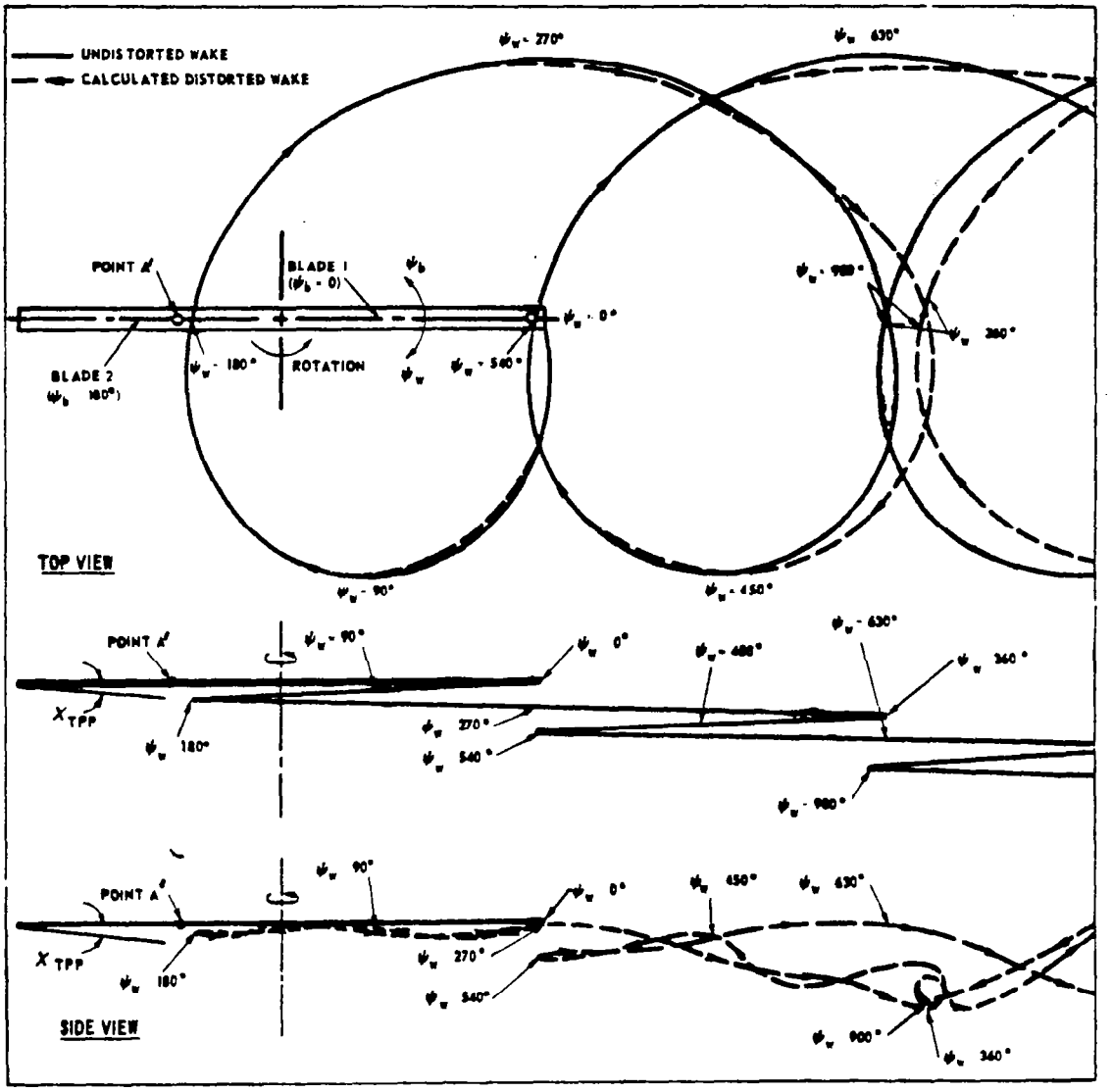

FIGURE 6. THEORETICAL WAKE PATTERN FROM ONE BLADE OF AN UH-1A ROTOR, V=89 KT, μ=0.21, C_T=0.0037 (REPRODUCED FROM REF.5)

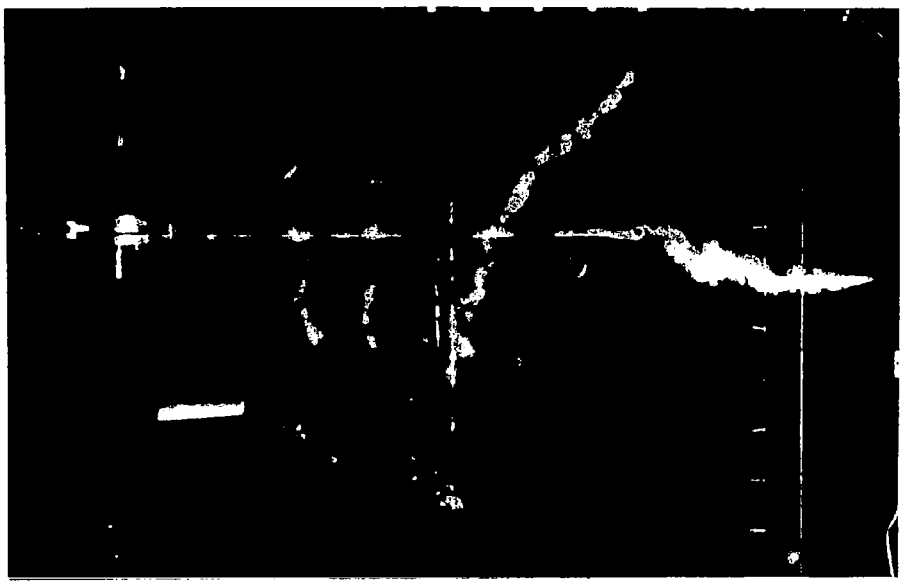

V = 0 (HOVER)

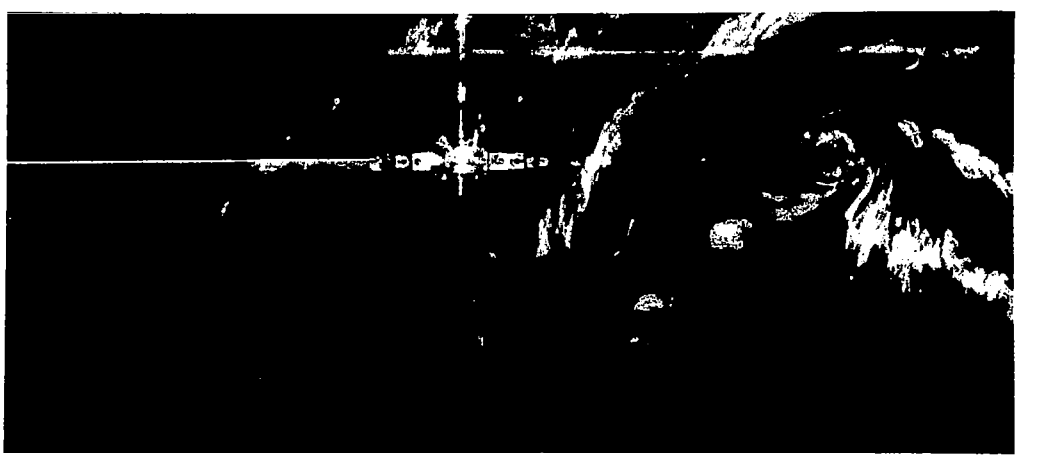

V = 15 KTS

FIGURE 7. SMOKE FLOW VISUALIZATION OF ROTOR WAKE FOR HOVER AND LOW SPEED FORWARD FLIGHT. (REPRODUCED FROM REF. 6)

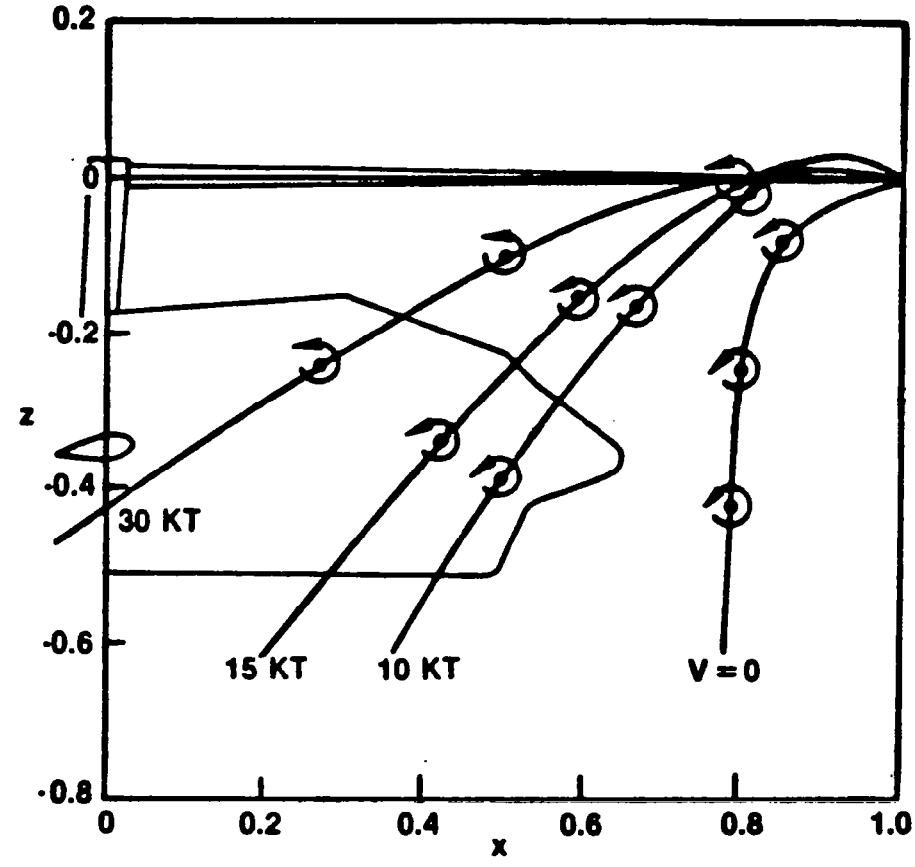

TIP VORTEX CROSS SECTIONS WHEN BLADES ARE AT 0,180 DEGREES AZIMUTH.

FIGURE 8. COMPARISON OF MEASURED ROTOR WAKE BOUNDARIES AND TIP VORTEX LOCATIONS FOR HOVER AND LOW SPEED FLIGHT (REPRODUCED FROM REF. 6)

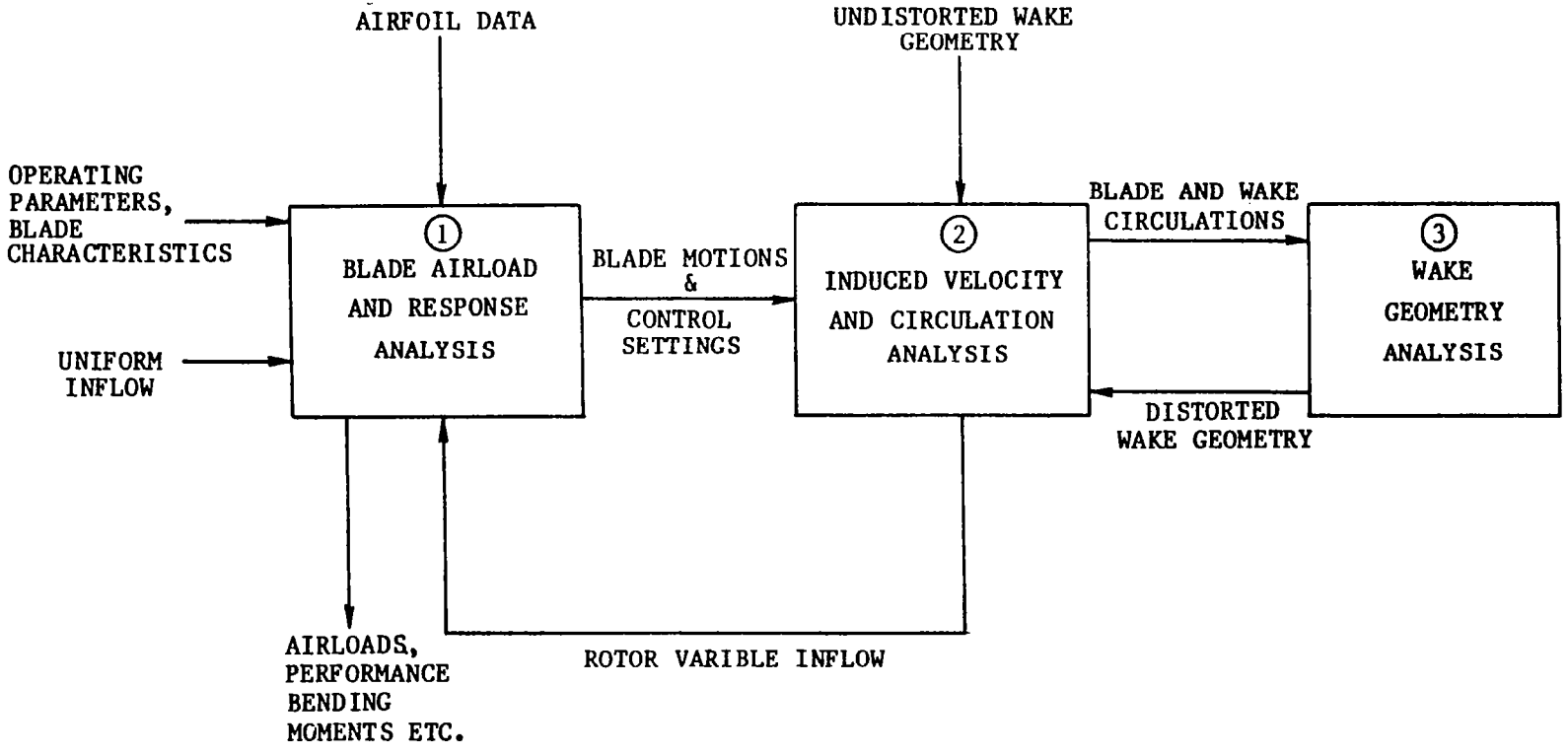

COMPONENT COMPUTER ANALYSES USED

(1) SIKORSKY GENERALIZED ROTOR PERFORMANCE ANALYSIS AND SIKORSKY NORMAL MODES ROTOR AEROELASTIC ANALYSIS(Y200)

(2) UTRC PRESCRIBED WAKE ROTOR INFLOW ANALYSIS(F389SR)

(3) UTRC ROTOR WAKE GEOMETRY ANALYSIS(F506)

FIGURE 9. ROTOR ANALYSIS COMPONENTS AND COUPLING

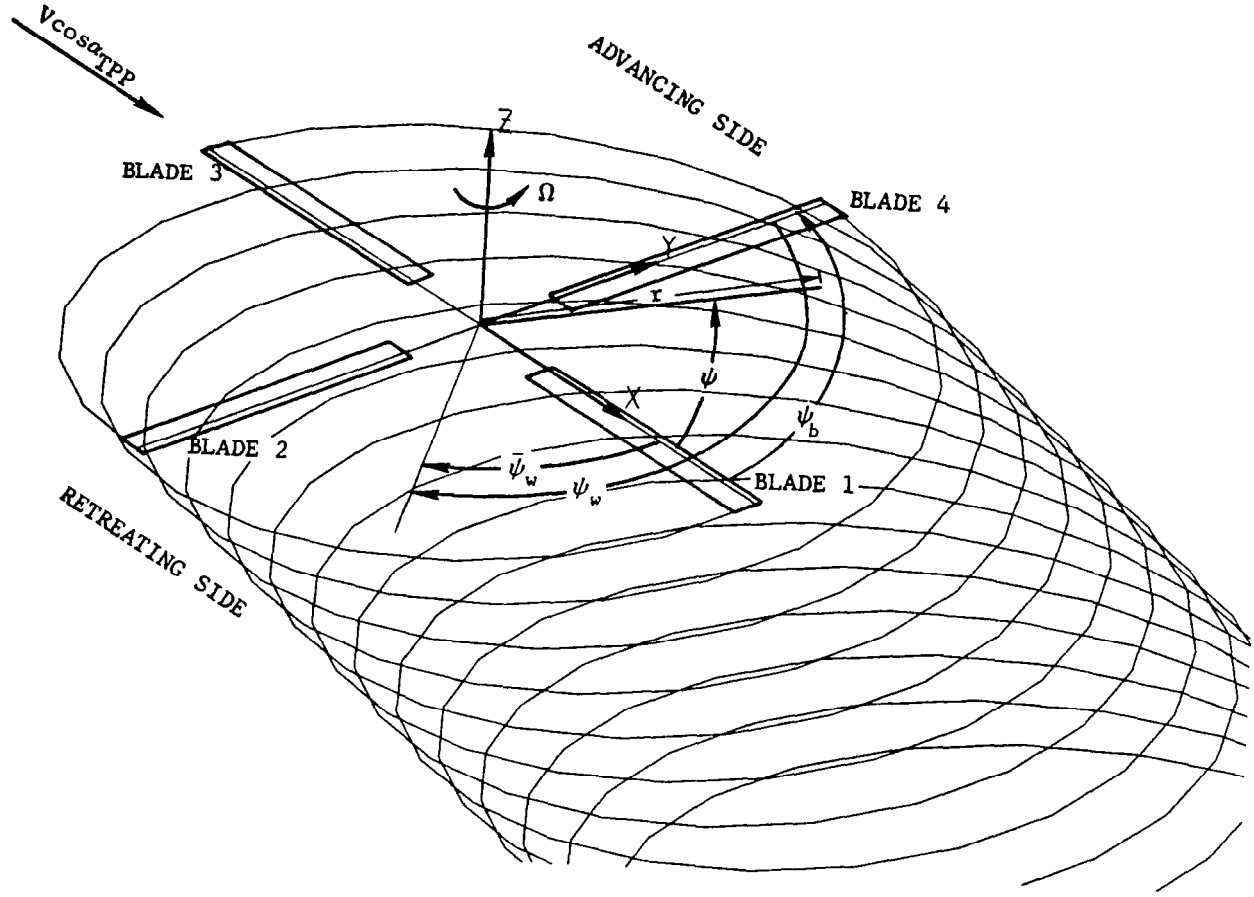

ψ_w, $\bar{\psi}_w$, and ψ_b are shown for Blade 4

FIGURE 10. COORDINATE DEFINITION AND BLADE NUMBERING SYSTEM

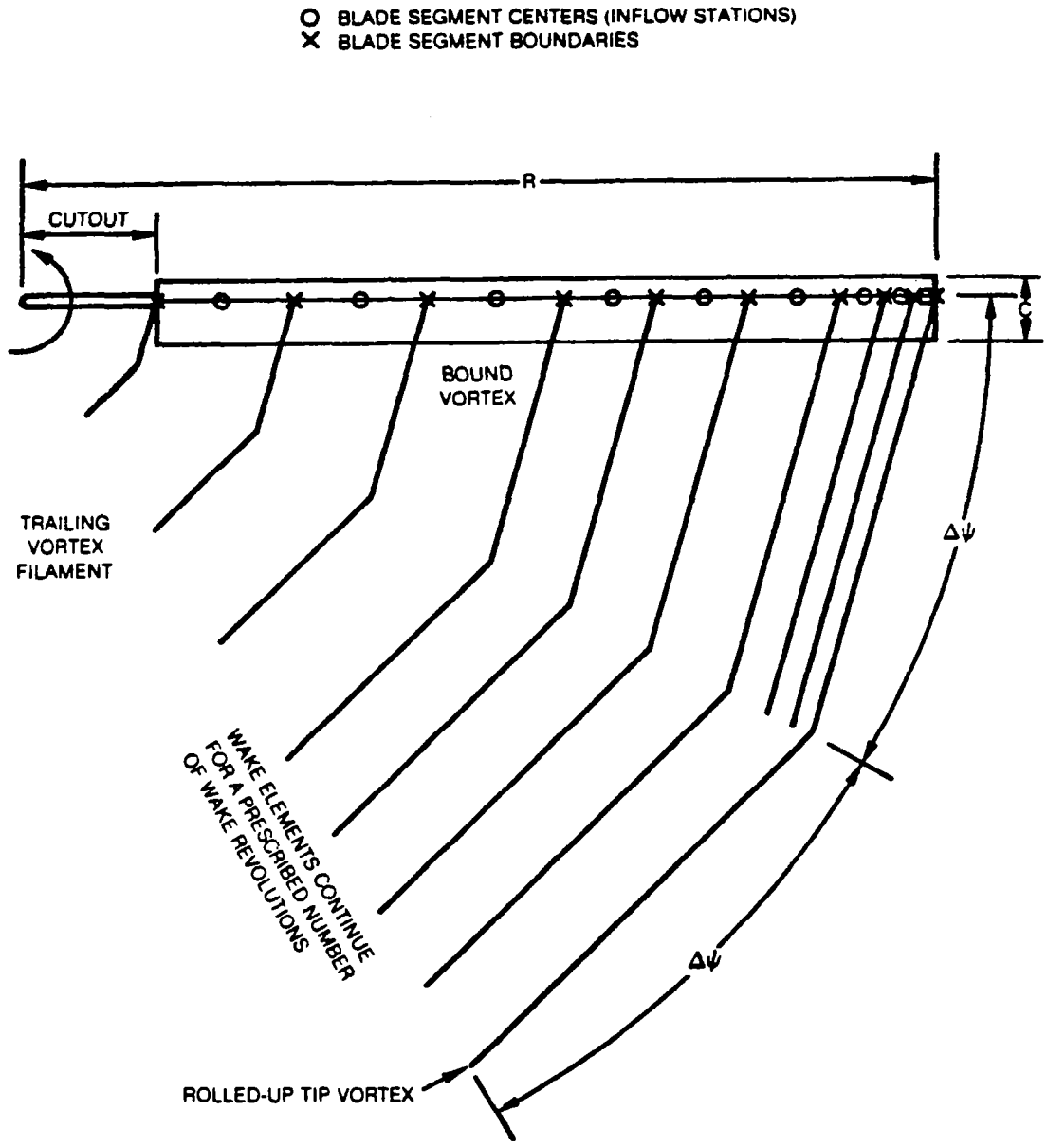

FIGURE 11. REPRESENTATION OF BLADE AND WAKE BY BOUND AND TRAILING VORTEX SEGMENTS

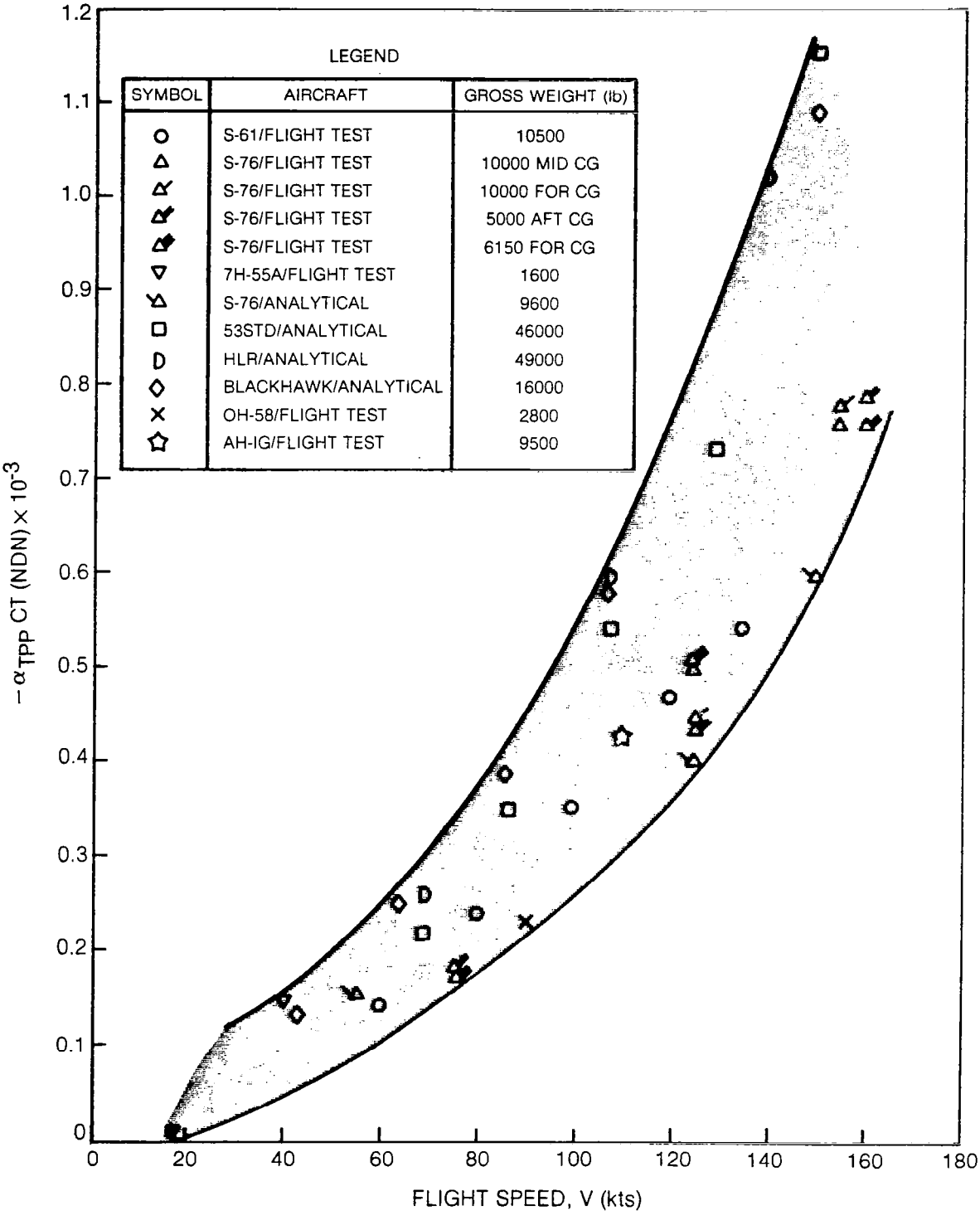

Figure 12. Results of Rotor Attitude, Thrust Coefficient Study

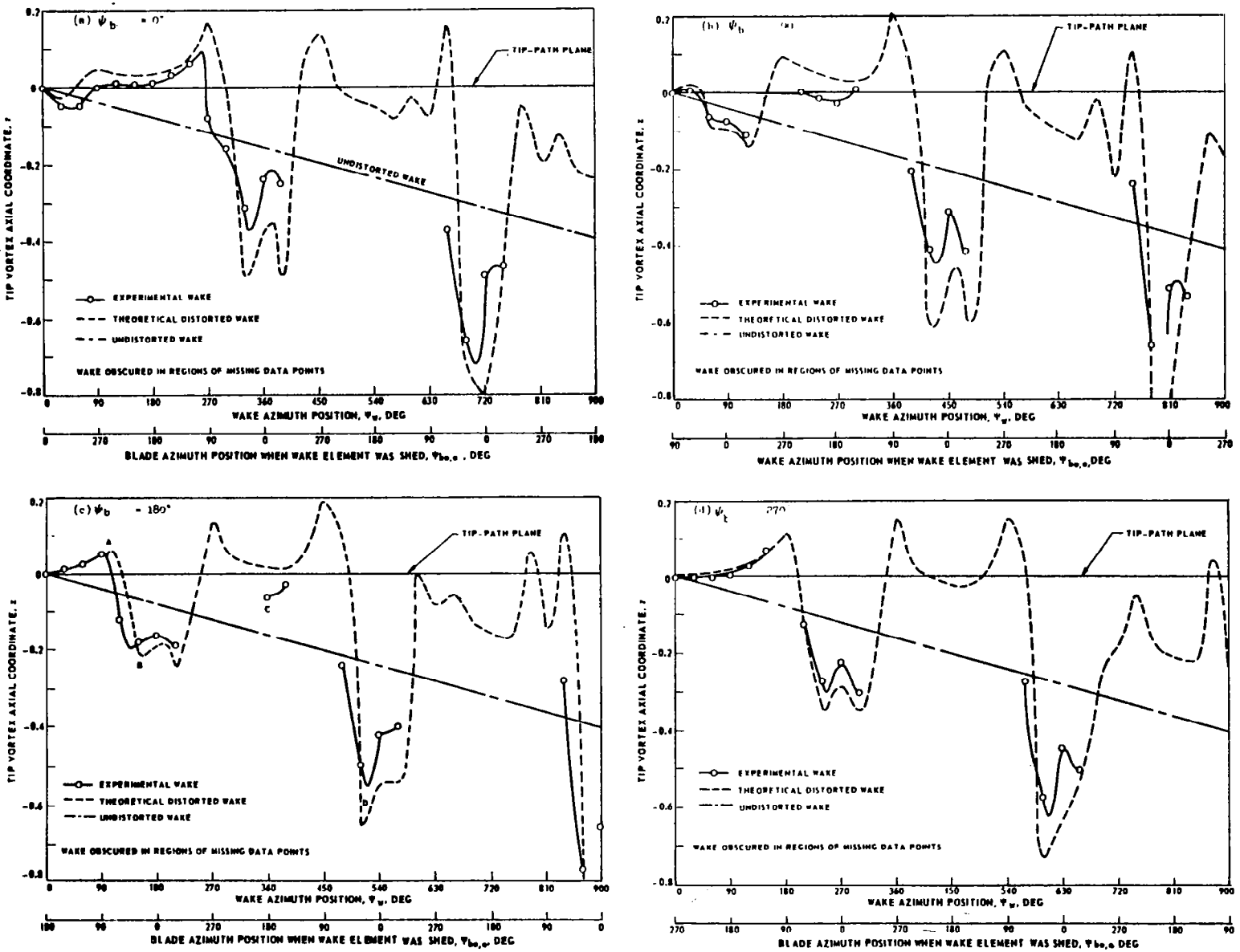

FIGURE 13. COMPARISON OF EXPERIMENTAL AND THEORETICAL WAKE AXIAL COORDINATES-MODEL ROTOR, SIMULATED 35 KT, 10,000-LB LIFT(μ=0.074) (REPRODUCED FROM REF. 5)

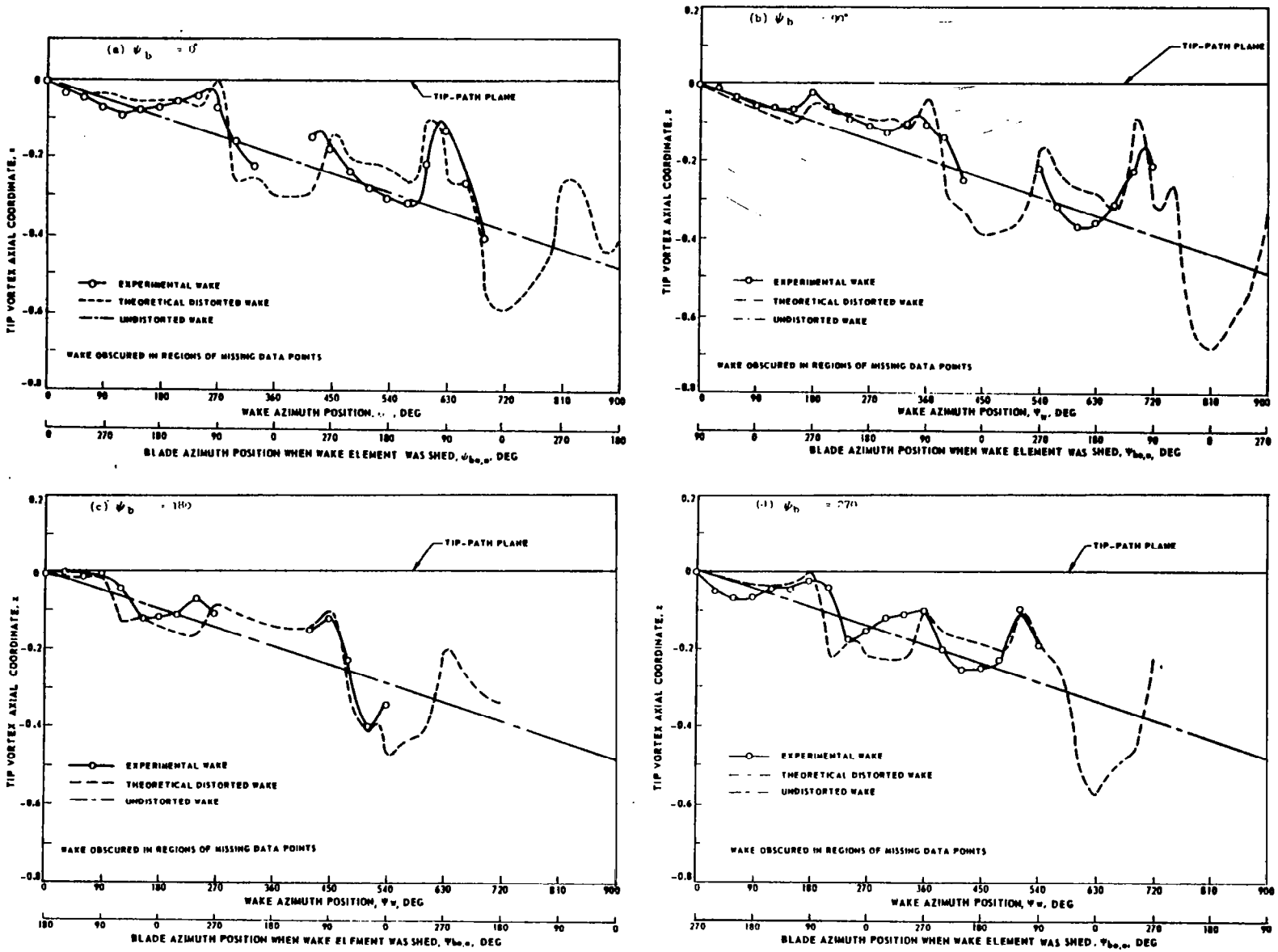

FIGURE 14. COMPARISON OF EXPERIMENTAL AND THEORETICAL WAKE AXIAL COORDINATES MODEL ROTOR, SIMULATED 90 KT, 10,000-LB LIFT(μ=0.19) (REPRODUCED FROM REF. 5)

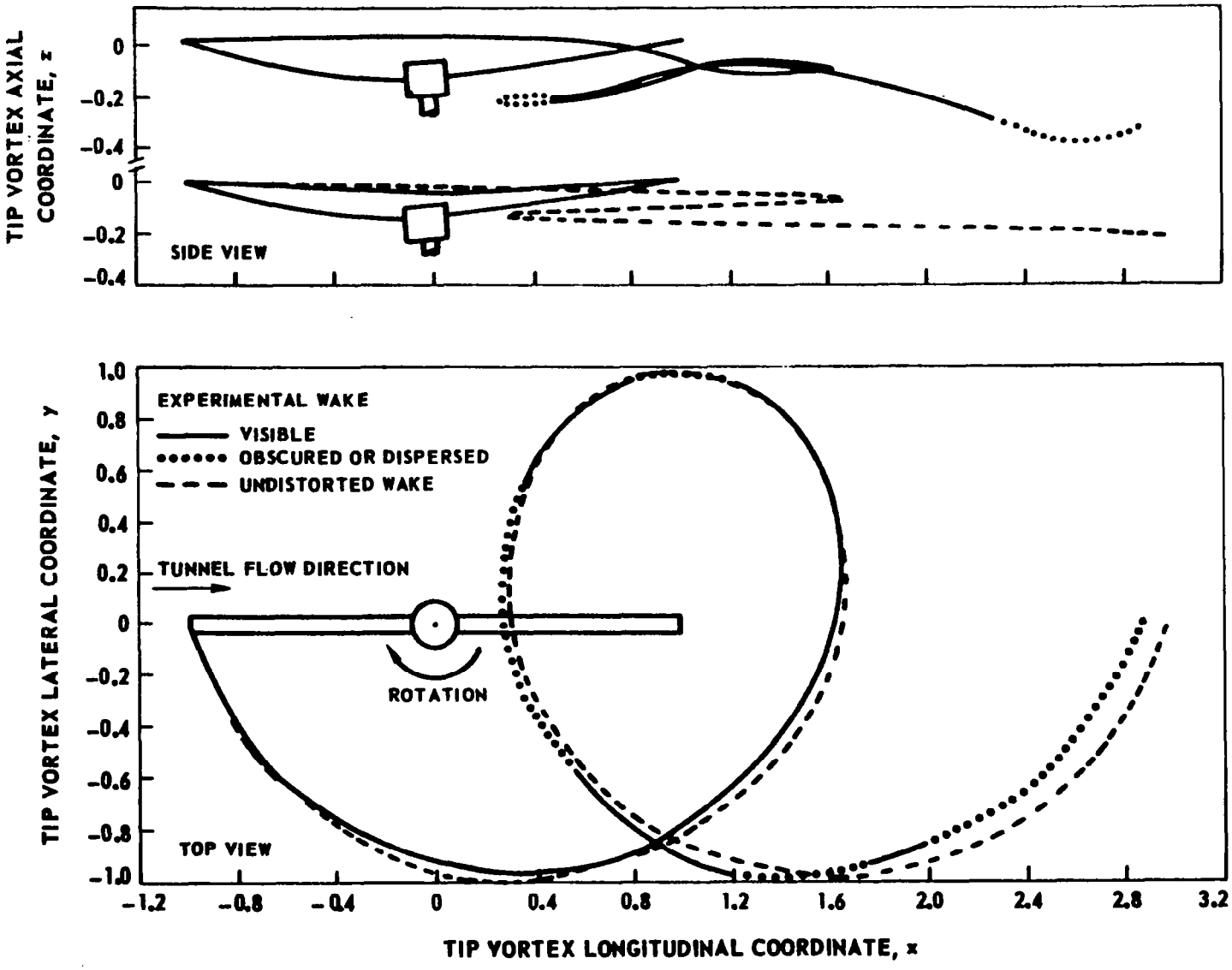

FIGURE 15. COMPARISON OF EXPERIMENTAL AND UNDISTORTED WAKE PATTERNS--MODEL ROTOR, SIMULATED 90 KT, 10,000-LB LIFT (REPRODUCED FROM REF. 5)

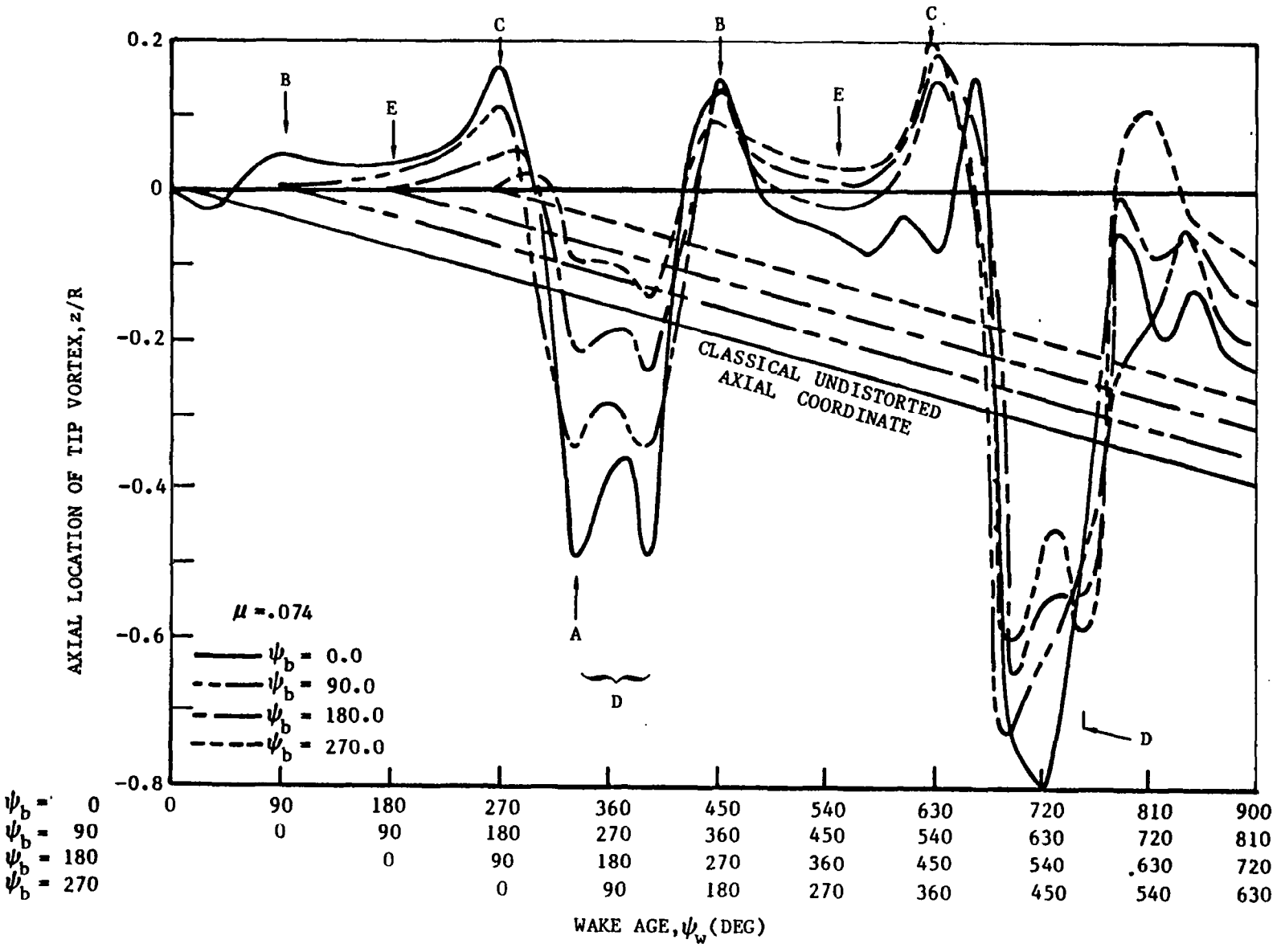

FIGURE 16. SUPERPOSITION OF AXIAL WAKE LOCATION FOR VARIOUS BLADE AZIMUTH POSITION

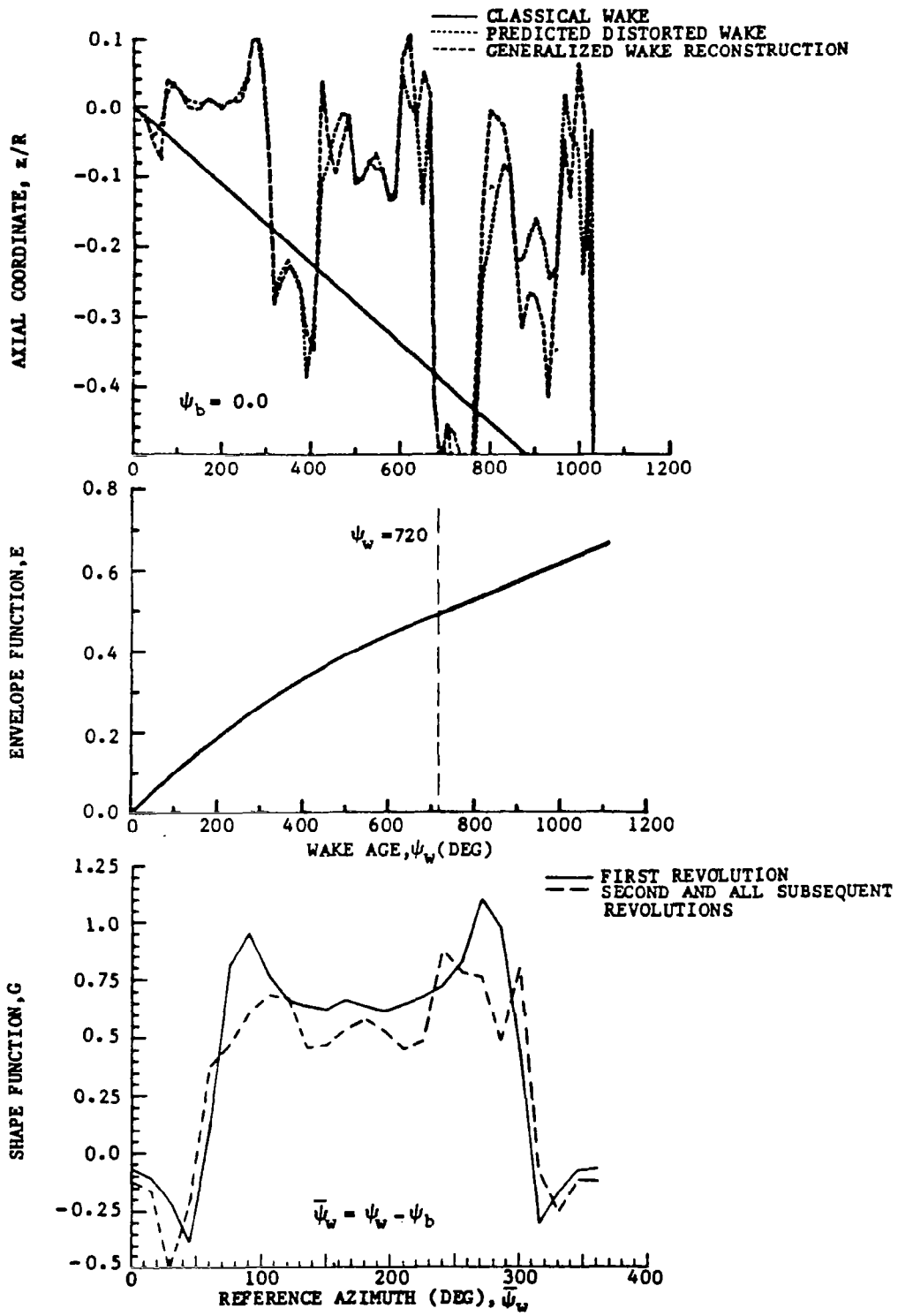

FIGURE 17. EXAMPLE OF THE GENERALIZED WAKE GEOMETRY FORMULATION FEATURES

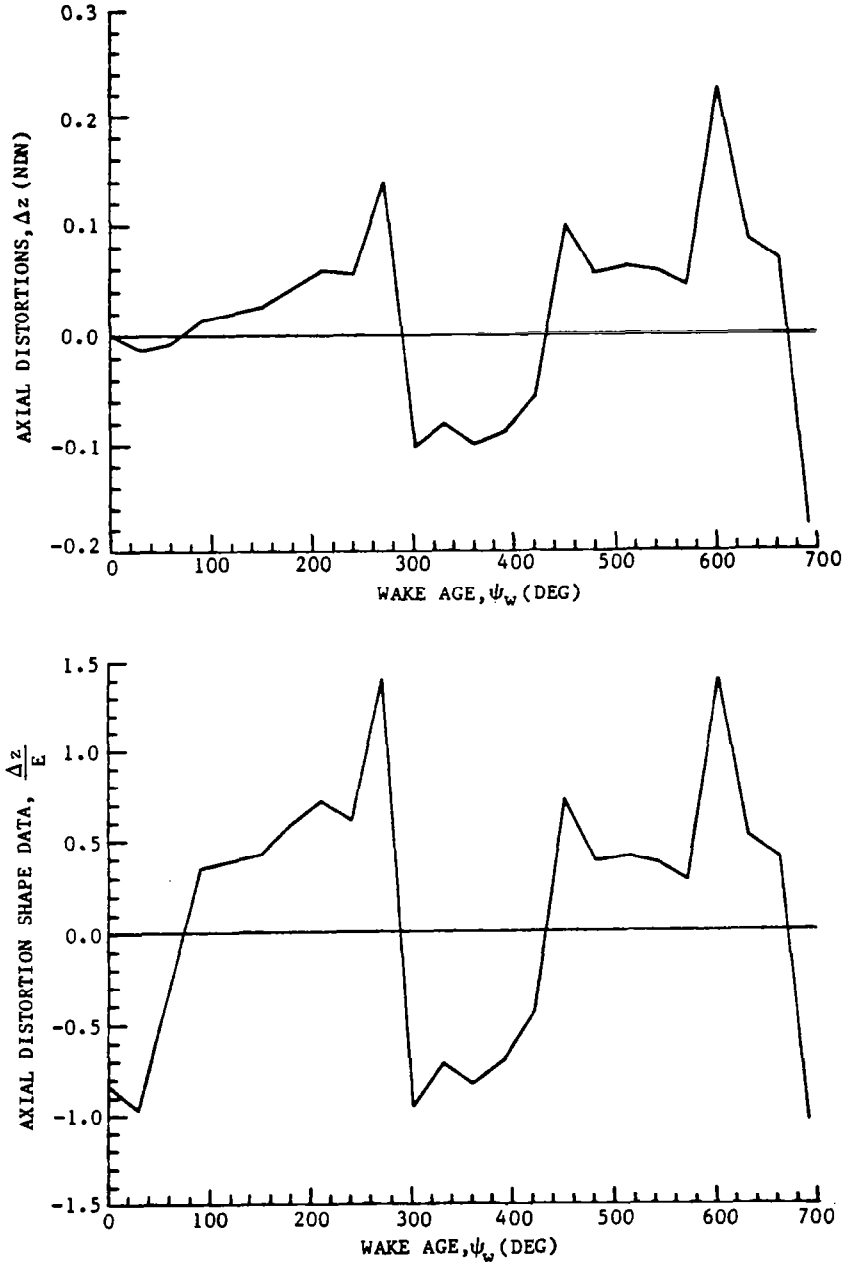

FIGURE 18. EFFECT OF NORMALIZATION OF THE AXIAL WAKE DISTORTIONS BY THE ENVELOPE FUNCTION($\psi_b = 0^\circ$)

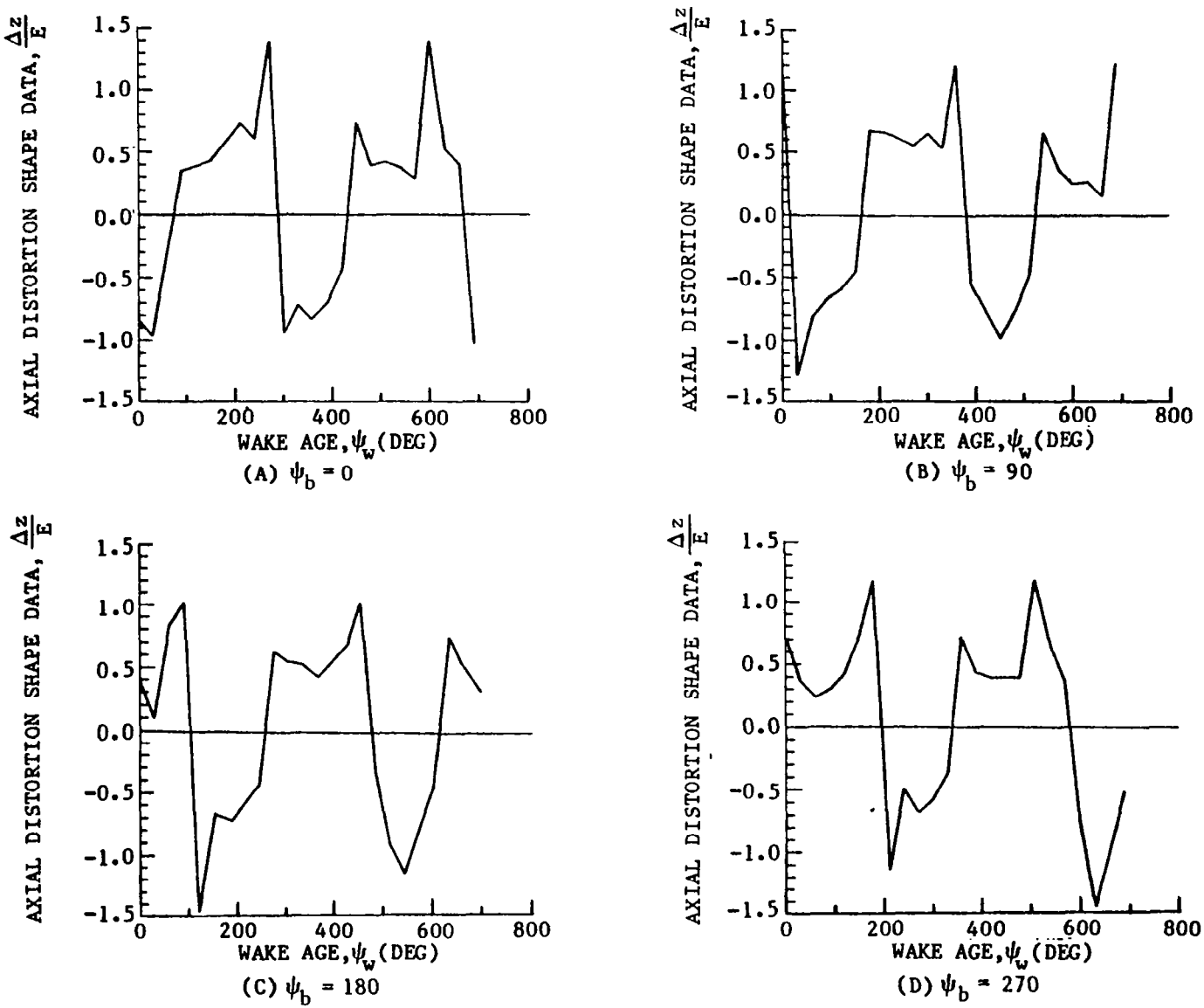

FIGURE 19. COMPARISON OF NORMALIZED AXIAL DISTORTIONS

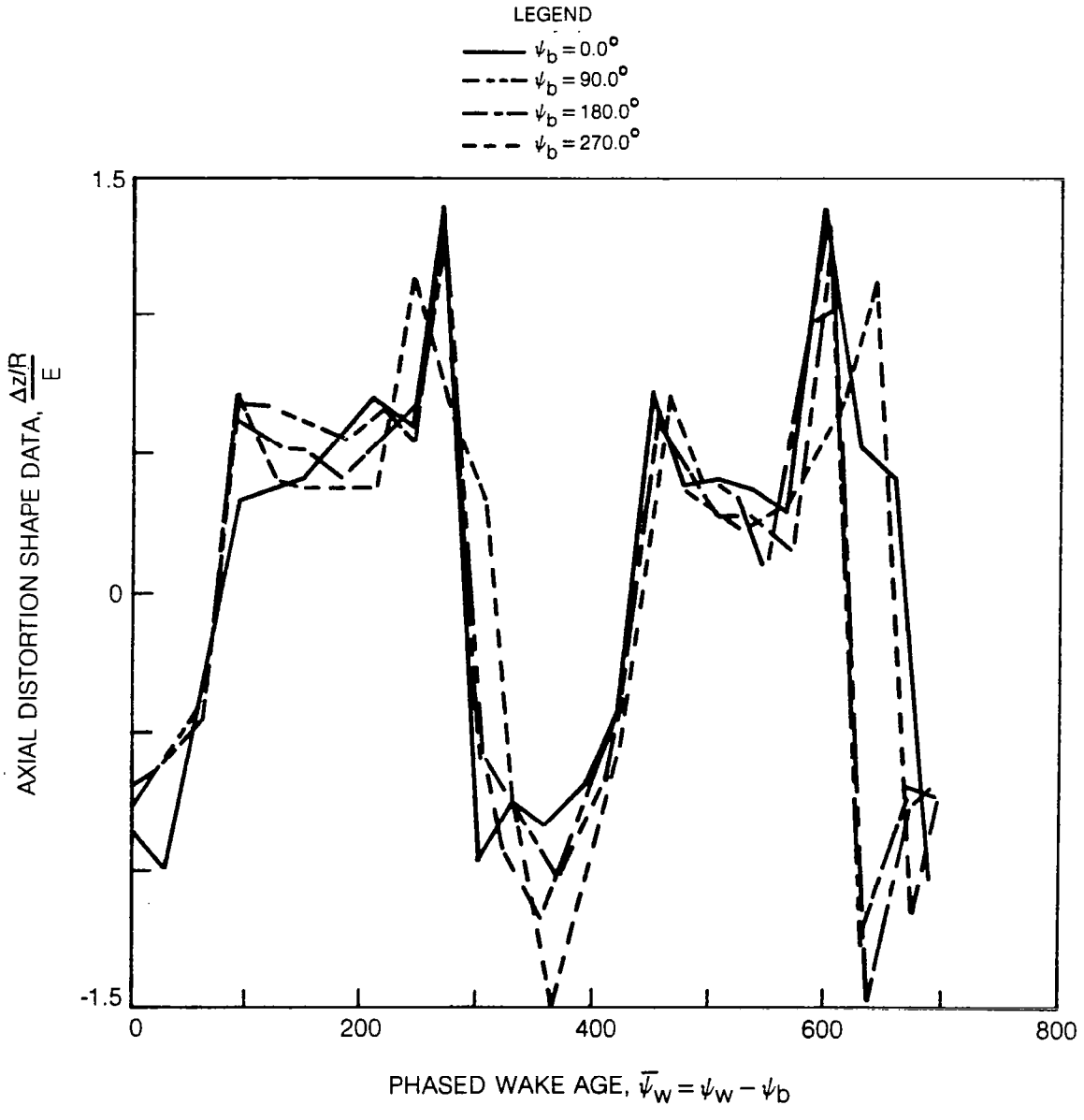

Figure 20. Superposition of Axial Distortion Shape Calculations Phased for Blade Azimuth Positions

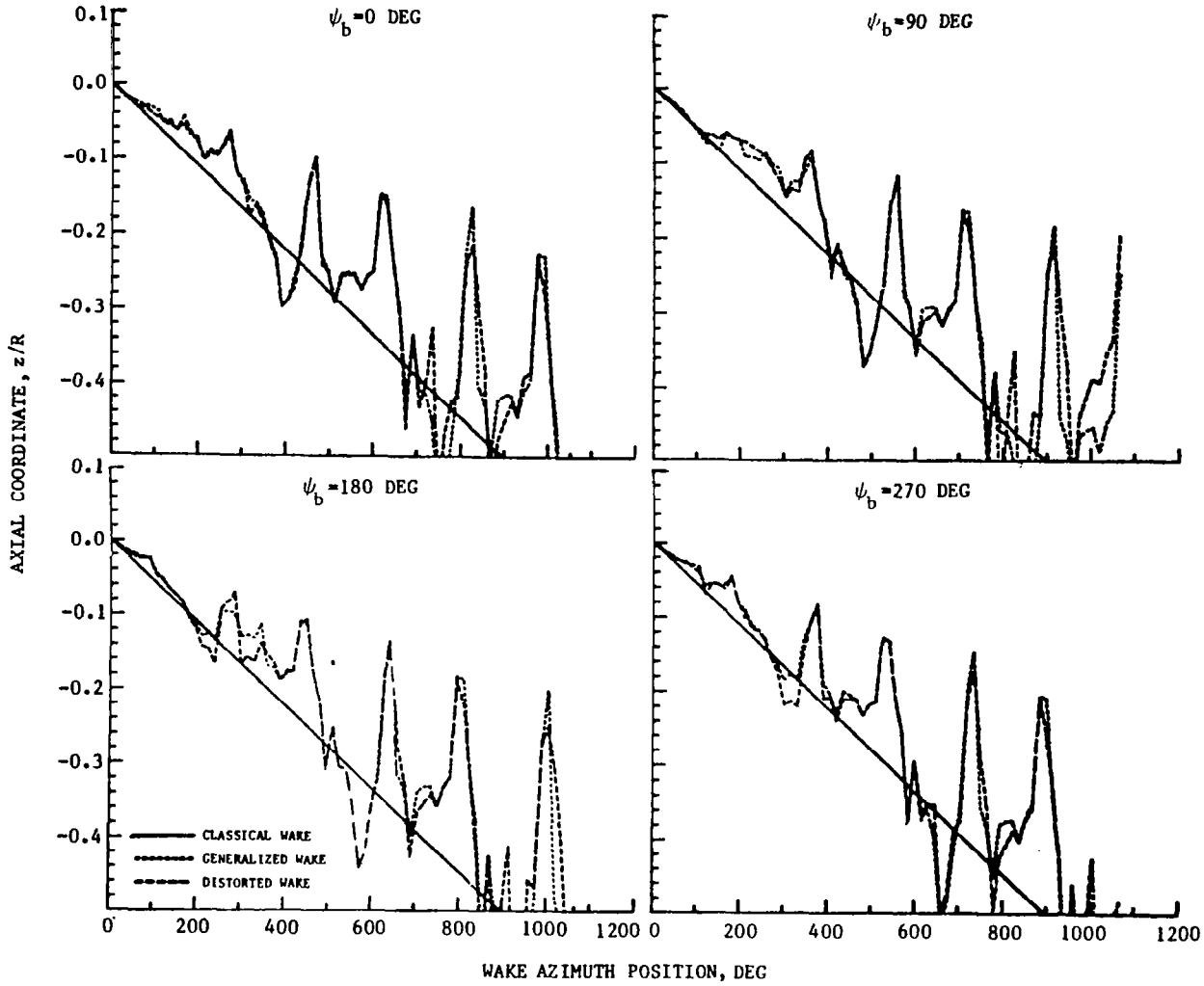

FIGURE 21. SAMPLE COMPARISONS OF THE PREDICTED WAKE AXIAL COORDINATE AT SELECTED BLADE AZIMUTH POSITIONS, ($b=4$, $C_T=.0064$, $\alpha_{TPP}=-4$, $\mu=.3$)

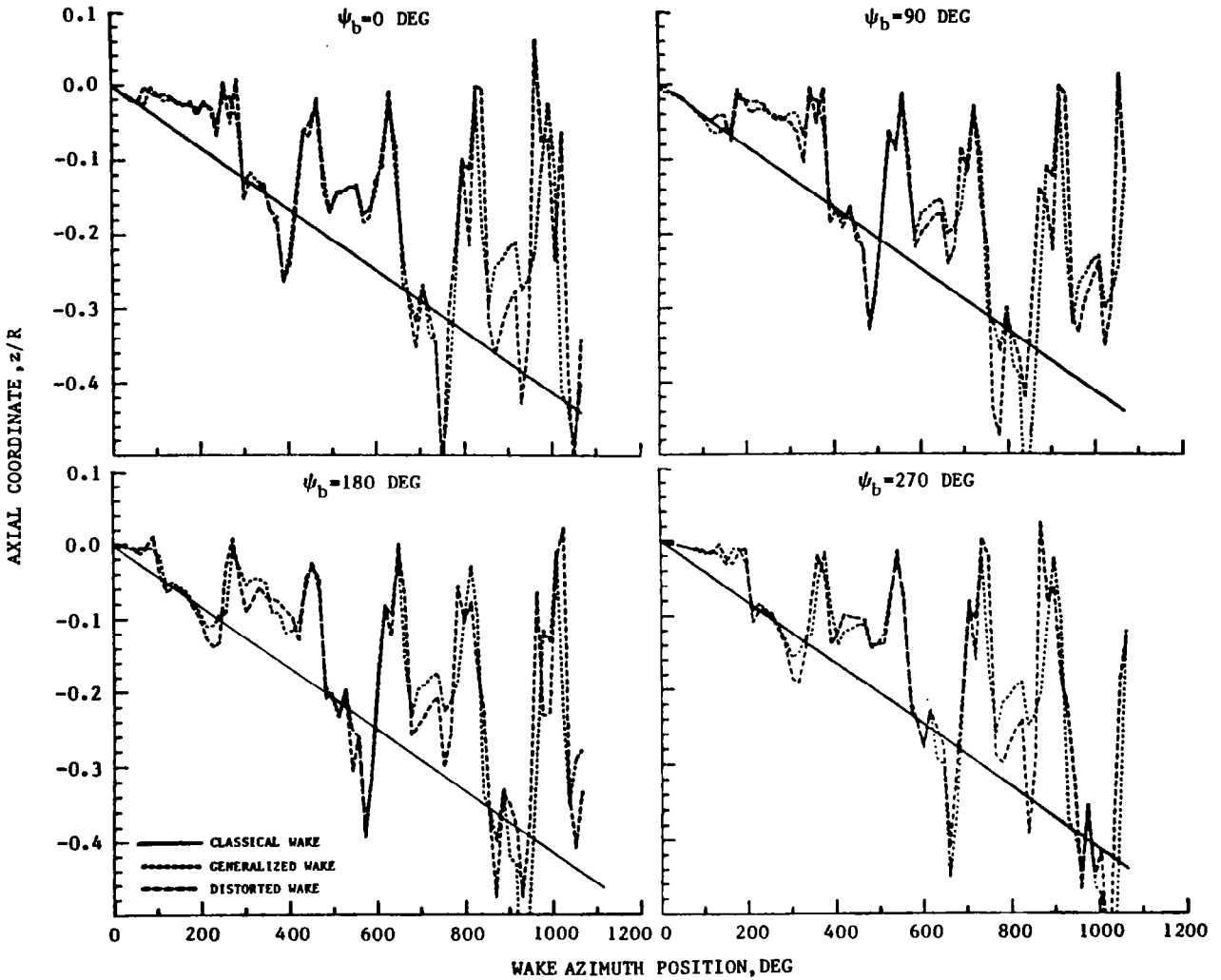

FIGURE 22. SAMPLE COMPARISONS OF THE PREDICTED WAKE AXIAL COORDINATE AT SELECTED BLADE AZIMUTH POSITIONS, ($b=4$, $C_T=.0064$, $\alpha_{TPP}=-2.25$, $\mu=.2$)

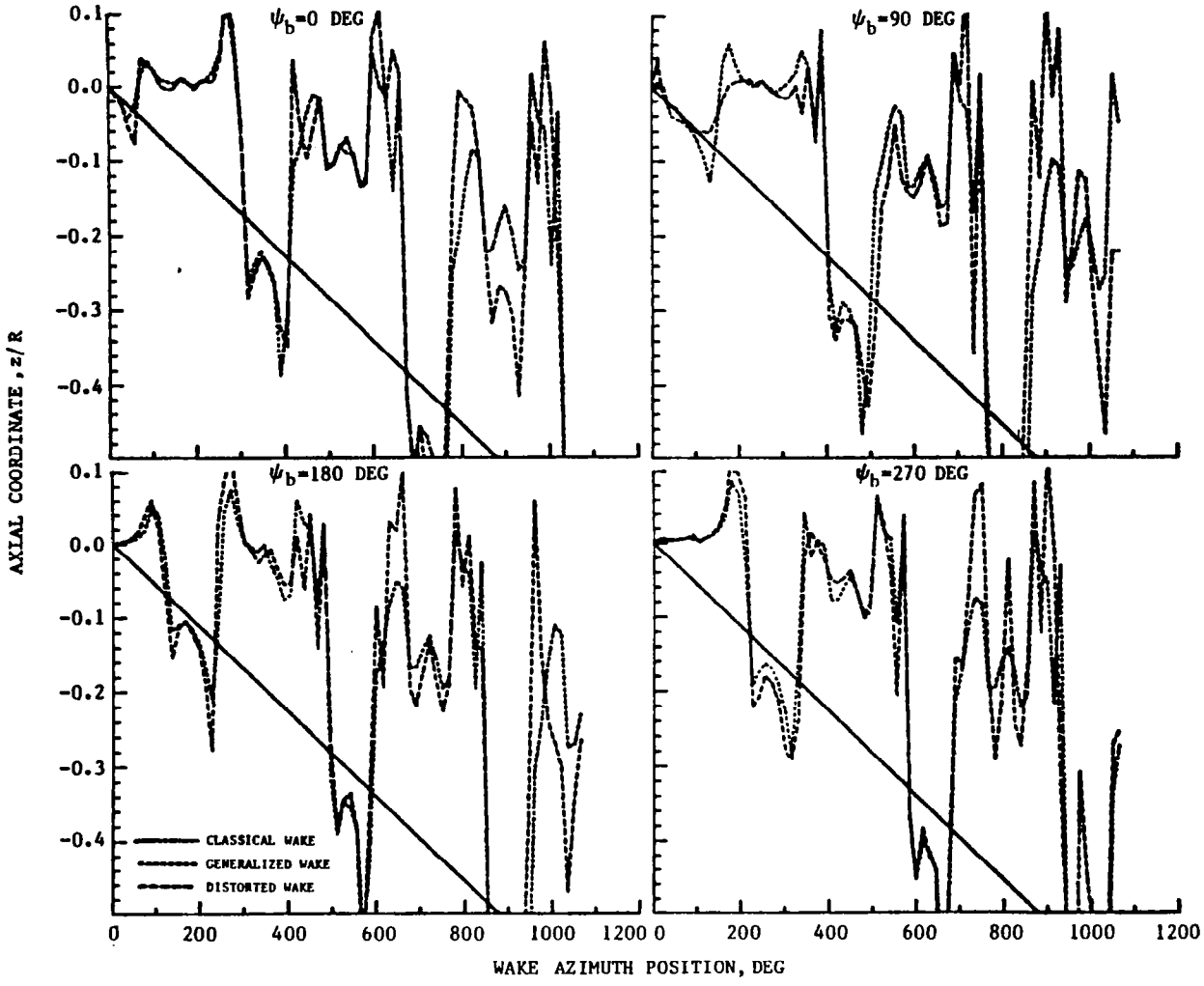

FIGURE 23. SAMPLE COMPARISONS OF THE PREDICTED WAKE AXIAL COORDINATE AT SELECTED BLADE AZIMUTH POSITIONS, ($b=4$, $C_T=.0064$, $\alpha_{TPP}=-1$, $\mu=.1$)

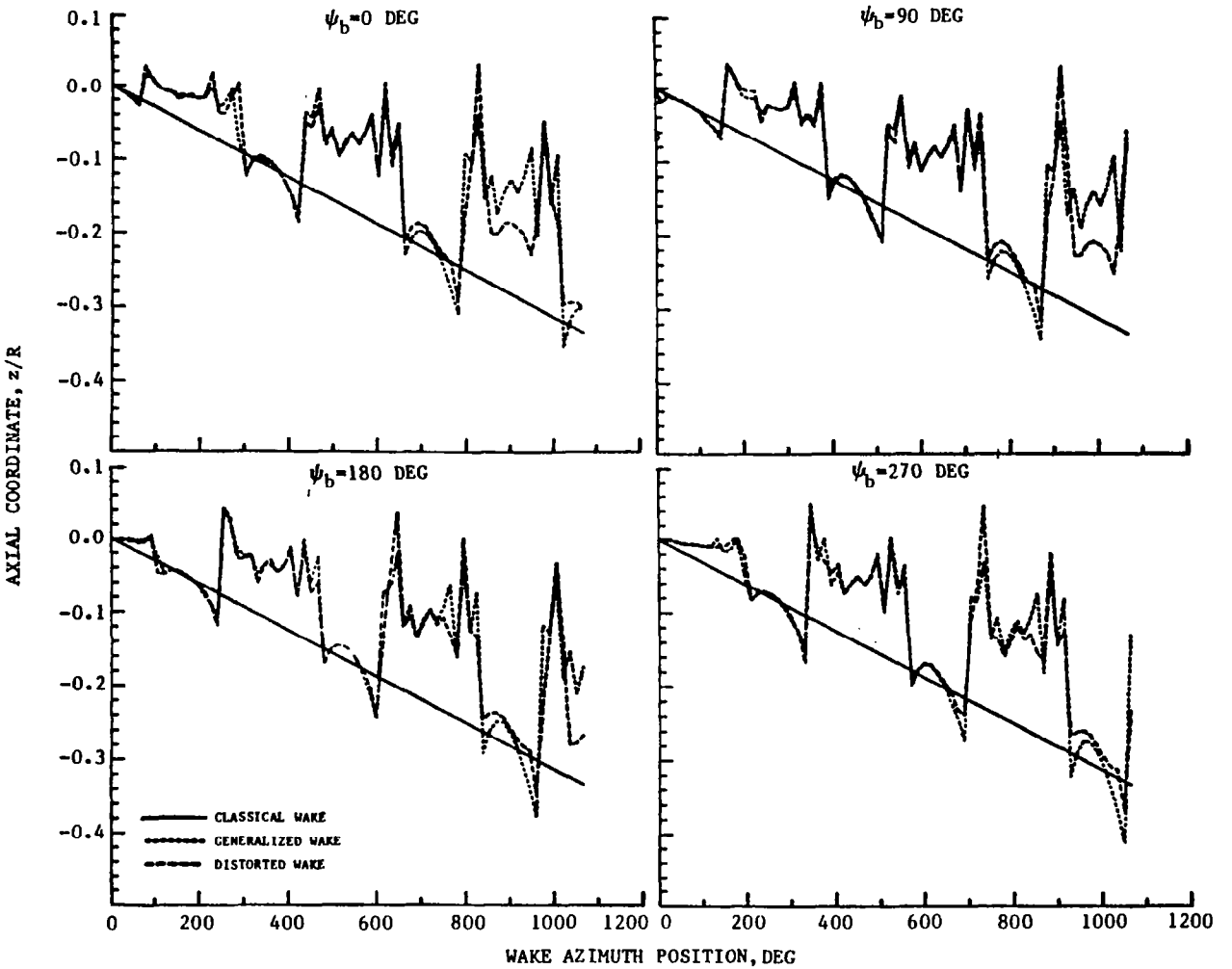

FIGURE 24. SAMPLE COMPARISONS OF THE PREDICTED WAKE AXIAL COORDINATE AT SELECTED BLADE AZIMUTH POSITIONS, ($b=2$, $C_T=.00257$, $\alpha_{TPP}=-3$, $\mu=.1$)

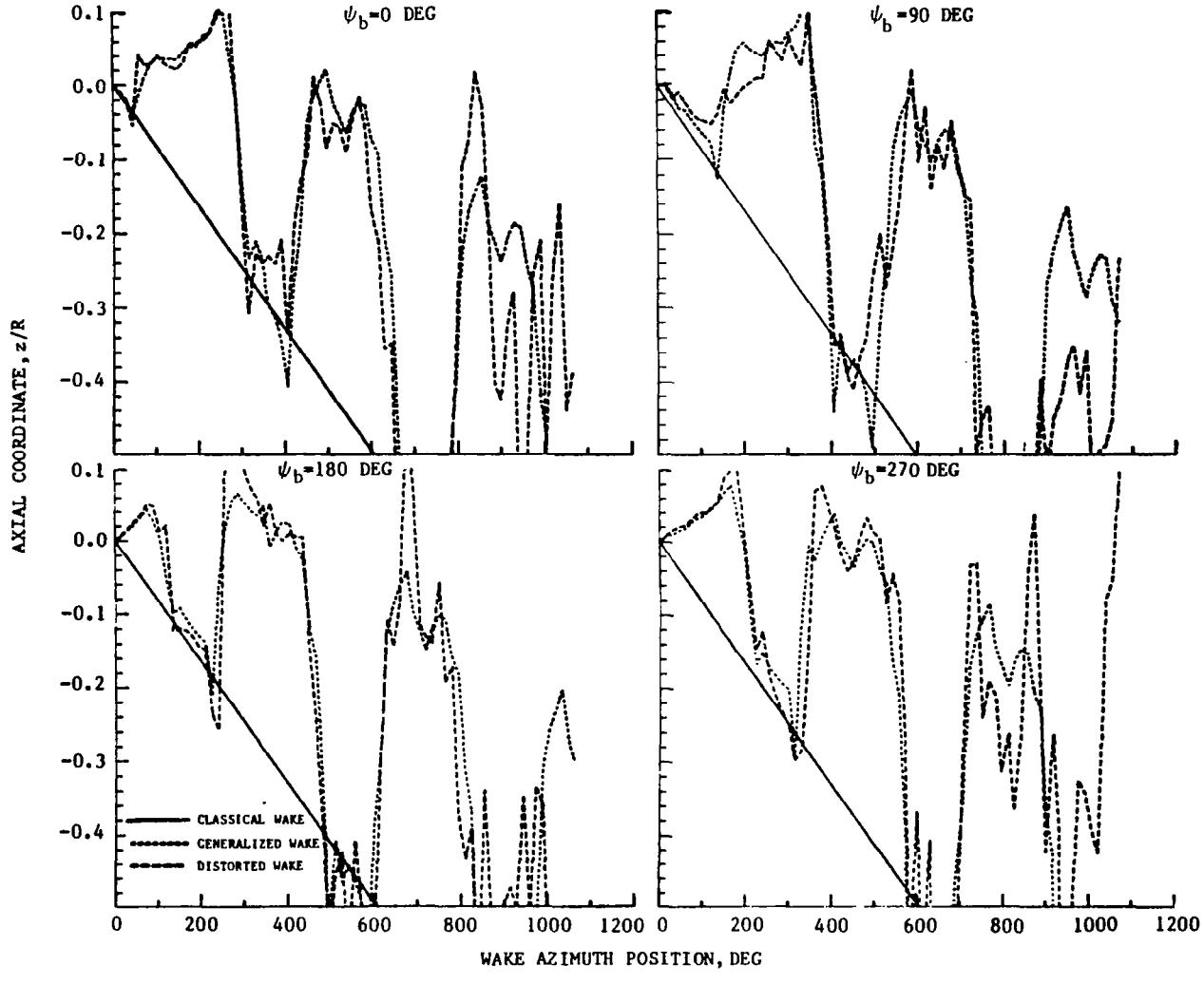

FIGURE 25. SAMPLE COMPARISONS OF THE PREDICTED WAKE AXIAL COORDINATE AT SELECTED BLADE AZIMUTH POSITIONS, ($b=4$, $C_T=.0064$, $\alpha_{TPP}=-.5$, $\mu=.05$)

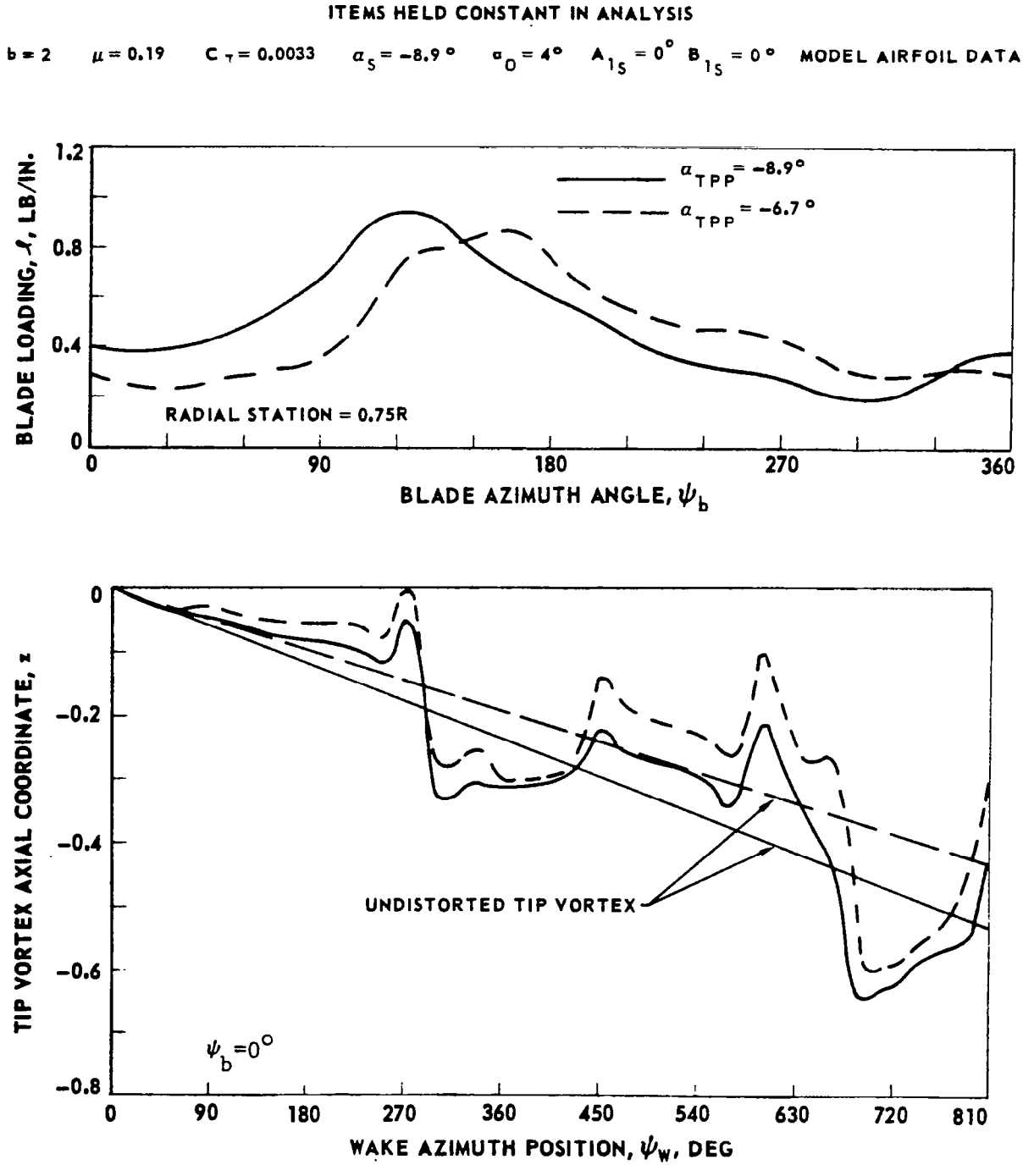

FIGURE 26. EFFECT OF ROTOR TIP-PATH PLANE ANGLE ON MODEL ROTOR LOADING AND WAKE GEOMETRY (REPRODUCED FROM REF. 5)

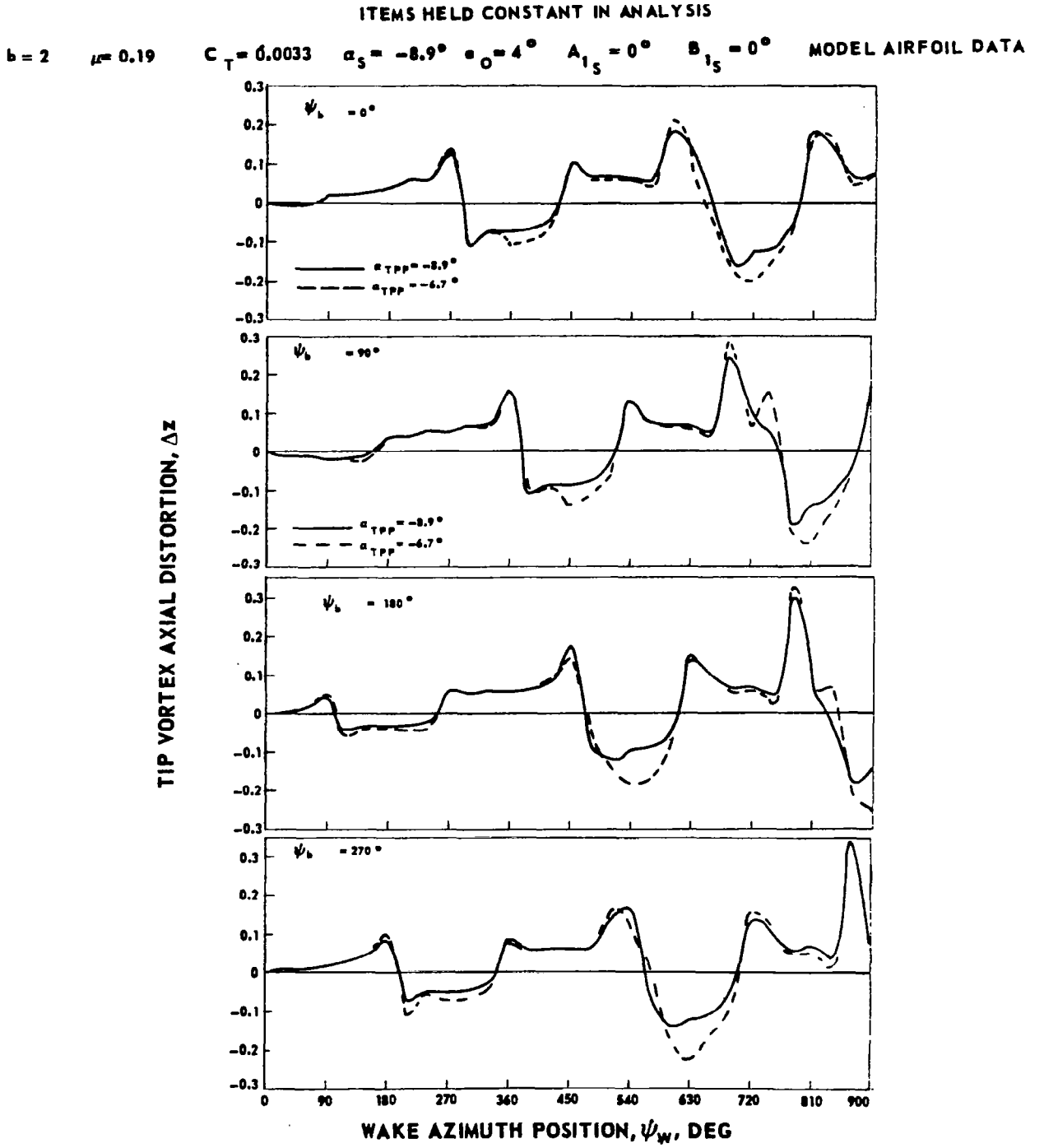

FIGURE 27. EFFECT OF ROTOR TIP-PATH PLANE ANGLE ON MODEL ROTOR WAKE DISTORTIONS (REPRODUCED FROM REF. 5)

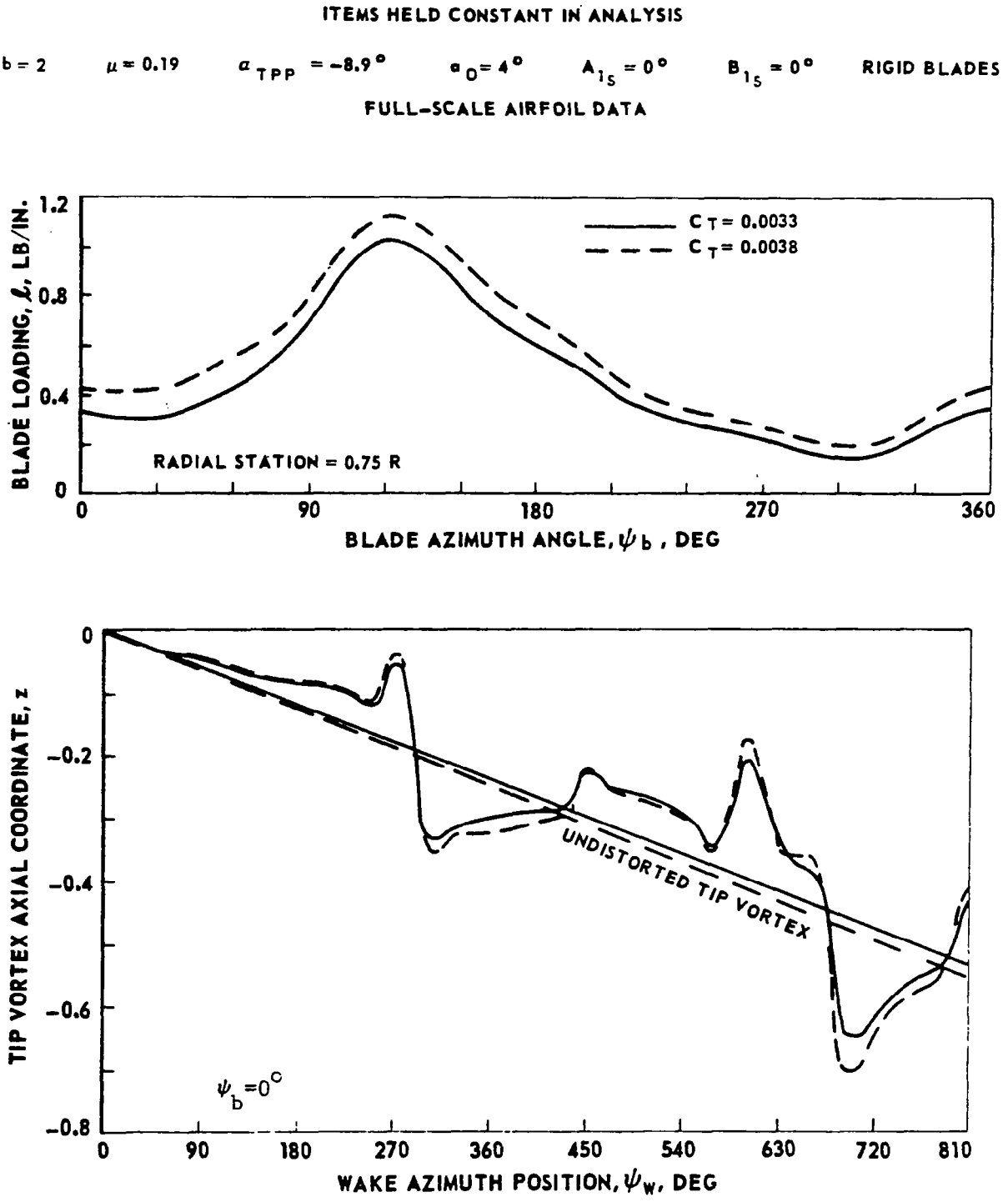

FIGURE 28. EFFECT OF THRUST COEFFICIENT ON MODEL ROTOR LOADING AND WAKE GEOMETRY (REPRODUCED FROM REF. 5)

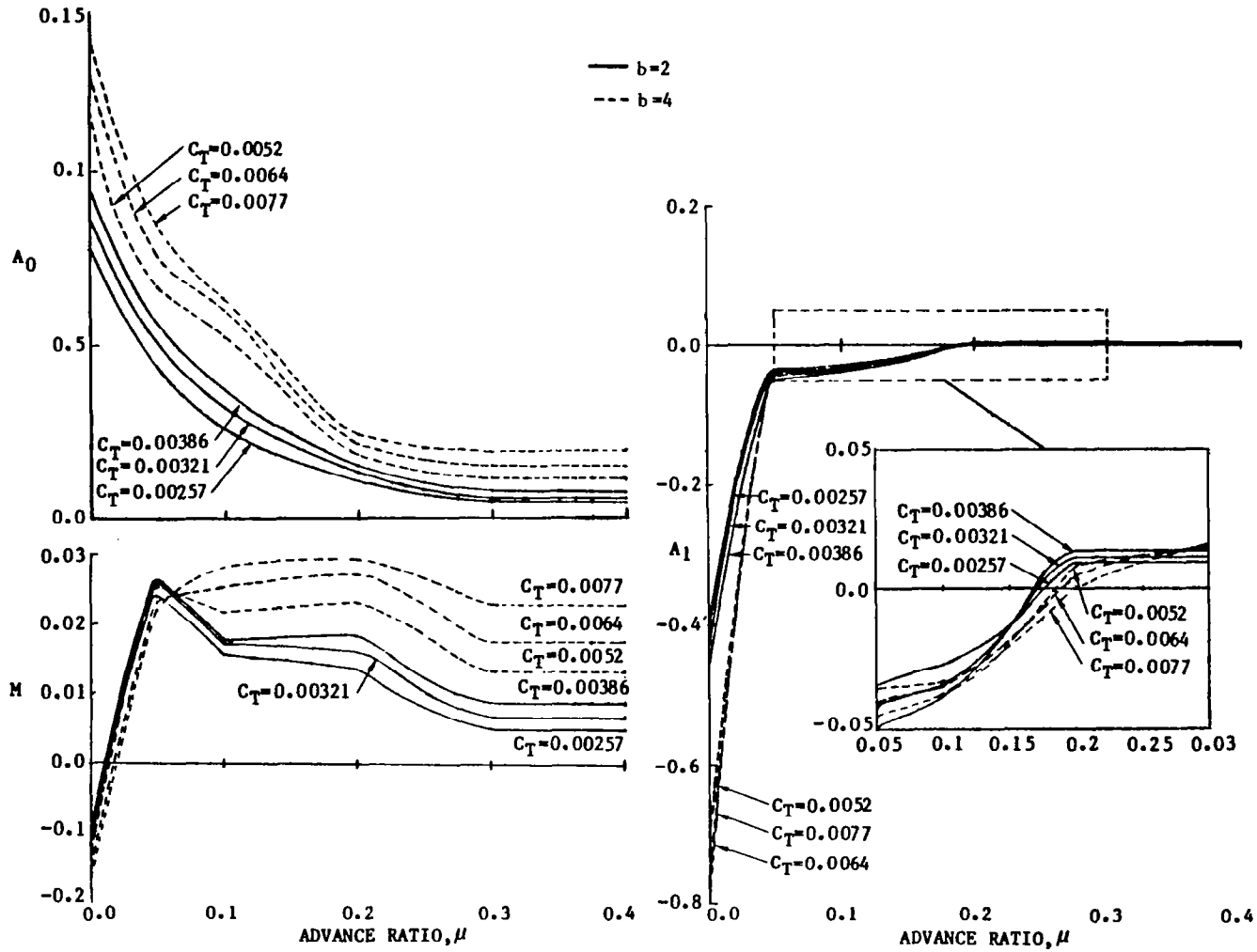

FIGURE 29. VARIATION OF THE ENVELOPE FUNCTION COEFFICIENTS FOR THE GENERALIZED WAKE MODULE

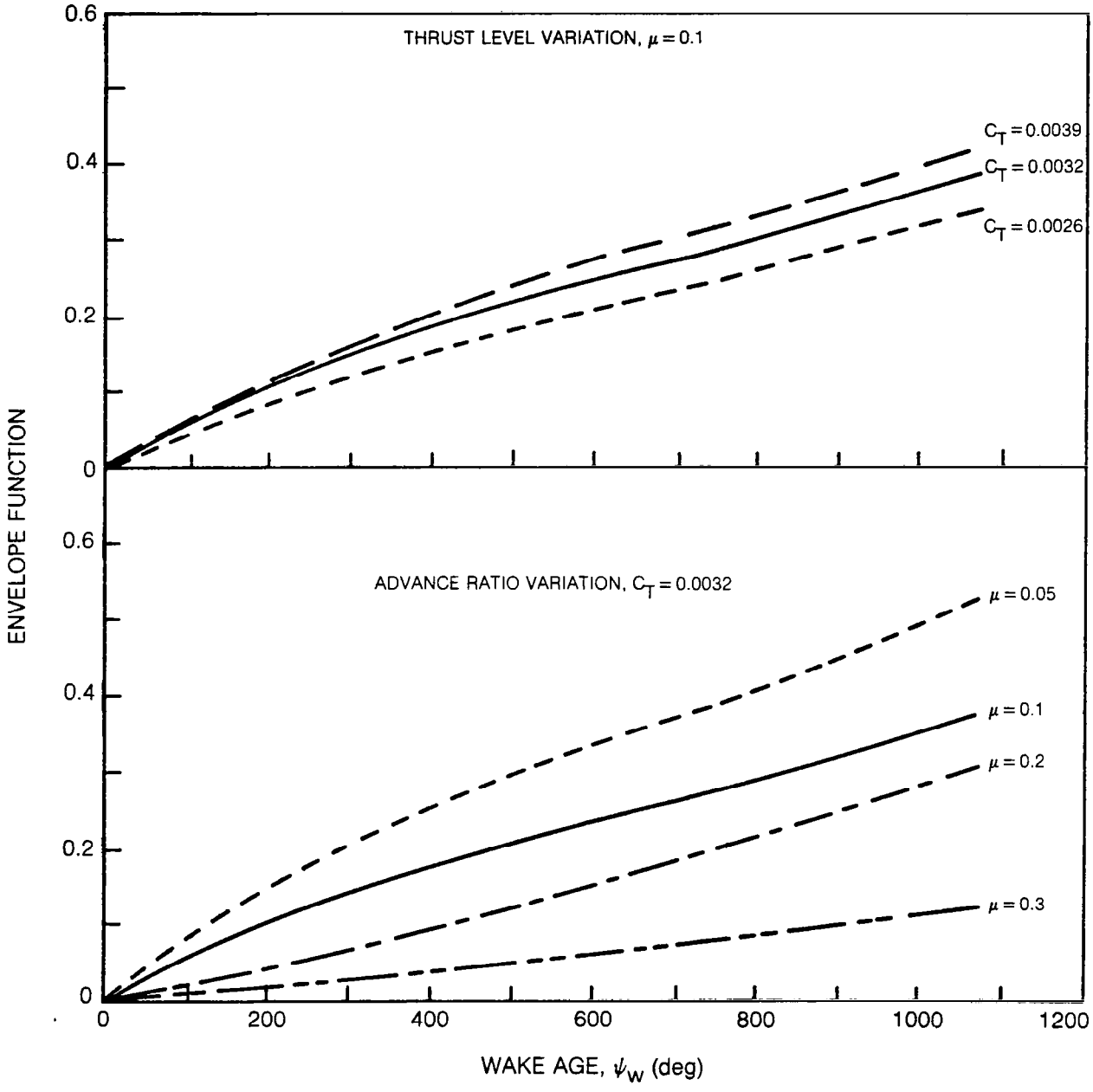

Figure 30. Variations of the Generalized Wake Envelope Function with Advance Rotor and Thrust Level for the Two Bladed Representative Rotor

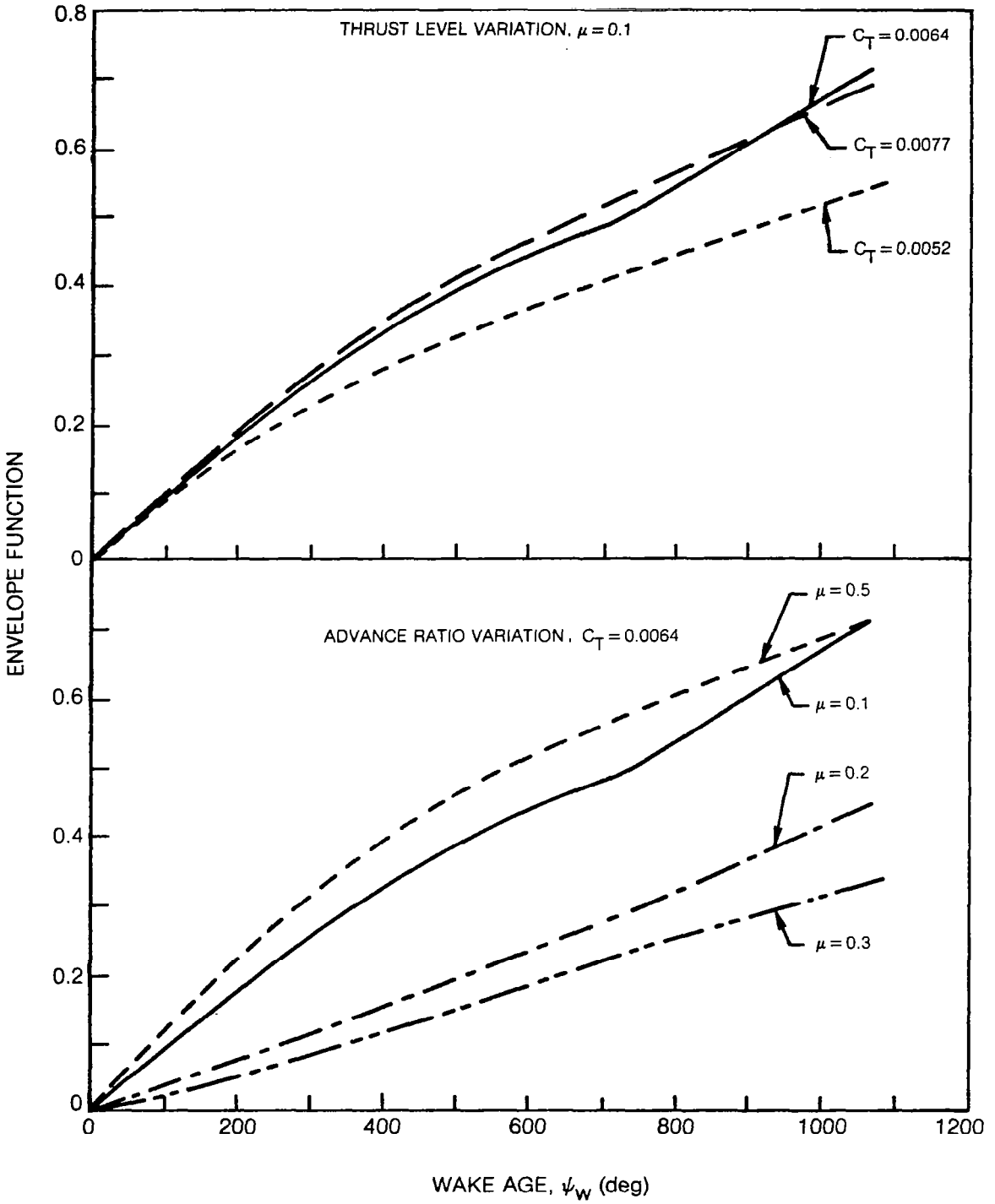

Figure 31. Variations of the Generalized Wake Envelope Function with Advance Rotor and Thrust Level for the Four Bladed Representative Rotor

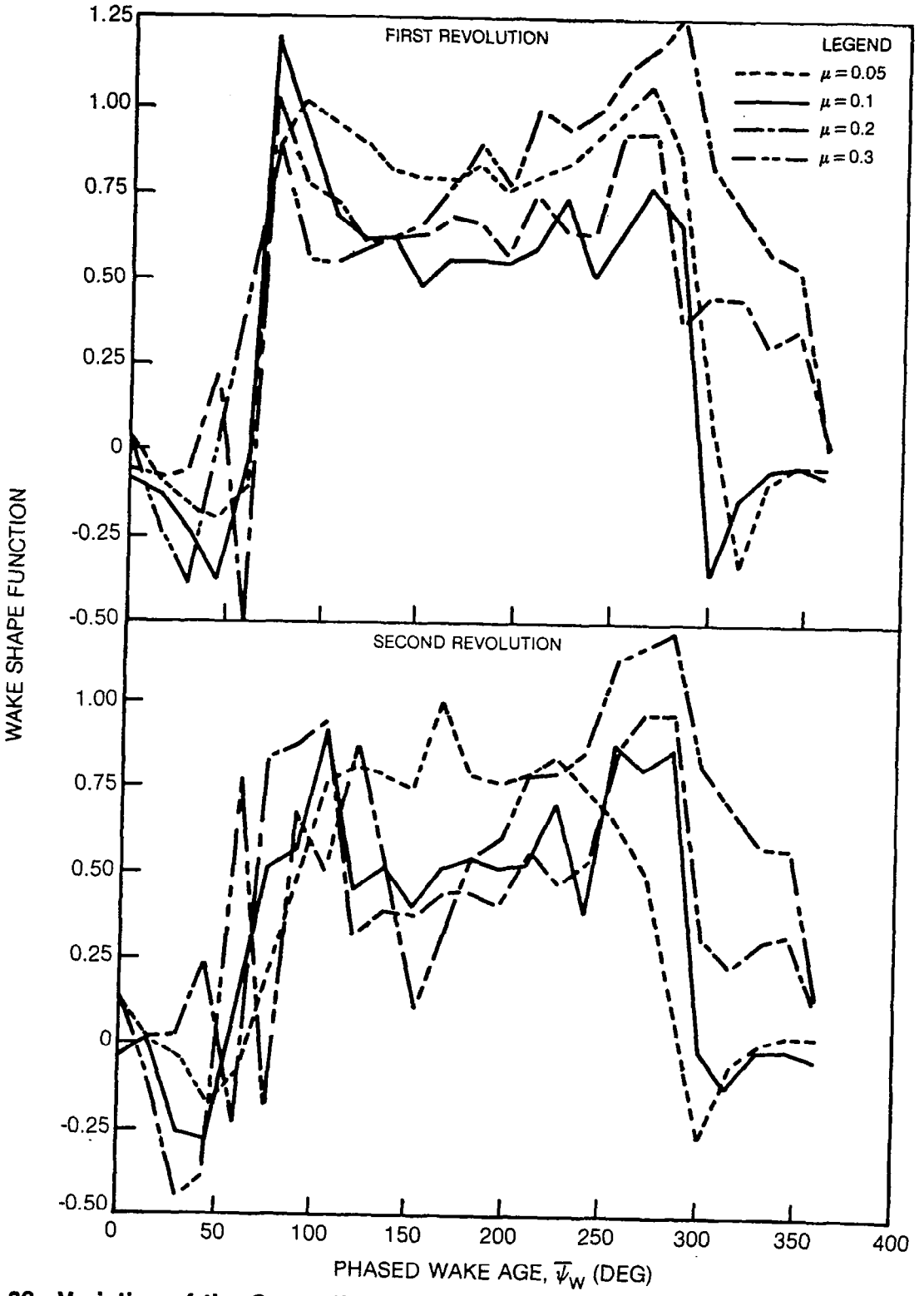

Figure 32. Variation of the Generalized Wake Shape Function with Advance Rotor for the Two-Bladed Representative Rotor

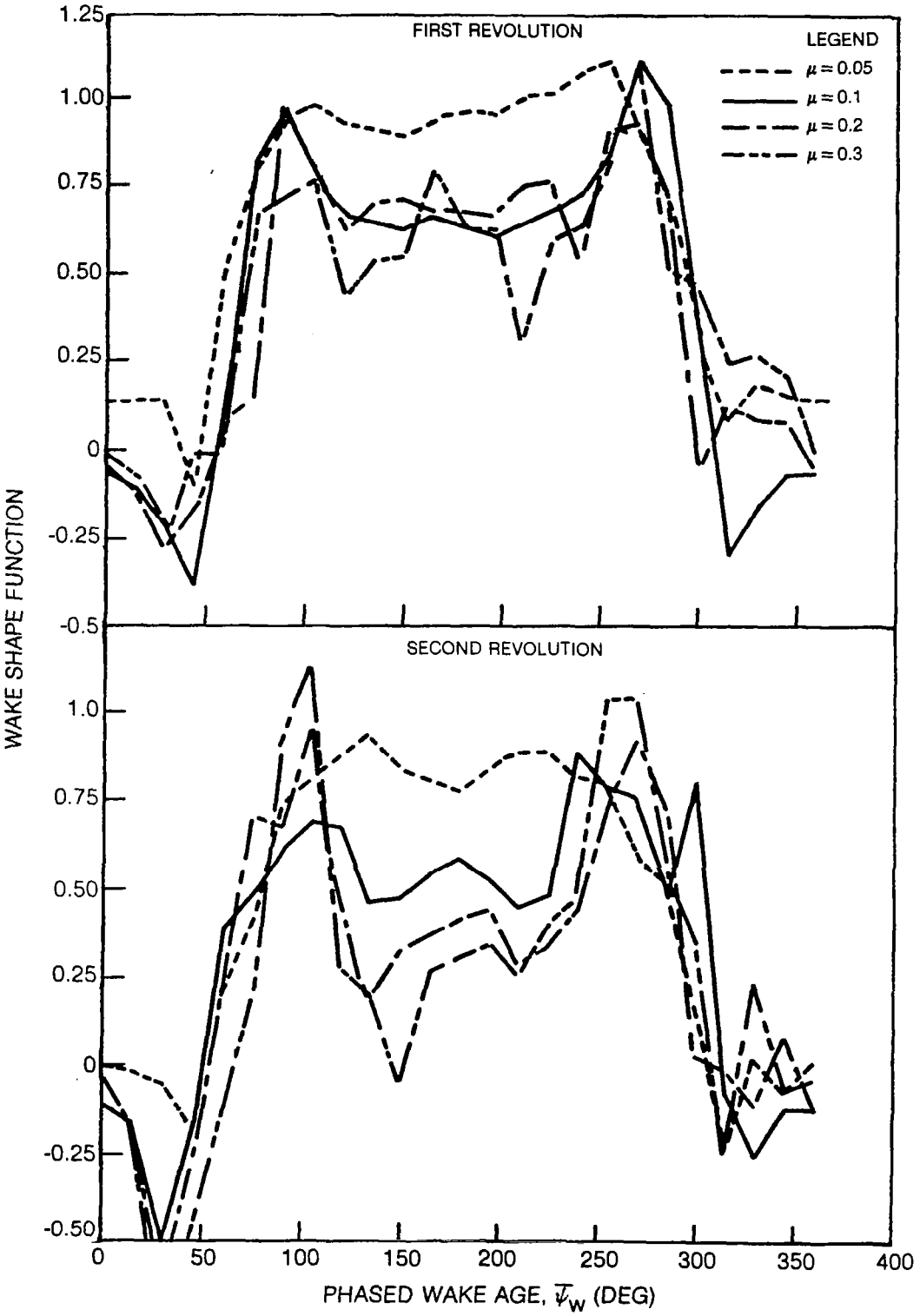

Figure 33. Variation of the Generalized Wake Shape Function with Advance Ratio for the Four-Bladed Representative Rotor

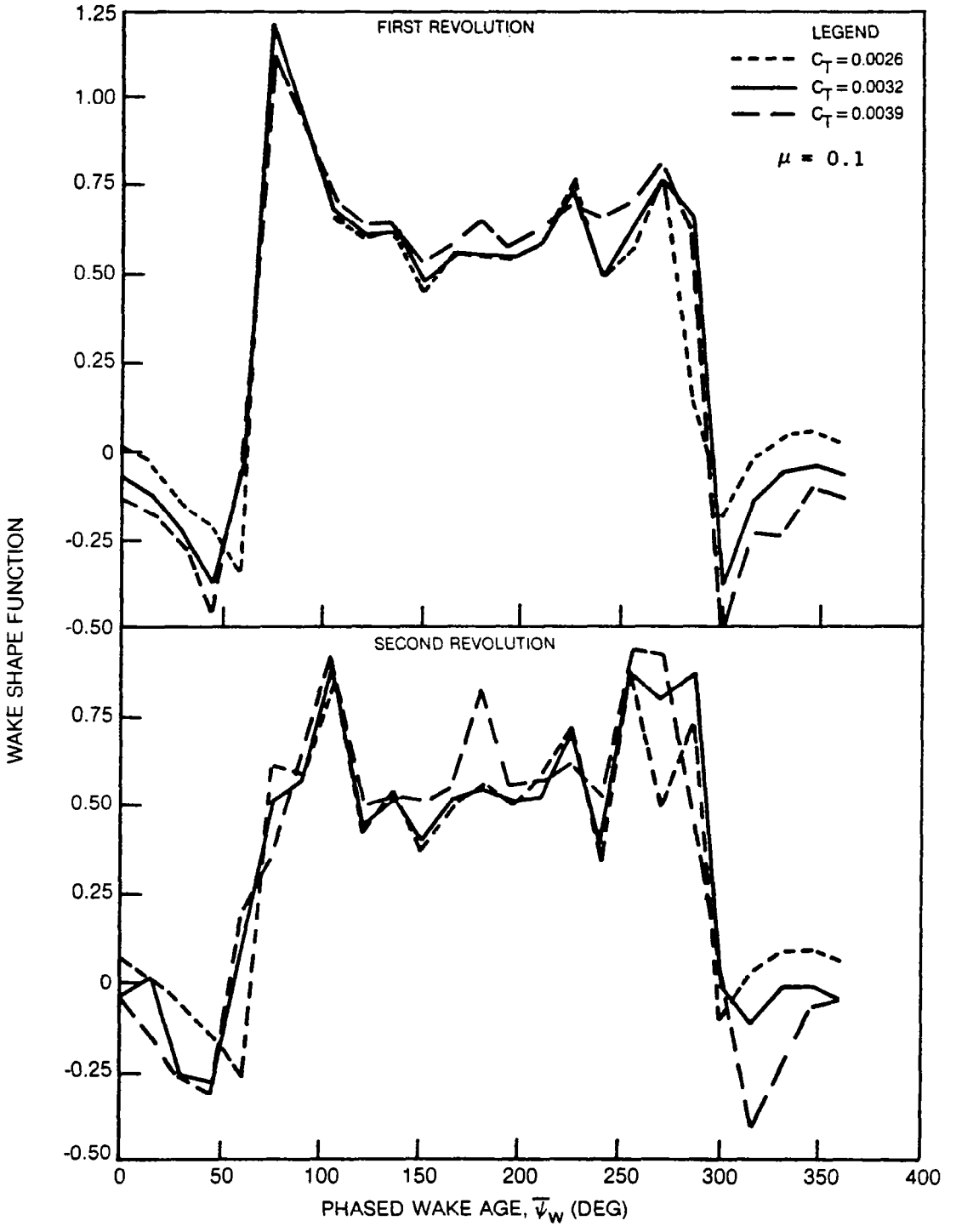

FIGURE 34. VARIATION OF THE GENERALIZED WAKE SHAPE FUNCTION WITH THRUST LEVEL FOR THE TWO-BLADED REPRESENTATIVE ROTOR (μ=0.1)

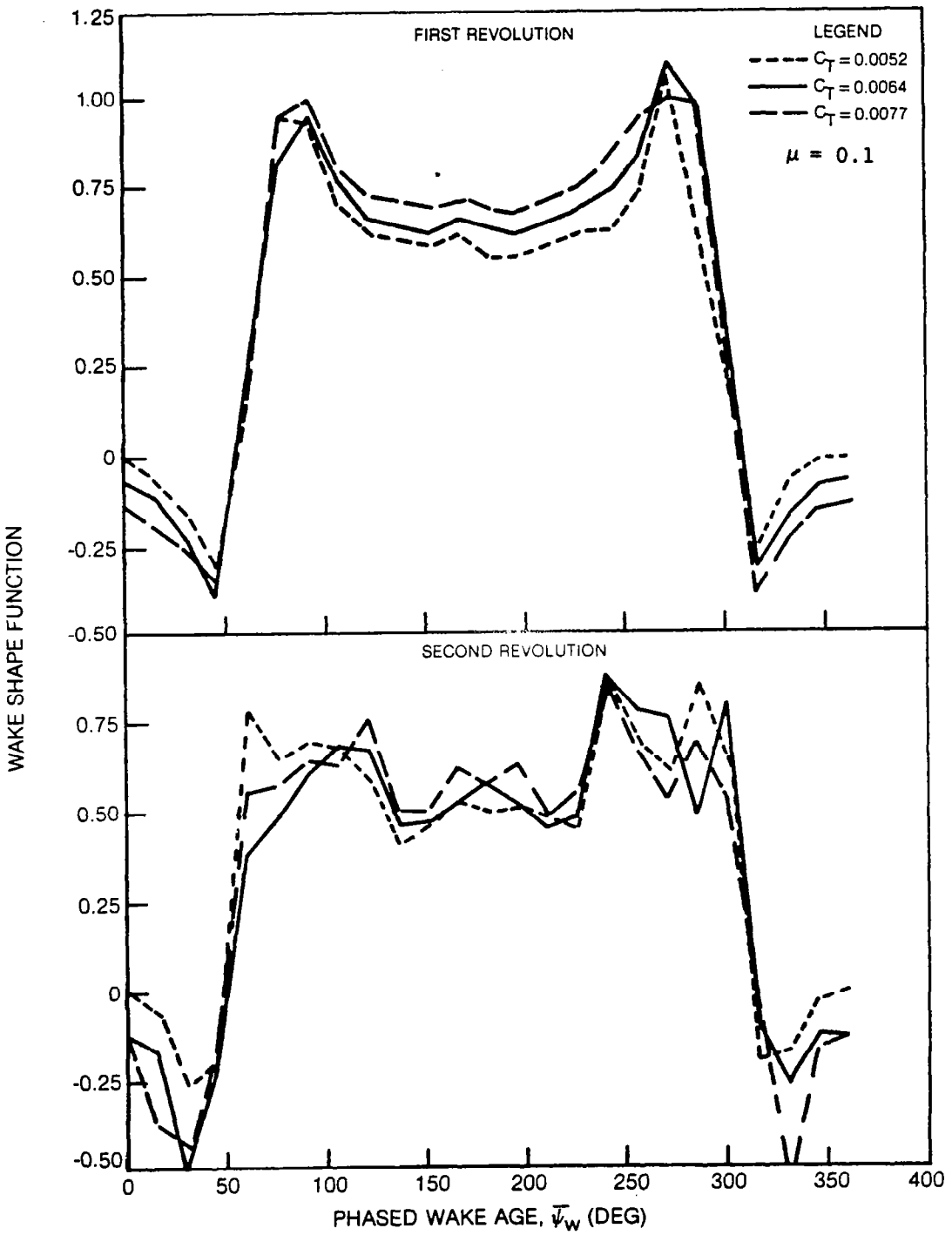

FIGURE 35. VARIATION OF THE GENERALIZED WAKE SHAPE FUNCTION WITH THRUST LEVEL FOR THE FOUR-BLADED REPRESENTATIVE ROTOR (μ=0.1)

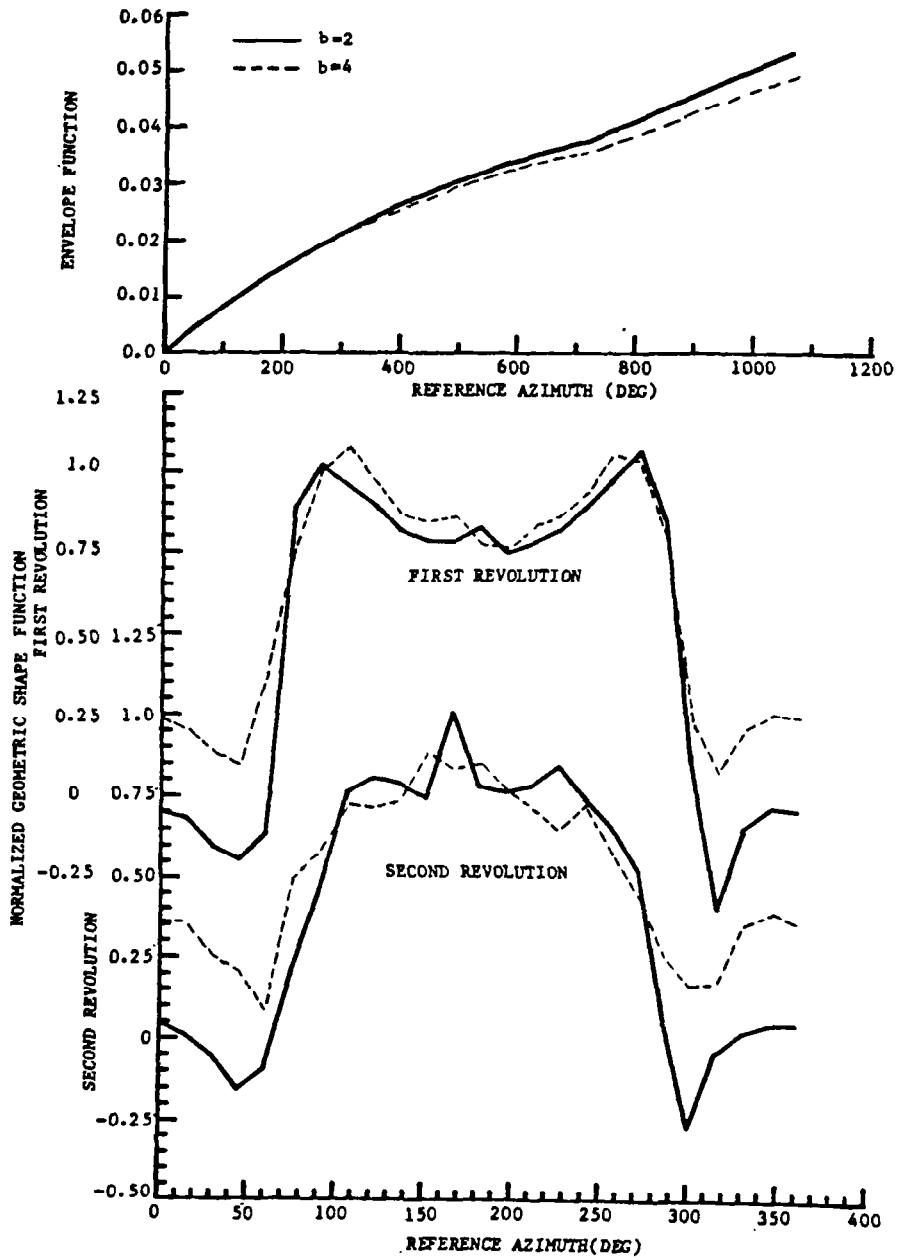

FIGURE 36. COMPARISON OF THE GENERALIZED WAKE FORMULATION FOR TWO AND FOUR BLADES FOR THE SAME THRUST AND ADVANCE RATIO (C_T=0.00321,μ=0.05)

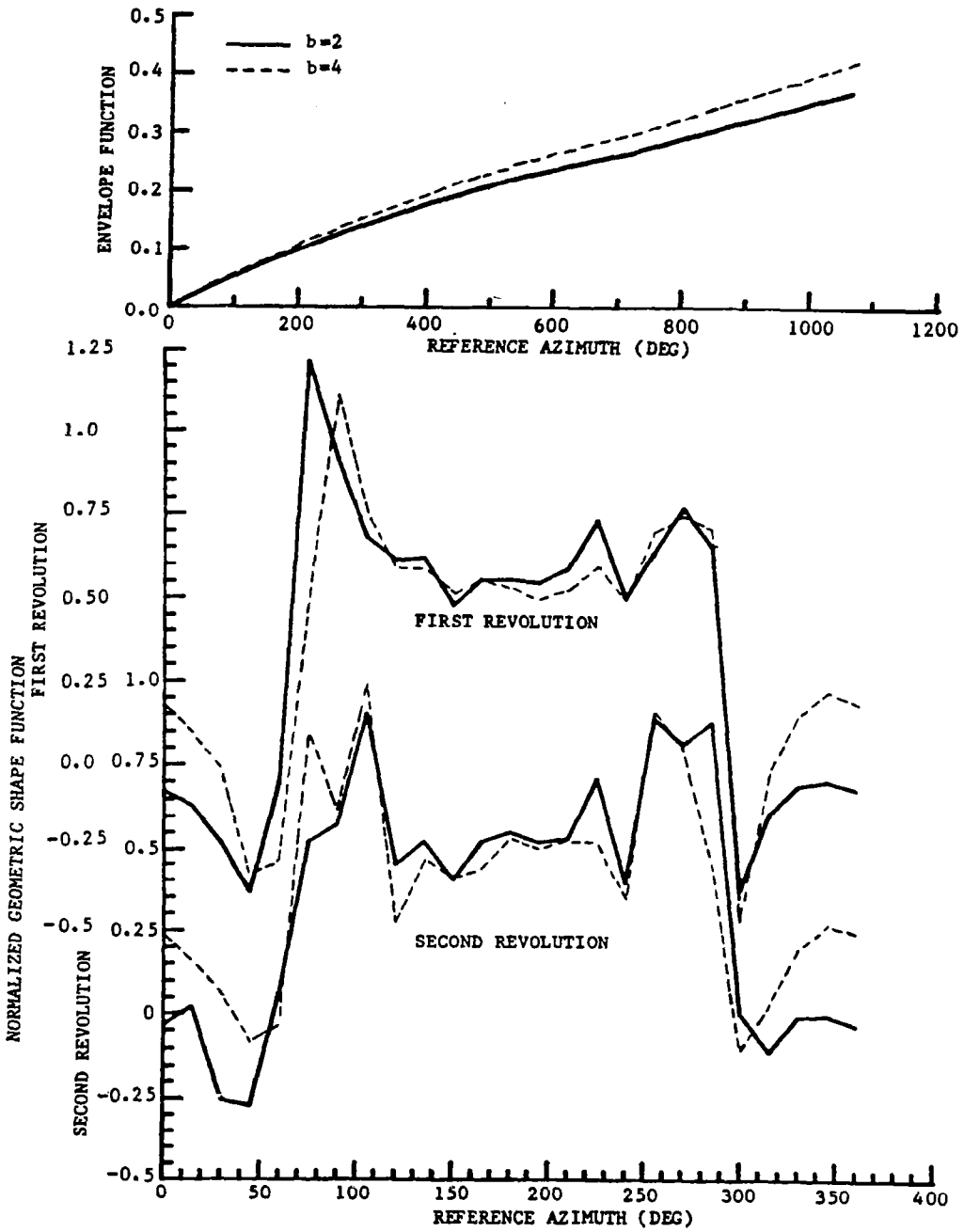

FIGURE 37. COMPARISON OF THE GENERALIZED WAKE FORMULATION FOR TWO AND FOUR BLADES FOR THE SAME THRUST AND ADVANCE RATIO (C_T=0.00321,μ=0.1)

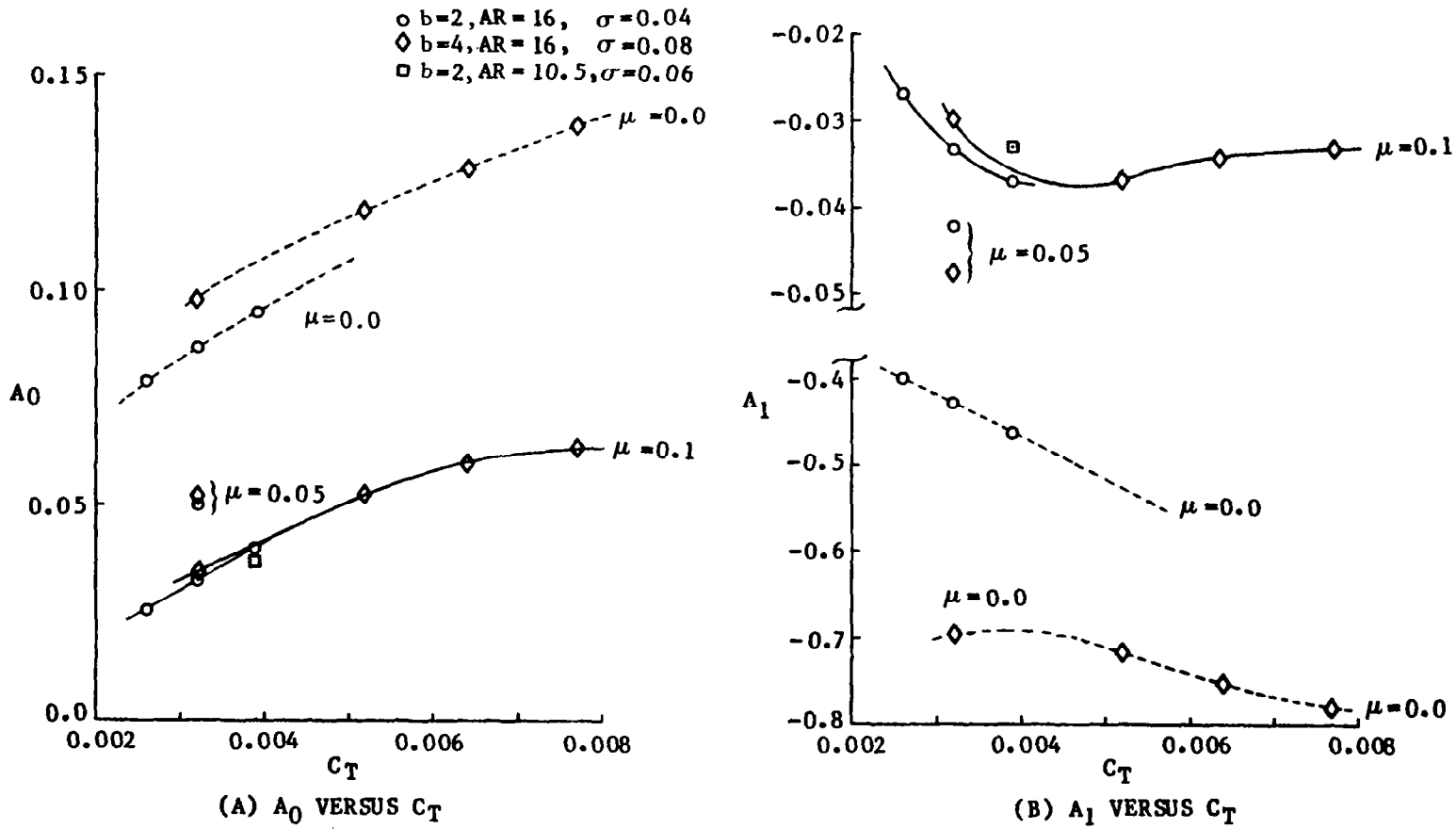

FIGURE 38. VARIATIONS IN THE ENVELOPE FUNCTION COEFFICIENTS FOR THRUST LEVEL AND BLADE NUMBER

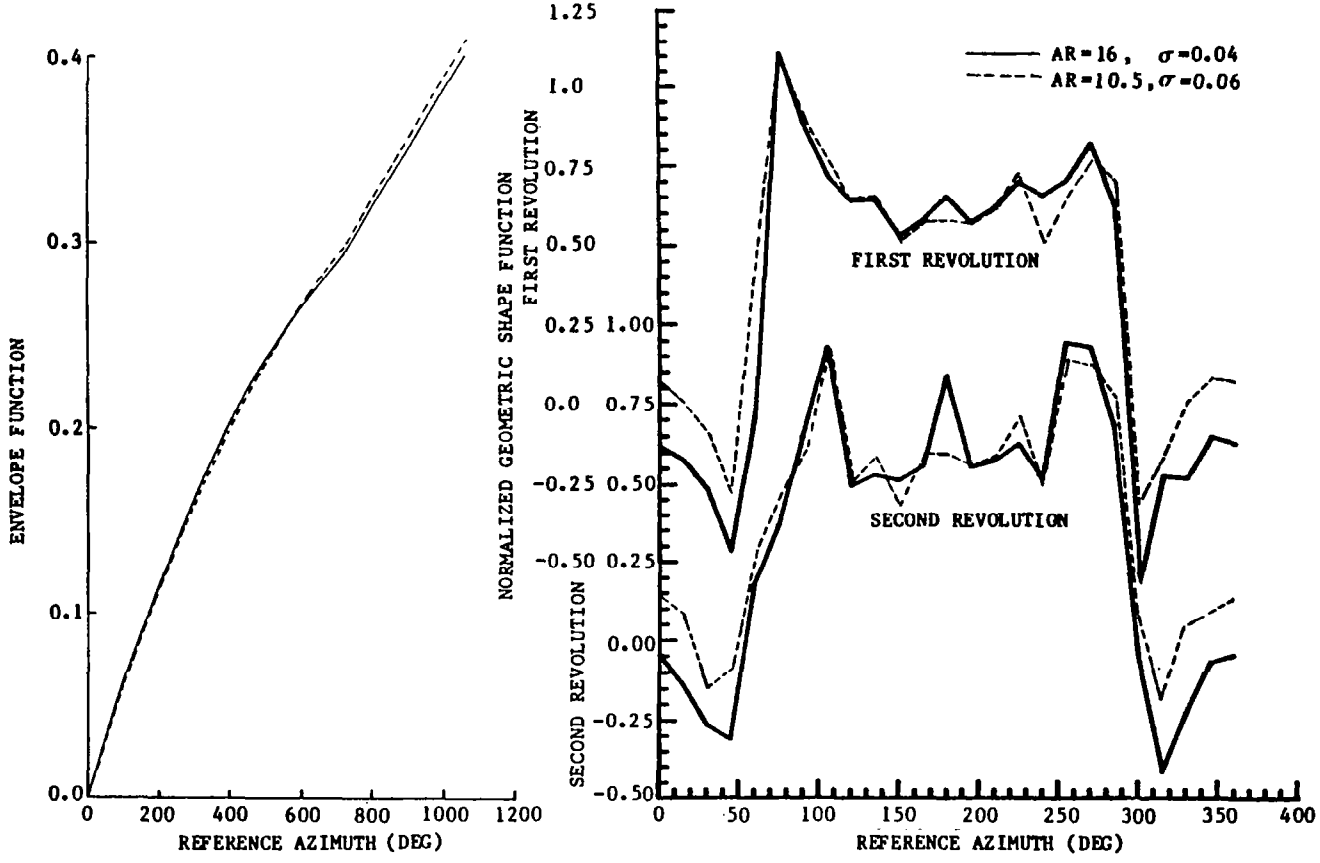

FIGURE 39. COMPARISON OF THE ENVELOPE FUNCTION AND NORMALIZED GEOMETRIC SHAPE FUNCTION FOR TWO ROTOR SOLIDITIES (ASPECT RATIO) AT THE SAME CONDITION (C_T=0.0039,μ=0.1) FOR THE TWO BLADED ROTOR

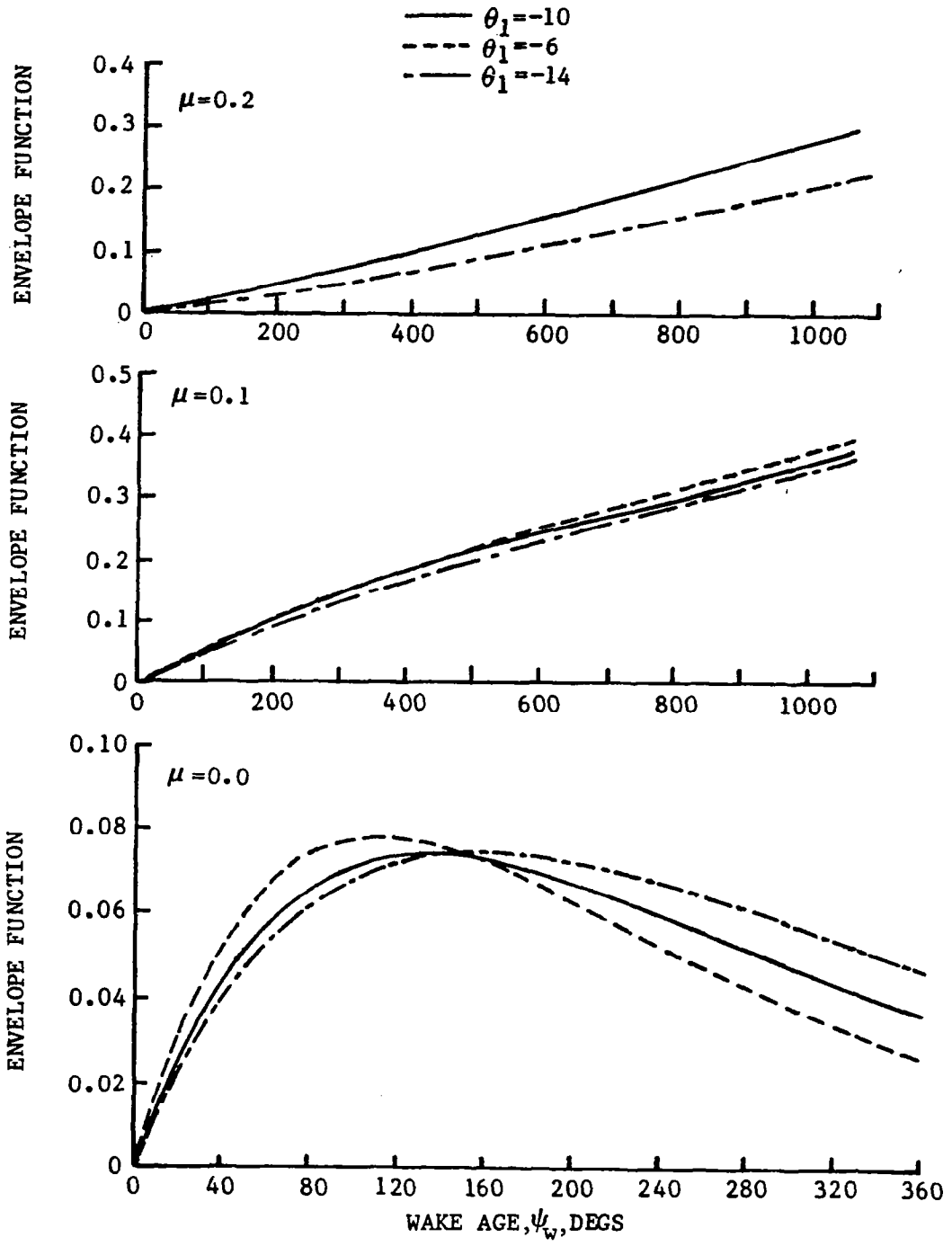

FIGURE 40a. COMPARISON OF THE ENVELOPE FUNCTION VARIATIONS WITH TWIST (b=2, C_T =0.0032)

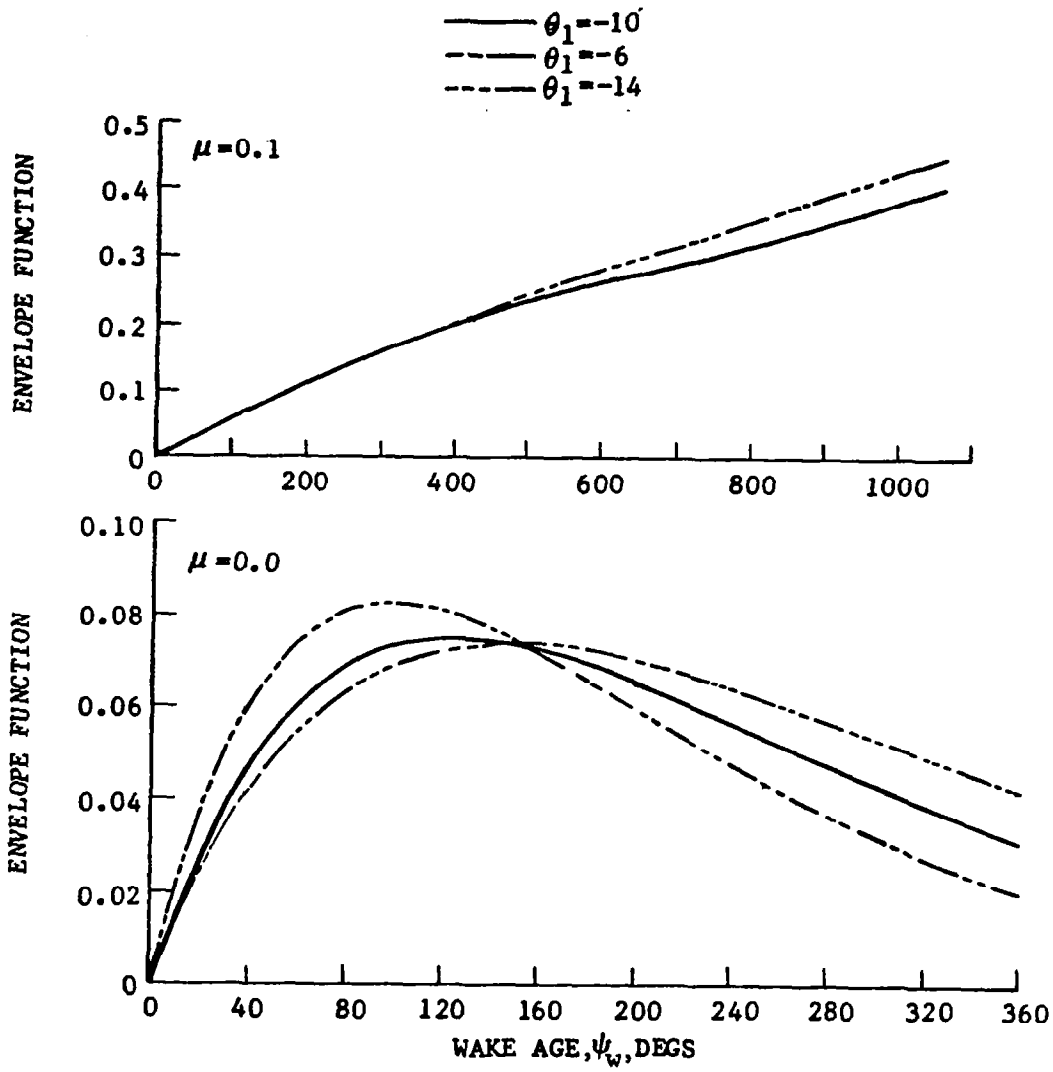

FIGURE 40b. COMPARISON OF THE ENVELOPE FUNCTION VARIATIONS WITH TWIST ($b=2, C_T=0.0039$)

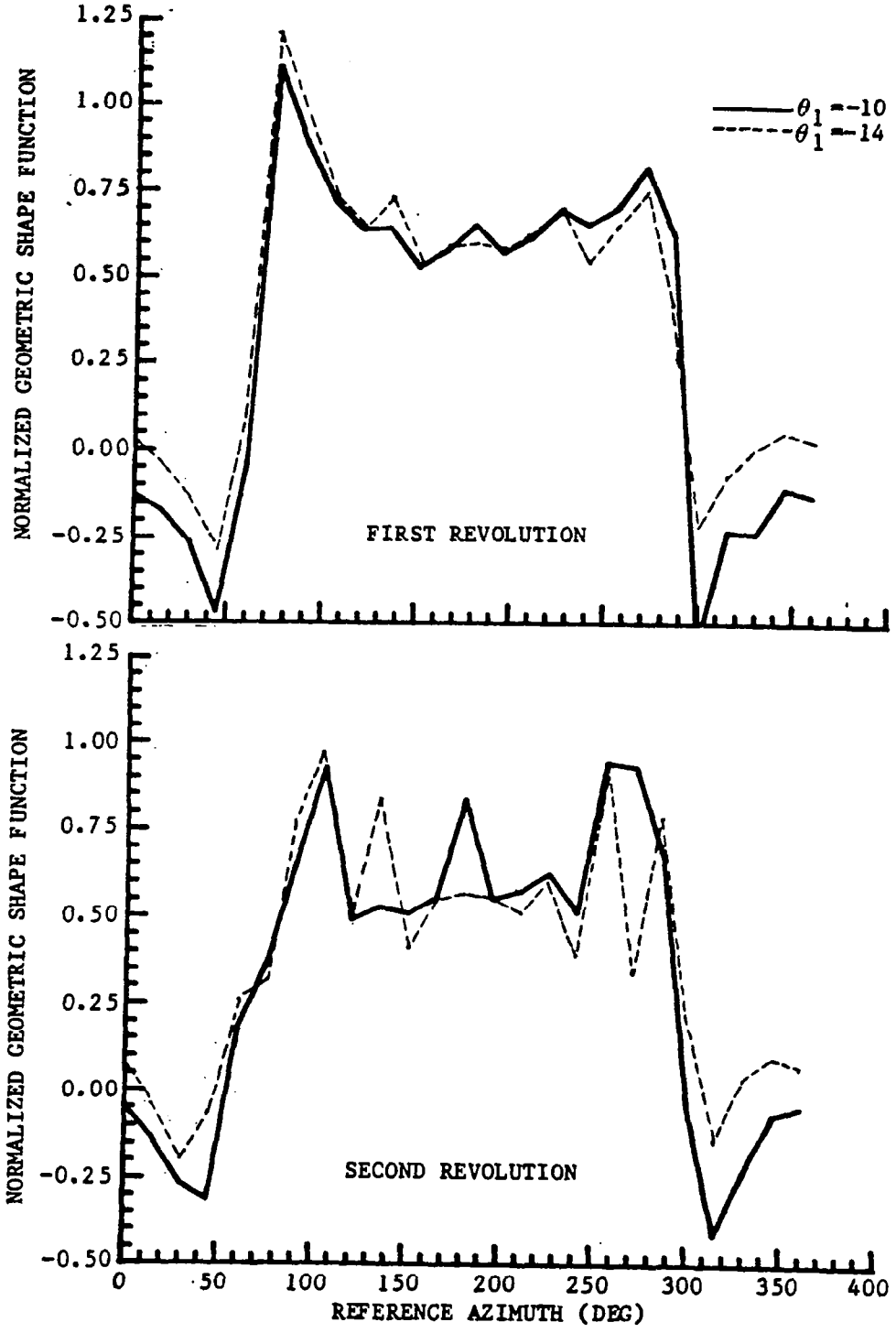

FIGURE 41. COMPARISON OF THE NORMALIZED GEOMETRIC SHAPE FUNCTION FOR TWO DIFFERENT TWIST CONDITIONS AT ONE FLIGHT CONDITION (C_T=0.0039, μ=0.1)

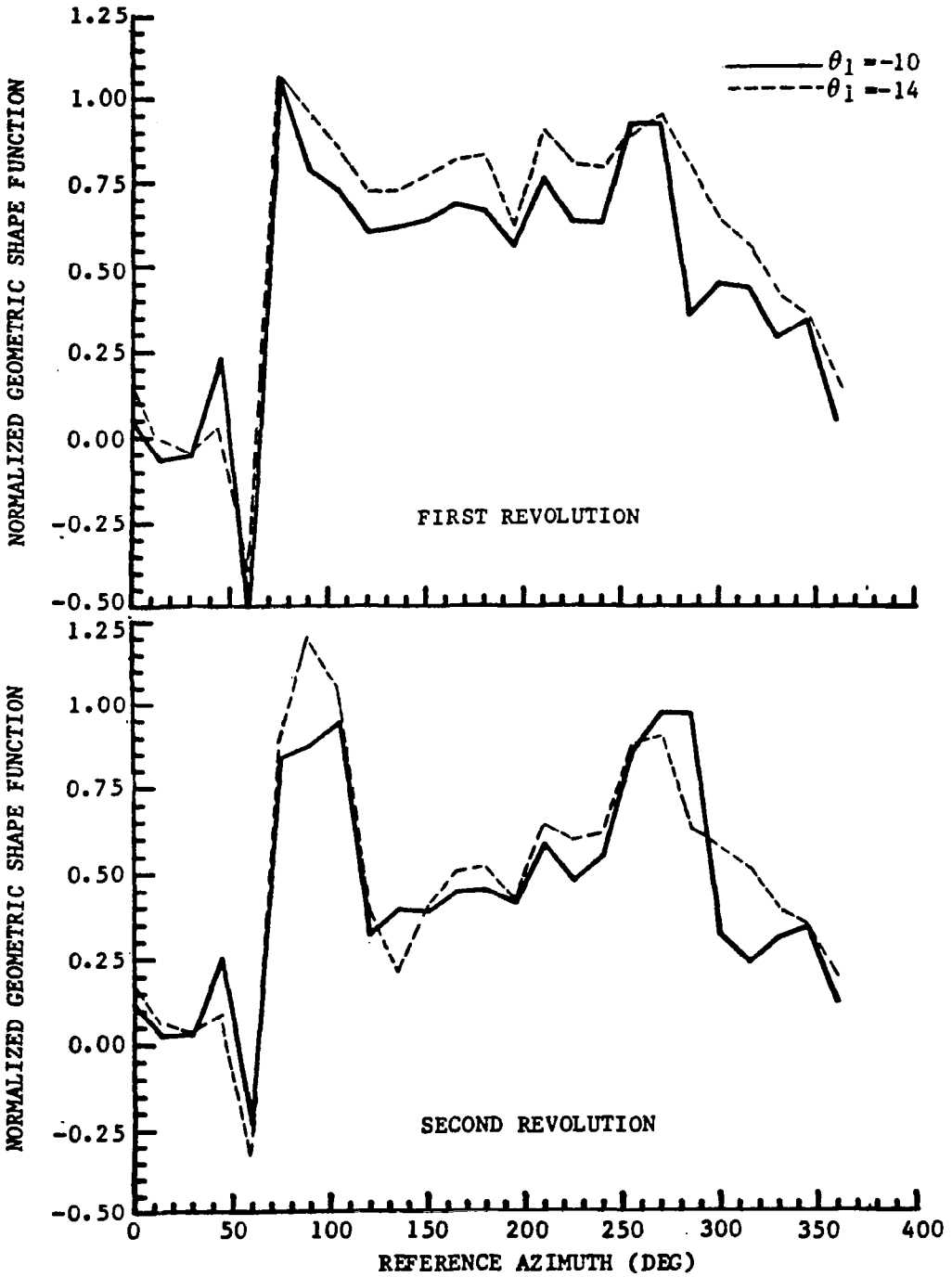

FIGURE 42. COMPARISON OF THE NORMALIZED GEOMETRIC SHAPE FUNCTION FOR TWO DIFFERENT TWIST CONDITIONS AT ONE FLIGHT CONDITION (C_T =0.032, μ=0.2)

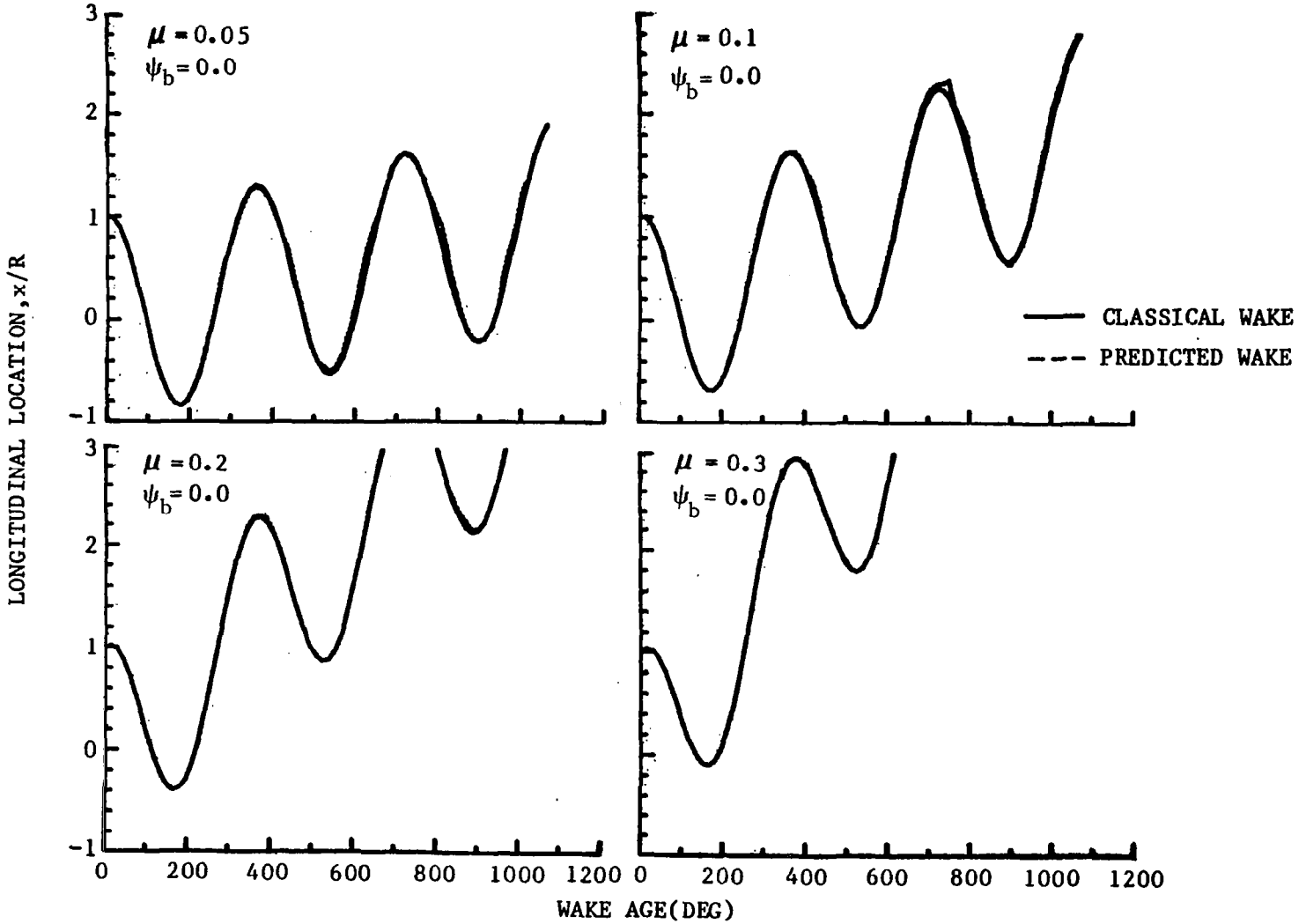

FIGURE 43. DISTORTED AND CLASSICAL TIP VORTEX LONGITUDINAL COORDINATE VERSUS WAKE AGE FOR VARIOUS ADVANCE RATIOS FOR THE REPRESENTATIVE ROTOR (C_T=0.0032, b=2.0)

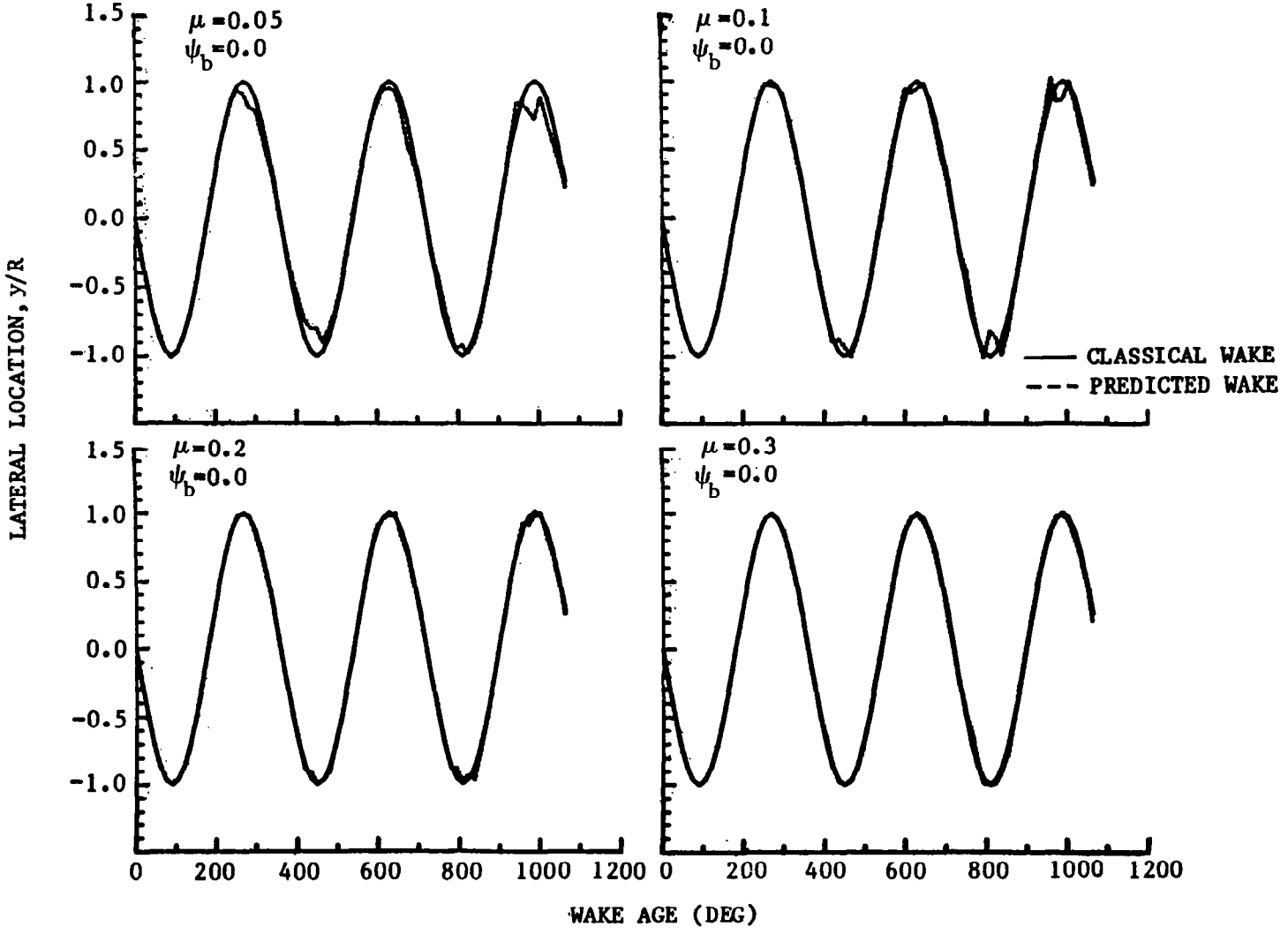

FIGURE 44. DISTORTED AND CLASSICAL TIP VORTEX LATERAL COORDINATE VERSUS WAKE AGE FOR VARIOUS ADVANCE RATIOS FOR THE REPRESENTATIVE ROTOR (C_T=0.0032,b=2.0)

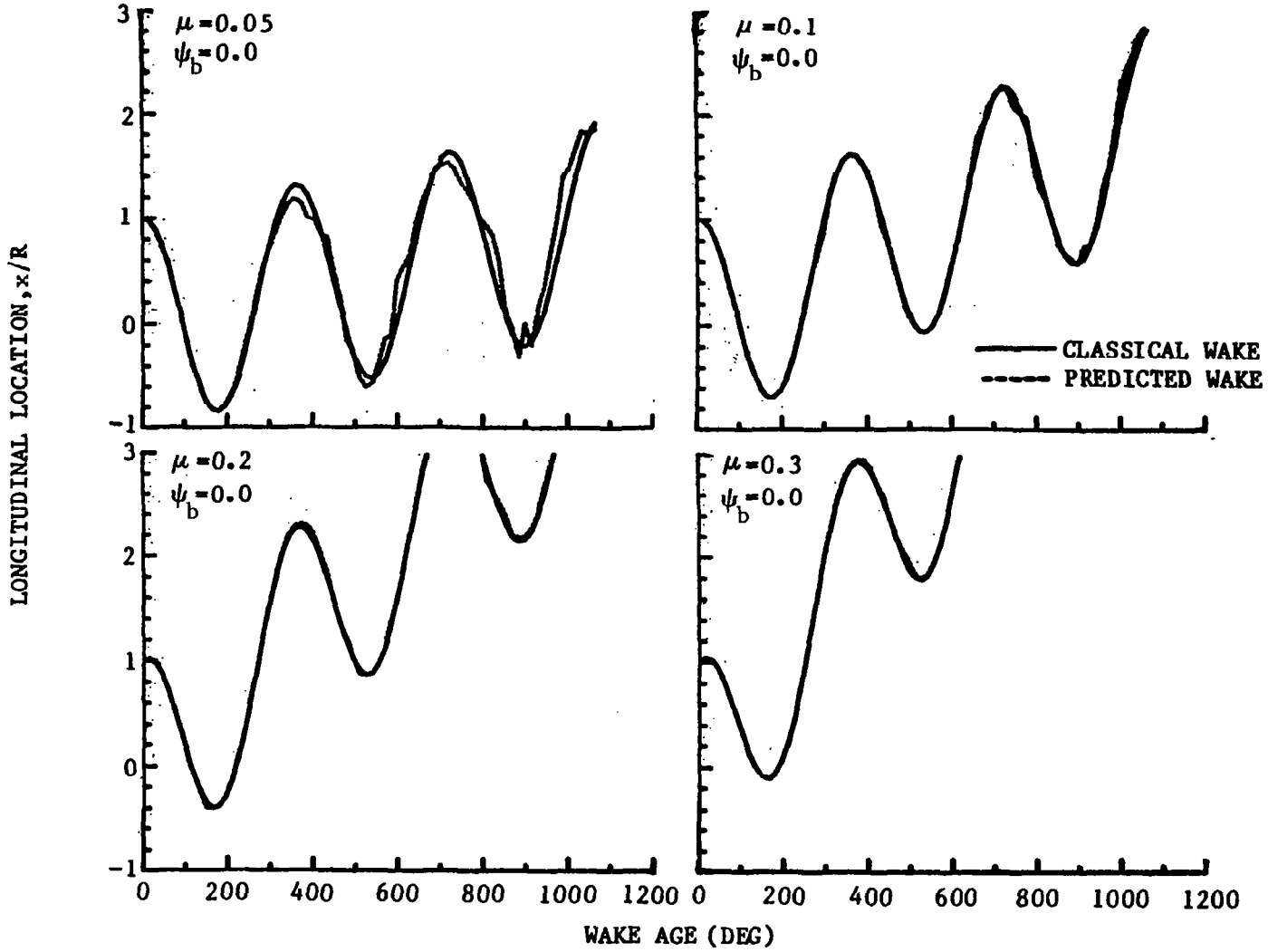

FIGURE 45. DISTORTED AND CLASSICAL TIP VORTEX LONGITUDINAL COORDINATE VERSUS WAKE AGE FOR VARIOUS ADVANCE RATIOS FOR THE REPRESENTATIVE ROTOR (C_T=0.0064,b=4.0)

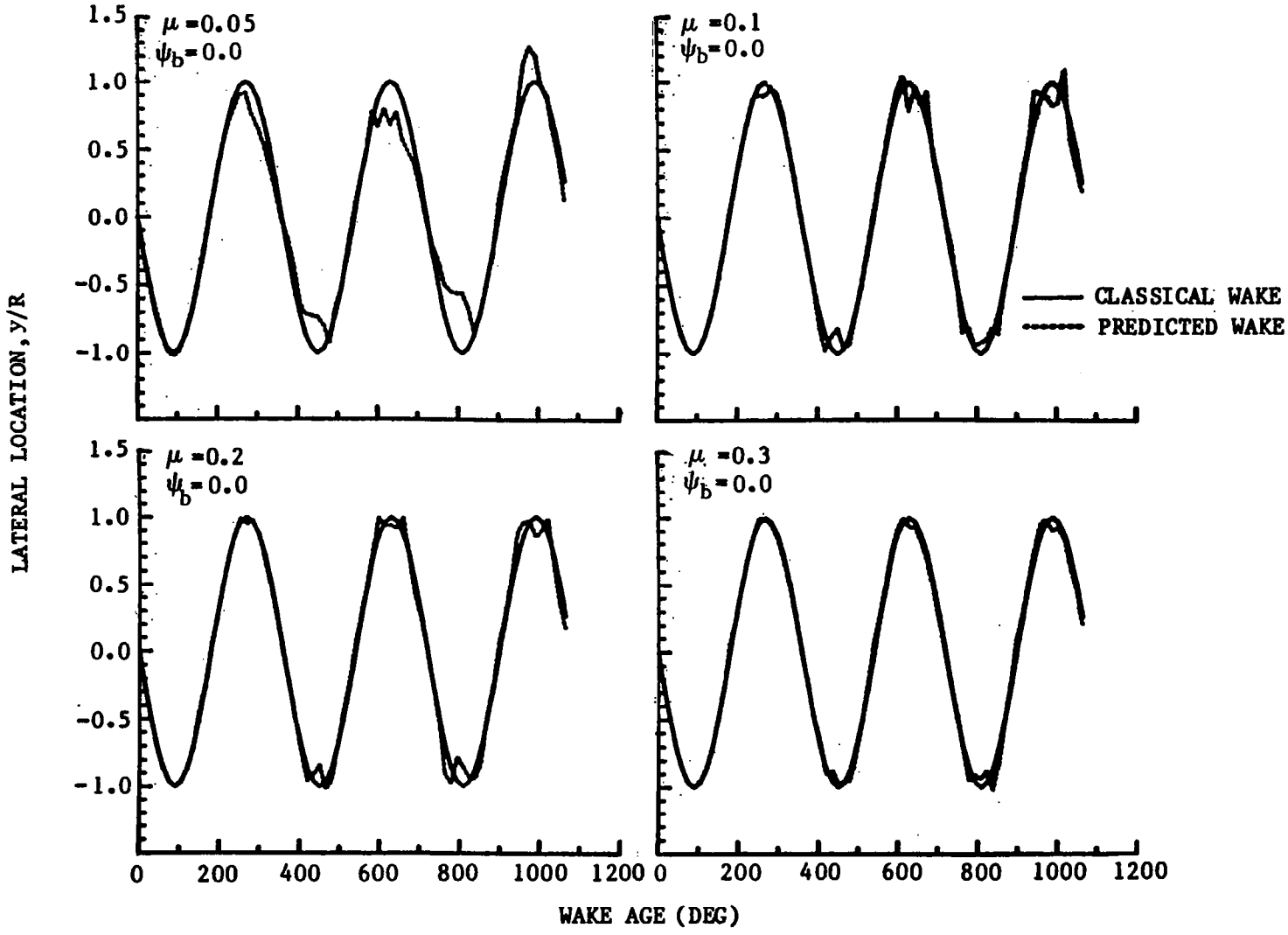

FIGURE 46. DISTORTED AND CLASSICAL TIP VORTEX LATERAL COORDINATE VERSUS WAKE AGE FOR VARIOUS ADVANCE RATIOS FOR THE REPRESENTATIVE ROTOR (C_T=0.0064, b=4.0)

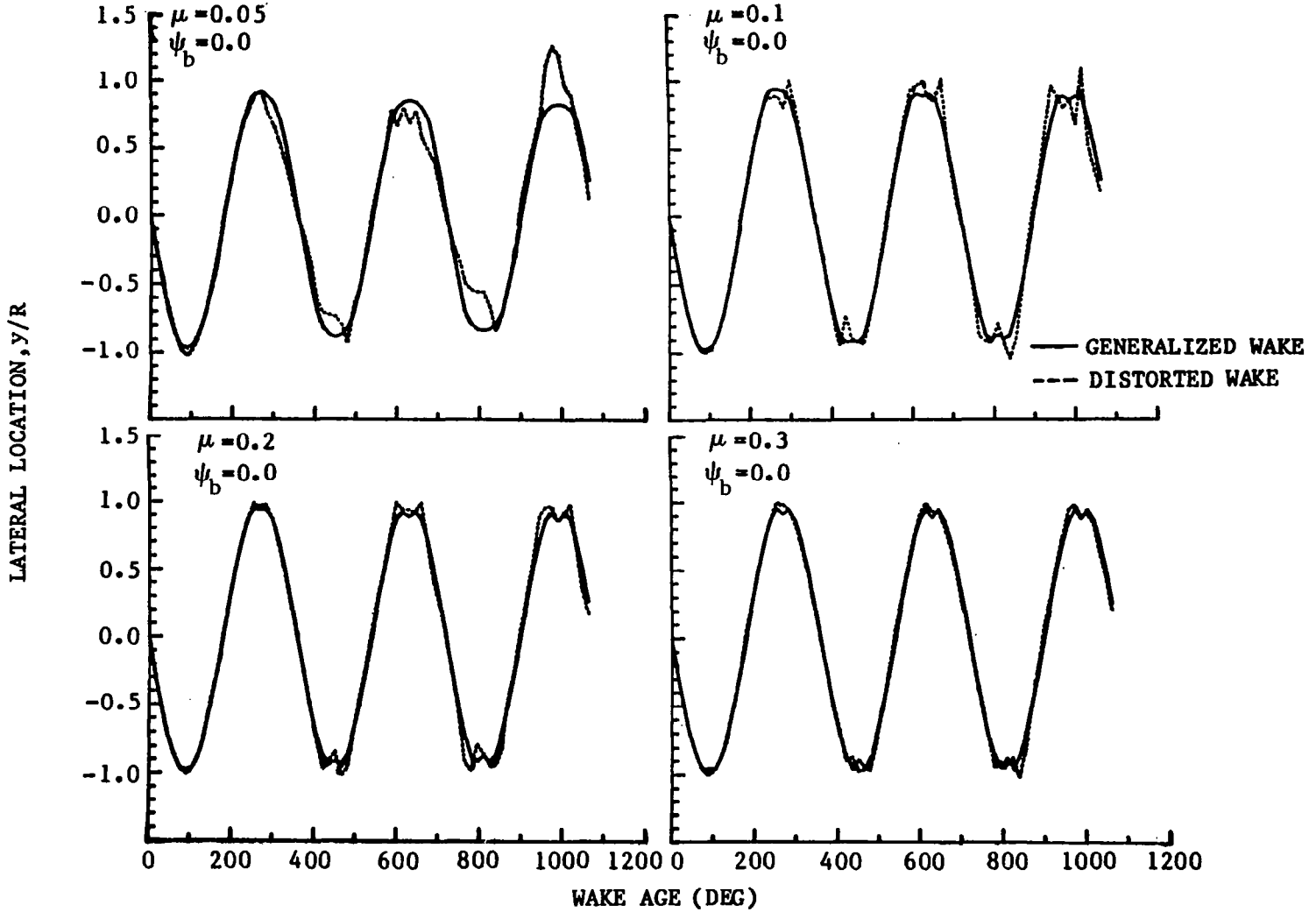

FIGURE 47. COMPARISON OF THE PREDICTED GENERALIZED AND DISTORTED LATERAL COORDINATE FOR VARIOUS ADVANCE RATIOS (C_T=0.0064, b=4.0)

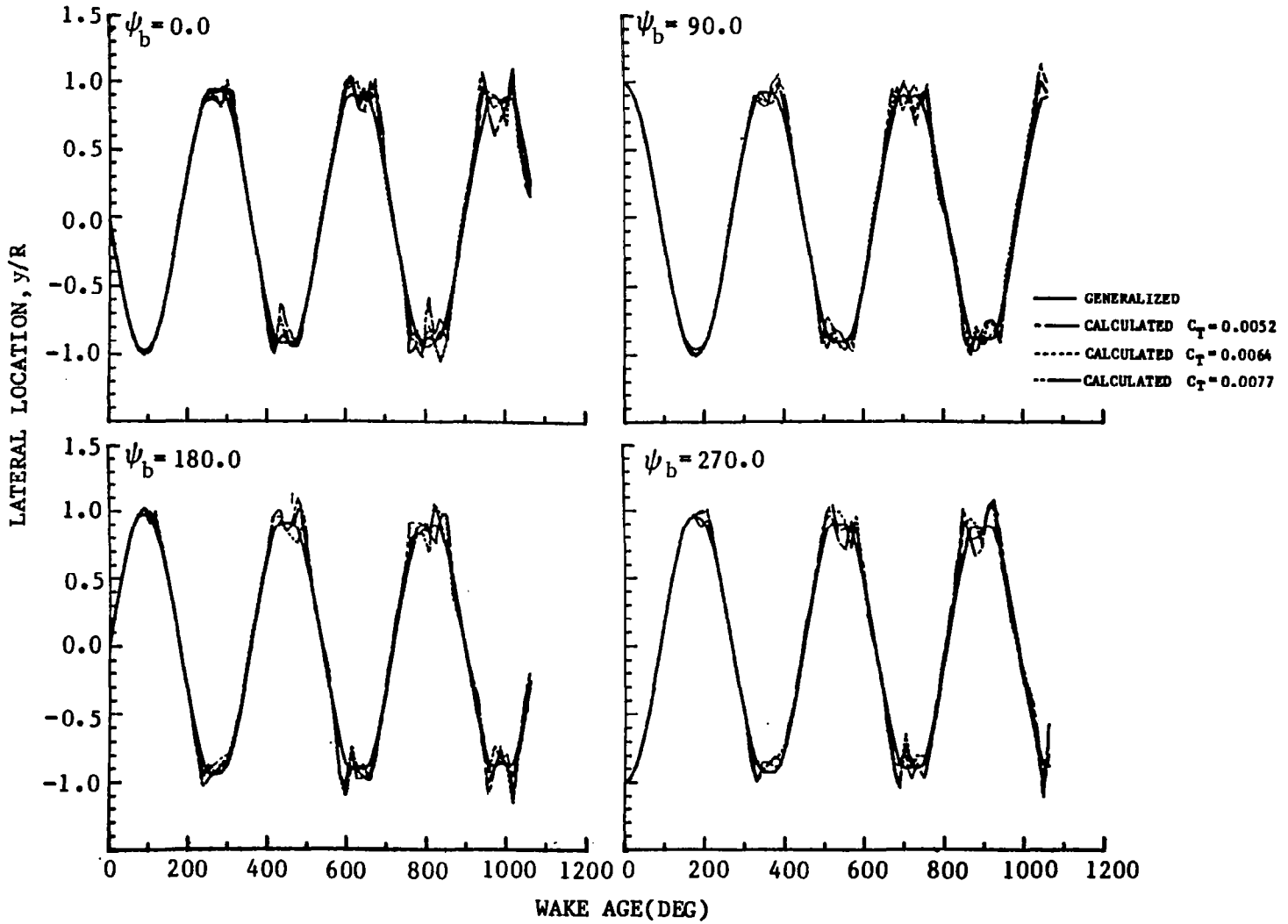

FIGURE 48. COMPARISON OF THE GENERALIZED LATERAL TIP VORTEX COORDINATE WITH THE PREDICTED DISTORTED LATERAL COORDINATES FOR SEVERAL THRUST LEVELS AT SELECTED BLADE AZIMUTH POSITION (b=4)

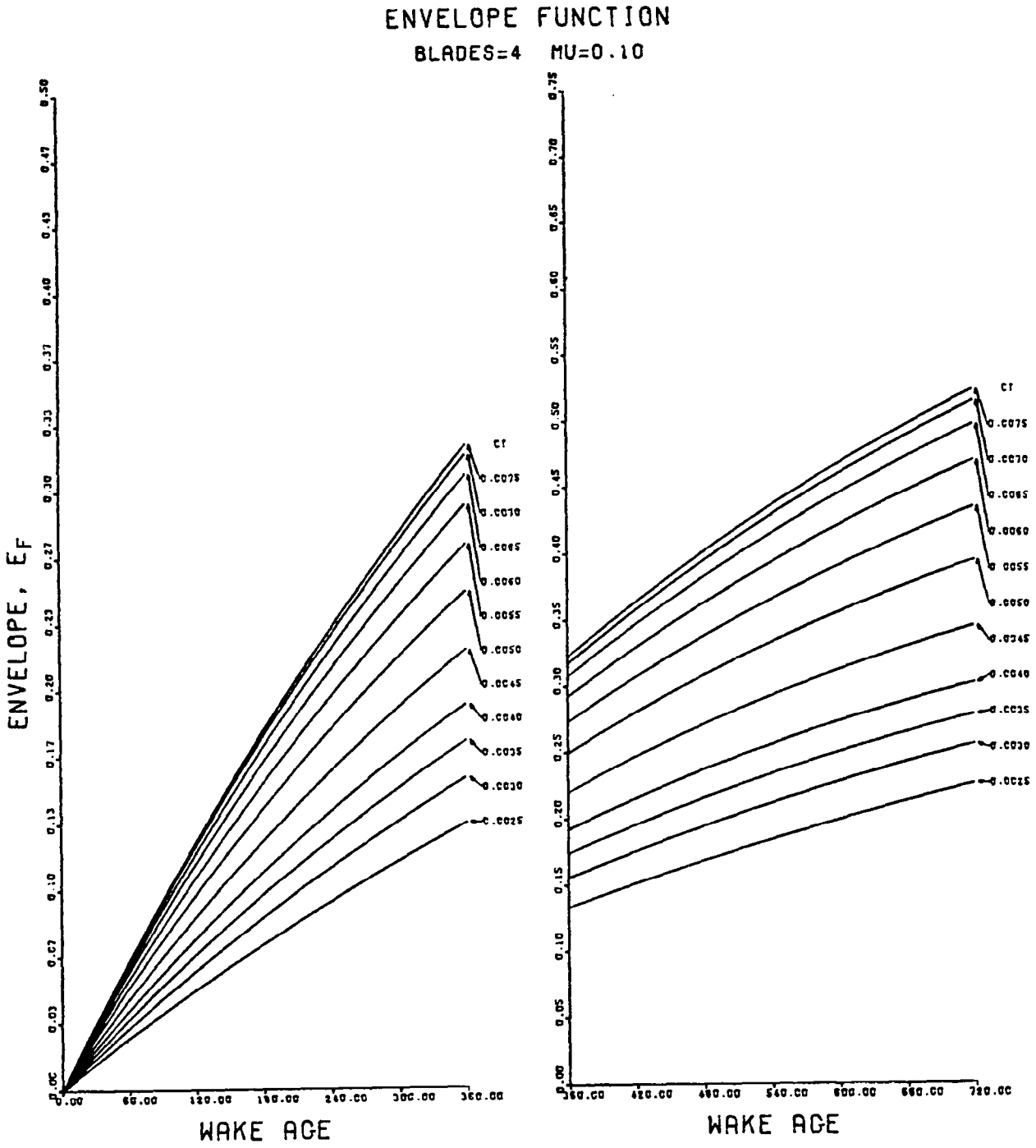

FIGURE 49a. GENERALIZED WAKE ENVELOPE FUNCTION CHARTS FOR FOUR BLADES (μ = .10)

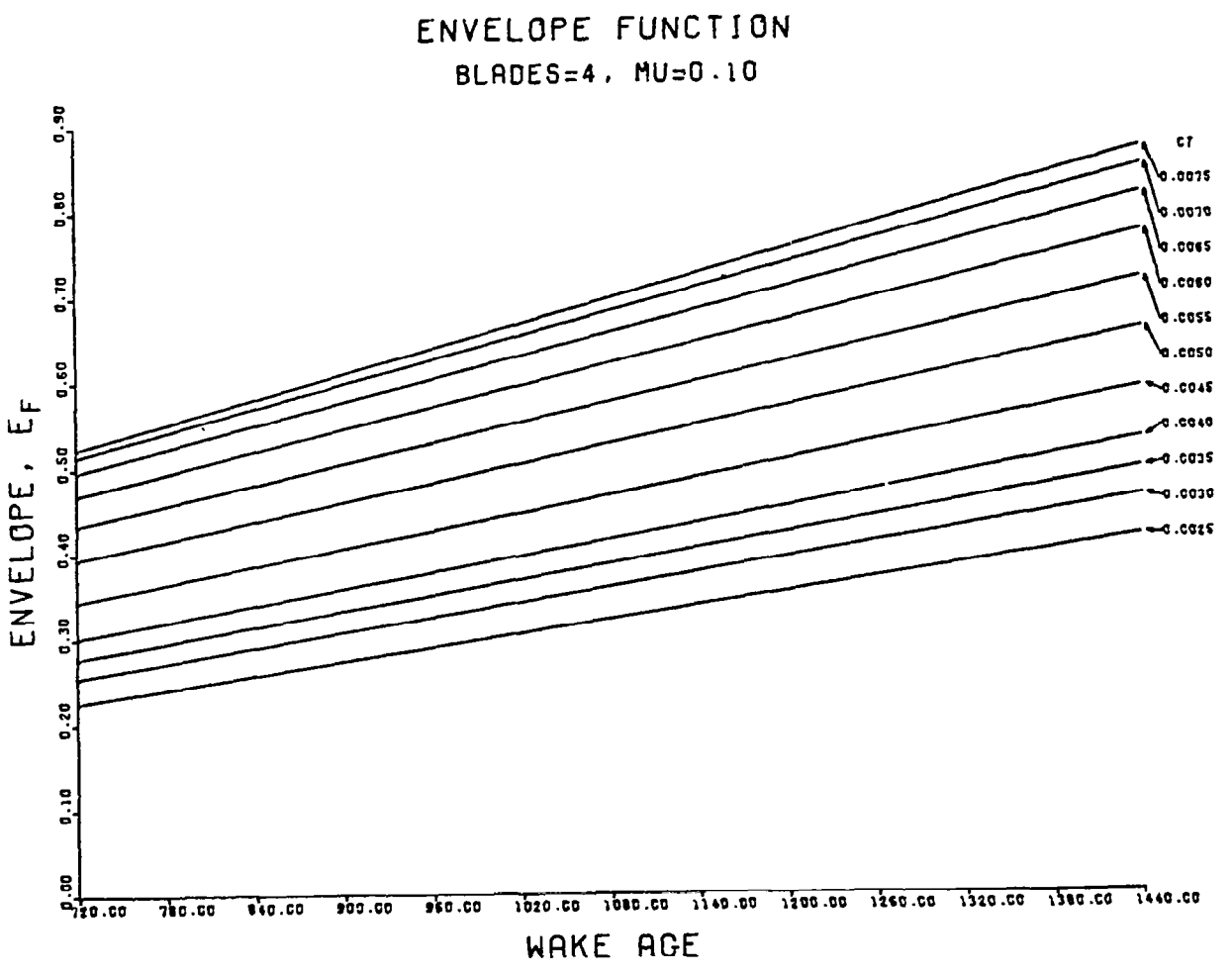

FIGURE 49b. CONTINUED

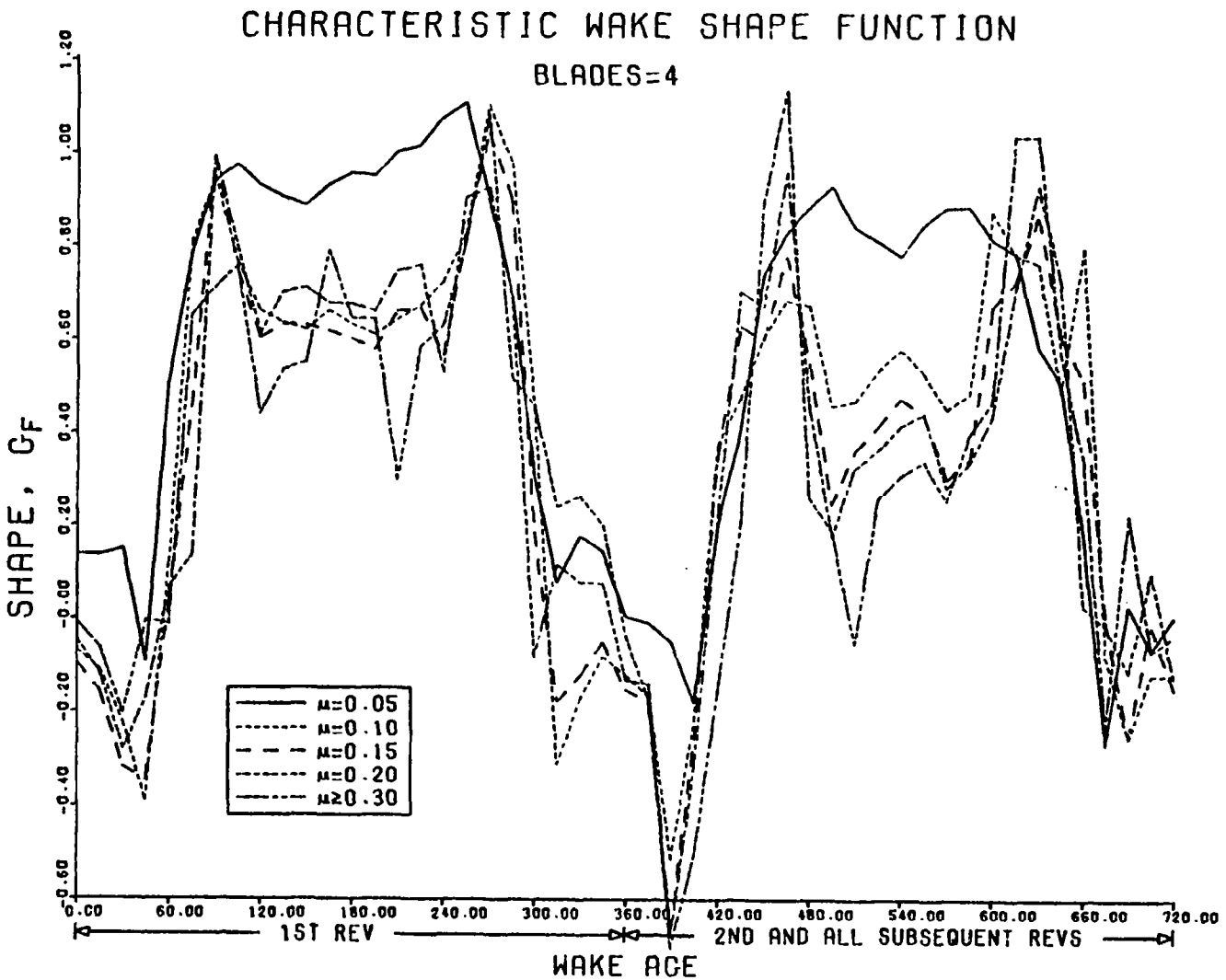

FIGURE 50. GENERALIZED WAKE SHAPE FUNCTION CHART FOR FOUR BLADES

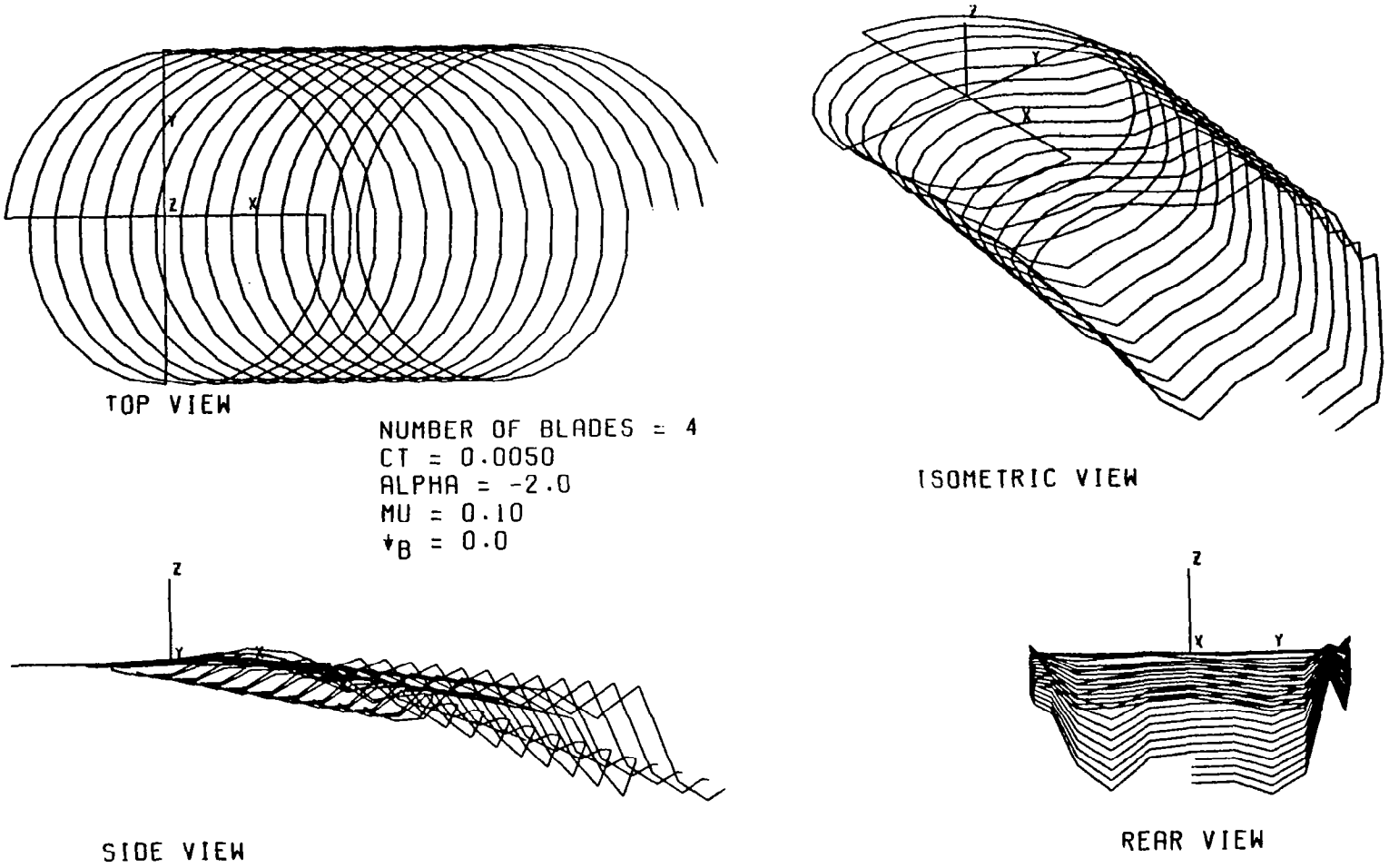

FIGURE 51. PROJECTION AND ISOMETRIC VIEWS FOR GENERALIZED DISTORTED TIP VORTEX, VARYING ADVANCE RATIO (V/ΩR = .10)

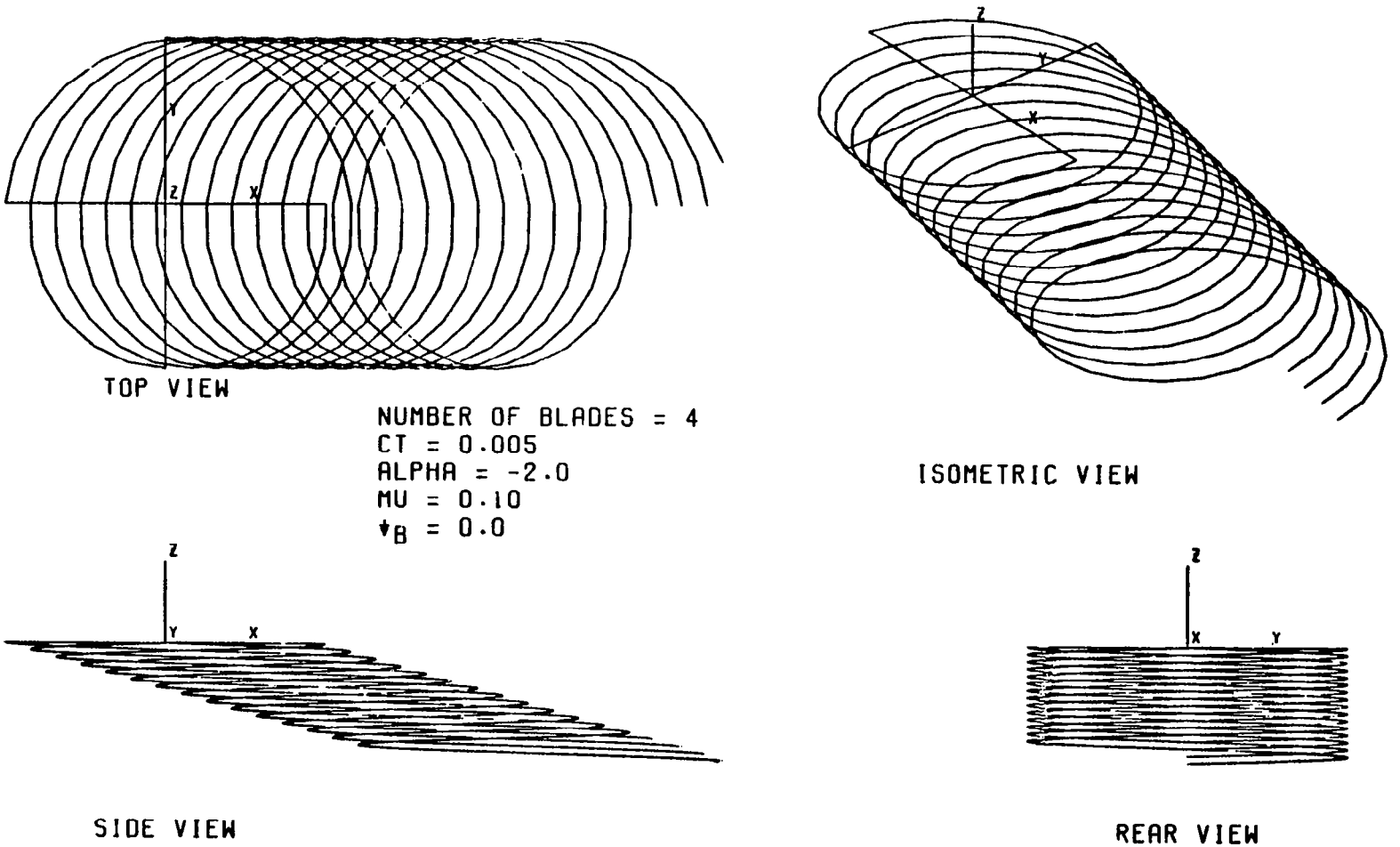

FIGURE 52. PROJECTION AND ISOMETRIC VIEWS OF UNDISTORTED TIP VORTEX, VARYING ADVANCE RATIO ($V/\Omega R$ = .10)

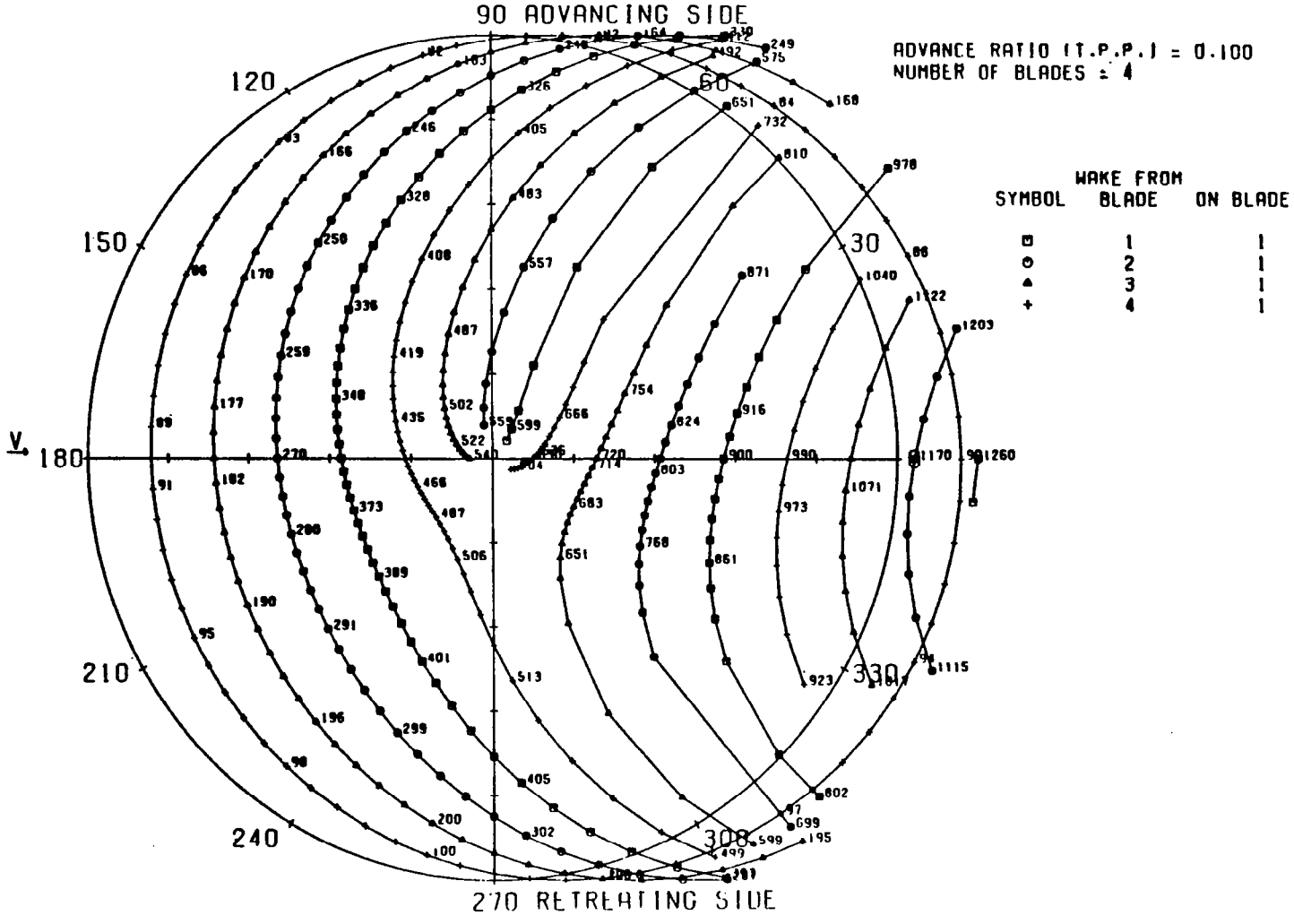

FIGURE 53. POTENTIAL BLADE/TIP VORTEX INTERSECTION PLOT FOR FOUR BLADES (POLAR FORMAT), μ = .10

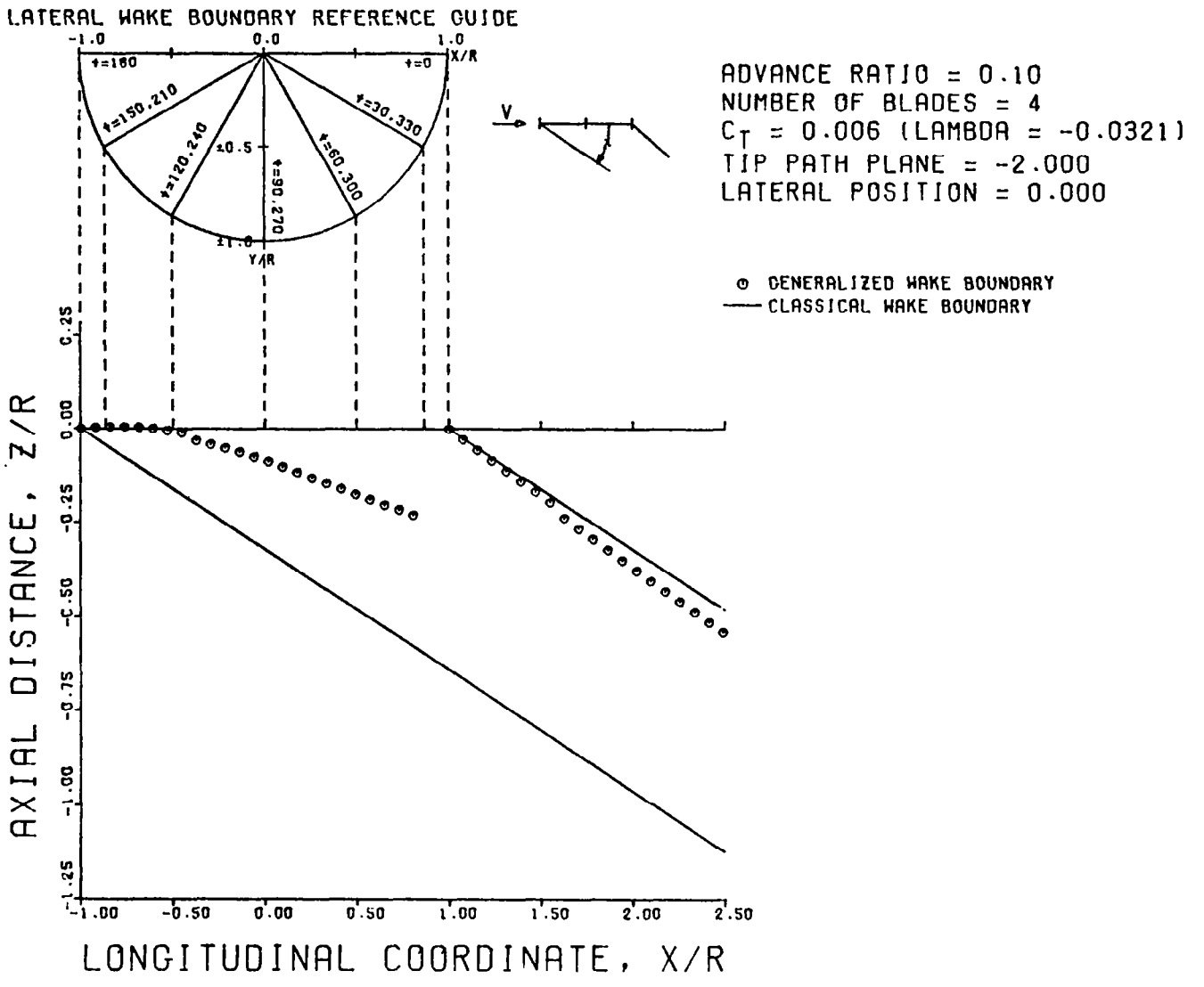

FIGURE 54. FORE AND AFT WAKE BOUNDARY CHARTS FOR THE GENERALIZED DISTORTED TIP VORTEX (μ = .1, B = 4, C_T = .006, α = -2), Y/R = 0.0

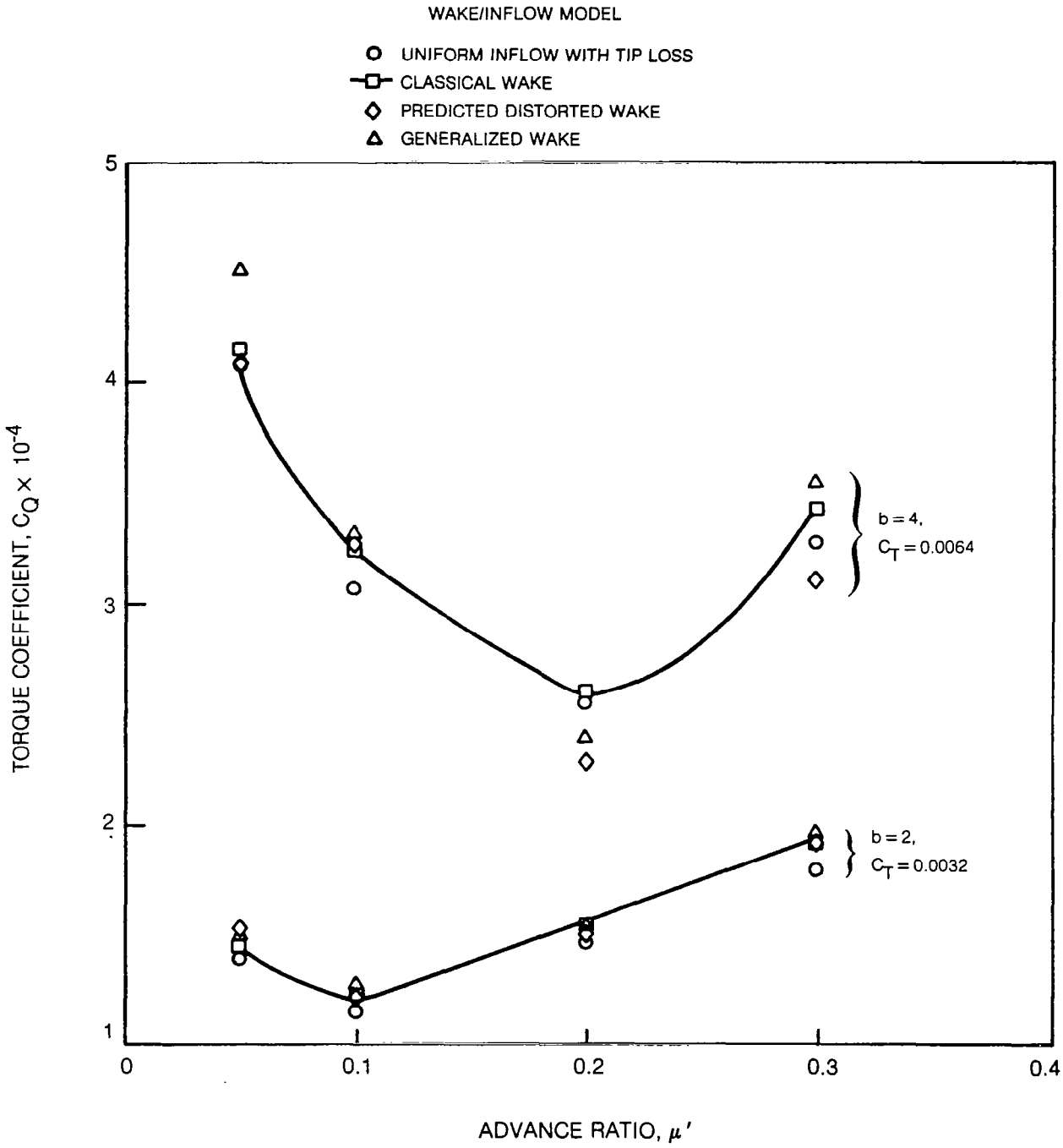

Figure 55. Influence of Inflow Models on Rotor Torque

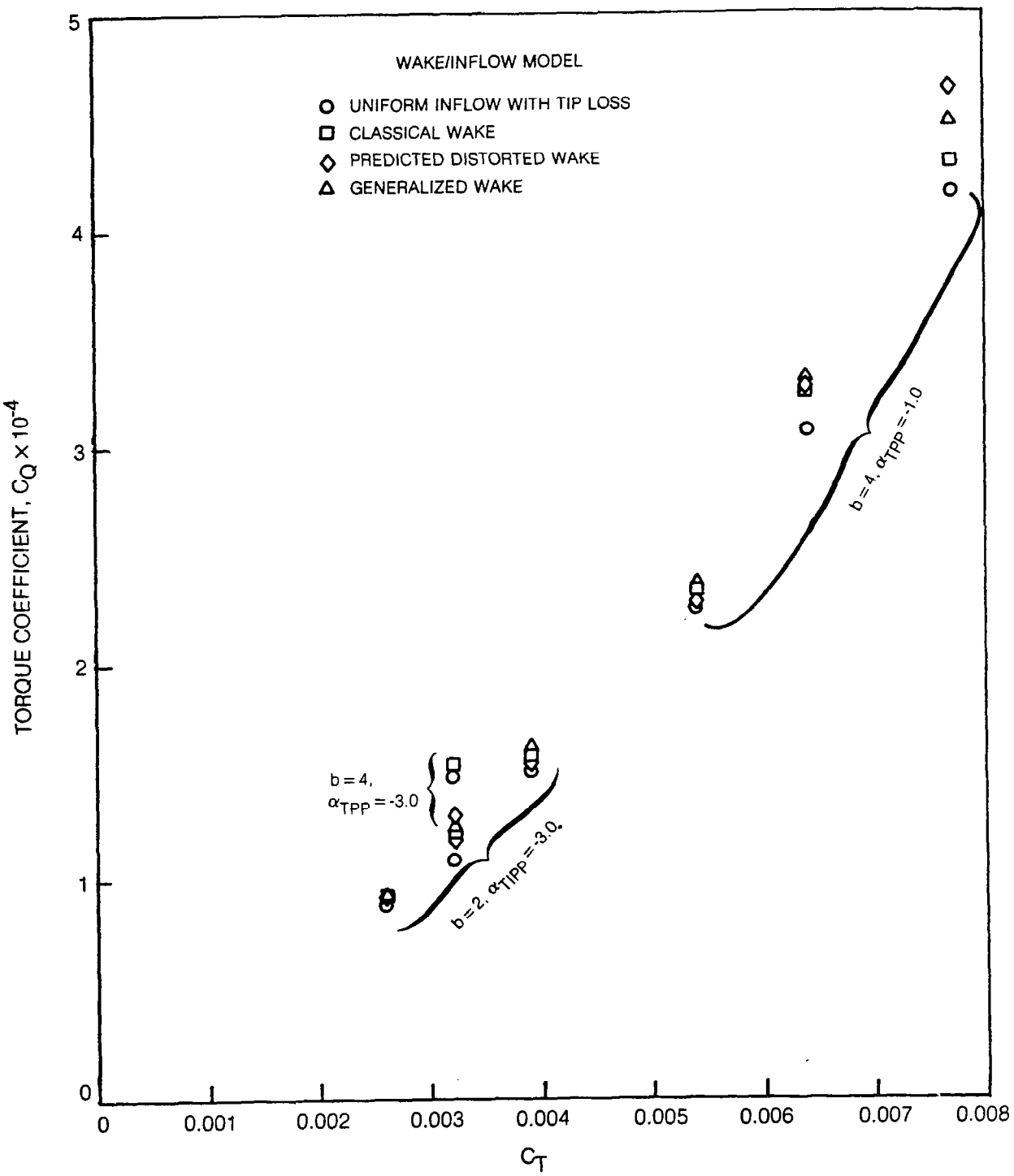

Figure 56. Comparison of Torque Versus Thrust for Various Inflow Models ($\mu = 0.1$)

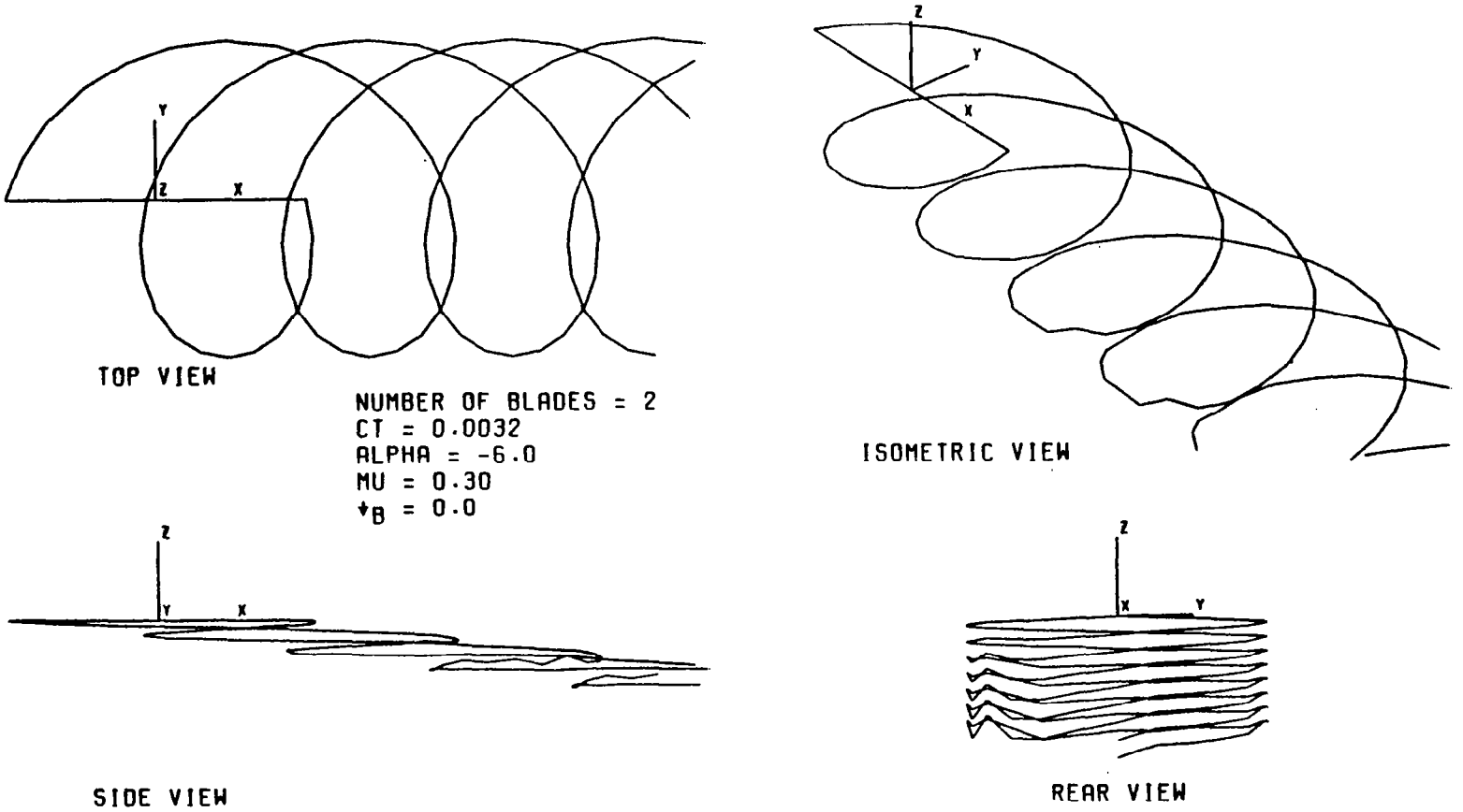

FIGURE 57. GENERALIZED TIP VORTEX GEOMETRY FOR TWO-BLADED REPRESENTATIVE ROTOR, μ=0.3

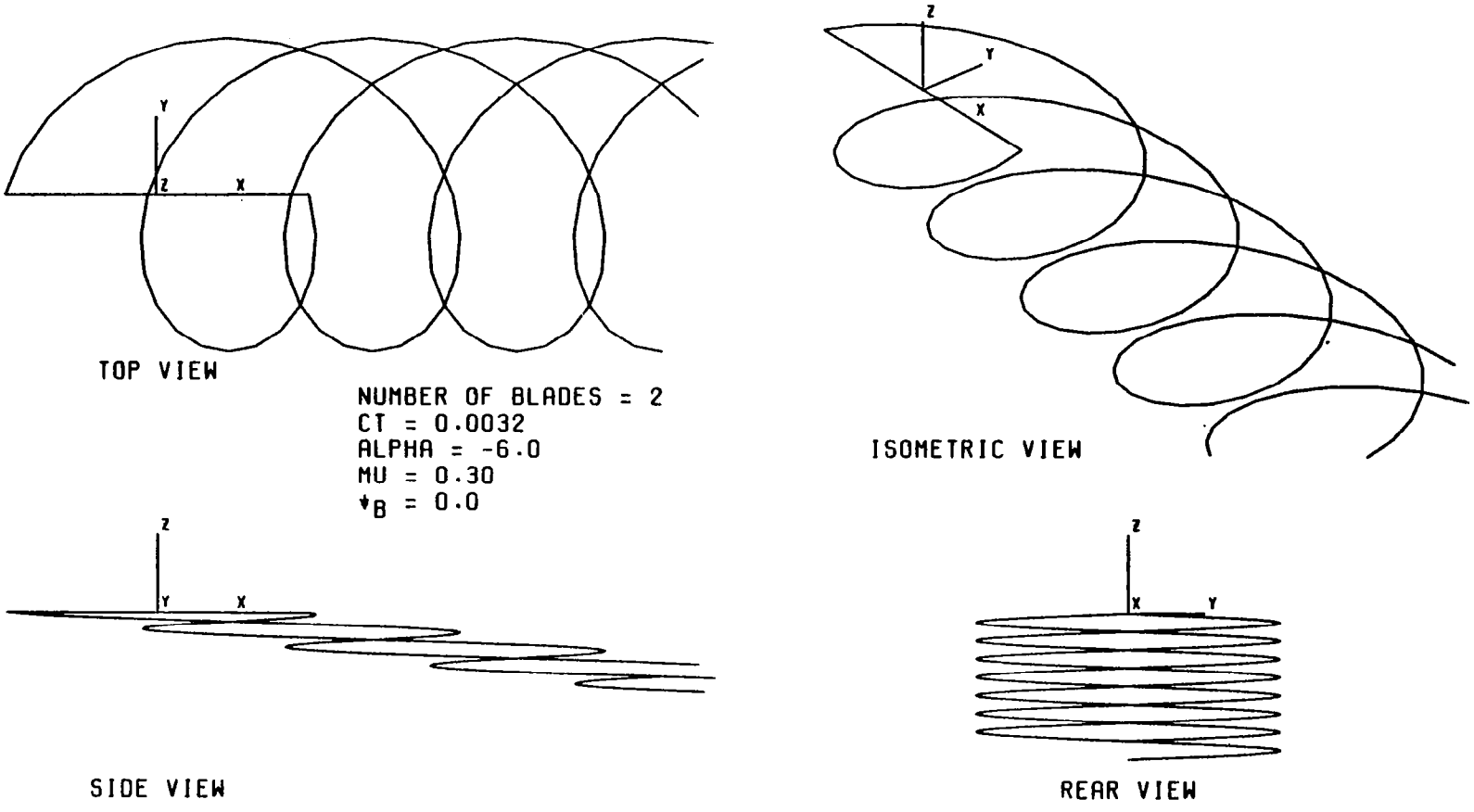

FIGURE 58. UNDISTORTED TIP VORTEX GEOMETRY FOR TWO-BLADED REPRESENTATIVE ROTOR, μ=0.3

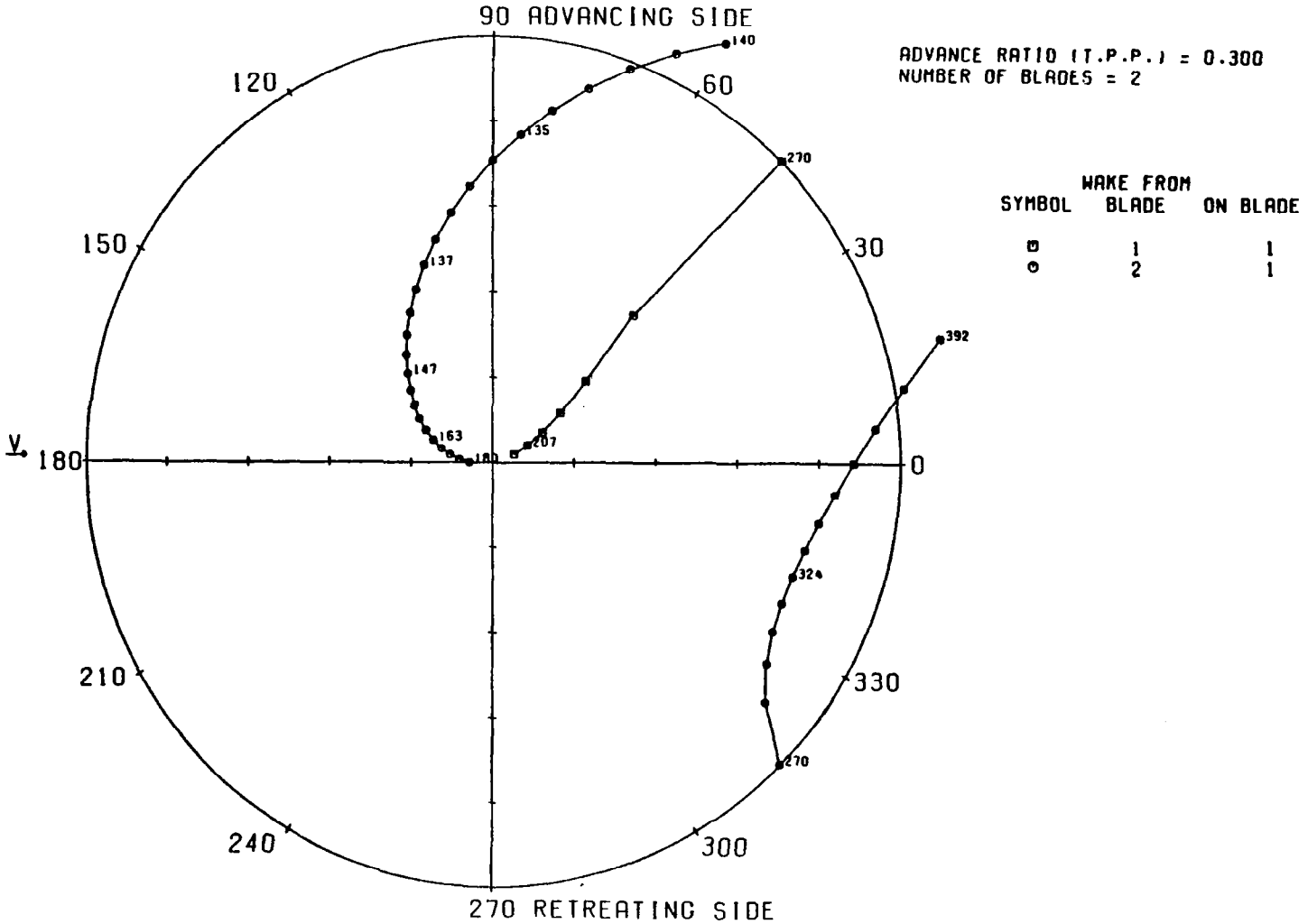

FIGURE 59. POTENTIAL BLADE/TIP VORTEX INTERSECTION PLOT FOR TWO BLADES (POLAR FORMAT), μ = .30

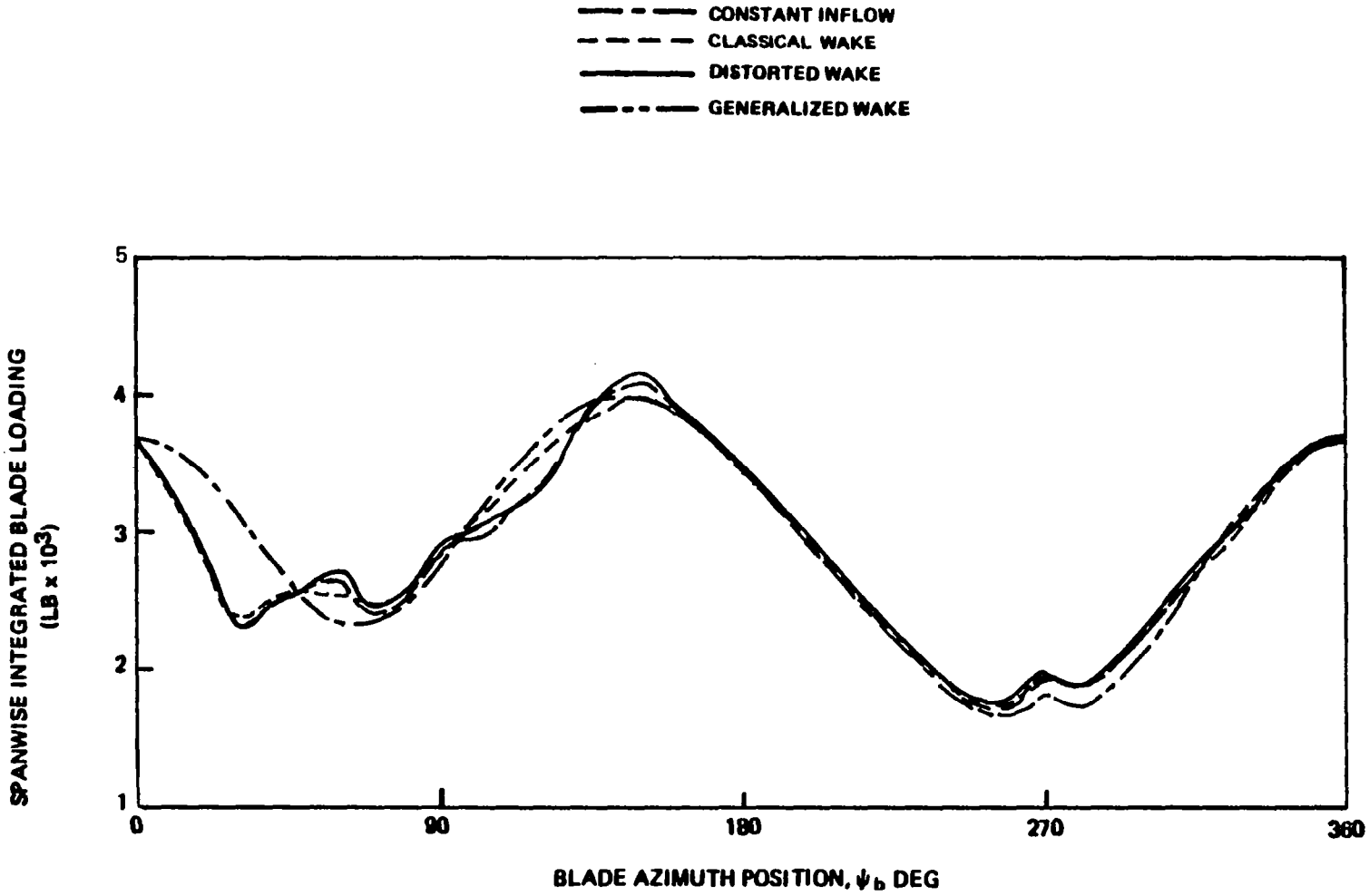

FIGURE 60. SPANWISE INTEGRATED BLADE LOADING TIME HISTORIES FOR VARIOUS WAKE MODELS AT AN ADVANCE RATIO OF 0.3

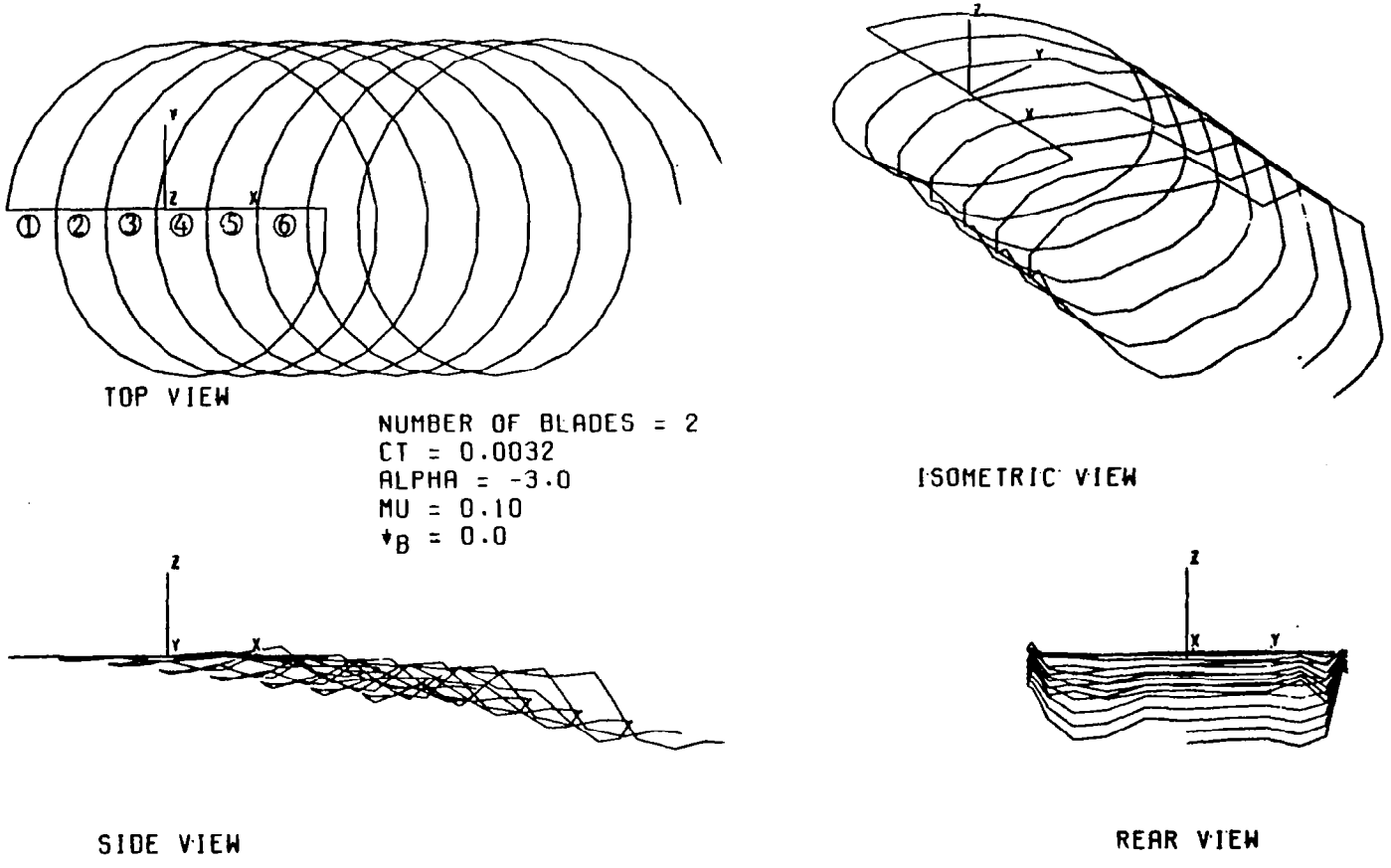

FIGURE 61. GENERALIZED TIP VORTEX GEOMETRY FOR TWO-BLADED REPRESENTATIVE ROTOR, (μ=0.1; ψ_b=0°,180°)

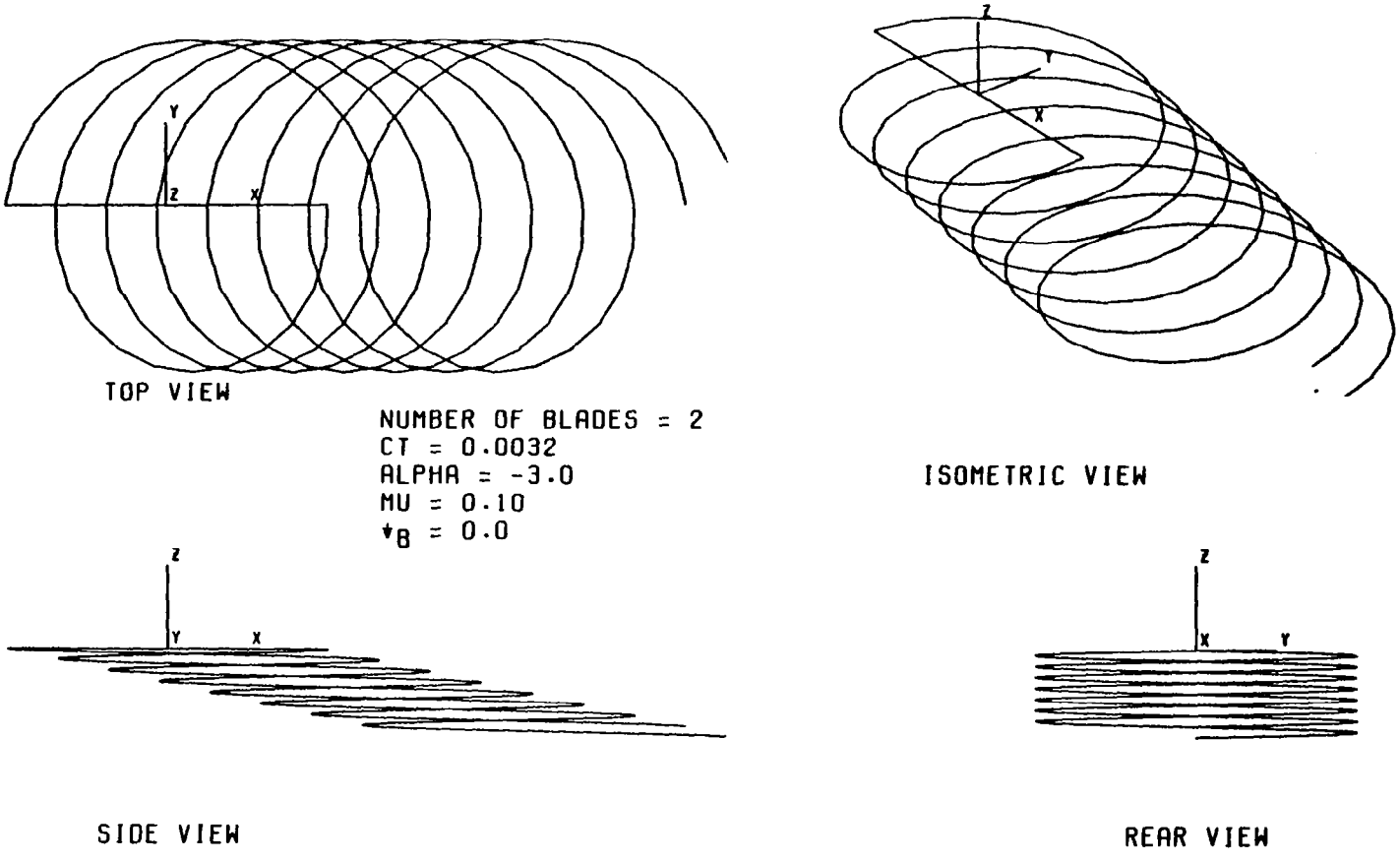

FIGURE 62. UNDISTORTED TIP VORTEX GEOMETRY FOR TWO-BLADED REPRESENTATIVE ROTOR, (μ=0.1; ψ_b=0°,180°)

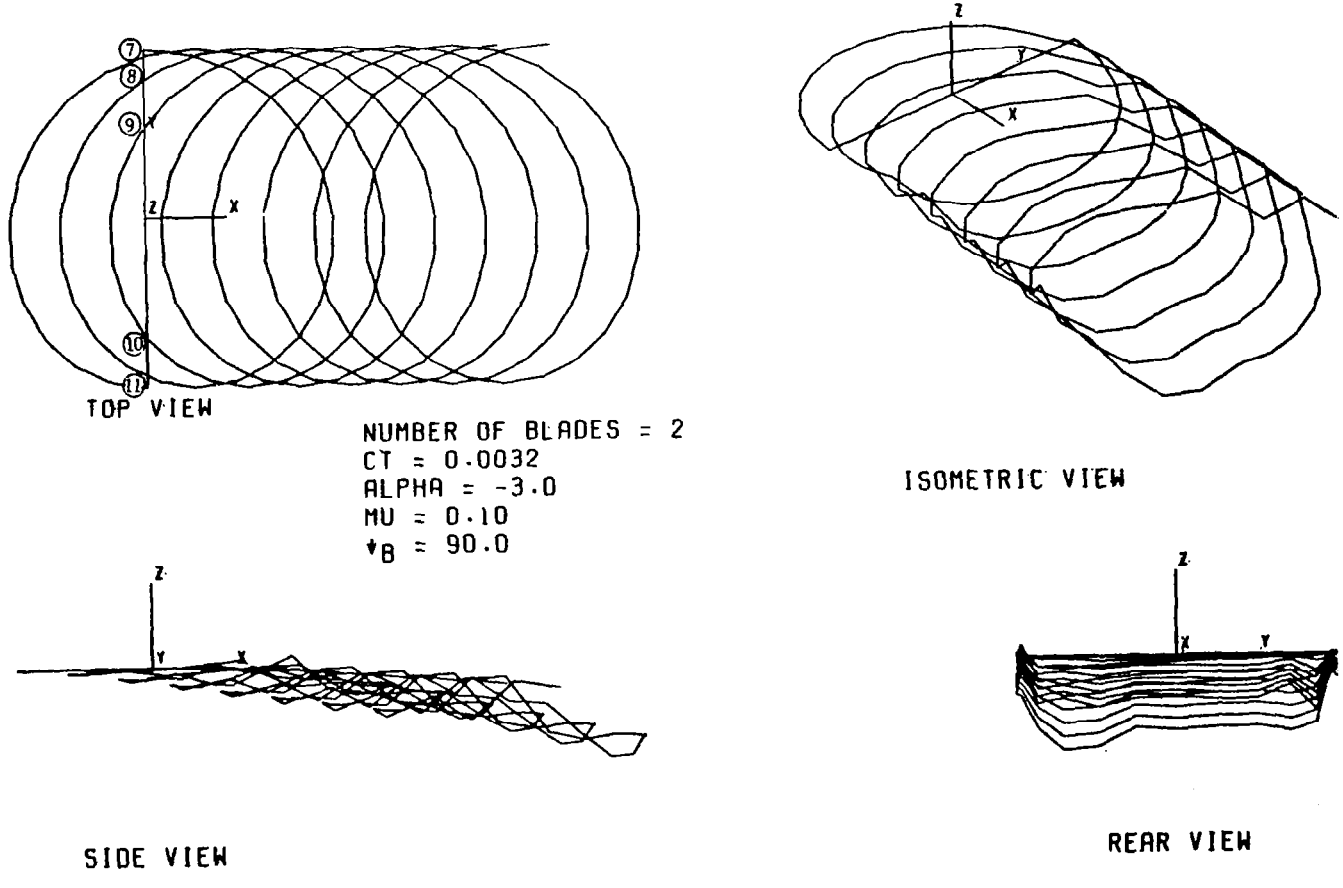

FIGURE 63. UNDISTORTED TIP VORTEX GEOMETRY FOR TWO-BLADED REPRESENTATIVE ROTOR, (μ=0.1; ψ_b=90°,270°)

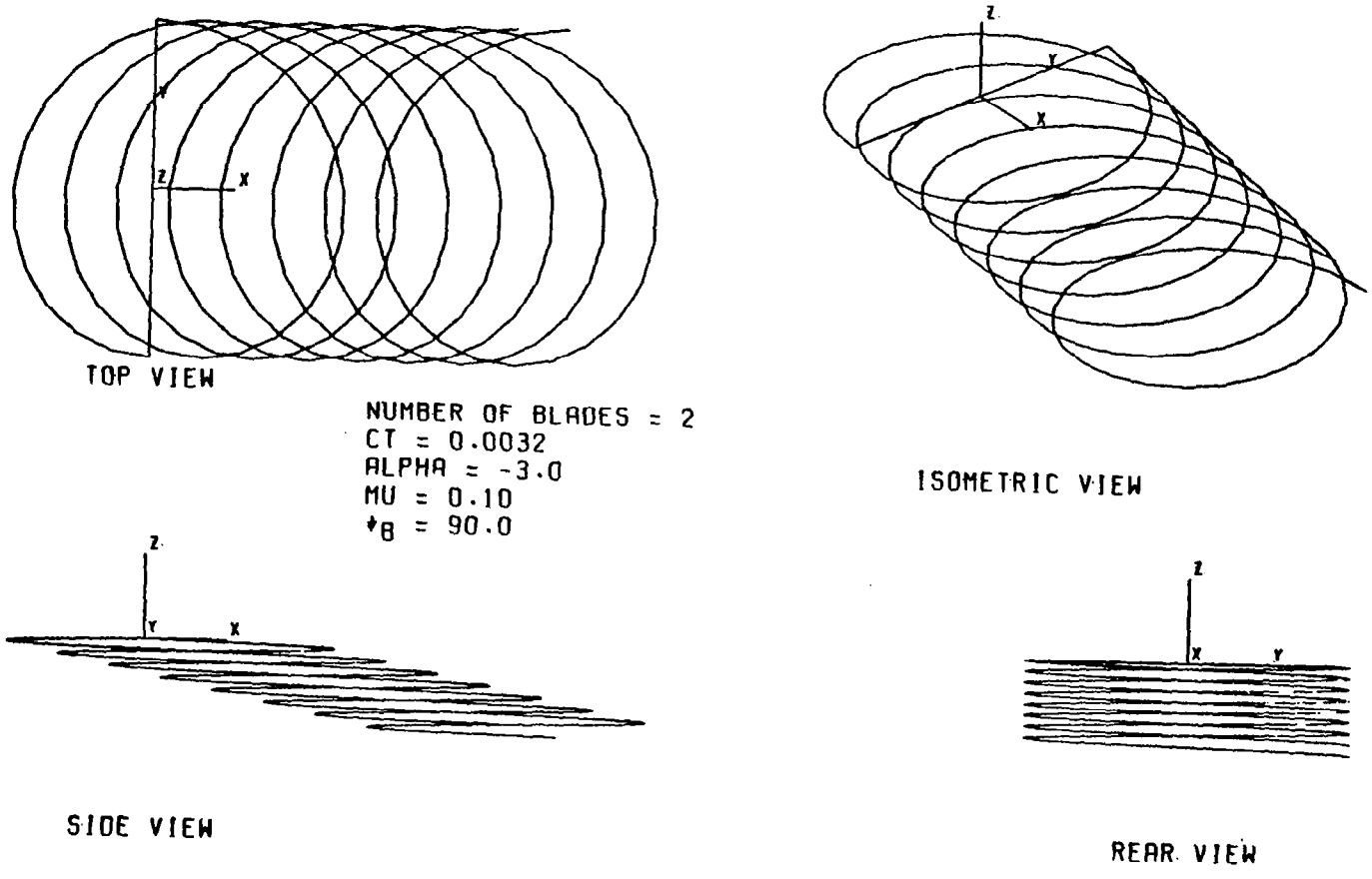

FIGURE 64. UNDISTORTED TIP VORTEX GEOMETRY FOR TWO-BLADED REPRESENTATIVE ROTOR, (μ=0.1; ψ =90°, 270°)

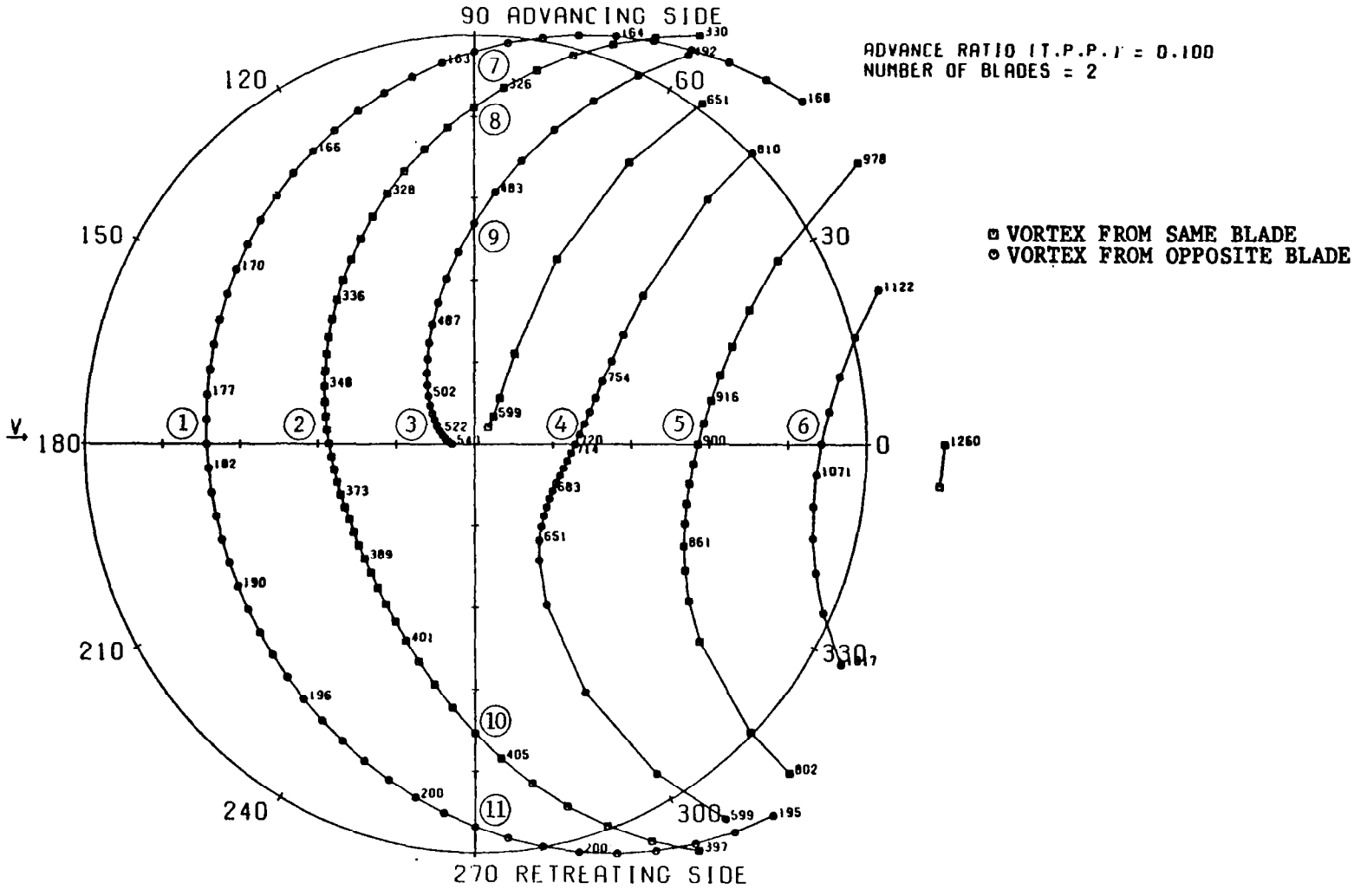

FIGURE 65. POTENTIAL BLADE/TIP VORTEX INTERSECTION PLOT FOR TWO BLADES (POLAR FORMAT), μ = .10

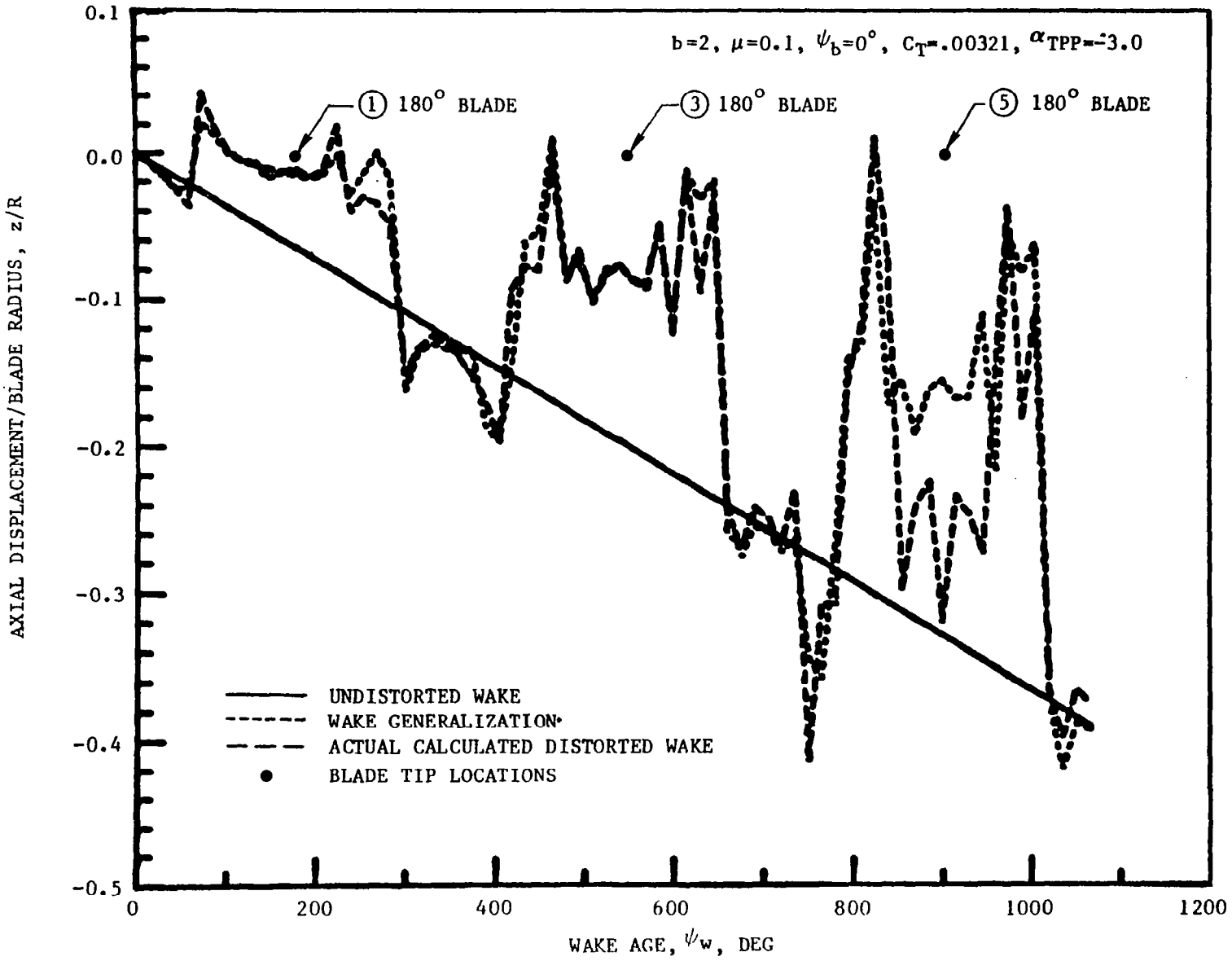

FIGURE 66a. AXIAL POSITION OF THE TIP VORTEX FROM THE BLADE AT $\psi_b = 0°$

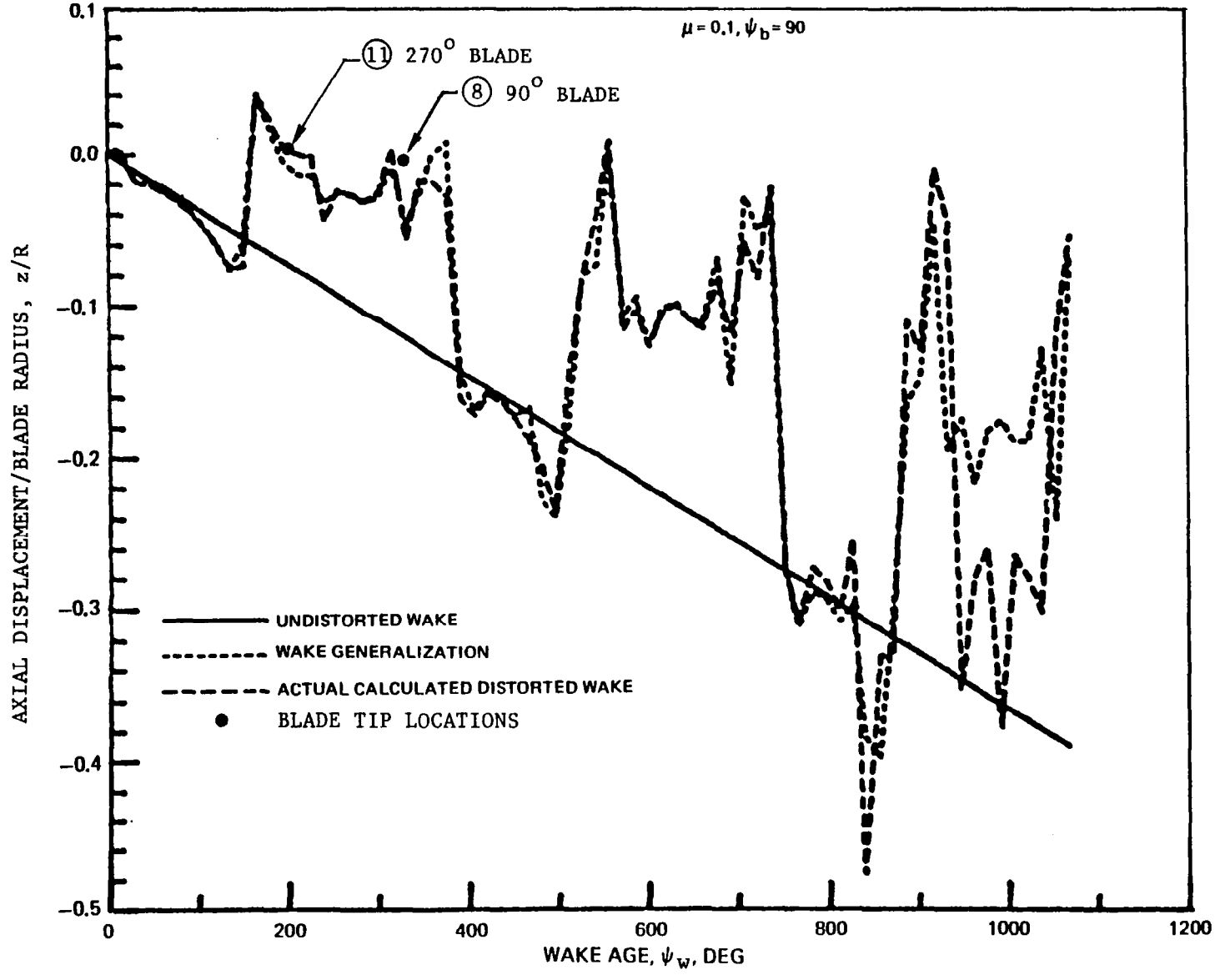

FIGURE 66b. AXIAL POSITION OF THE TIP VORTEX FROM THE BLADE AT $\psi_b = 90°$

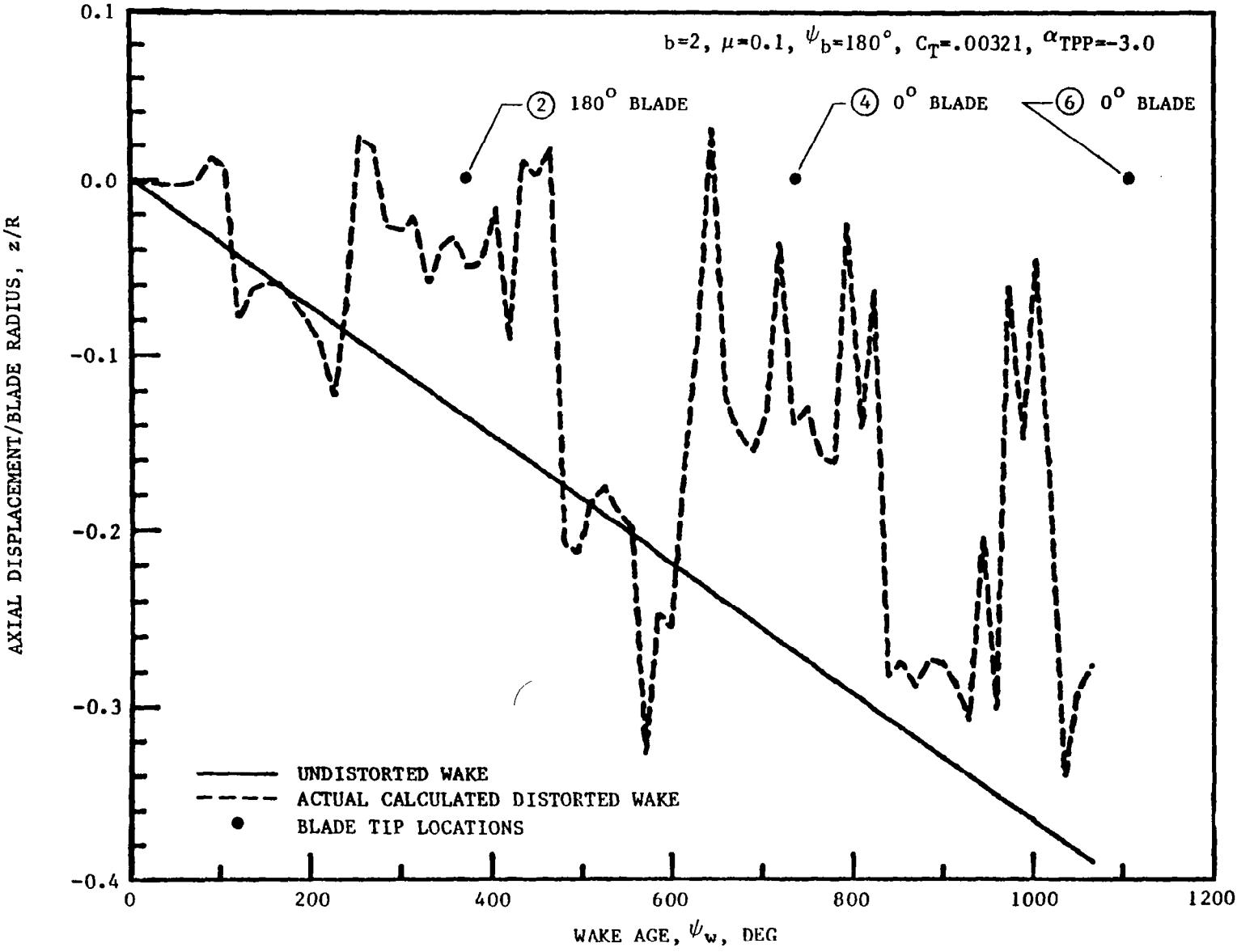

FIGURE 66c. AXIAL POSITION OF THE TIP VORTEX FROM THE BLADE AT $\psi_b = 180°$

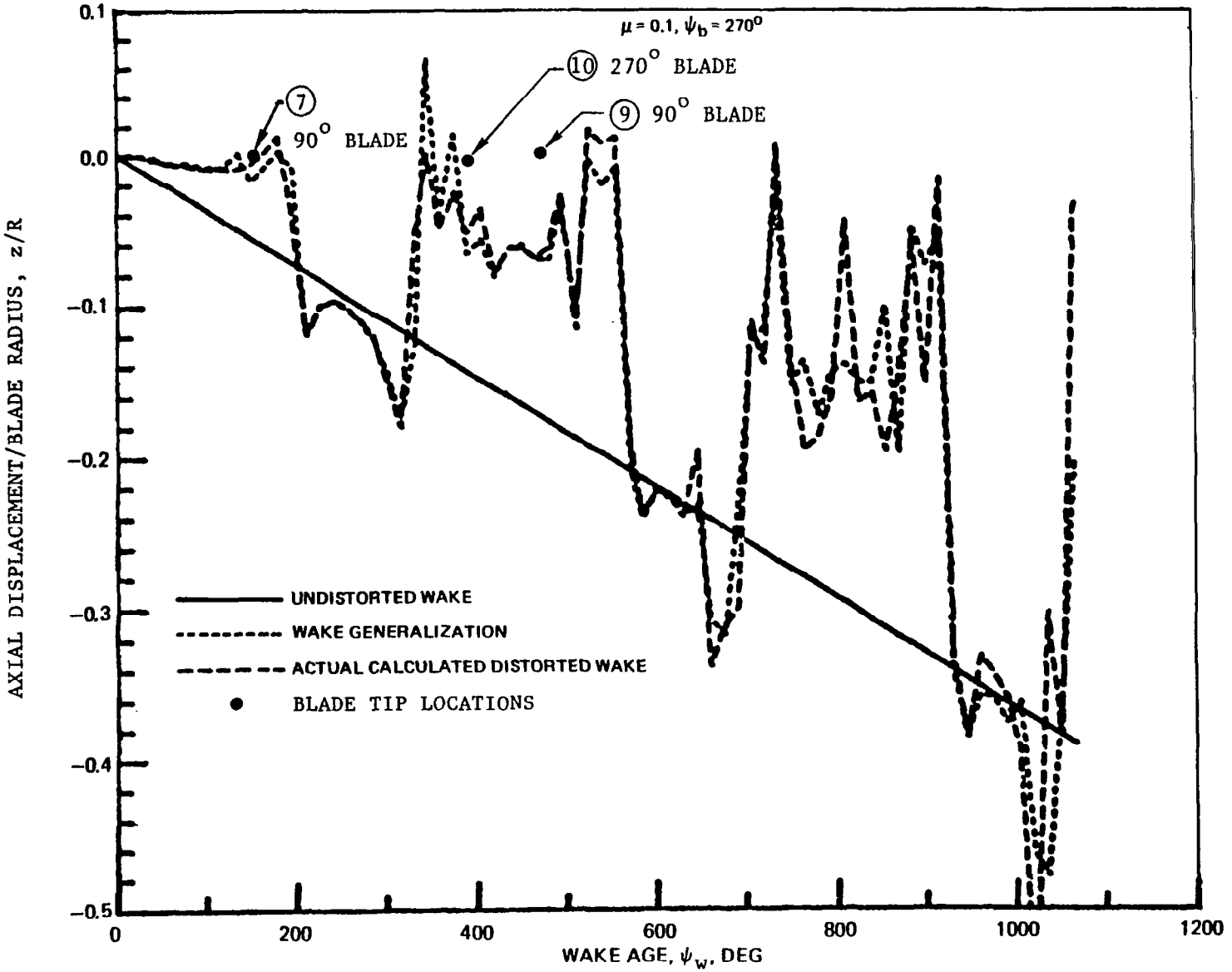

FIGURE 66d. AXIAL POSITION OF THE TIP VORTEX FROM THE BLADE AT $\psi_b = 270^o$

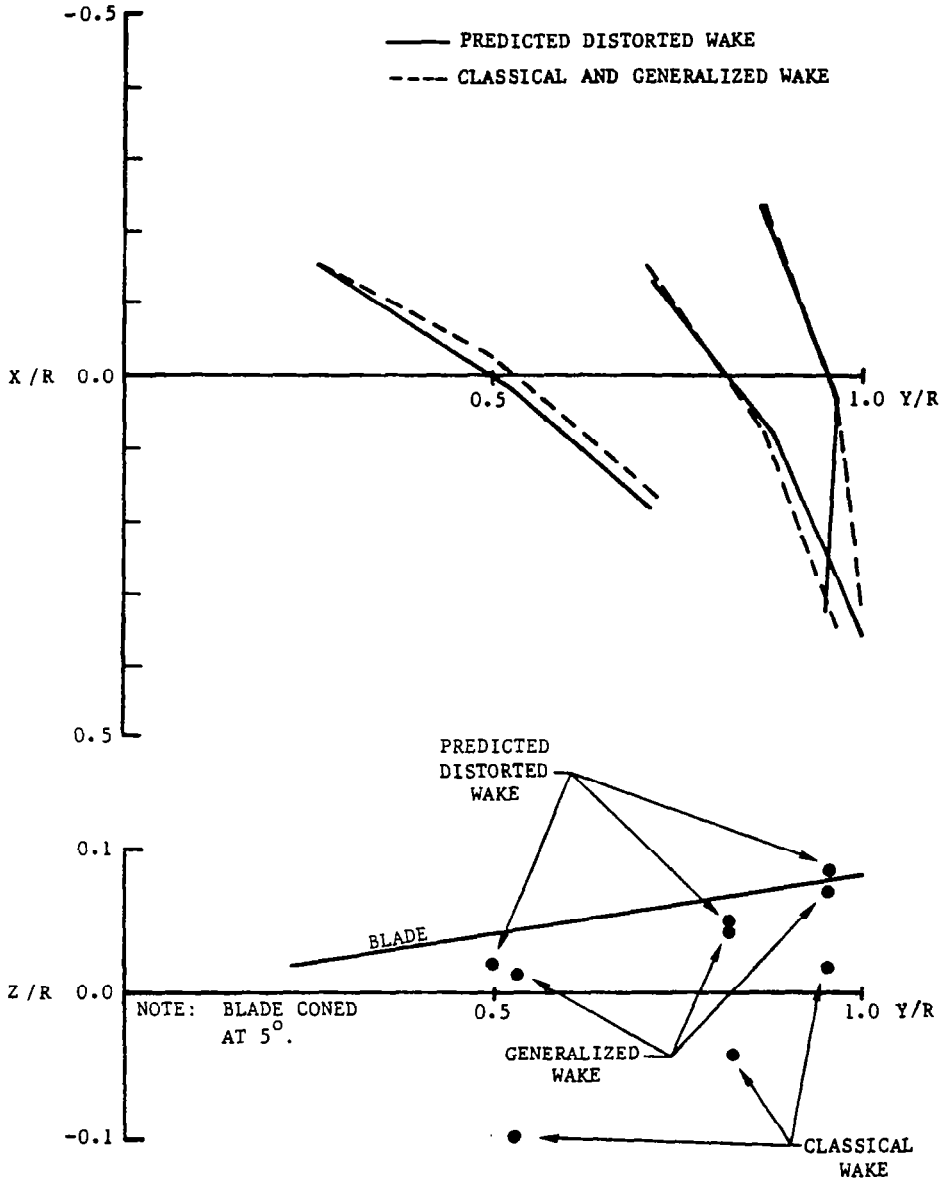

FIGURE 67. COMPARISON OF LOCAL WAKE GEOMETRIES AT $\psi_b = 90^\circ$ FOR $b = 2$, $\mu = 0.1$, $\alpha_{TPP} = -3$ AT A C_T OF 0.0032

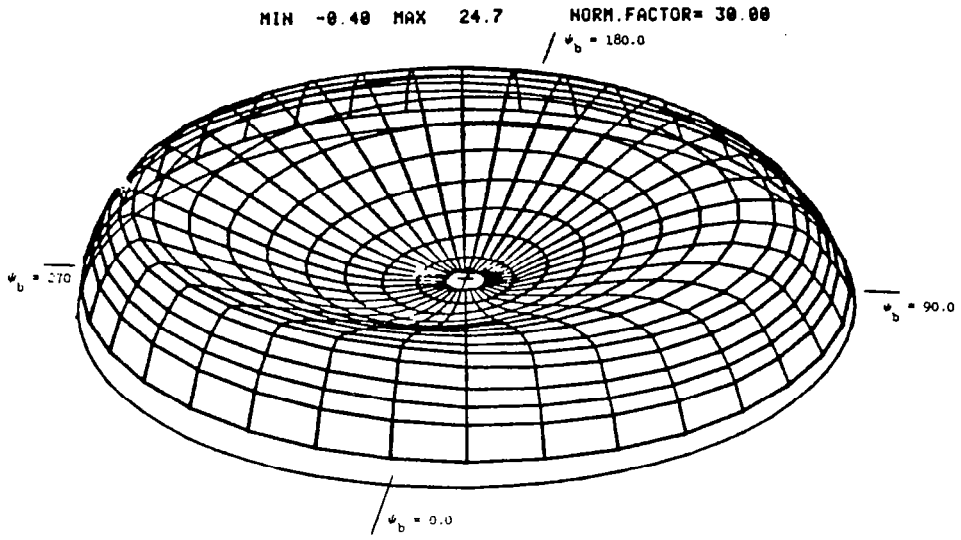

UNIFORM INFLOW

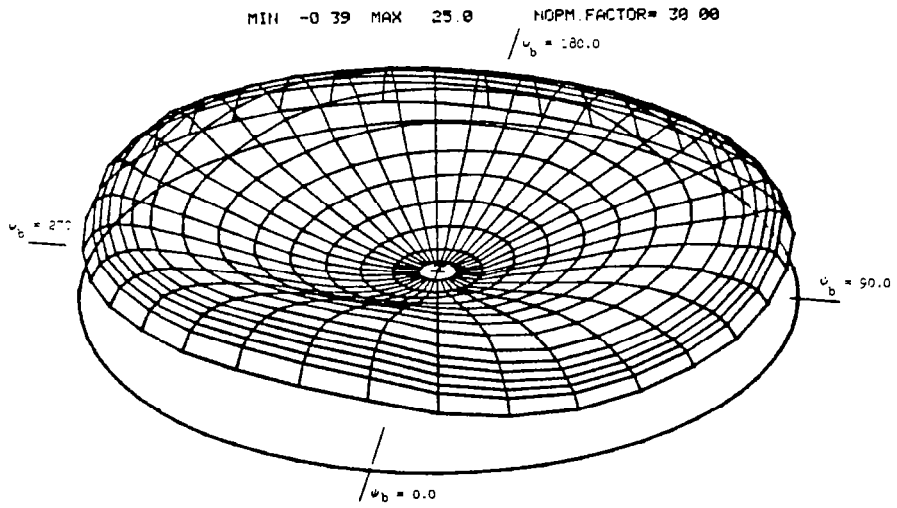

CLASSICAL WAKE

$b = 2, \mu = 0.1, C_T = 0.0032, \alpha_{TPP} = -0.3$

FIGURE 68a. ROTOR LIFT DISTRIBUTIONS, UNIFORM INFLOW VERSUS CLASSICAL WAKE PREDICTIONS

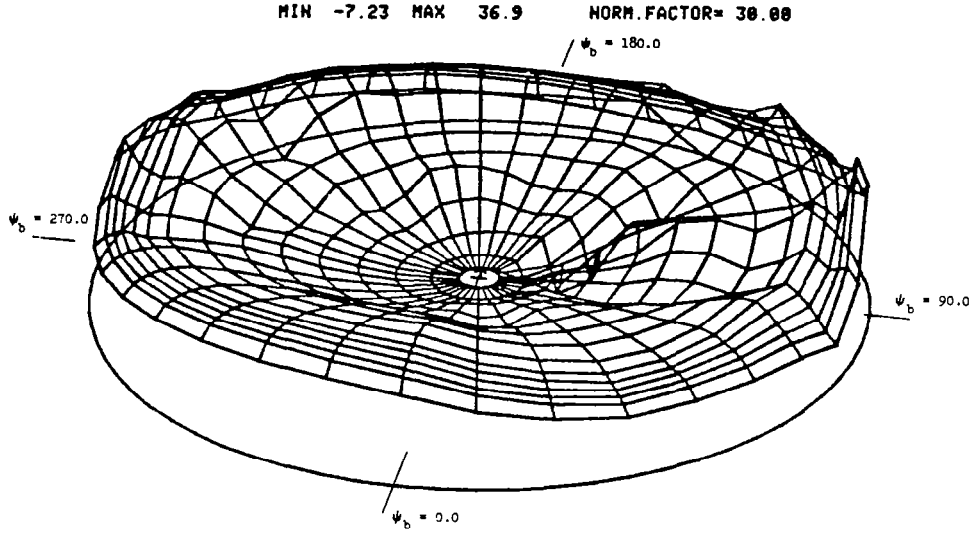

DISTORTED WAKE

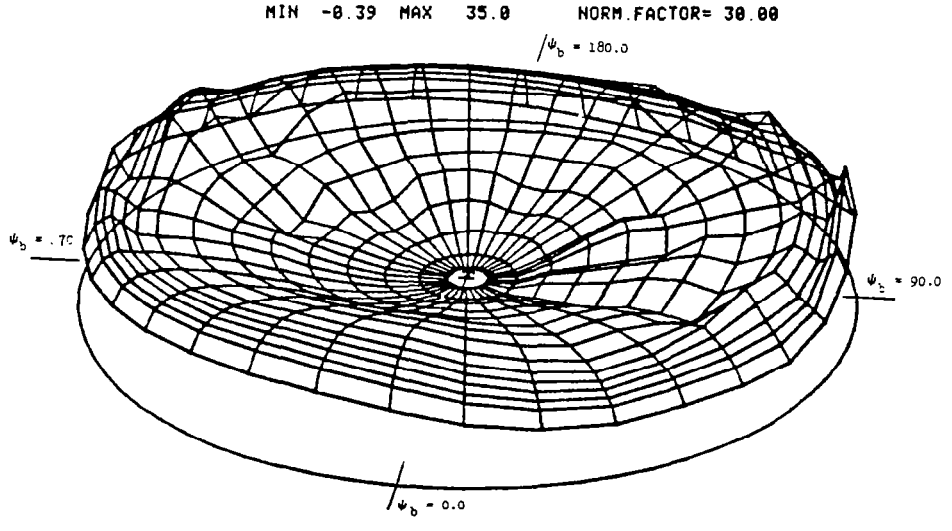

GENERALIZED WAKE

$b=2, \mu = 0.1, C_T = 0.0032, \alpha_{TPP} = -0.3$

FIGURE 68b. ROTOR LIFT DISTRIBUTIONS, DISTORTED WAKE VERSUS GENERALIZED WAKE PREDICTIONS

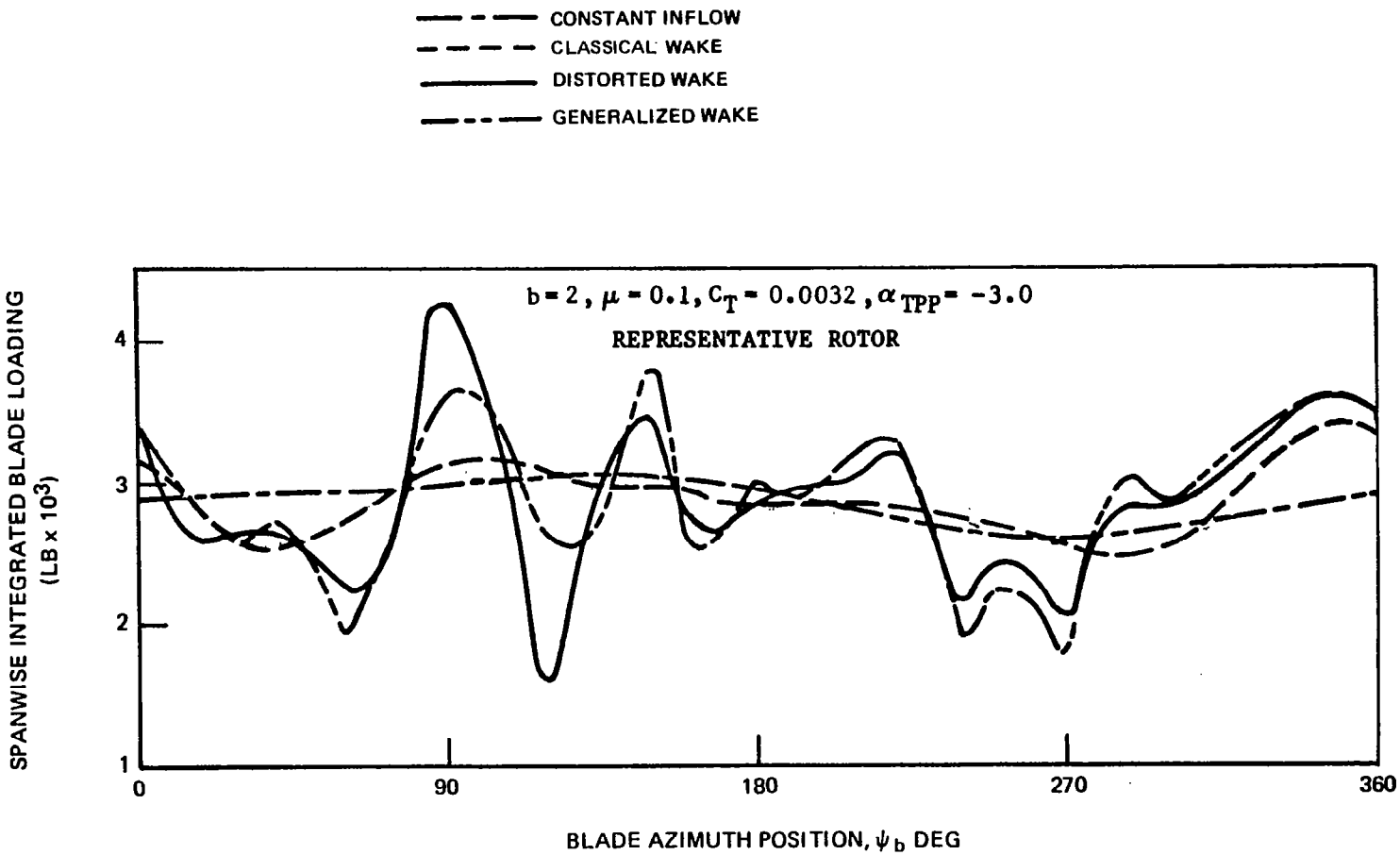

FIGURE 69. SPANWISE INTERGRATED BLADE LOADING TIME HISTORIES FOR VARIOUS WAKE MODELS AT AN ADVANCE RATIO OF 0.1

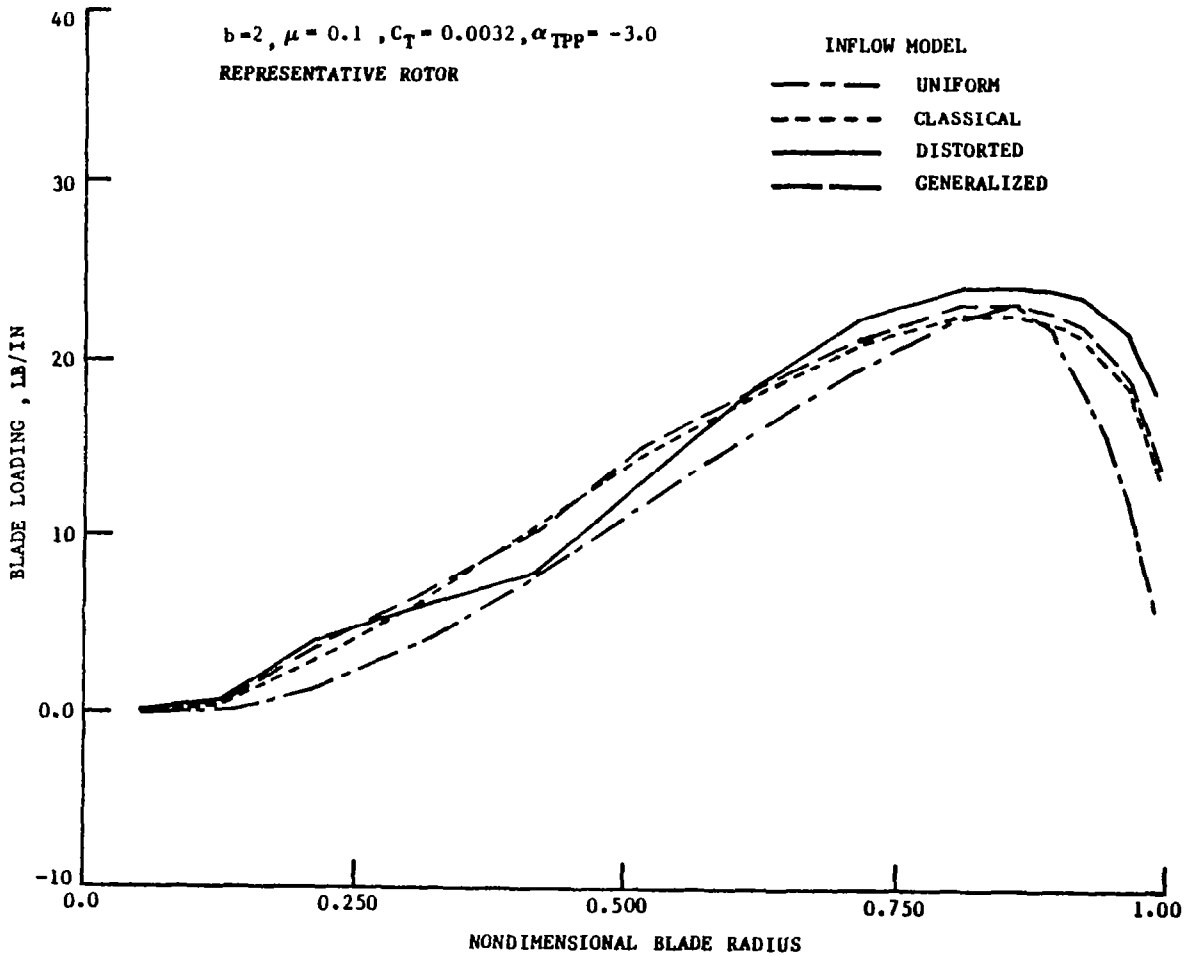

FIGURE 70a. COMPARISON OF PREDICTED SPANWISE LIFT DISTRIBUTION FOR VARIOUS INFLOW MODELS AT $\psi_b = 0^\circ$

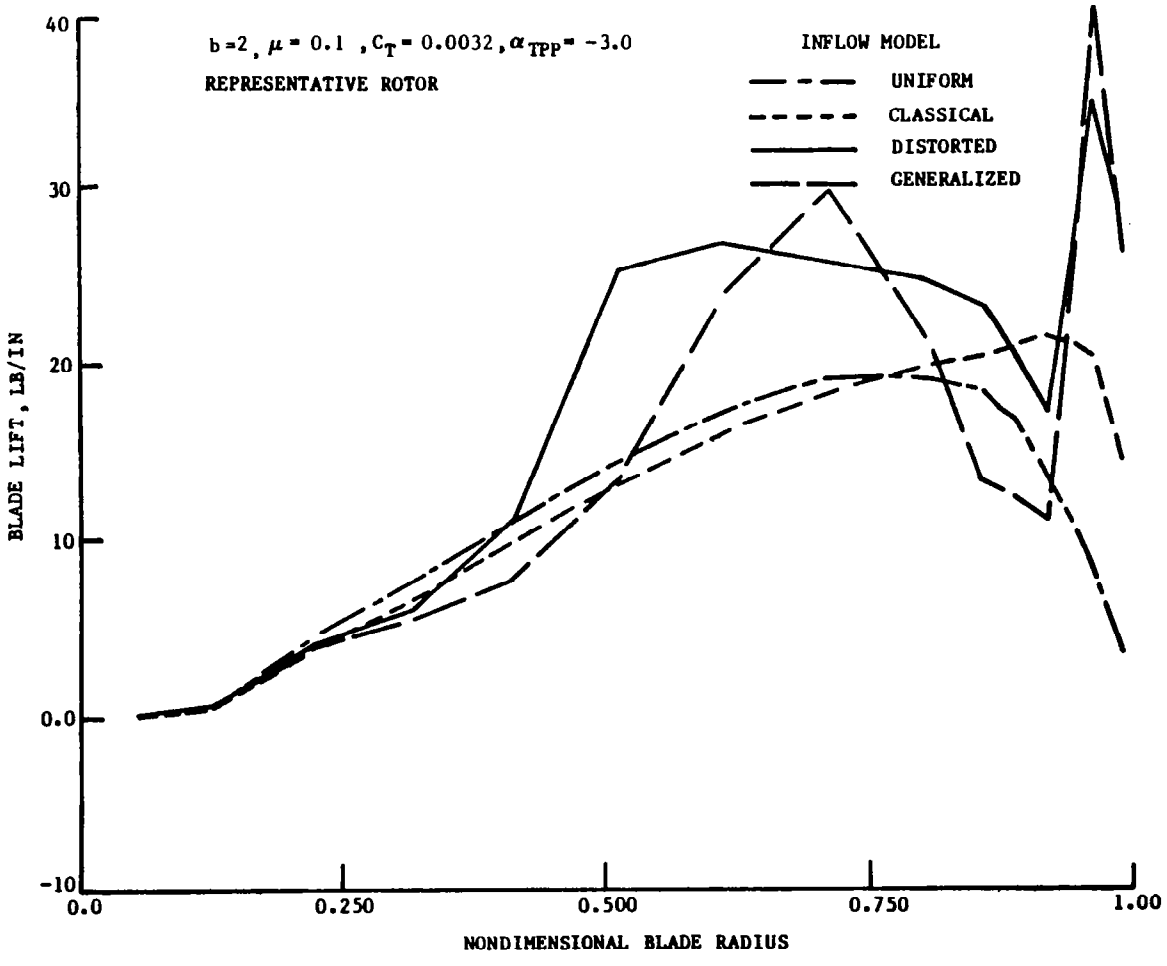

FIGURE 70b. COMPARISON OF PREDICTED SPANWISE LIFT DISTRIBUTION FOR VARIOUS INFLOW MODELS AT $\psi_b = 90°$

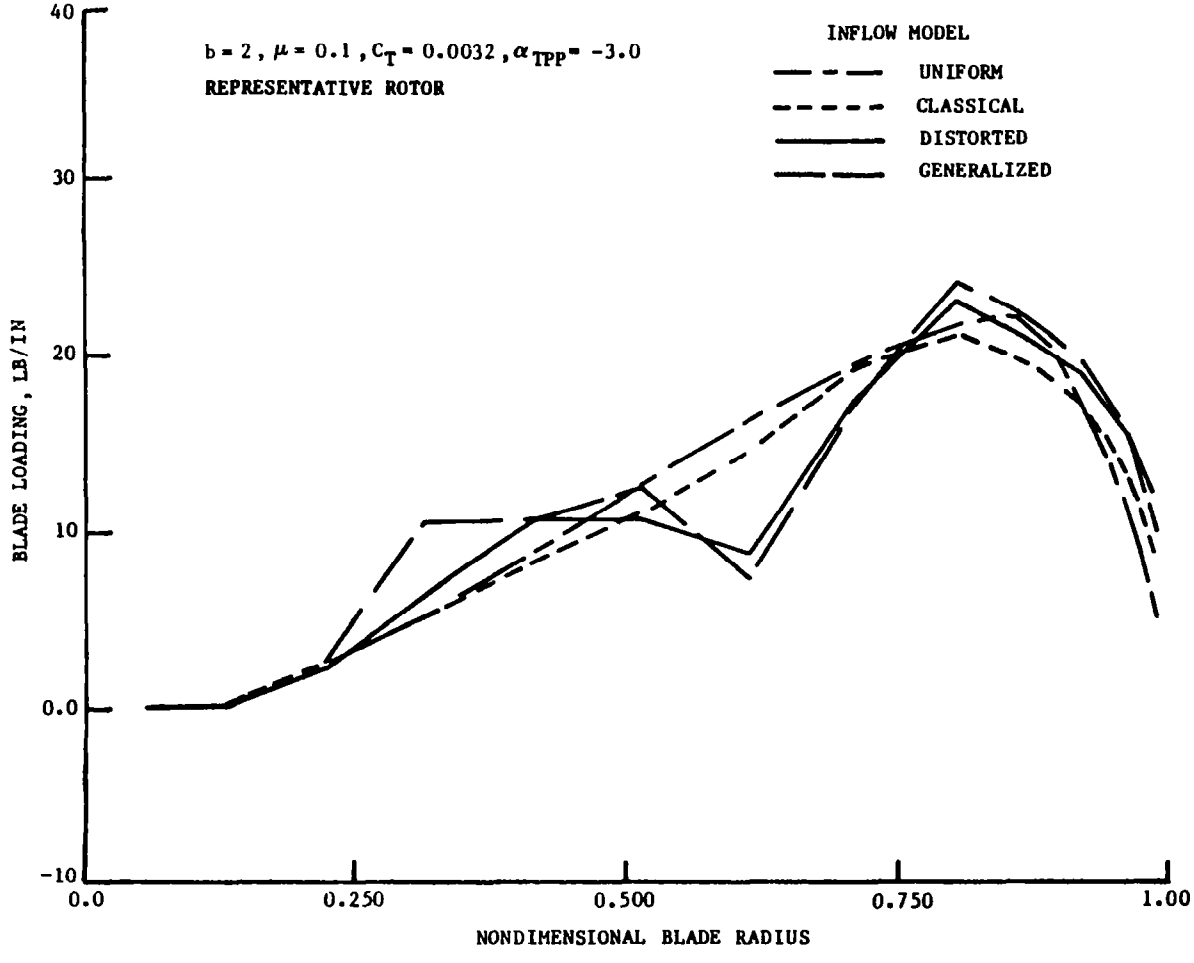

FIGURE 70c. COMPARISON OF PREDICTED SPANWISE LIFT DISTRIBUTION FOR VARIOUS INFLOW MODELS AT $\psi_b = 180°$

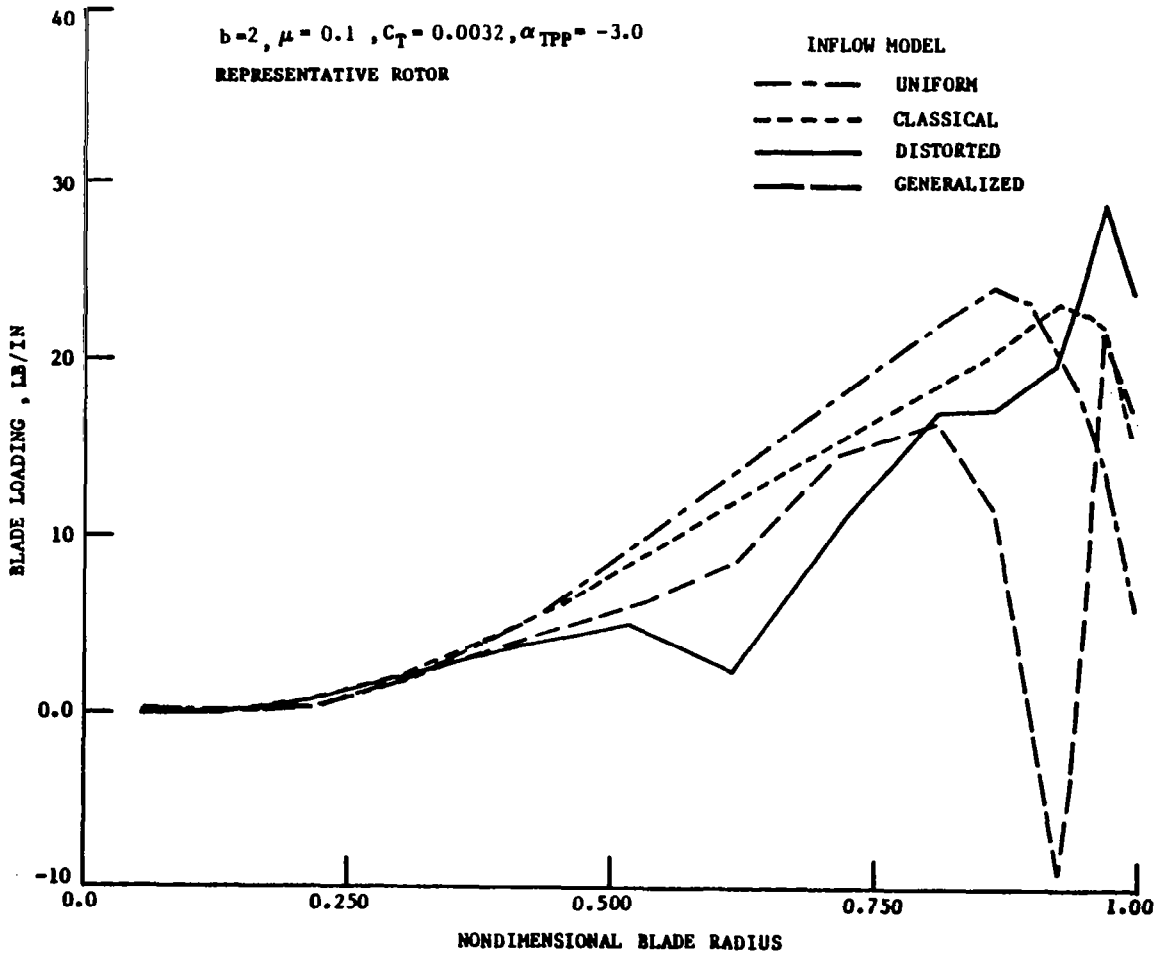

FIGURE 70d. COMPARISON OF PREDICTED SPANWISE LIFT DISTRIBUTION FOR VARIOUS INFLOW MODELS AT $\psi_b = 270^\circ$

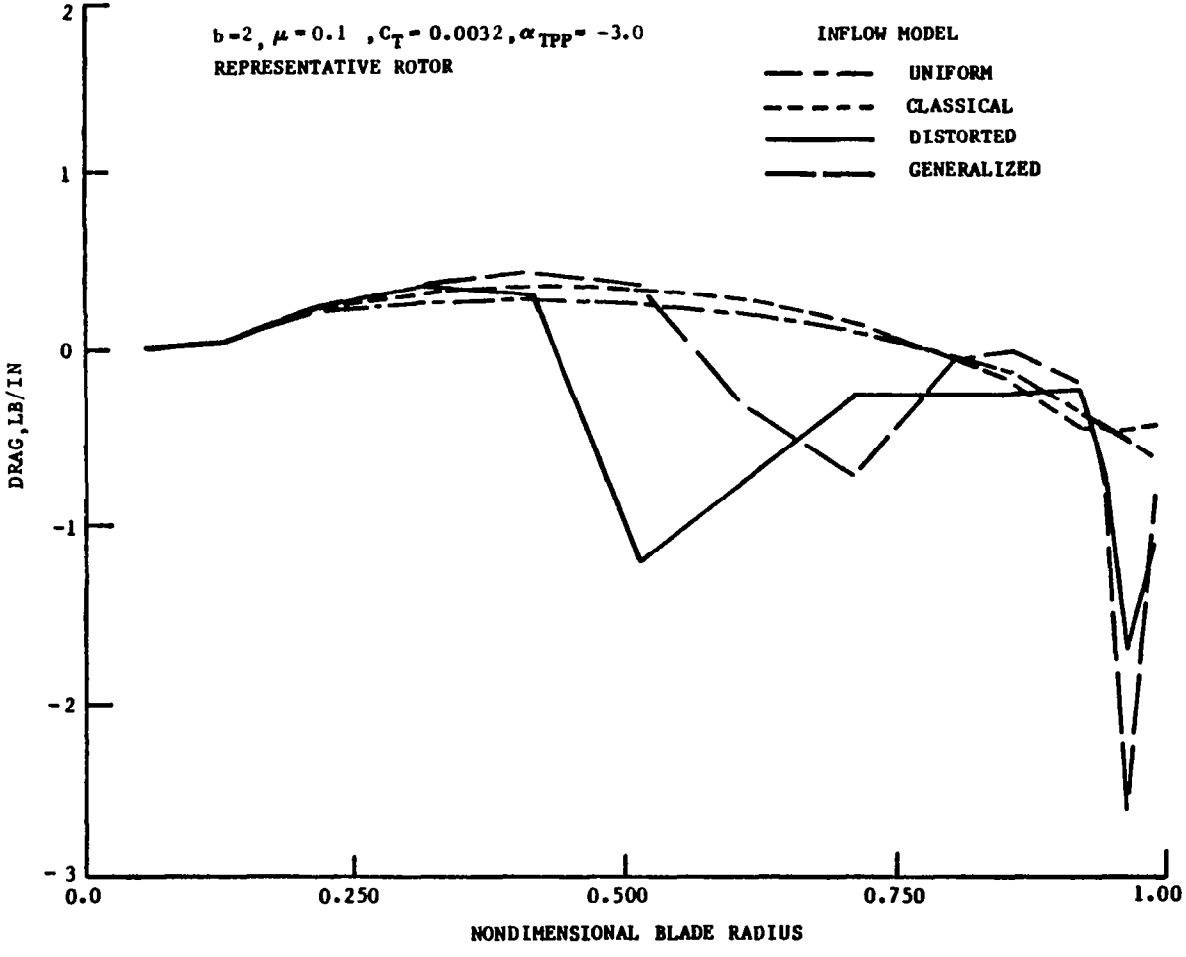

FIGURE 71. COMPARISON OF PREDICTED SPANWISE DRAG DISTRIBUTION FOR VARIOUS INFLOW MODELS AT $\psi_b = 90°$

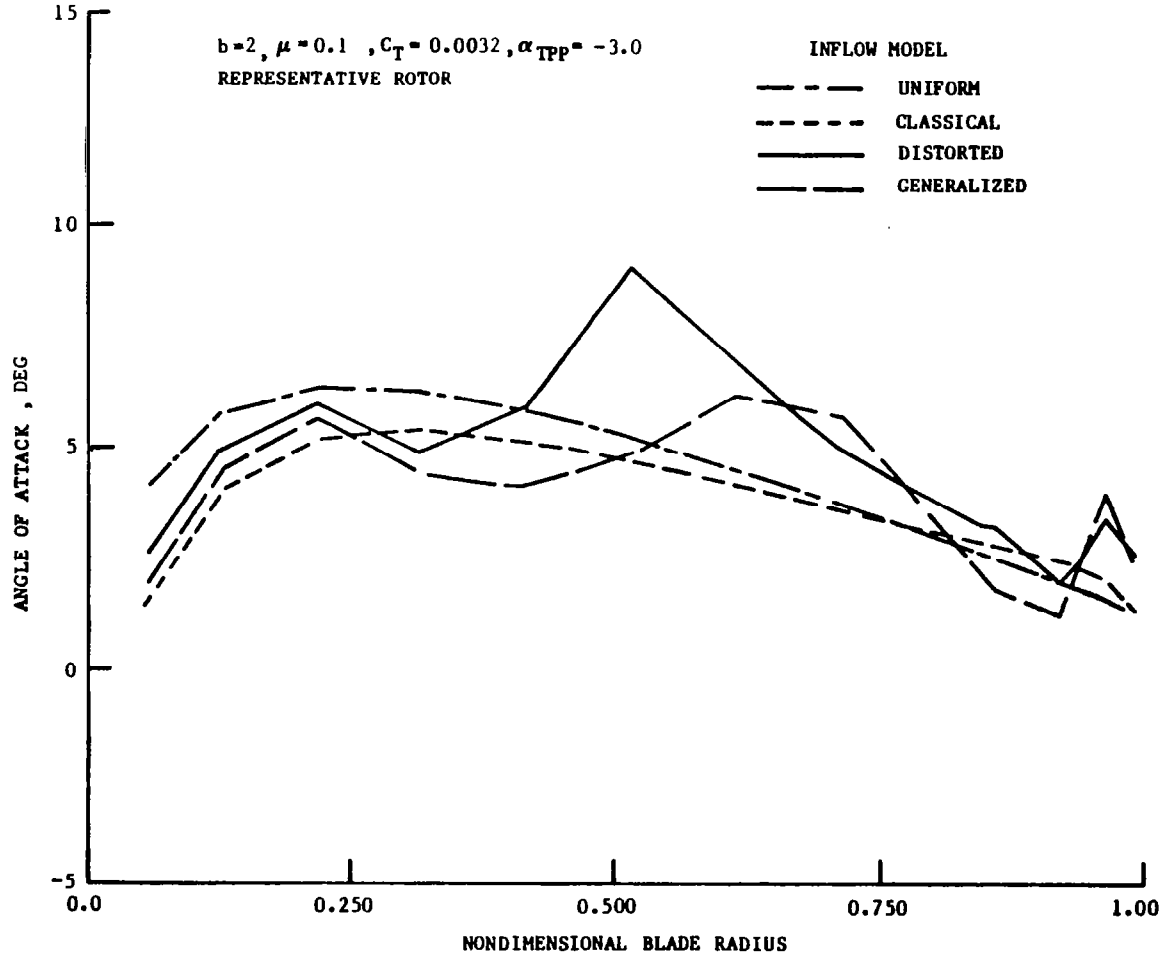

FIGURE 72. COMPARISON OF PREDICTED SPANWISE ANGLE OF ATTACK DISTRIBUTION FOR VARIOUS INFLOW MODELS AT $\psi_b = 90^o$

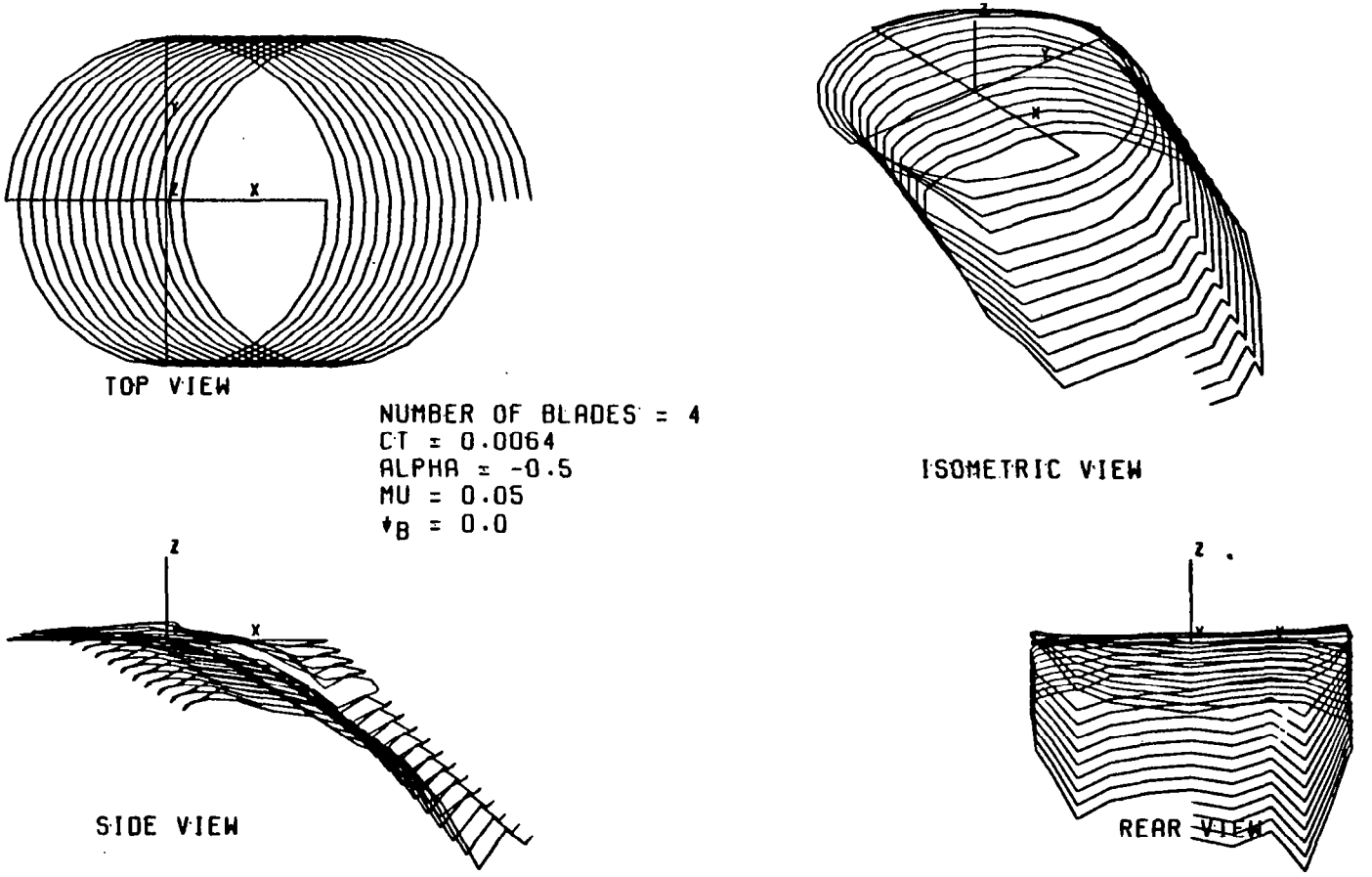

FIGURE 73. DISTORTED TIP VORTEX GEOMETRY FOR FOUR-BLADED REPRESENTATIVE ROTOR, μ=0.05

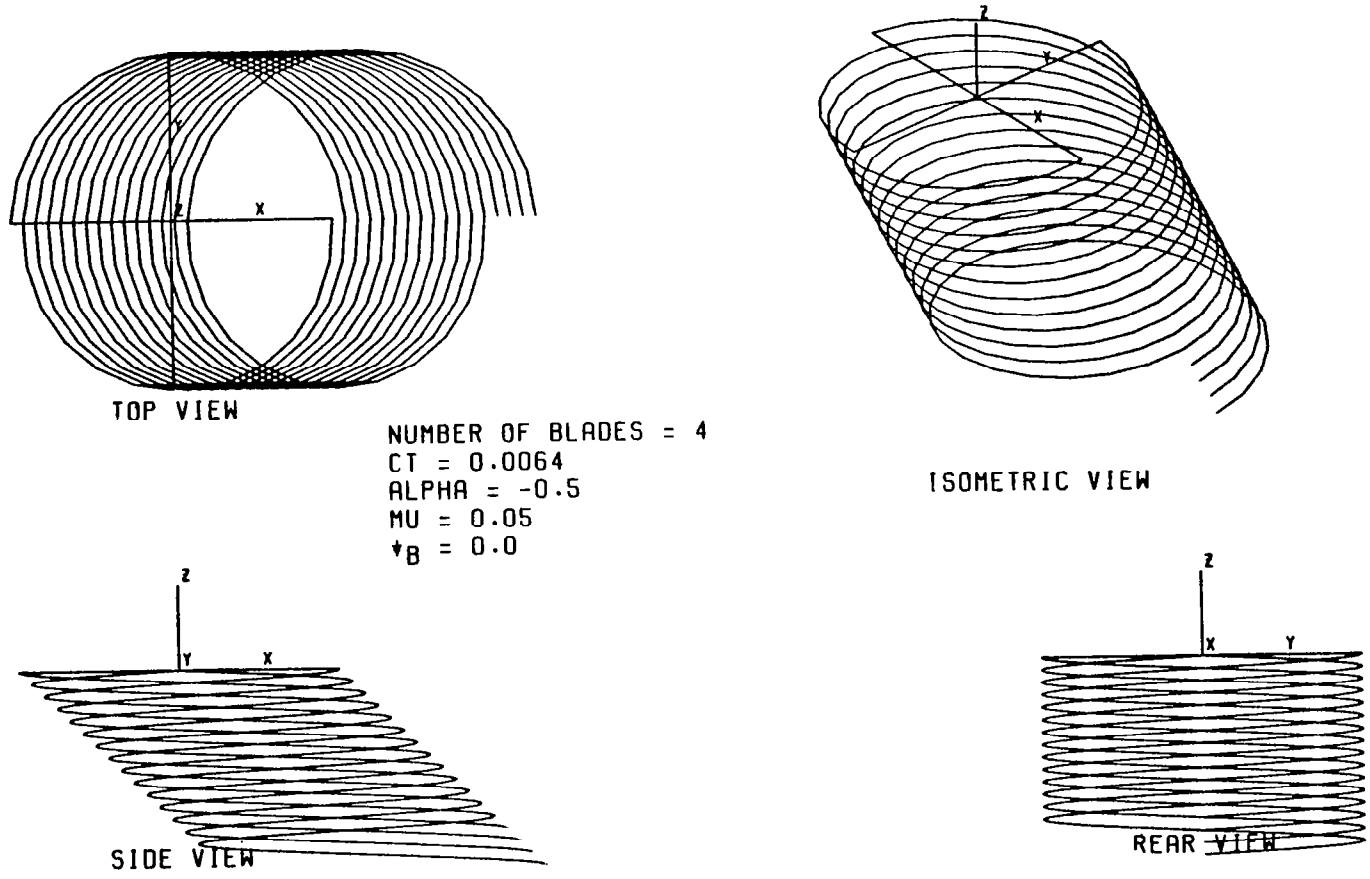

FIGURE 74. UNDISTORTED TIP VORTEX GEOMETRY FOR FOUR-BLADED REPRESENTATIVE ROTOR, μ=0.05

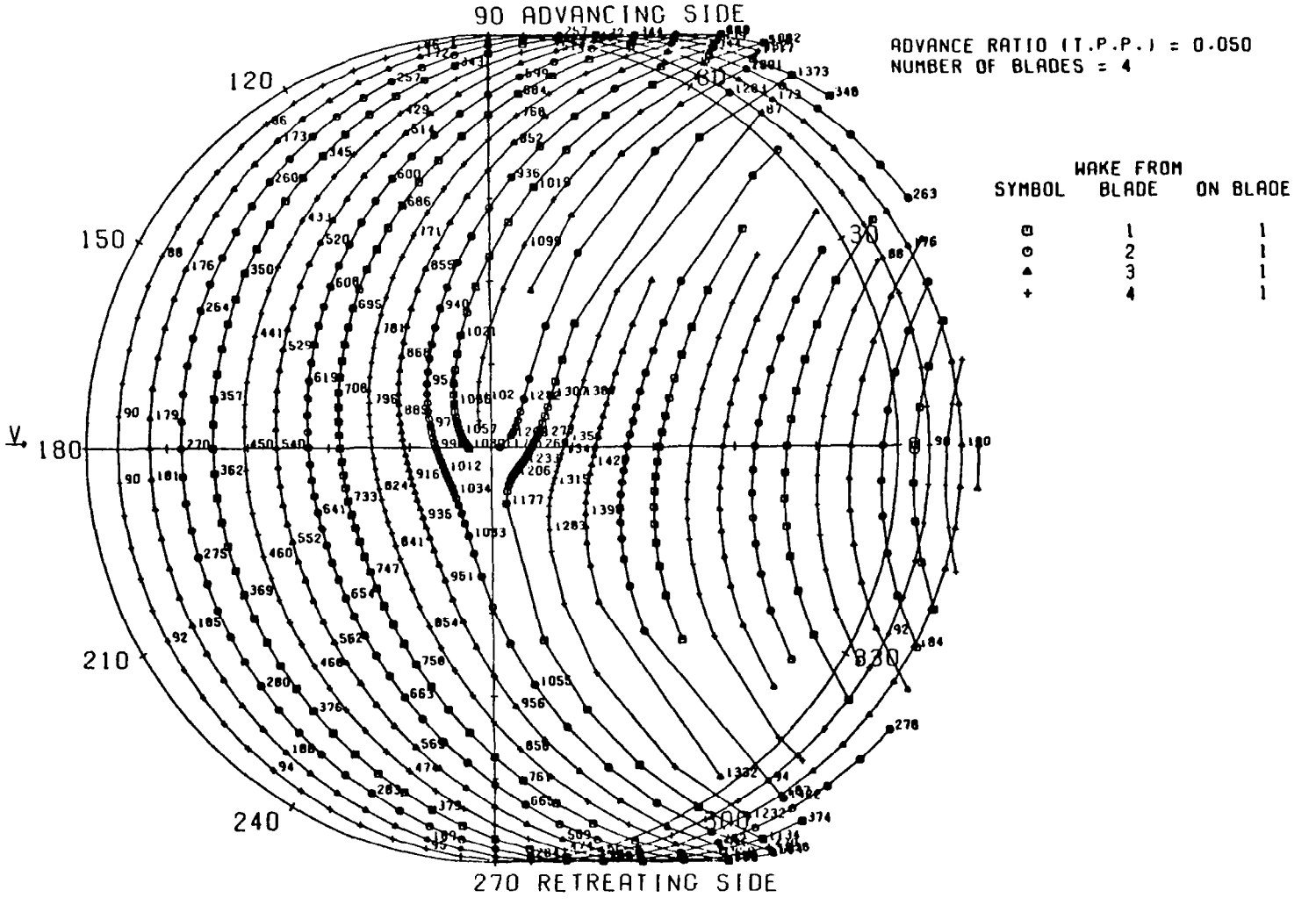

FIGURE 75. POTENTIAL BLADE/TIP VORTEX INTERSECTION PLOT FOR FOUR BLADES (POLAR FORMAT), μ = .05

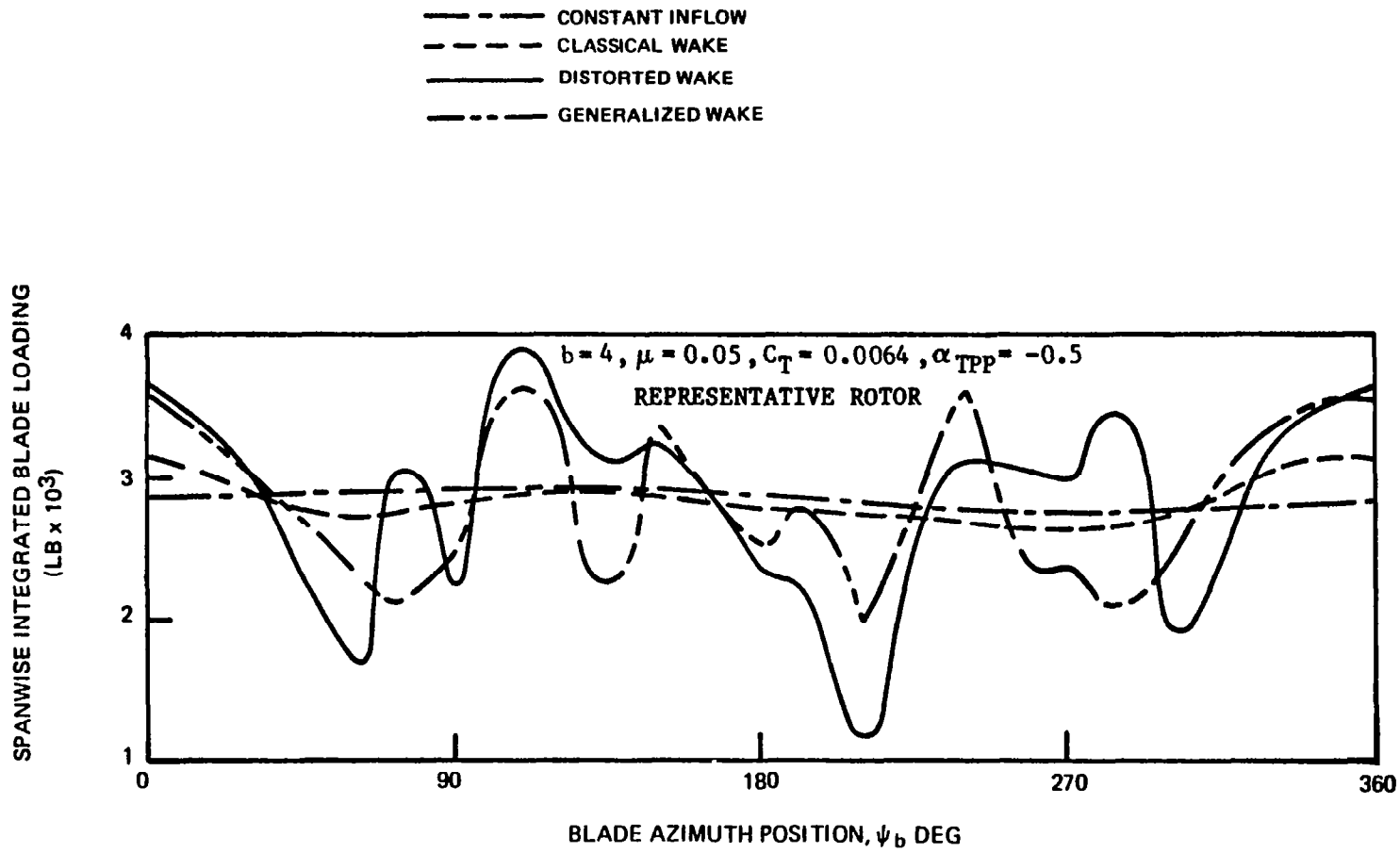

FIGURE 76. SPANWISE INTEGRATED BLADE LOADING TIME HISTORIES FOR VARIOUS WAKE MODELS AT AN ADVANCE RATIO OF 0.05

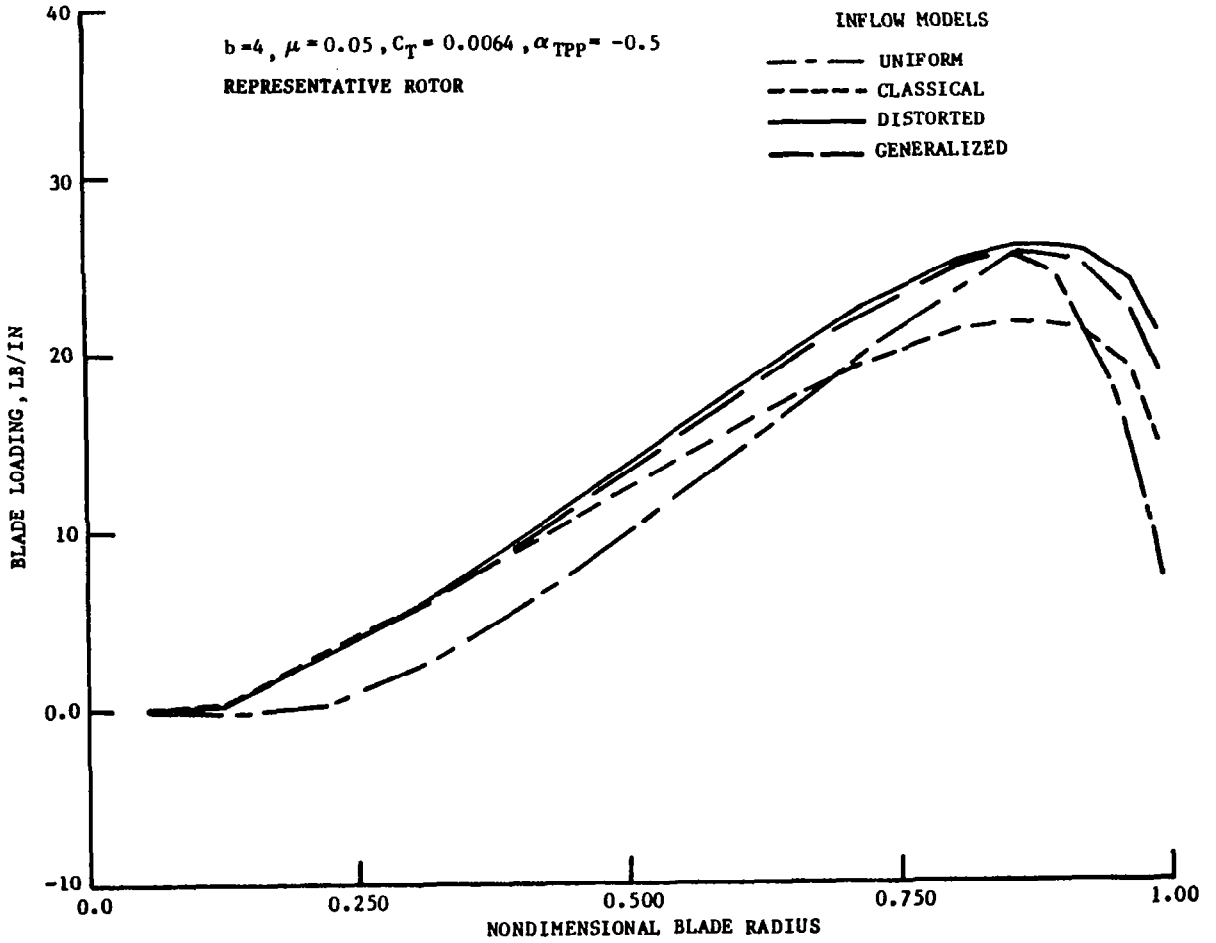

FIGURE 77. COMPARISON OF PREDICTED SPANWISE LIFT DISTRIBUTION FOR VARIOUS INFLOW MODELS AT $\psi_b = 0°$

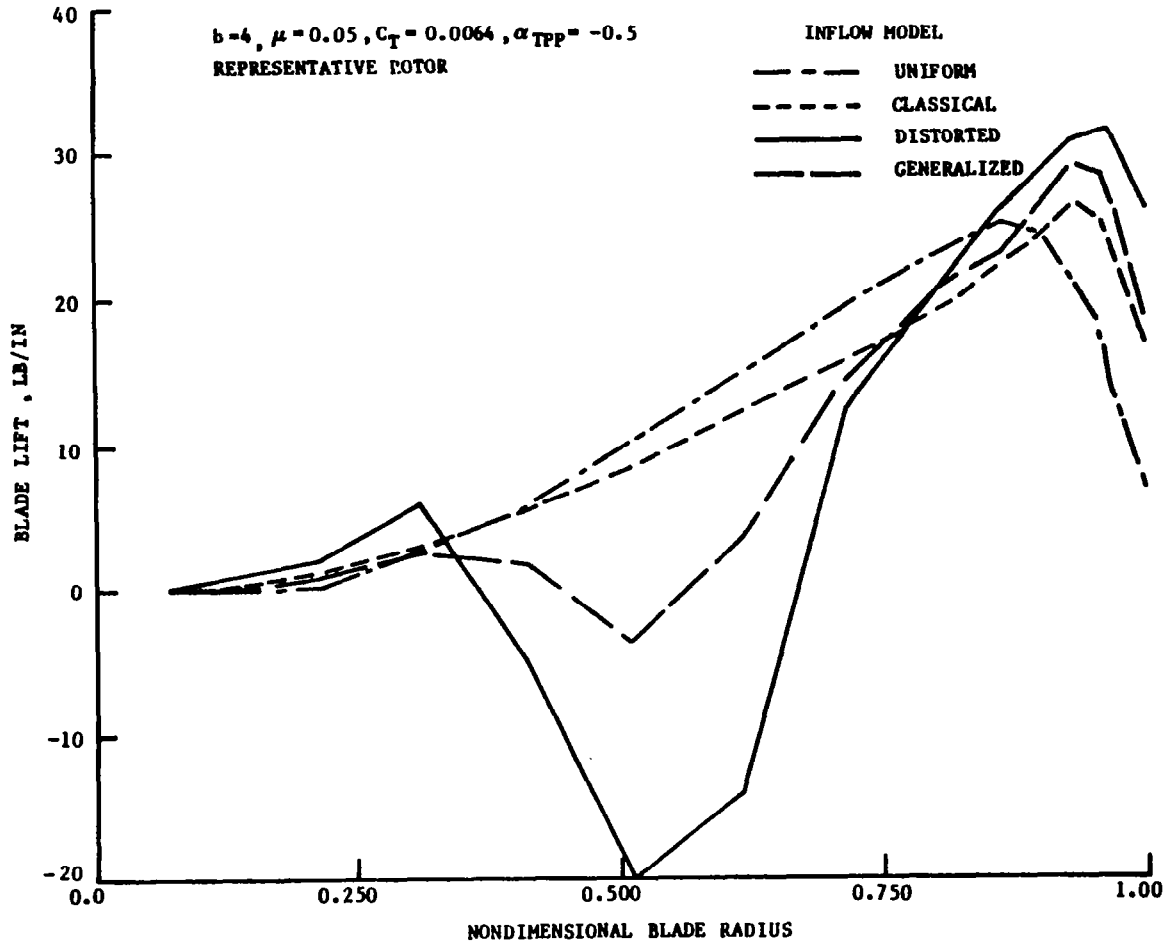

FIGURE 78. COMPARISON OF PREDICTED SPANWISE LIFT DISTRIBUTION FOR VARIOUS INFLOW MODELS AT ψ_b=210°

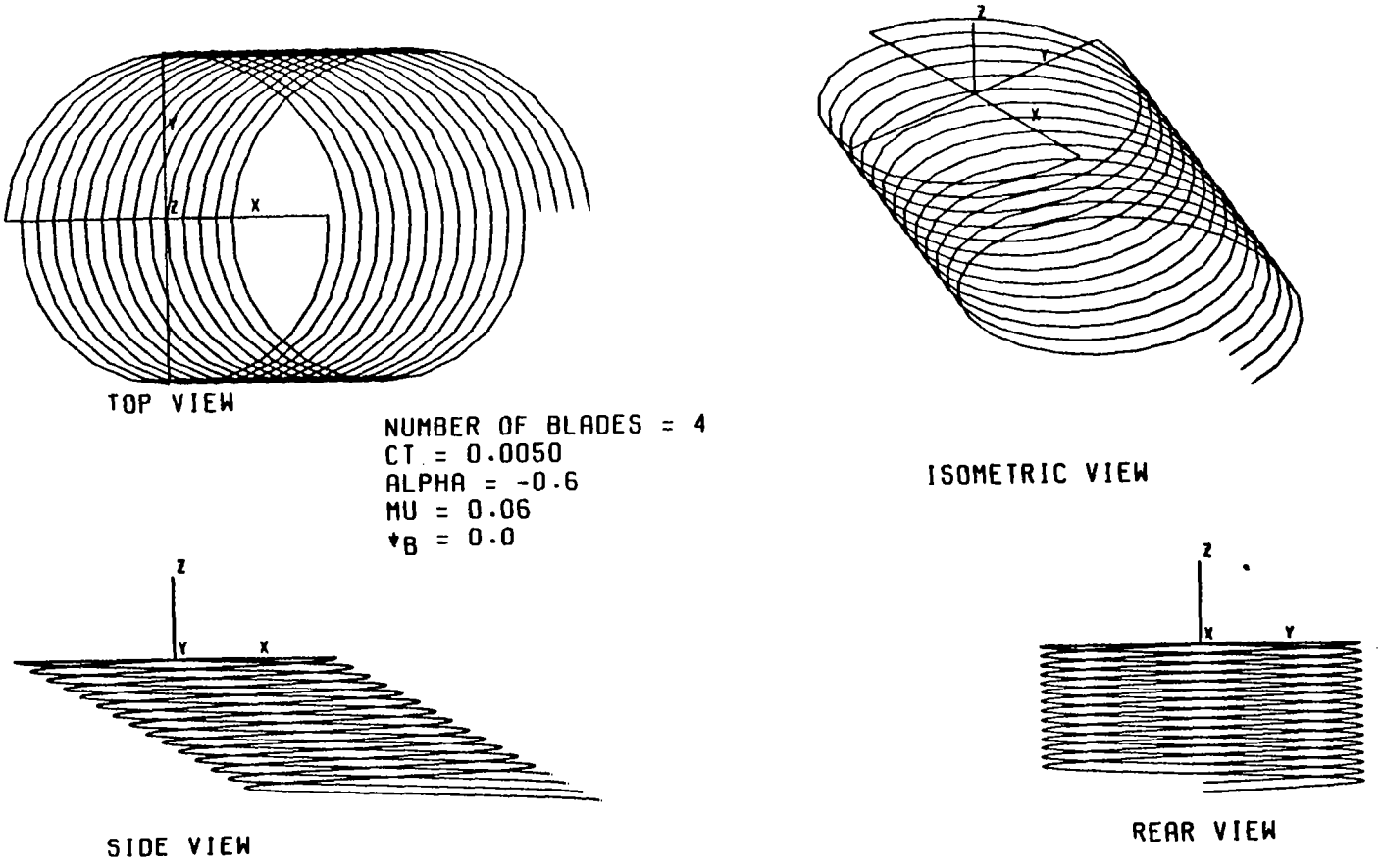

FIGURE 79. UNDISTORTED TIP VORTEX GEOMETRY FOR H-34 ROTOR, μ=0.064

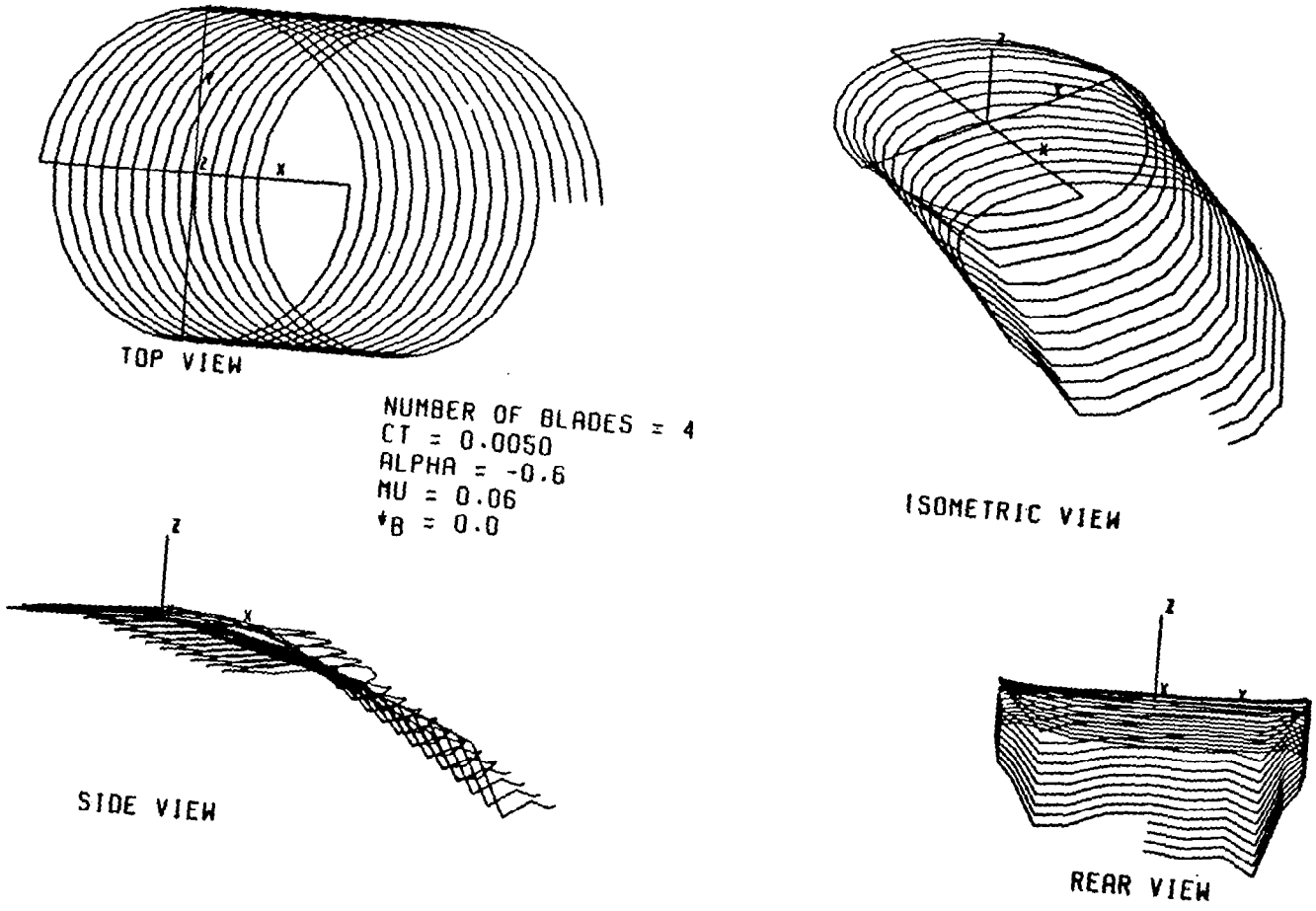

FIGURE 80. DISTORTED TIP VORTEX GEOMETRY FOR H-34 ROTOR, μ=0.064

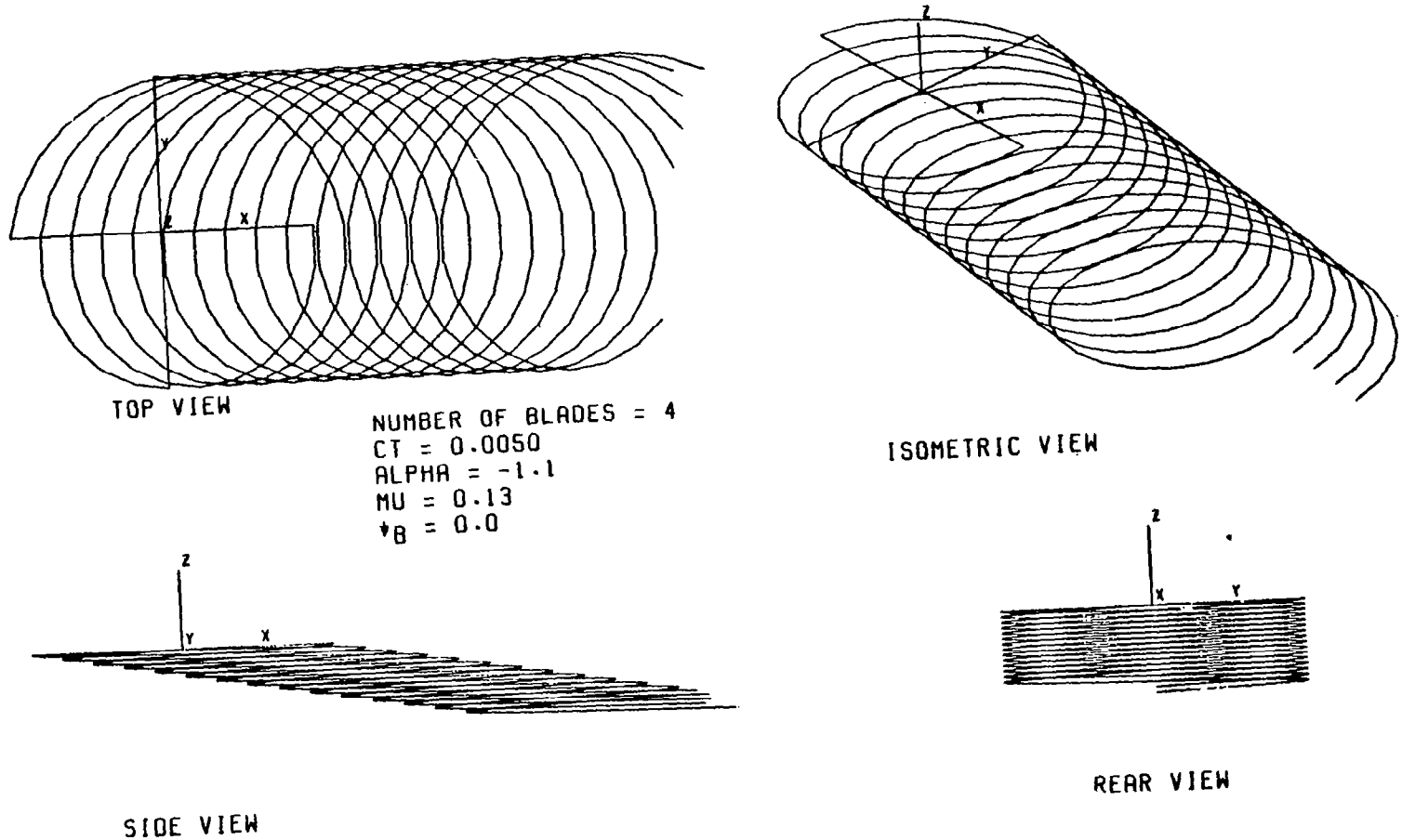

FIGURE 81. UNDISTORTED TIP VORTEX GEOMETRY FOR H-34 ROTOR, μ=0.129

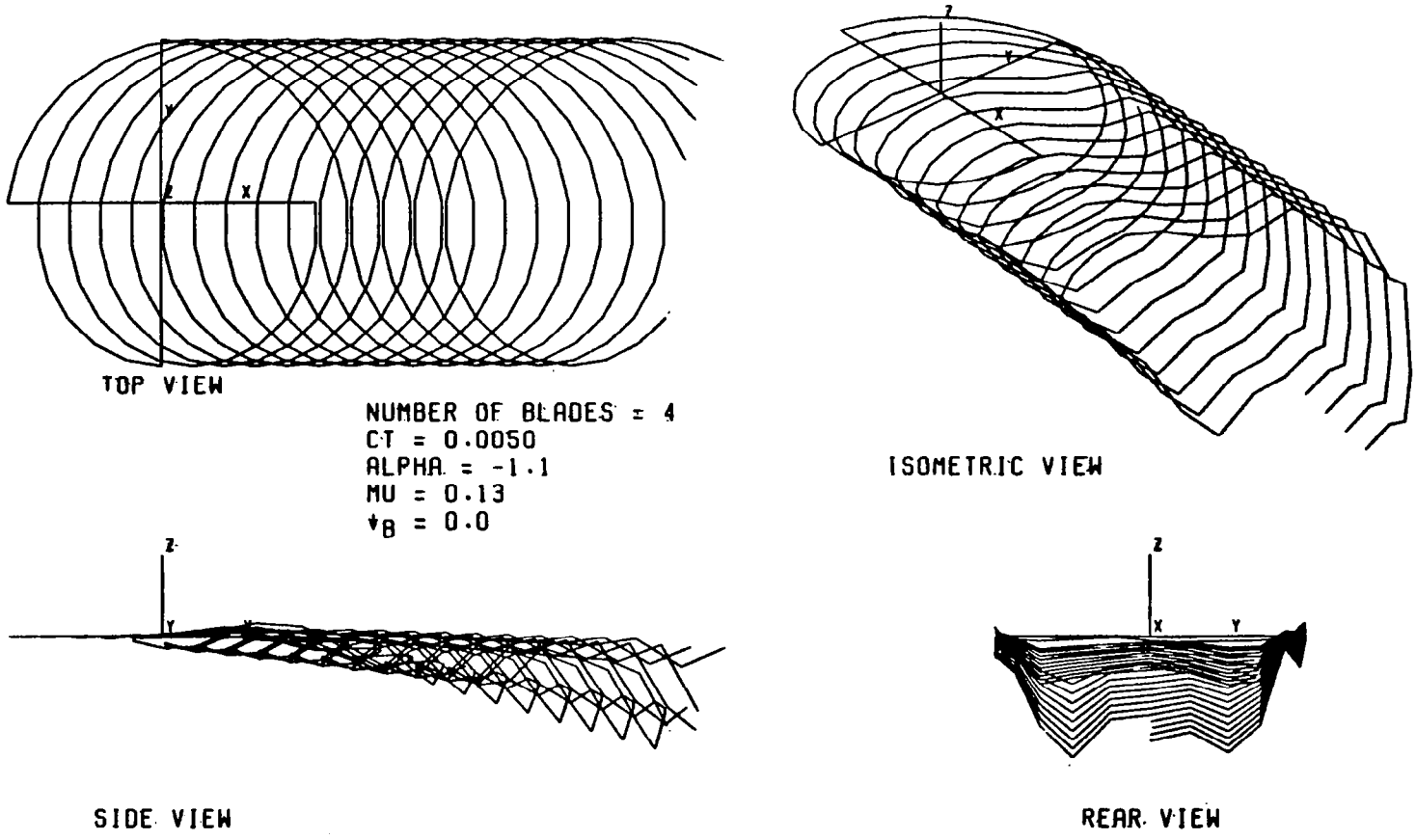

FIGURE 82. DISTORTED TIP VORTEX GEOMETRY FOR H-34 ROTOR, μ=0.129

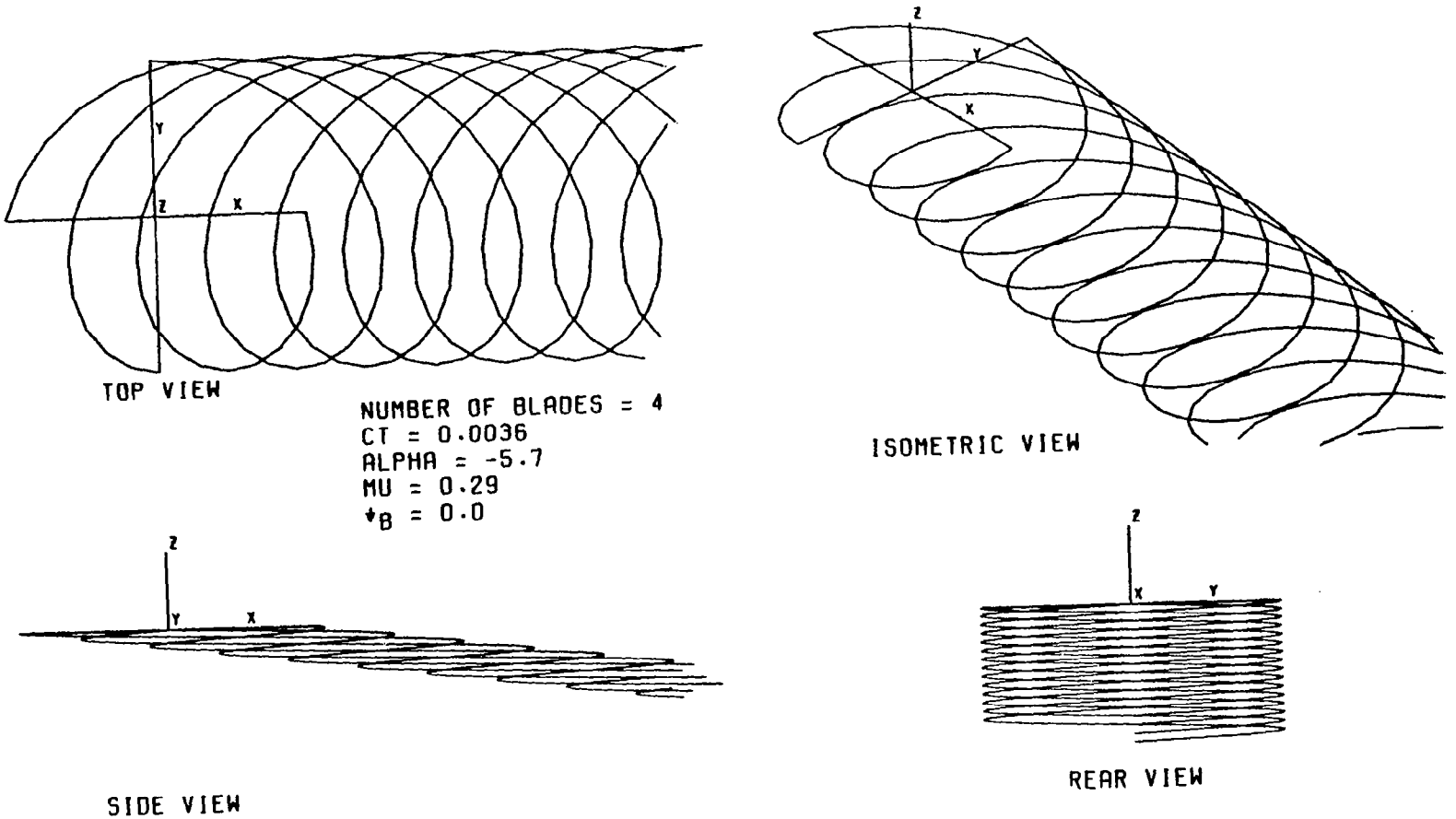

FIGURE 83. UNDISTORTED TIP VORTEX GEOMETRY FOR H-34 ROTOR, μ=0.29

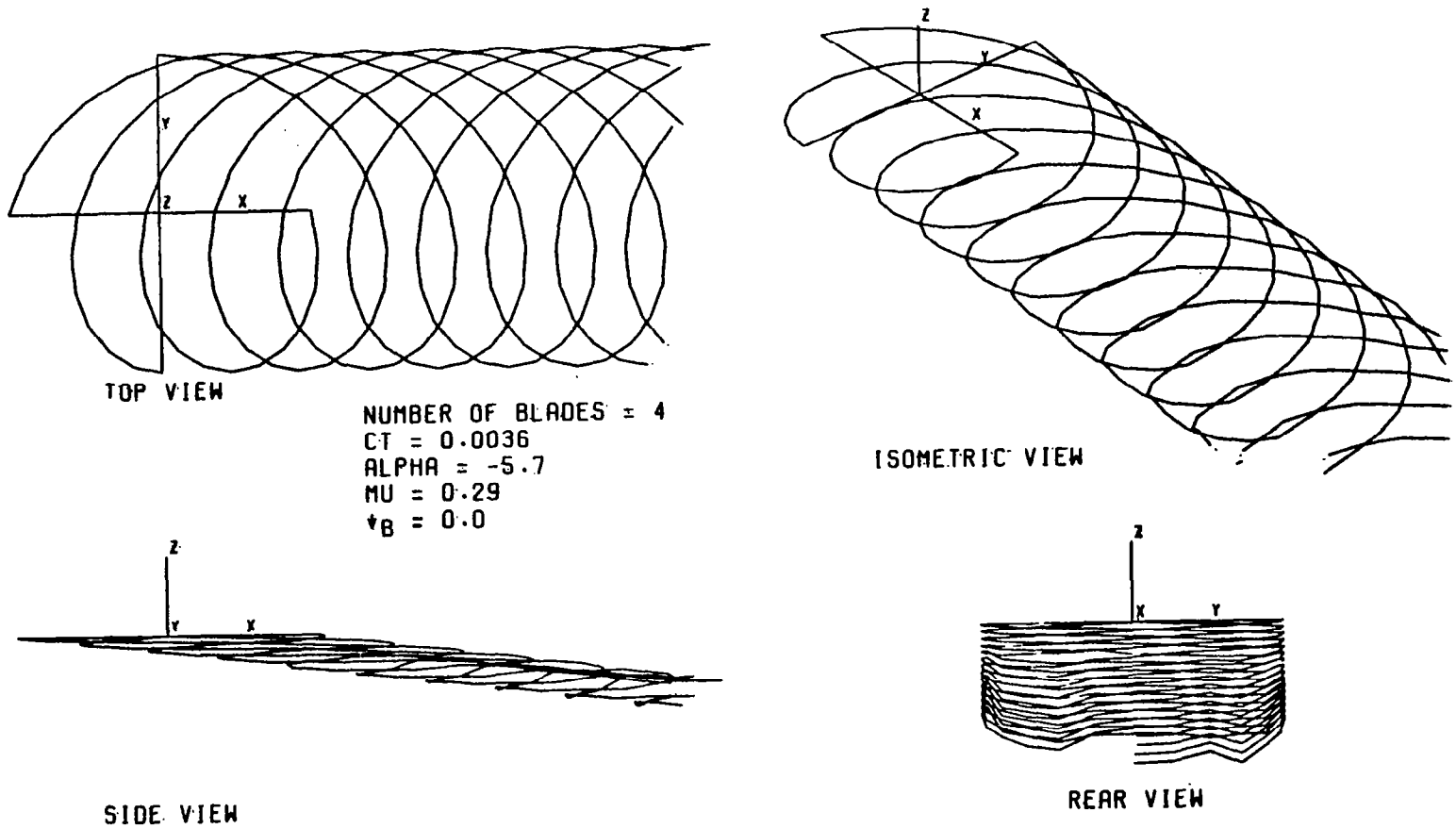

FIGURE 84. DISTORTED TIP VORTEX GEOMETRY FOR H-34 ROTOR, μ=0.29

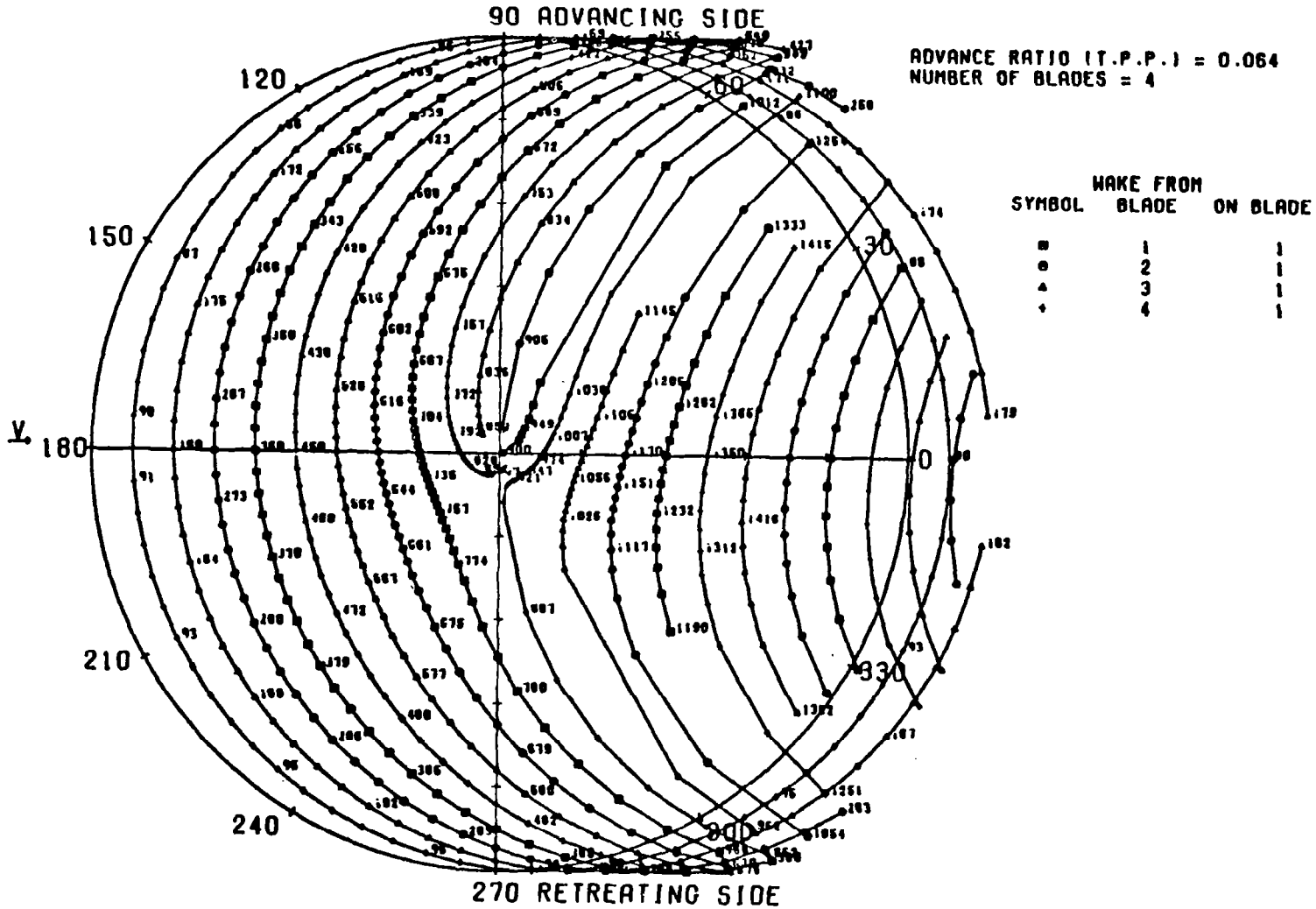

FIGURE 85. POTENTIAL BLADE/TIP VORTEX INTERSECTION PLOT FOR FOUR BLADED ROTOR AT AN ADVANCE RATIO OF 0.064

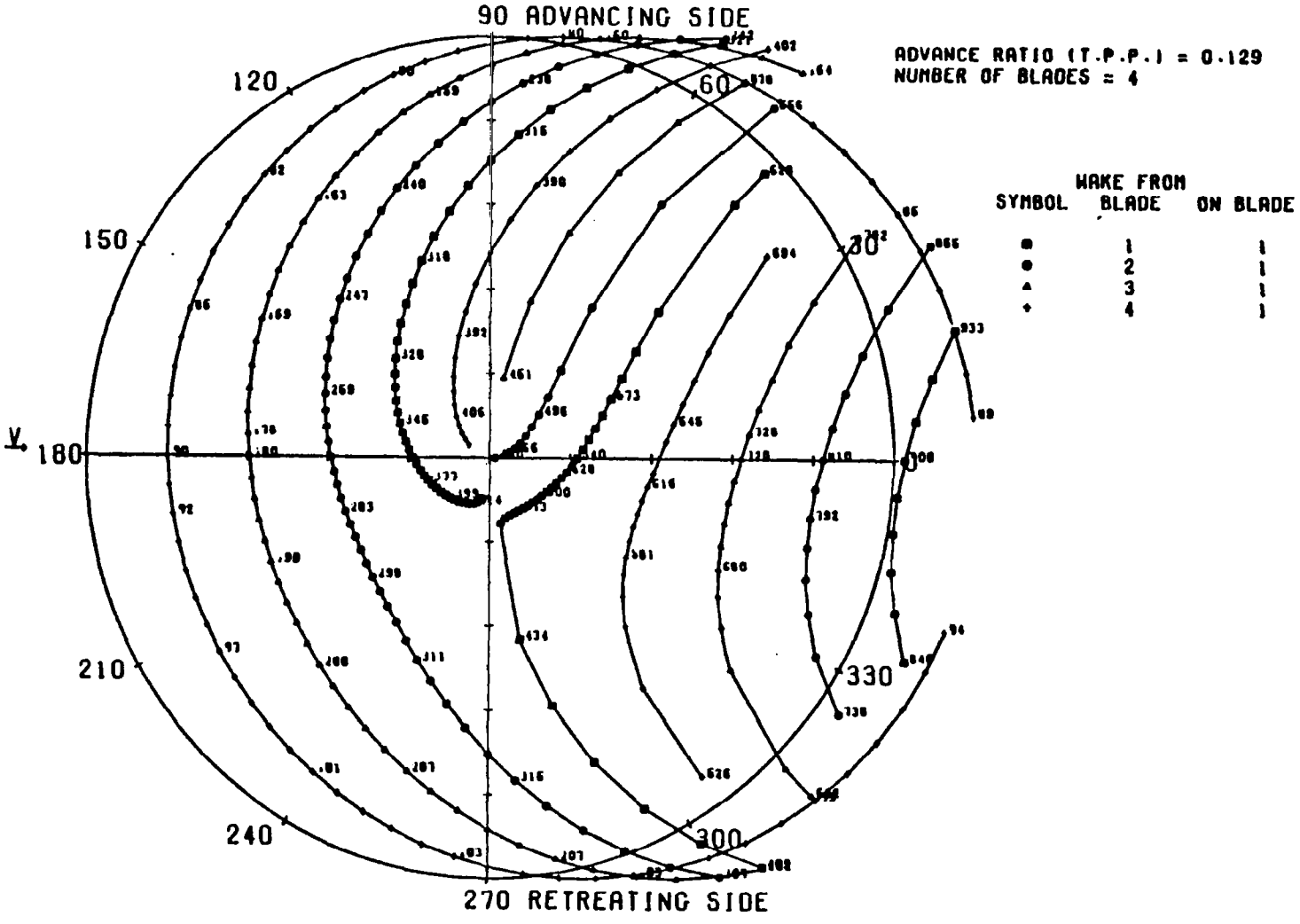

FIGURE 86. POTENTIAL BLADE / TIP VORTEX INTERSECTION PLOT FOR TWO BLADED ROTOR AT AN ADVANCE RATIO OF 0.129

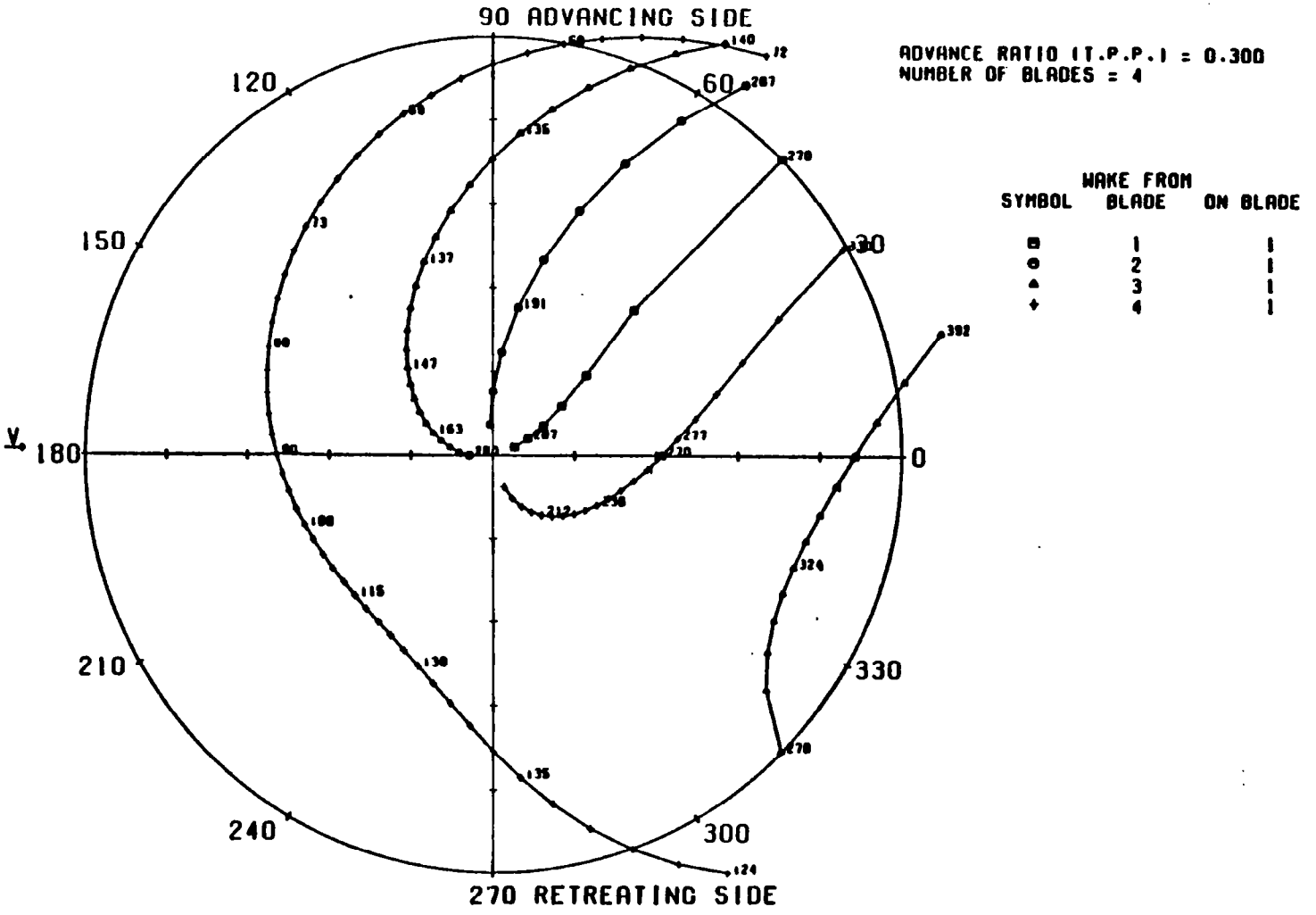

FIGURE 87. POTENTIAL BLADE/TIP VORTEX INTERSECTION PLOT FOR FOUR BLADES (POLAR FORMAT), μ = .30

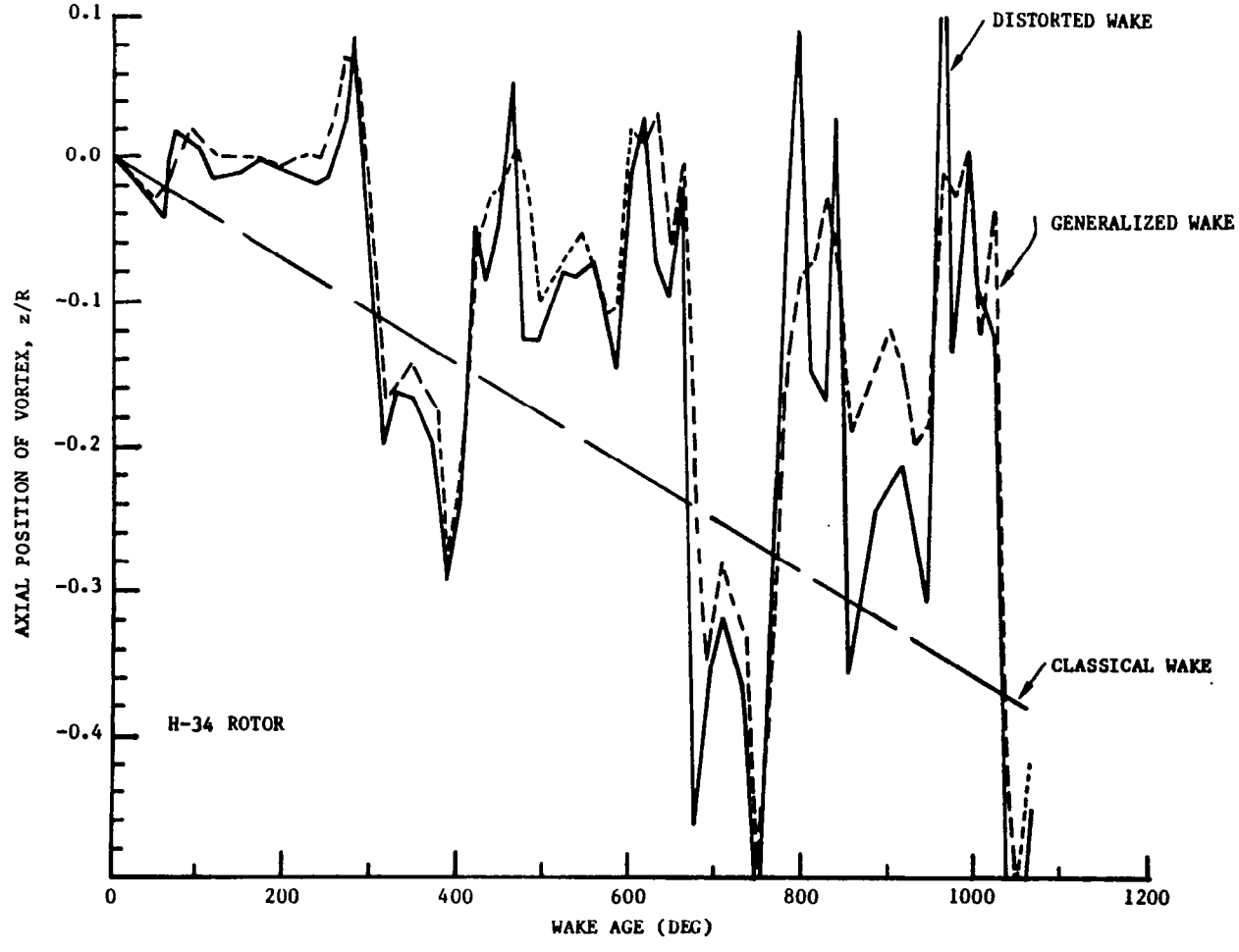

FIGURE 88. COMPARISON OF THE GENERALIZED WAKE AND THE ACTUAL PREDICTED DISTORTED WAKE GEOMETRY FOR A SELECTED BLADE AZIMUTH POSITION, ψ_b=0.0°, μ=.129, b=4, C_T=.0047, α_{TPP}=-1.13

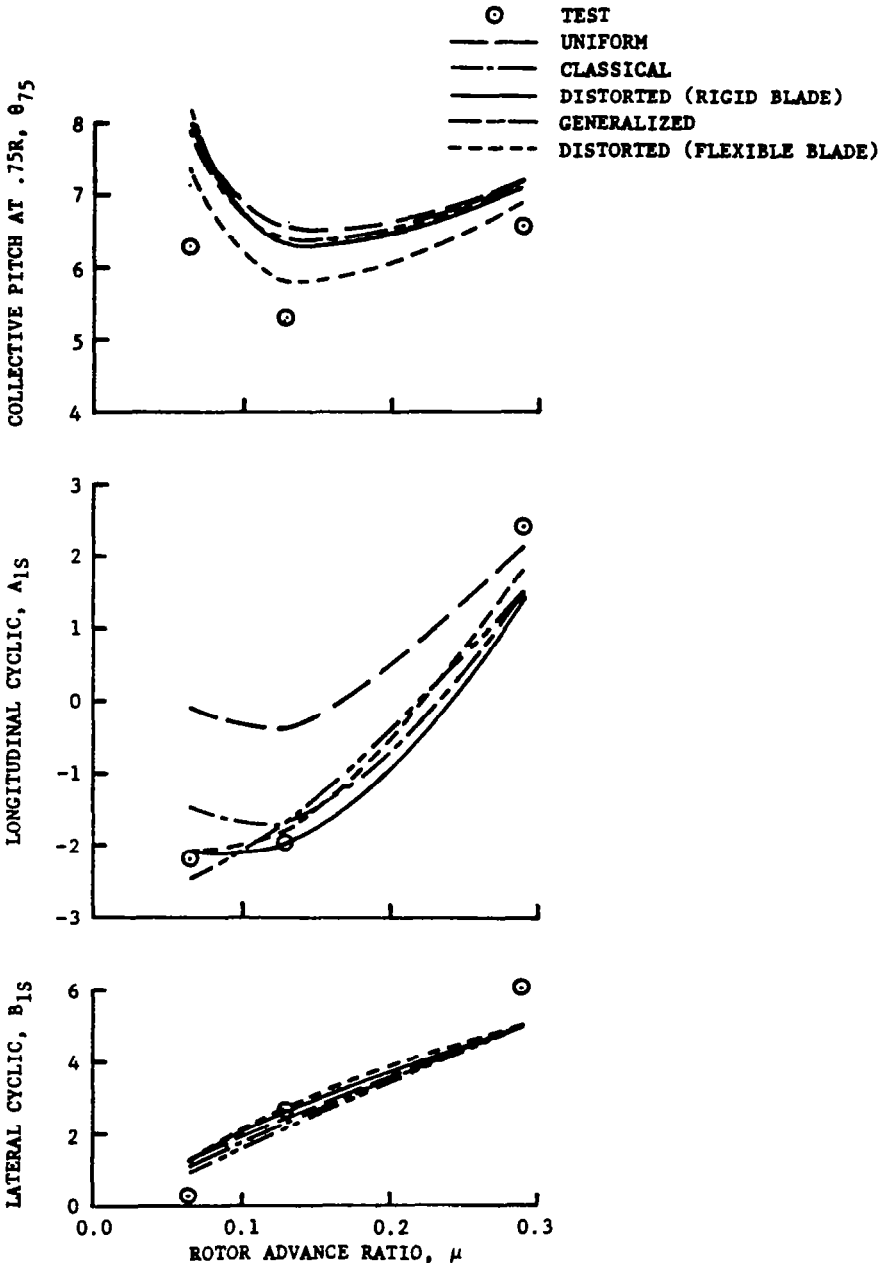

FIGURE 89. COMPARISON OF PREDICTED AND MEASURED BLADE PITCH CONTROL ANGLE SETTINGS

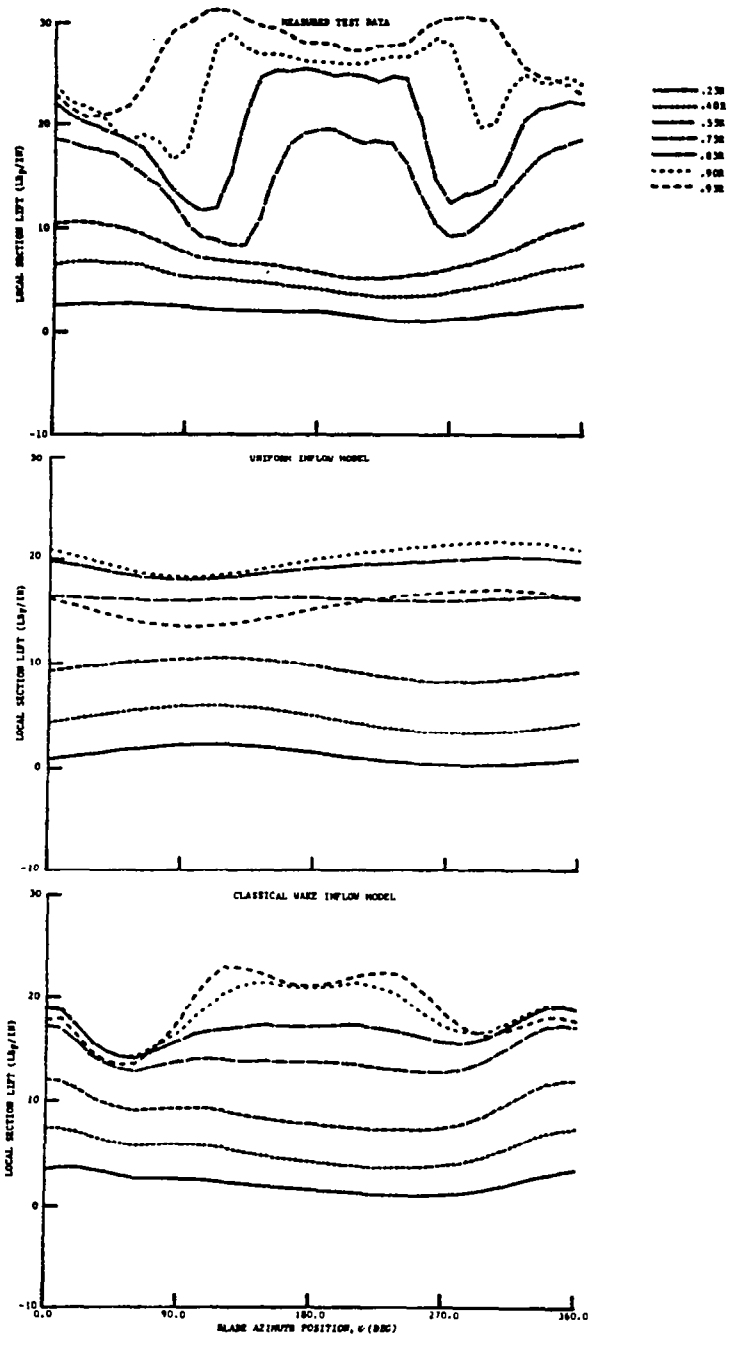

FIGURE 90a. H-34 LOCAL LIFT DISTRIBUTIONS, FOR AN ADVANCE RATIO OF .064 (23 KT)

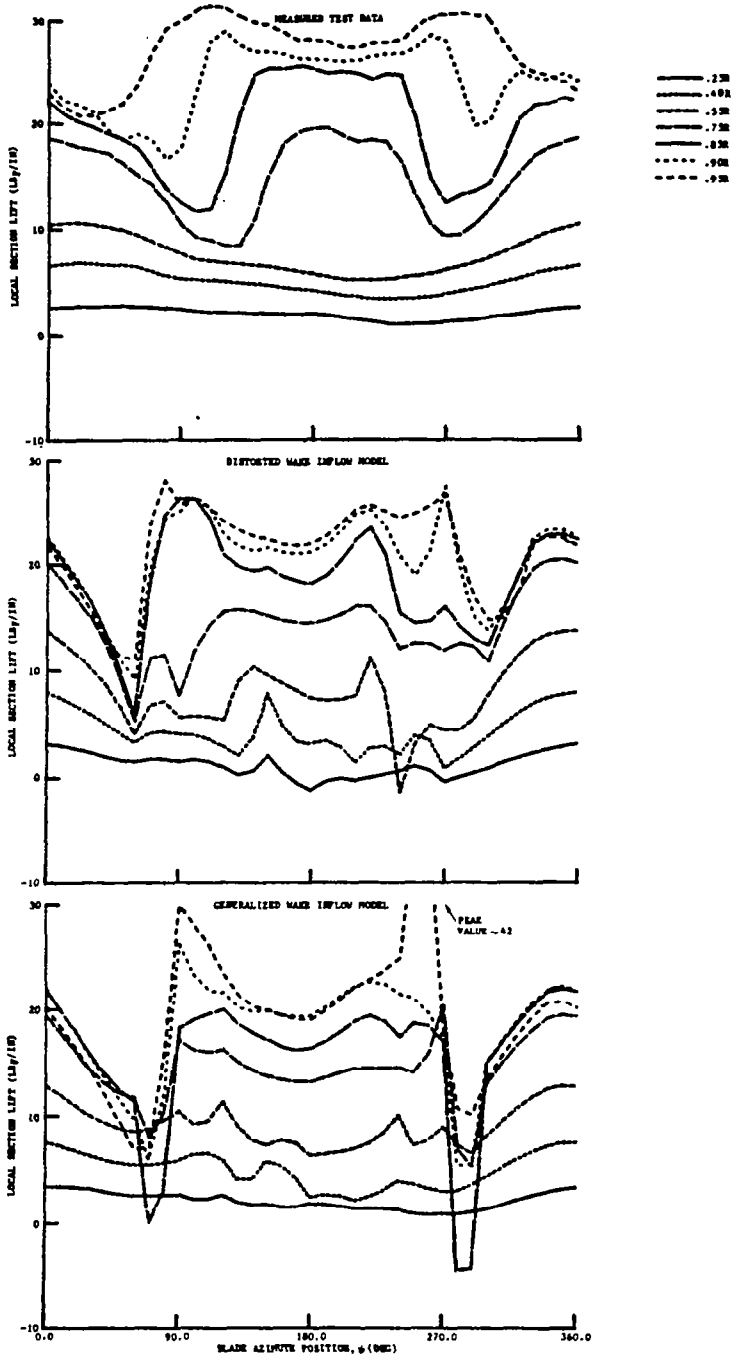

FIGURE 90b. R-34 LOCAL LIFT DISTRIBUTIONS, FOR AN ADVANCE RATIO OF .064 (23 KT)

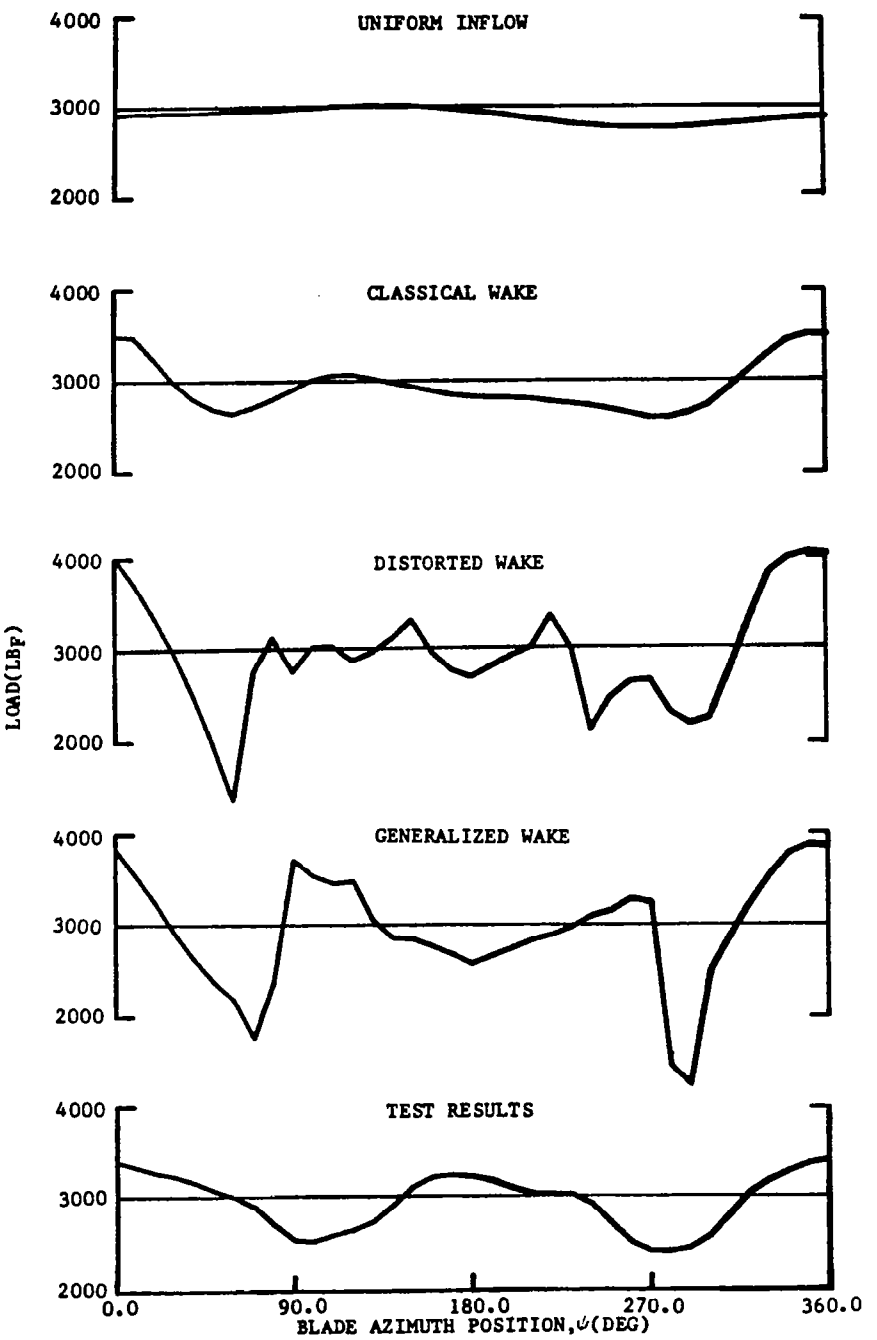

FIGURE 91. H-34 INTEGRATED SPANWISE LOADING RESULTS FOR VARIOUS INFLOW MODELS AND TEST RESULTS AT AN ADVANCE RATIO OF .064 (23 KT)

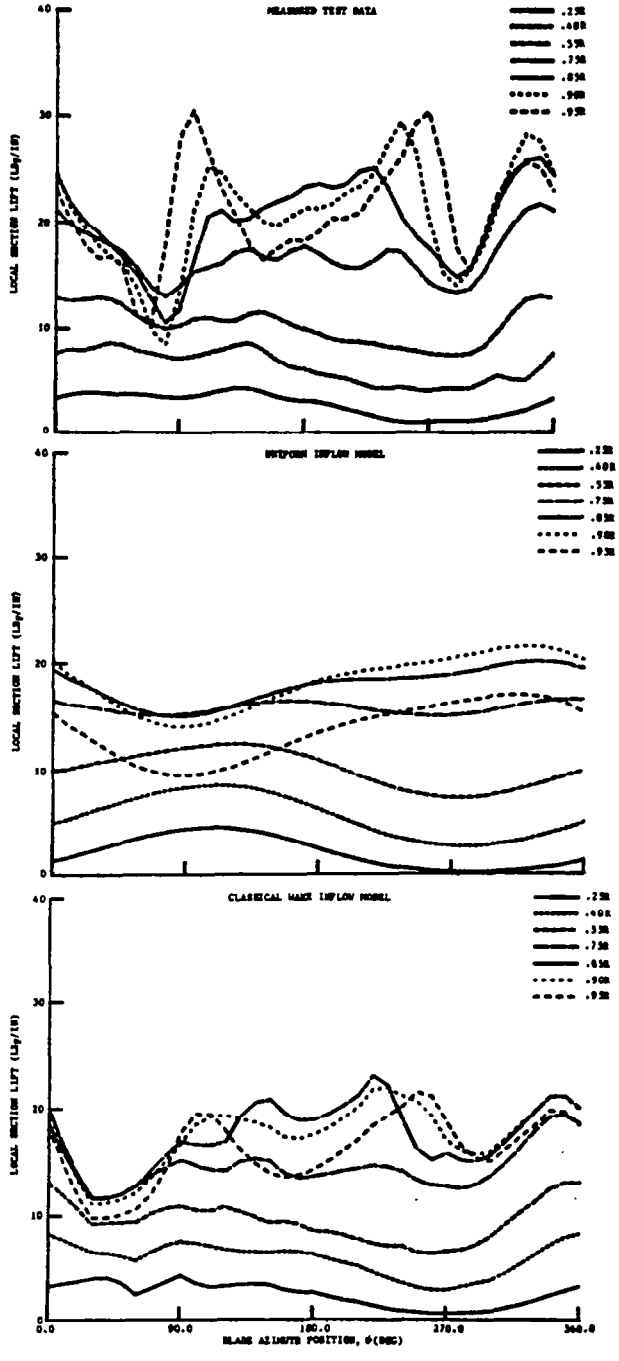

FIGURE 92a. H-34 LOCAL LIFT DISTRIBUTIONS, FOR AN ADVANCE RATIO OF .129

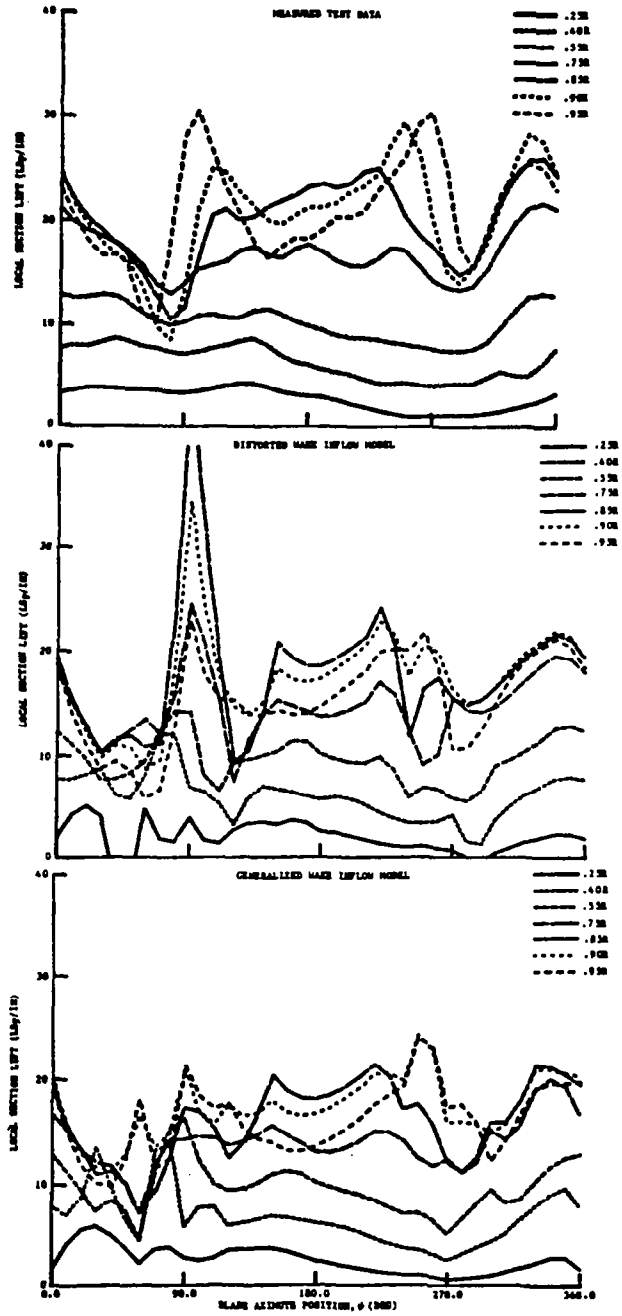

FIGURE 92b. H-34 LOCAL LIFT DISTRIBUTIONS, FOR AN ADVANCE RATIO OF .129

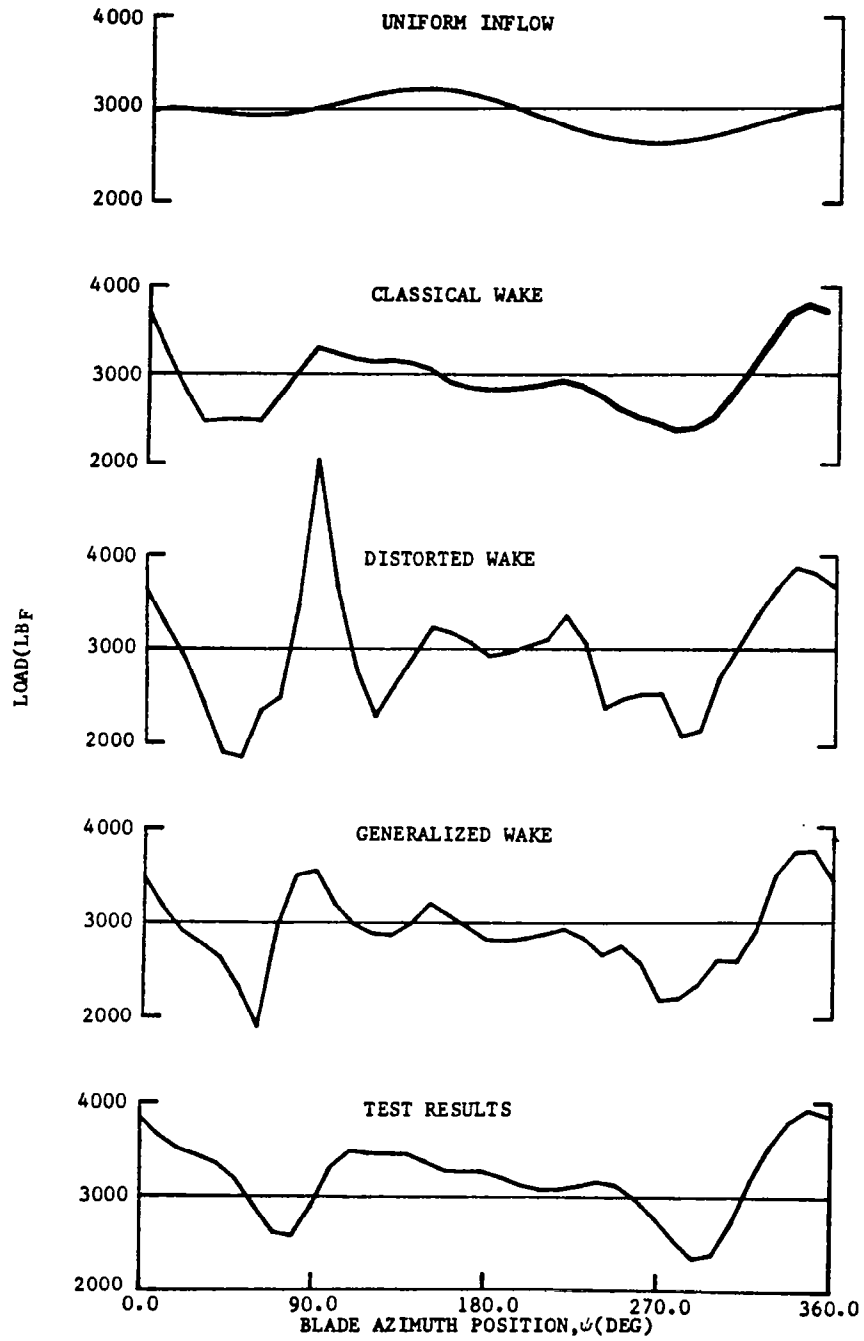

FIGURE 93. H-34 INTEGRATED SPANWISE LOADING RESULTS FOR VARIOUS INFLOW MODELS AND TEST RESULTS AT AN ADVANCE RATIO OF .129.

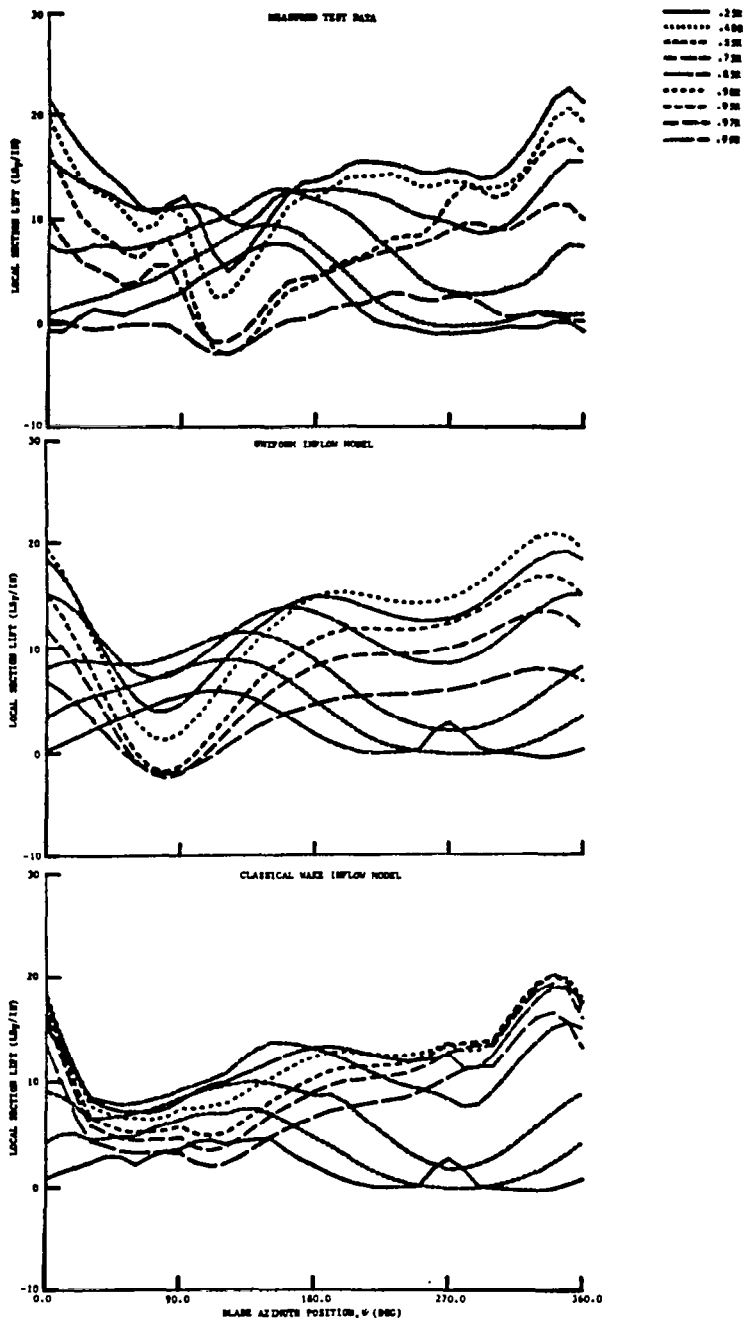

FIGURE 94 a. H-34 LOCAL LIFT DISTRIBUTIONS, FOR AN ADVANCE RATIO OF .29

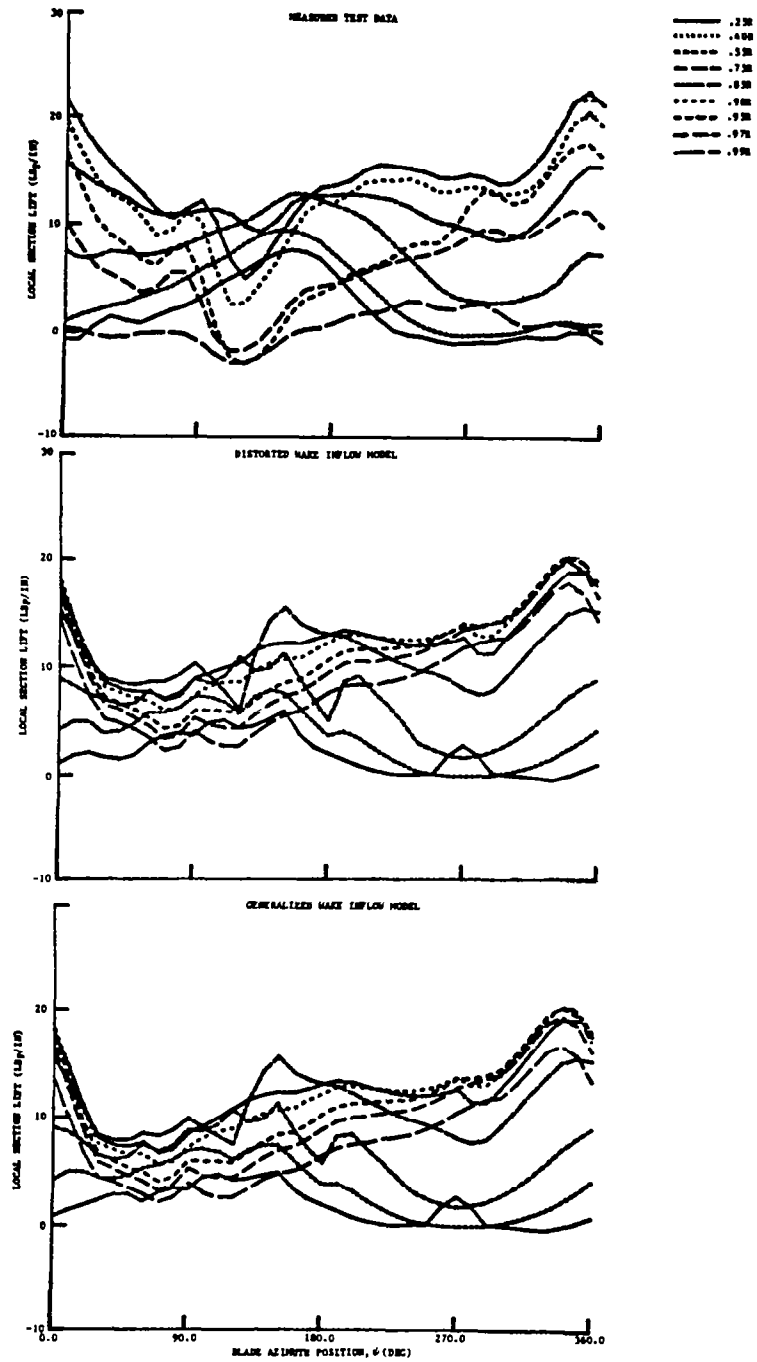

FIGURE 94b. H-34 LOCAL LIFT DISTRIBUTIONS, FOR AN ADVANCE RATIO OF .29

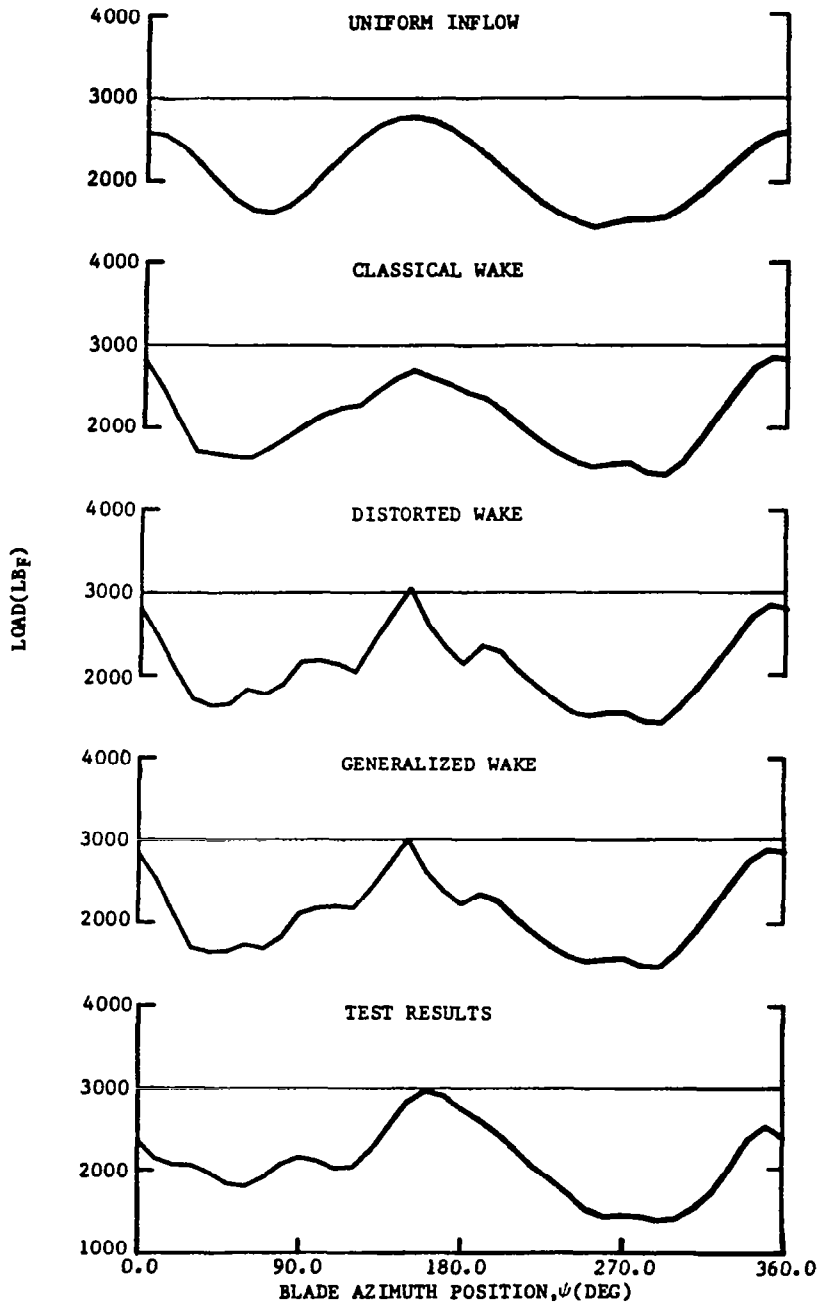

FIGURE 95. H-34 INTEGRATED SPANWISE LOADING RESULTS FOR VARIOUS INFLOW MODELS AND TEST RESULTS AT AN ADVANCE RATIO OF .29.

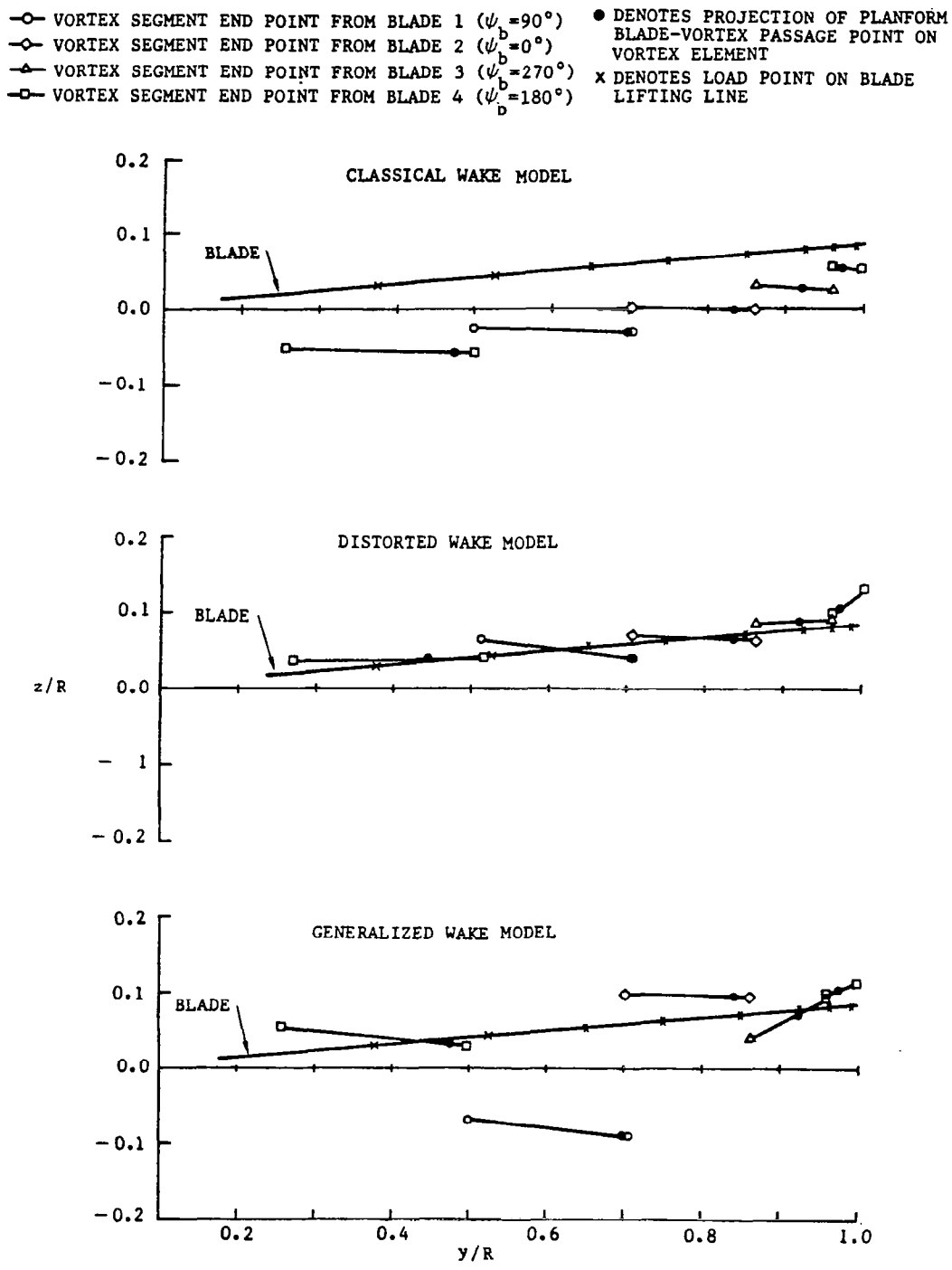

FIGURE 96. COMPARISON OF PREDICTED AXIAL LOCATIONS OF LOCAL VORTEX SEGMENTS FOR THE H-34 ROTOR AT AN ADVANCE RATIO OF .129, ψ_b=90°

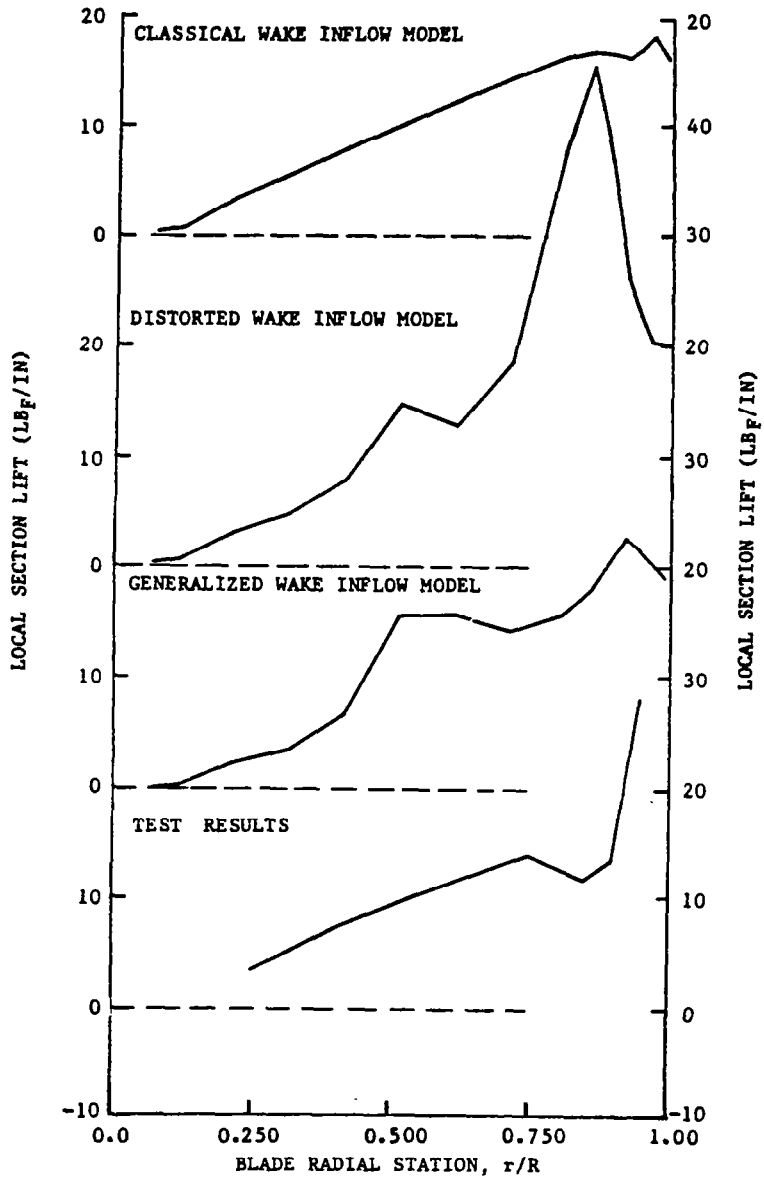

FIGURE 97. COMPARISON OF PREDICTED SPANWISE LOADING FOR H-34 ROTOR AT AN ADVANCE RATIO OF .129, $\psi_b = 90°$

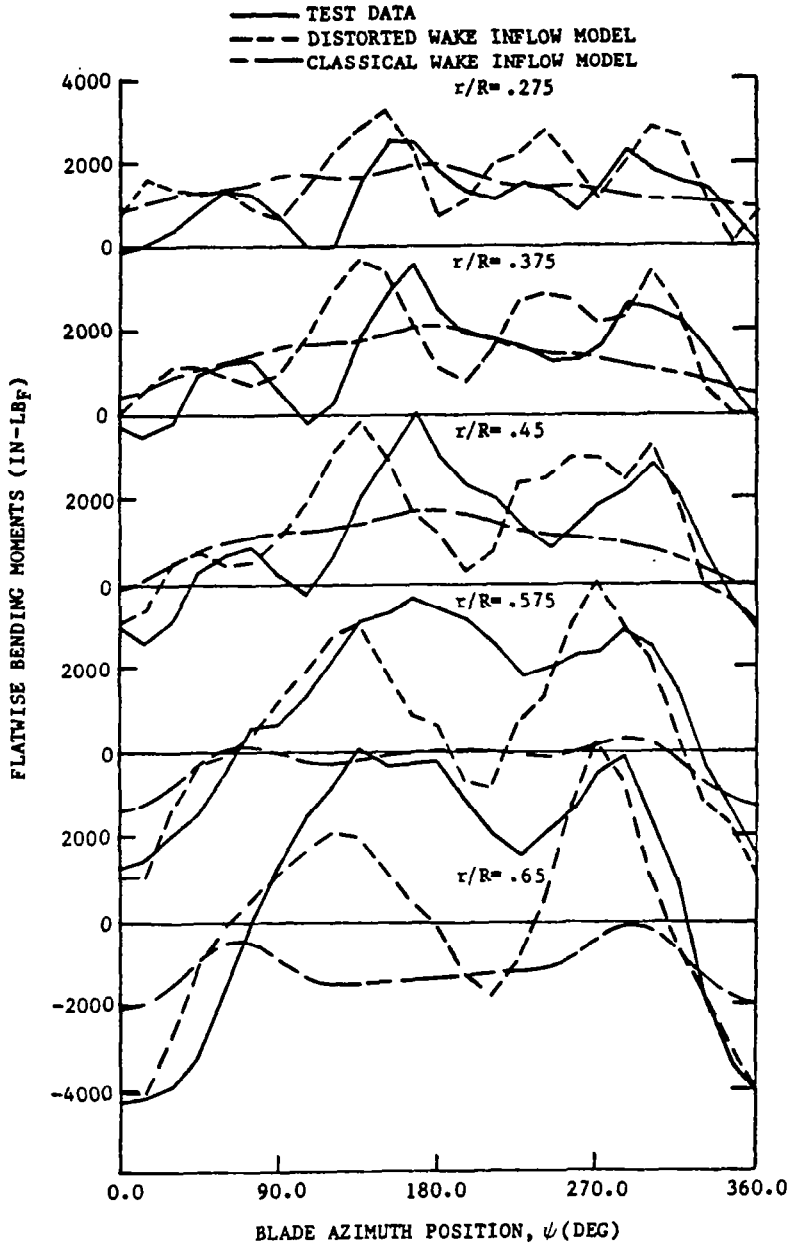

FIGURE 98. COMPARISON OF PREDICTED FLATWISE BENDING MOMENTS USING THE DISTORTED WAKE INFLOW MODEL VERSUS TEST RESULTS FOR AN ADVANCE RATIO OF .064

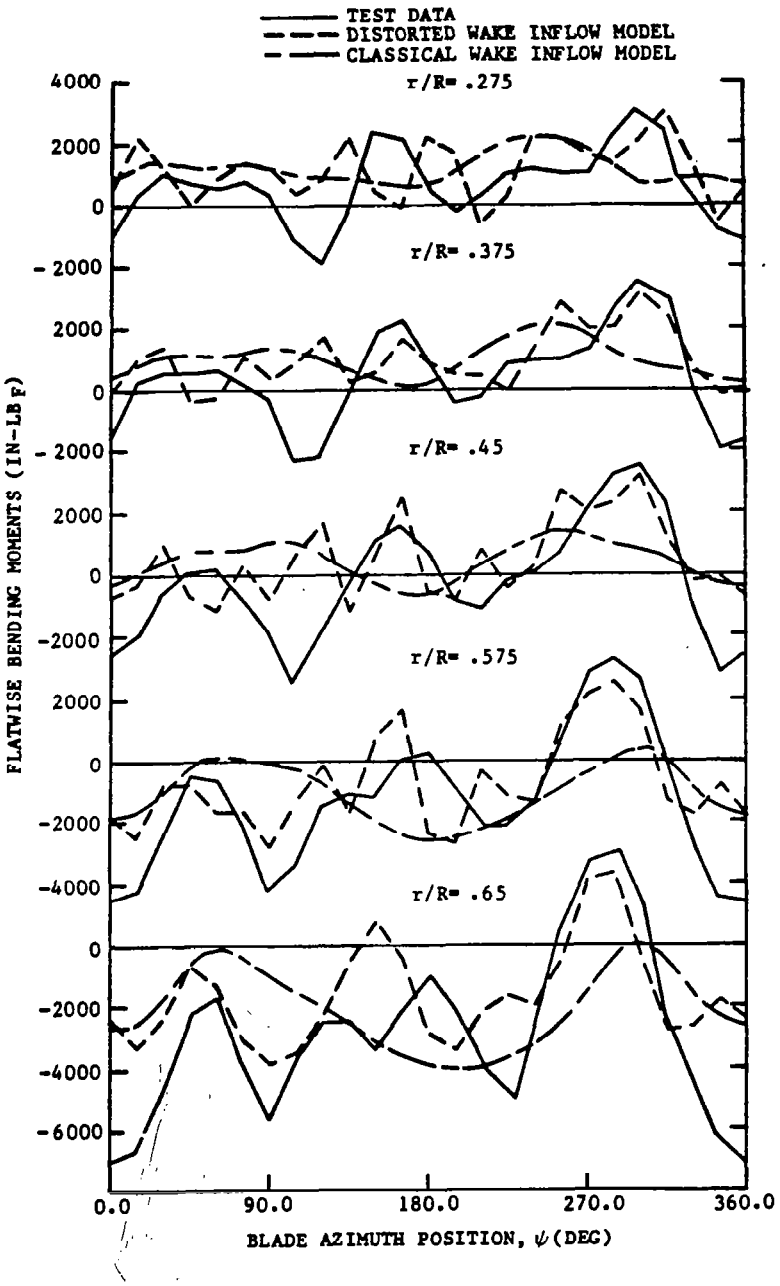

FIGURE 99. COMPARISON OF PREDICTED FLATWISE BENDING MOMENTS USING THE DISTORTED WAKE INFLOW MODEL VERSUS TEST RESULTS FOR AN ADVANCE RATIO OF .129

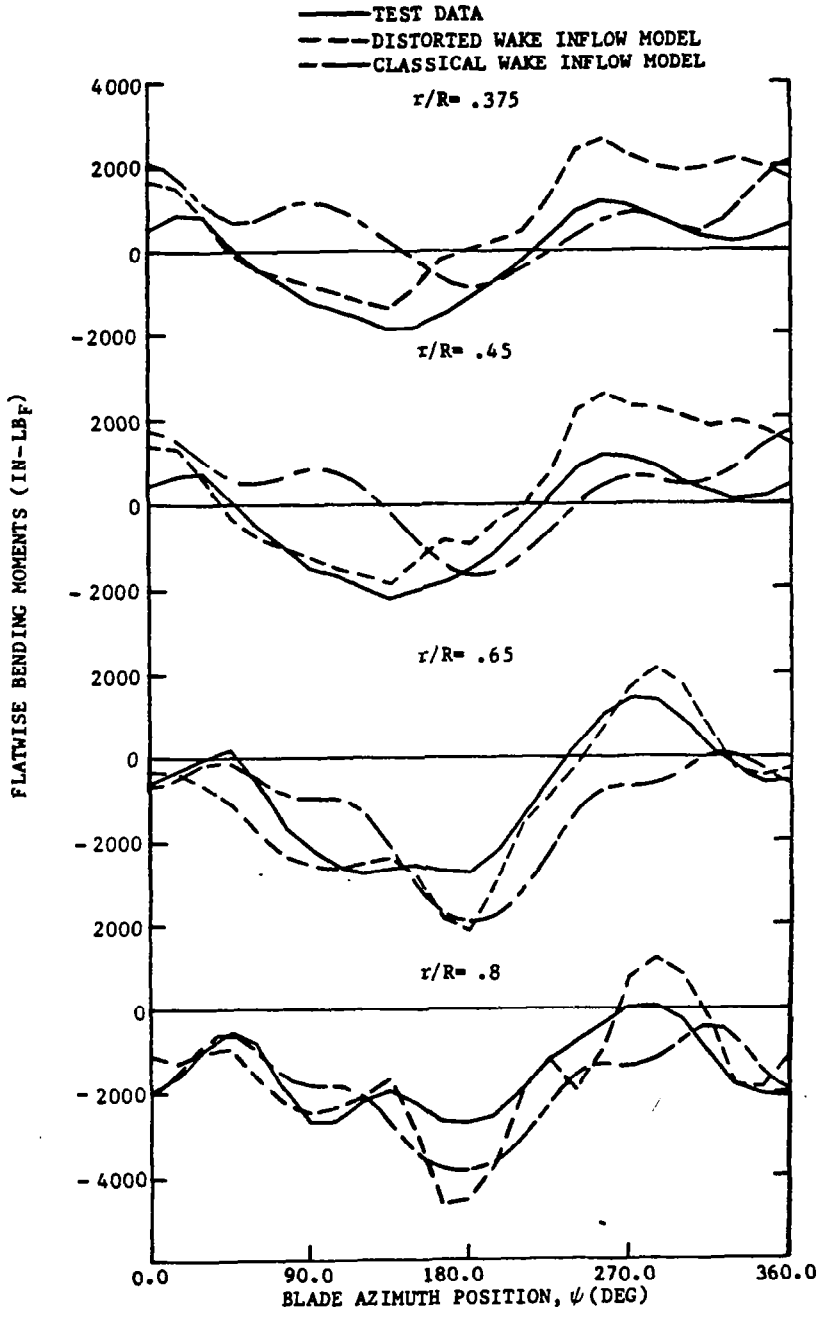

FIGURE 100. COMPARISON OF PREDICTED FLATWISE BENDING MOMENTS USING THE DISTORTED WAKE INFLOW MODEL VERSUS TEST RESULTS FOR AN ADVANCE RATIO OF .29

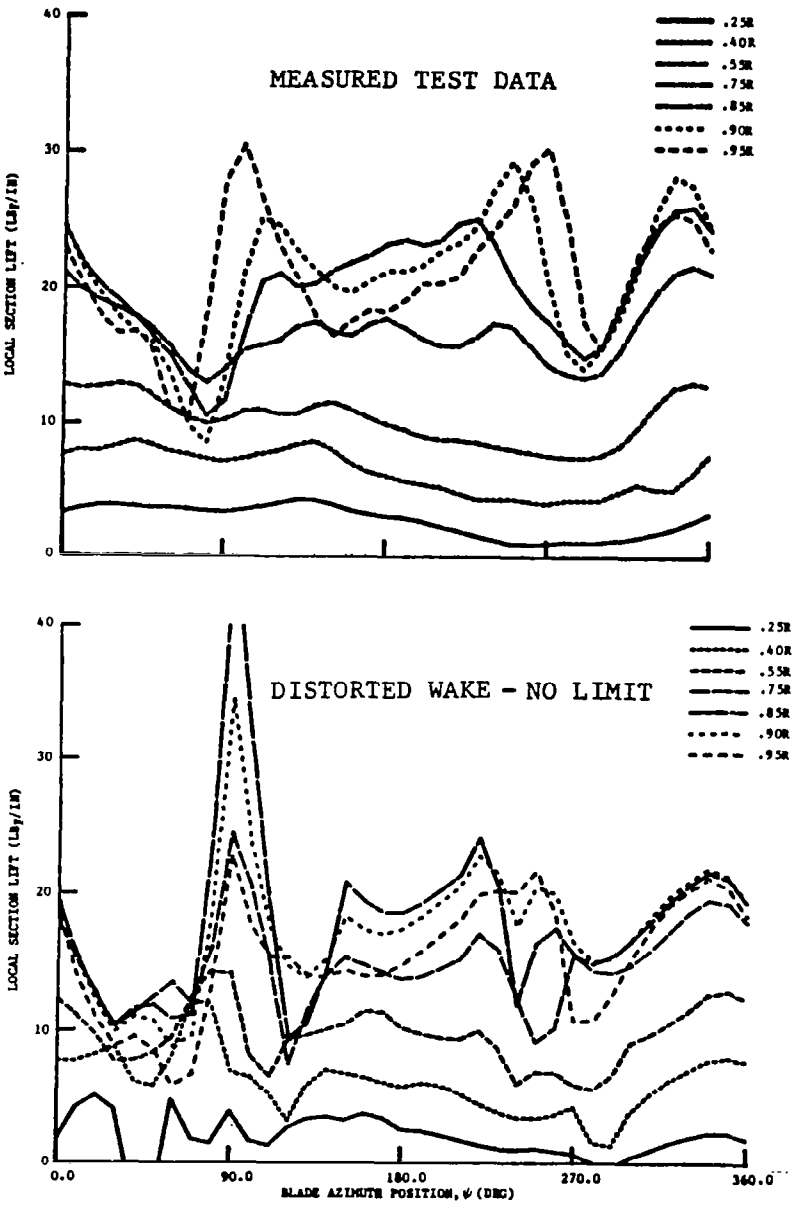

FIGURE 101a. H-34 LOCAL LIFT DISTRIBUTIONS FOR AN ADVANCE RATIO OF .129 FOR COMPARISON WITH FIG. 101b

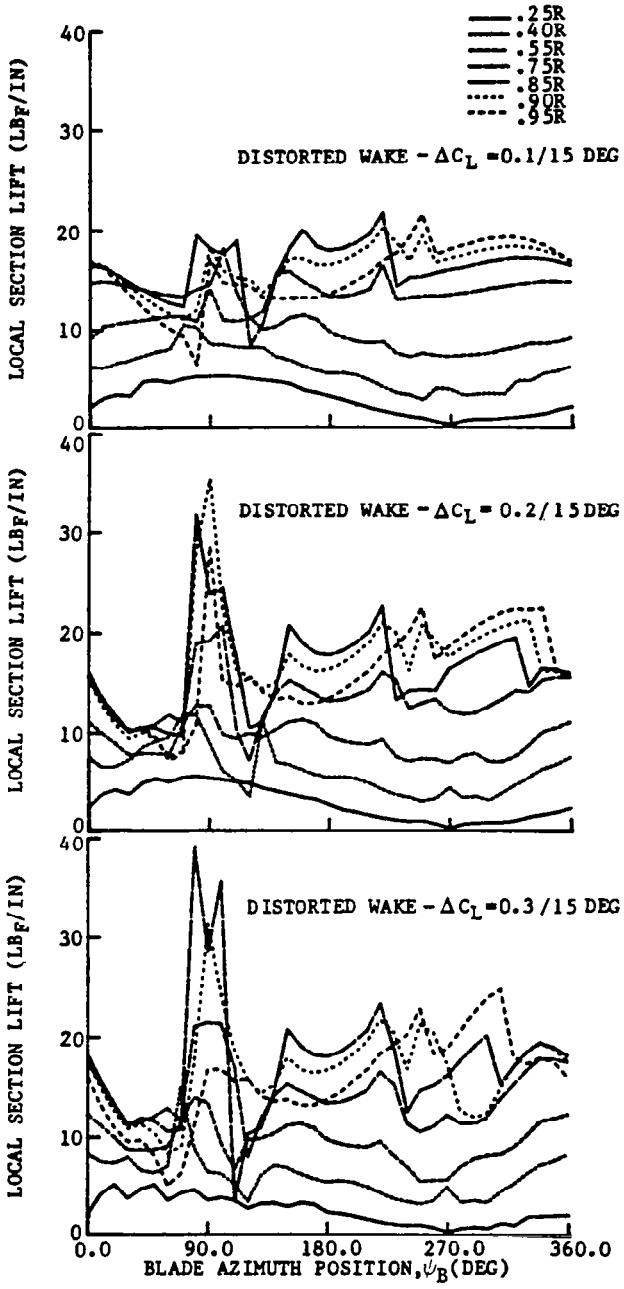

FIGURE 101b. PREDICTED H-34 LIFT DISTRIBUTION FOR VARIOUS BLADE VORTEX INTERACTION LIMITS AT AN ADVANCE RATIO OF .129

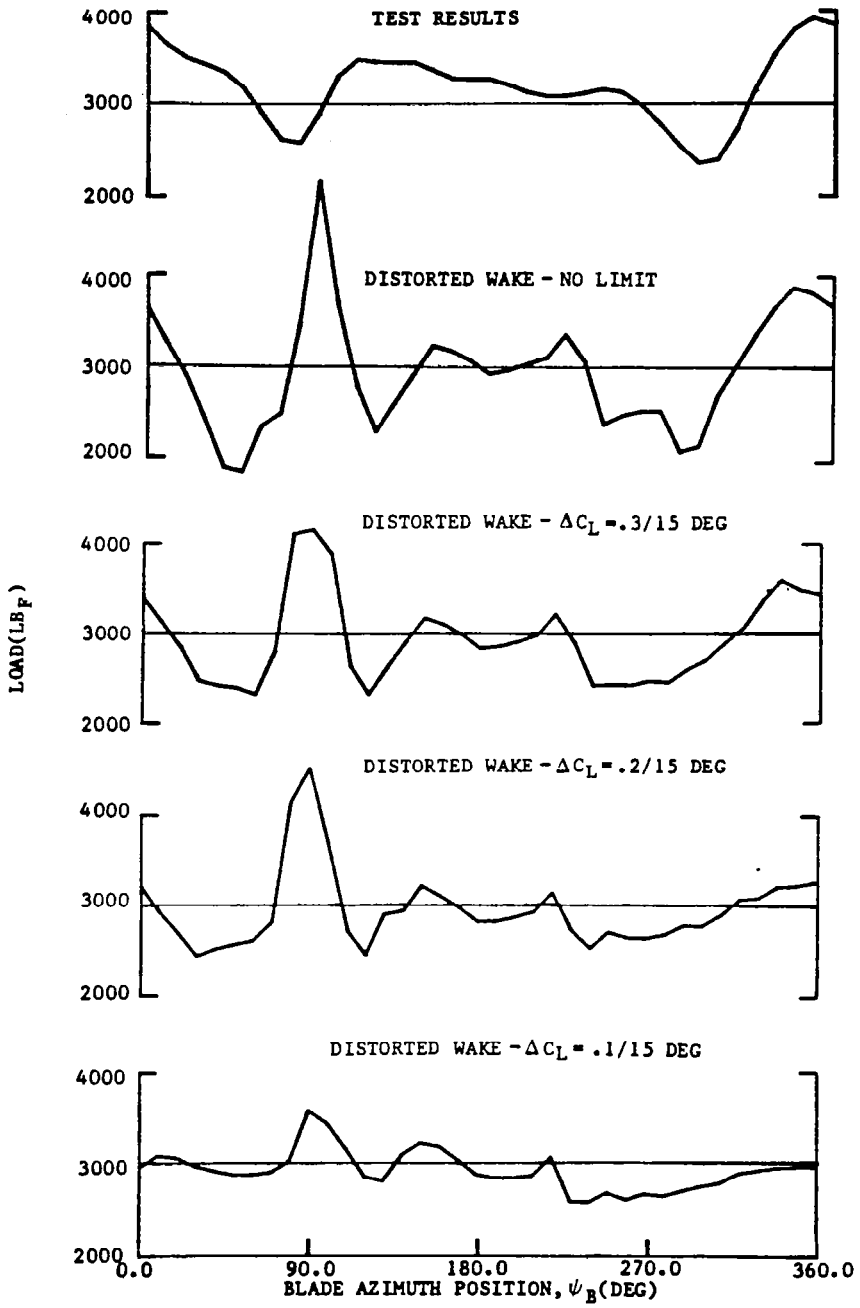

FIGURE 102. COMPARISON OF H-34 INTEGRATED SPANWISE LOAD DISTRIBUTIONS FOR VARIOUS BLADE VORTEX INTERACTION LIMITS AT AN ADVANCE RATIO OF .129

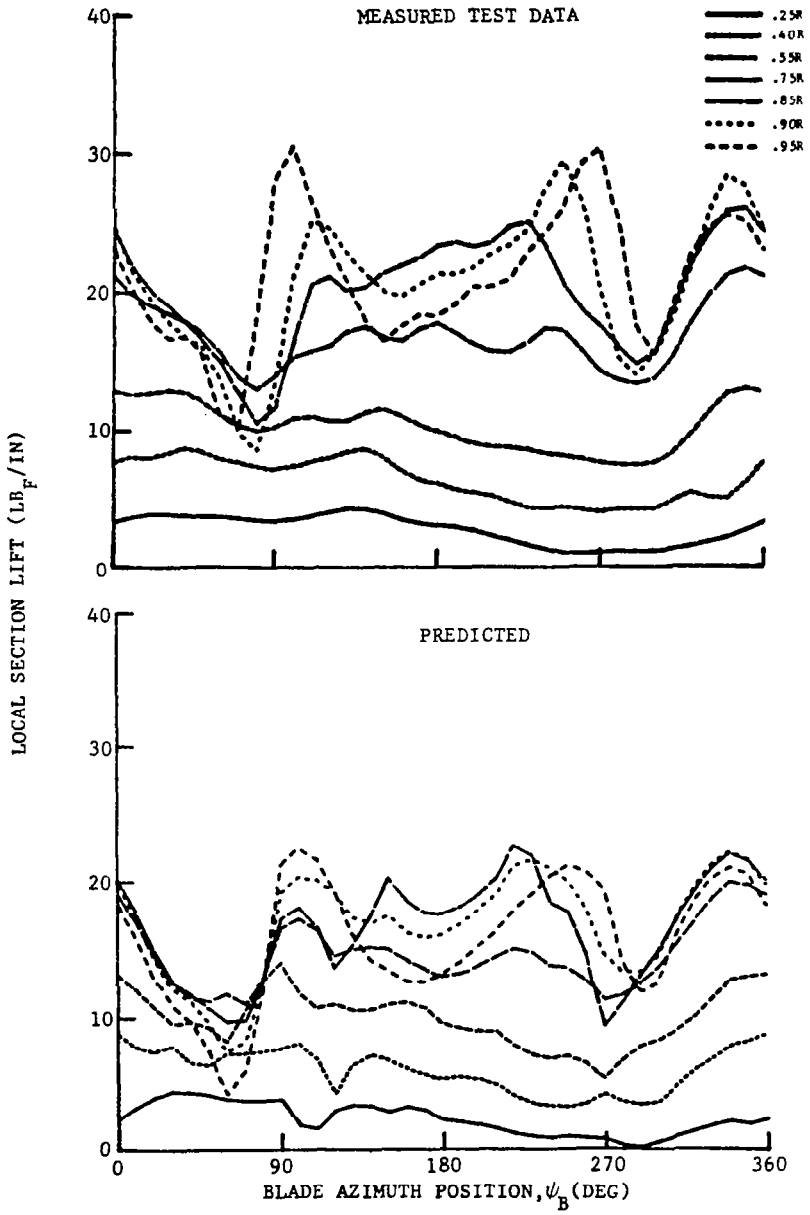

FIGURE 103. PREDICTED AIRLOADING FOR THE H-34 ROTOR AT AN ADVANCE RATIO OF 0.129 USING THE DISTORTED WAKE GEOMETRY WITH ZERO INDUCED INFLUENCE WITHIN A LARGE VORTEX CORE RADIUS (0.03R)

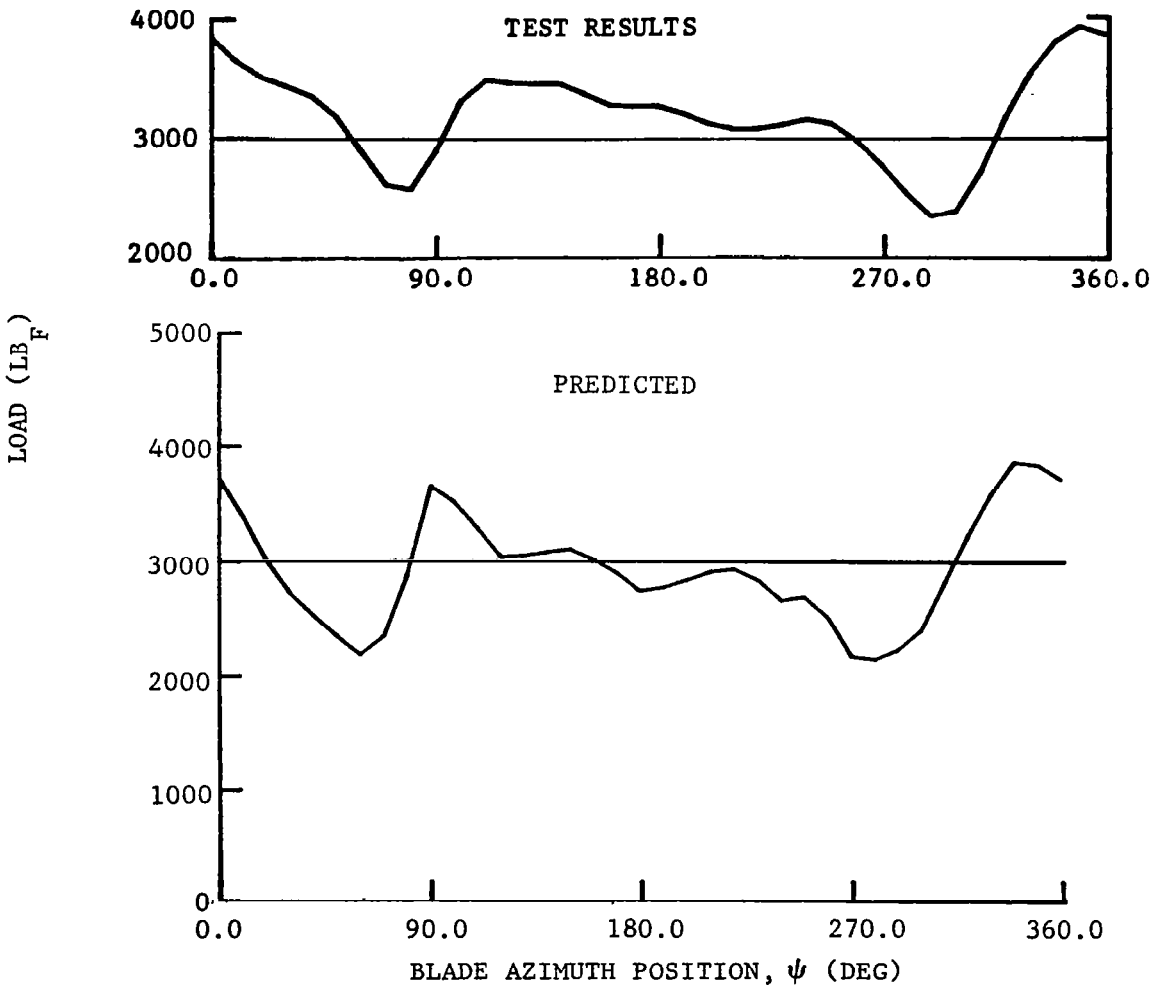

FIGURE 104. PREDICTED INTEGRATED BLADE LIFT FOR THE H-34 ROTOR AT AN ADVANCE RATIO OF 0.129 USING THE DISTORTED WAKE GEOMETRY WITH ZERO INDUCED INFLUENCE WITHIN A LARGE VORTEX CORE RADIUS (0.03R)

☆U.S. GOVERNMENT PRINTING OFFICE 1983 639 008/36

1. Report No.	2. Government Accession No.	3. Recipient's Catalog No.
NASA CR-3726		

4. Title and Subtitle	5. Report Date
HELICOPTER ROTOR WAKE GEOMETRY AND ITS INFLUENCE IN FORWARD FLIGHT. Volume I - Generalized Wake Geometry and Wake Effect on Rotor Airloads and Performance	October 1983
	6. Performing Organization Code
7. Author(s)	8. Performing Organization Report No.
T. Alan Egolf and Anton J. Landgrebe	R83-912666-58
	10. Work Unit No.
9. Performing Organization Name and Address	
United Technologies Research Center East Hartford, CT 06108	11. Contract or Grant No. NAS1-14568
	13. Type of Report and Period Covered
12. Sponsoring Agency Name and Address	Contractor Report
National Aeronautics and Space Administration Washington, DC 20546	14. Sponsoring Agency Code

15. Supplementary Notes The contract research effort which has led to the results in this report was financially supported by the structures Laboratory, USARTL, (AVRADCOM). Langley Technical Monitor: Wayne R. Mantay, Final Report - Volume I of two Volumes

16. Abstract An analytical investigation to generalize the wake geometry of a helicopter rotor in steady level forward flight and to demonstrate the influence of wake deformation in the prediction of rotor airloads and performance is described.

In Volume I, a first level generalized wake model is presented which is based on theoretically predicted tip vortex geometries for a selected representative blade design. The tip vortex distortions are generalized in equation form as displacements from the classical undistorted tip vortex geometry in terms of vortex age, blade azimuth, rotor advance ratio, thrust coefficient, and number of blades. These equations were programmed in a computer module to provide distorted wake coordinates at very low cost for use in rotor airflow and airloads prediction analyses. The sensitivity of predicted rotor airloads, performance, and blade bending moments to the modeling of the tip vortex distortion are demonstrated for low to moderately high advance ratios for a representative rotor and the H-34 rotor. Comparisons with H-34 rotor test data demonstrate the effects of the classical, predicted distorted, and the newly developed generalized wake models on airloads and blade bending moments. The use of distorted wake models results in the occurrence of numerous blade-vortex interactions on the forward and lateral sides of the rotor disk. The significance of these interactions is related to the number and degree of proximity to the blades of the tip vortices. The correlation obtained with the distorted wake models (generalized and predicted) is encouraging. However, the resulting high sensitivity of the predicted airloads to small deviations in tip vortex position demonstrate the requirement for improved blade-vortex interaction modeling.

A set of wake geometry charts are presented in Volume II to provide a convenient, readily accessible source for approximating rotor forward flight wake geometry and identifying wake boundaries and locations of blade-vortex passage.

17. Key Words (Suggested by Author(s))		18. Distribution Statement
Rotor Wake Geometry	Helicopter	Unclassified - Unlimited
Distorted Wake	Wake Geometry Charts	
Generalized Wake	Tip Vortex	
Rotor Airloads		
Rotor Performance		Subject Category 02

19. Security Classif. (of this report)	20. Security Classif. (of this page)	21. No. of Pages	22. Price
Unclassified	Unclassified	224	A10